Proceedings of the First PRC-US Workshop on Seismic Analysis and Design of Special Bridges

Edited by

Lichu Fan
State Key Laboratory for Disaster Reduction in Civil Engineering
Tongji University
Shanghai, China

George Lee
Multidisciplinary Center for Earthquake Engineering Research
University at Buffalo, State University of New York
Buffalo, New York

MCEER
MULTIDISCIPLINARY CENTER FOR EARTHQUAKE ENGINEERING RESEARCH
A National Center of Excellence in Advanced Technology Applications

ISSN 1520-295X

Technical Report MCEER-03-0004
July 15, 2003

This workshop was held October 8-10, 2002 and hosted by the State Key Laboratory for Disaster Reduction in Civil Engineering, Tongji University, Shanghai, China and was supported by the Federal Highway Administration under contract number DTFH61-92-C-00106.

NOTICE

This report was jointly prepared by Tongji University and the Multidisciplinary Center for Earthquake Engineering (MCEER) as a result of research sponsored by the Multidisciplinary Center for Earthquake Engineering Research (MCEER) through a contract from the Federal Highway Administration. Neither MCEER, associates of MCEER, its sponsors, Tongji University, nor any person acting on their behalf:

a. makes any warranty, express or implied, with respect to the use of any information, apparatus, method, or process disclosed in this report or that such use may not infringe upon privately owned rights; or

b. assumes any liabilities of whatsoever kind with respect to the use of, or the damage resulting from the use of, any information, apparatus, method, or process disclosed in this report.

Any opinions, findings, and conclusions or recommendations expressed in this publication are those of the author(s) and do not necessarily reflect the views of MCEER or the Federal Highway Administration.

Proceedings of the First PRC-US Workshop on Seismic Analysis and Design of Special Bridges

Held at
State Key Laboratory for Disaster Reduction in Civil Engineering
Tongji University
October 8-10, 2002

Edited by
Li-Chu Fan[1] and George C. Lee[2]

Publication Date: July 15, 2003

Technical Report MCEER-03-0004

Workshop Steering Committee
Lichu Fan, SLDRCE, Tongji University
Mengling Lou, Tongji University
Weigang Bao, PRC Ministry of Communication
George Lee, MCEER, University at Buffalo
Ian Buckle, University of Nevada, Reno
W. Phillip Yen, Federal Highway Administration

Local Organizing Committee
Lichu Fan, Shide Hu, Yan Xu and Suwen Chen, all of Tongji University, Shanghai, PRC

FHWA Contract Number DTFH61-98-00094

1 Professor, State Key Laboratory for Diasaster Reduction in Civil Engineering, Tongji University, Shanghai, PRC
2 Director, Multidisciplinary Center for Earthquake Engineering Research, University at Buffalo, State University of New York

MULTIDISCIPLINARY CENTER FOR EARTHQUAKE ENGINEERING RESEARCH
University at Buffalo, State University of New York
Red Jacket Quadrangle, Buffalo, NY 14261

Preface

This seismic analysis and design of special bridges (SADSB) workshop series is based on a Memorandum of Understanding (MOU) between the Multidisciplinary Center for Earthquake Engineering Research (MCEER), University at Buffalo, Buffalo, New York and the State Key Laboratory for Disaster Reduction in Civil Engineering (SLDRCE), Tongji University, Shanghai China. The MOU was signed by Professor George C. Lee of MCEER and Professor Lichu Fan of SLDRCE on May 26 2001, and resulted from the PRC-US earthquake engineering and earthquake disaster mitigation collaboration project. Four international workshops will be carried out in China and US between 2002-2005, alternating locations each year.

The first workshop was held on October 8 - 10, 2002 at Tongji University in Shanghai. A total of 35 participants, ten from the US 12 from China, and 11 observers attended this workshop. Following the two-day meeting and discussion, a technical tour to the LuPu Bridge, a tied arch bridge under construction over the Huangpu River in Shanghai, was arranged. The lead designer of the energy dissipation system in the main span was Professor Shi-de Hu, one of the workshop organizers.

Workshop themes included seismic design and retrofit of long span bridges, performance based design, seismic safety evaluation, soil-pile-structure interaction and pseudo-dynamic and hydrodynamic experimental study. These proceeding contain 22 papers covering a wide range of research fields, including a discussion of seismicity in China.

Contents

Introduction to the State Key Laboratory For Disaster Reduction in Civil Engineering (SLDRCE)

Li-chu Fan[1]

The State Key Laboratory for Disaster Reduction in Civil Engineering (SLDRCE) was established in 1988 at Tongji University, which is one of 81 state key laboratories led directly by the State Commission of Education & Science, and also the only state key laboratory in the field of civil engineering in China. The main objectives of the SLDRCE at Tongji University, as one of the main research centers for disaster reduction in China, are to:

- Improve basic understanding of disaster phenomena through fundamental studies
- Establish effective measures for disaster reduction
- Provide opportunity for domestic applicants through opening the laboratory to outside scientists
- Participate in international exchanges and collaboration with government and non-government organizations, universities and research institutes
- Serve as consultants in disaster reduction
- Organize training activities

In addition, the SLDRCE will make a due contribution to the "International Decade for Natural Disaster Reduction" organized by the United Nations.

The SLDRCE's main facilities include:

- Shaking Table
- Boundary layer wind tunnel (TJ-1,TJ-2 and TJ-3)
- Strong Ground Motion Instrumentation

Research is performed in the following areas:

- Fundamental Study of Earthquake Engineering
- Applied Study of Earthquake Engineering
- Fundamental Study of Architectural Aerodynamics and Aeroelastic Phenomena
- Applied Study of Wind Engineering

However, in this presentation, special attention is paid to the research projects, further development and study trends of the bridge seismic laboratory, which is a subarea of applied study in earthquake engineering.

---

[1] State Key Laboratory for Disaster Reduction in Civil Engineering, Tongji University, Shanghai 200092, PRC

Introduction to the Seismicity of China

Luo Qi-feng and Li Shi-dong[1]

ABSTRACT

In this paper, China seismicity is introduced, which includes seismic regions in China, seismic activity, fault model, attenuation model and its characteristic, and a seismic zoning map of China, etc.

Keywords: seismic region in China, seismic activity, seismic zonation map of China, fault model, attenuation model, estimation of ground motion

[1] Research Institute of Structural Engineering and Disaster Reduction, Tongji University, Shanghai 200092

PREFACE

China is a large country where there were many large earthquakes occurred in the past thousand years. In 1556 about 830,000 persons were killed in Guanzhong earthquake, Shaanxi province. In 1976 more than 230,000 persons were killed in Tangshan earthquake, Hebei province. In the past 50 years, there are 51 earthquakes with a magnitude larger than 7.0 occurred in China. Therefore how to predict earthquake and how to mitigate seismic loses are the main purposes for scientists and engineers of China, who are studying and working on seismology, geophysics, geology, earthquake engineering, civil engineering and sociality, etc. Here the authors will introduce some researches on seismic region of China, seismic activity, fault model, attenuation model and its characteristics, seismic zoning map of China, and estimation of ground motion, etc.

MAIN SEISMIC REGIONS AND SEISMIC ACTIVITY

Seven main seismic regions

Based on the analysis of the seismic activity and seismo-tectonic environment, 7 large seismic regions are divided in China. They are Northeast region, North China region, South China region, Taiwan region, South China Sea region, Xinjiang region and Qinghai-Tibet Plateau region (see Figure 1). Every region has its own characteristic of seismic activity. In Taiwan region, Xinjiang region and Qinghai-Tibet Plateau region, the seismic intensities are stronger and the frequencies of earthquake occurrence are higher. In North China region the seismic intensity is stronger and the frequency of earthquake occurrence is high. The seismic activity is medium in South China region, where the seismic intensity is between medium and strong, while the frequency of earthquake occurrence lower. In Northeast China region and South China Sea region, the seismic activities are not active, where the seismic intensities are weaker and the frequencies of earthquake occurrence lower.

Taiwan seismic region is suited on the west boundary of Pacific plate and it belongs to Circum-Pacific seismic zone. And South China Sea region is mainly influenced by Philippine plate. Beside the earthquakes occurred in the two regions, most of others belong to intra-plat earthquakes. Some seismologists in United States also take China into an intra-plate region (Butler et al. 1979).

Also there are other methods to divide seismic regions. For example, Sichuan-Yunnan seismic belt, which is in the central area of Qinghai-Tibet Plateau region, and Shanxi fault belt in North China region compose one seismic belt, which is named Great Central Seismic Belt or Great North-South Seismic Belt (see Figure 1).

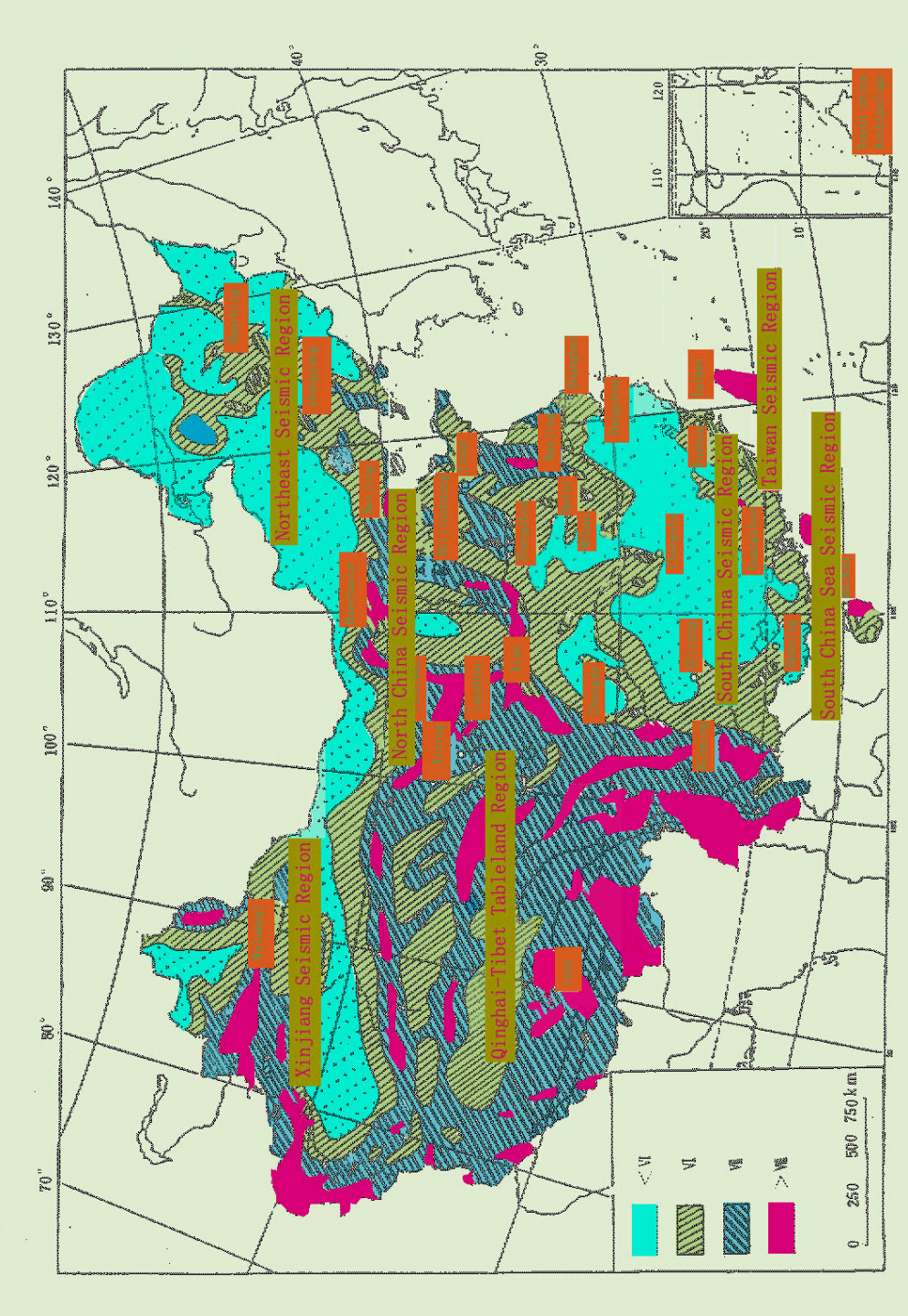

Figure 1 Distribution of 7 seismic regions and revised seismic intensity zoning map of China (1990)

Since 1900 there are many serious disaster earthquakes occurred in China, among which there are 9 earthquakes with a magnitude larger than 8.0. All the epicenters of earthquakes occurred in China with magnitude $M \geq 4\frac{3}{4}$ from 1901 to 1950 are shown in Figure 2.

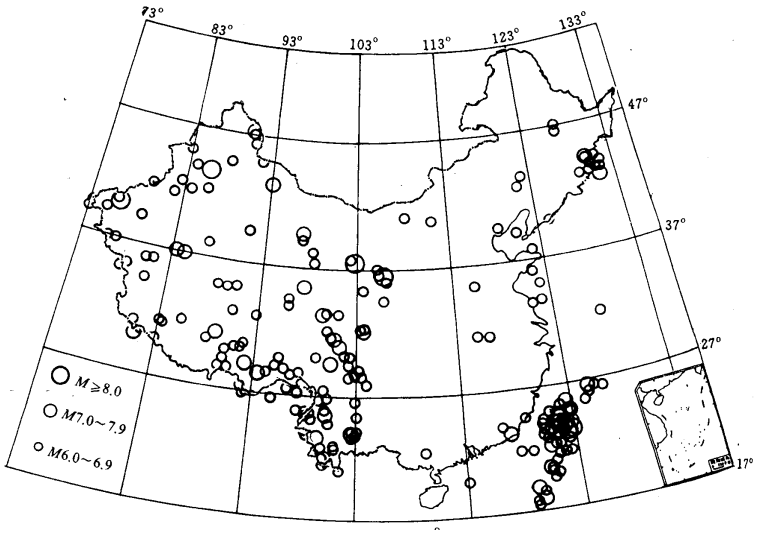

Figure 2 Distribution of epicenters of earthquakes ($M \geq 4\frac{3}{4}$)

Occurring in China from 1901 to 1950

According to the data we've collected, in the past 50 years there are about 51 earthquakes with magnitude larger than 7.0 occurring in China. Their distribution in different seismic regions is shown in Table 1. Figure 2 and Table 1 all show the characteristics of seismicity in different seismic regions in China.

Table 1 Distribution of large earthquakes (M ≥ 7.0, Since 1950)

Region	Northeast China	North China	Xinjiang	Qinghai-Tibet Plateau	Taiwan	South China	South China Sea	Total
Times	3	6	4	18	20	0	0	51

From Table 1 we can see that there are many large earthquakes occurred in Qinghai-Tibet Plateau region and Taiwan region. Because the population in Qinghai-Tibet Plateau is very small and most of the earthquakes took place in the wild field, these earthquakes did not cause serious disasters. For example, Kunlun Mountain Pass earthquake (*Ms* 8.1) on 14th Nov.2001 is only one great earthquake with magnitude larger than 8 occurred in Chinese continent since 1951. Fortunately, its epicenter is in frigid zone, where there are no people. And the Qinghai-Tibet railway, which runs across the near field of the earthquake, is still under construction, so that the great earthquake did not cause serious disaster.

Because of the dense population in North China region, although there are only a few earthquakes occurred there in the past 50 years, if one great earthquake occurs it will cause

serious disaster. The lesson embedded in our mind is the tragedy caused by the great Tangshan earthquake (Ms7.8) on 28th July 1976.

Seismic occurrence period

There are more than 3800 years of historical seismic records in China; Seismic activities can be analyzed from these records. Figure 3 shows the active periods and non-active periods of seismic activity in different seismic regions (Figure 3 is a revised figure, reference to Hu, 1988). Comparison of seismic activities shows that the active and non-active periods in one region are almost the same, but the periods in different regions vary from each other. In North China, South China, Taiwan and Qinghai-Tibet Plateau regions, the active period is about 300~400 years. In Xinjiang region, it is about 100 years, while in Taiwan it is only about decades. Figure 3 also implies that China is now in active seismic period.

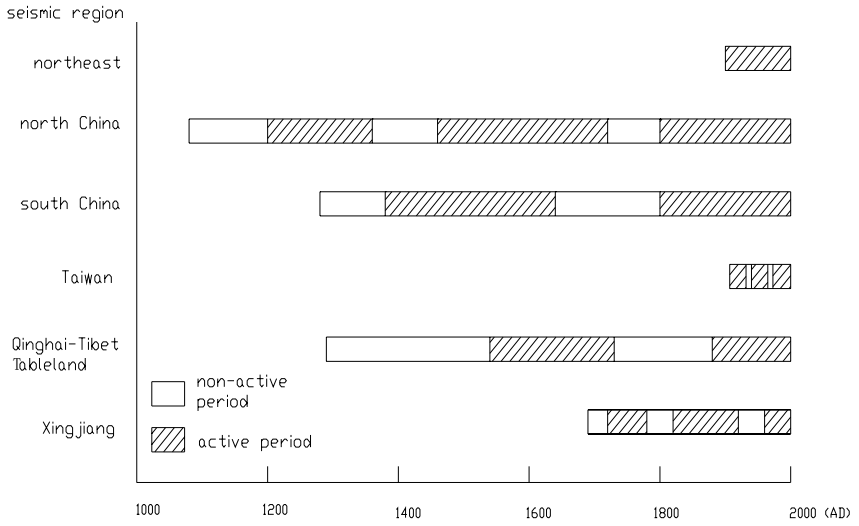

Figure 3 Seismic active periods in main seismic regions

The magnitude-frequency relationship can be described by equation

$$\lg N = a - bM \text{ .} \tag{1}$$

Where M is the earthquake magnitude, N is the occurring times of earthquakes whose magnitudes are M. a and b are constants. Figure 4 shows the magnitude-frequency relationships in the main seismic regions (Figure 4 is a revised figure, reference to Hu, 1988).

Comparing Figure 3 with Figure 4, we can know that if the active period is shorter in one seismic region, the constants a and b are larger in its magnitude-frequency relationship. For example, the values a and b in Taiwan region are larger than those in North China, while the active periods in the two regions are opposite.

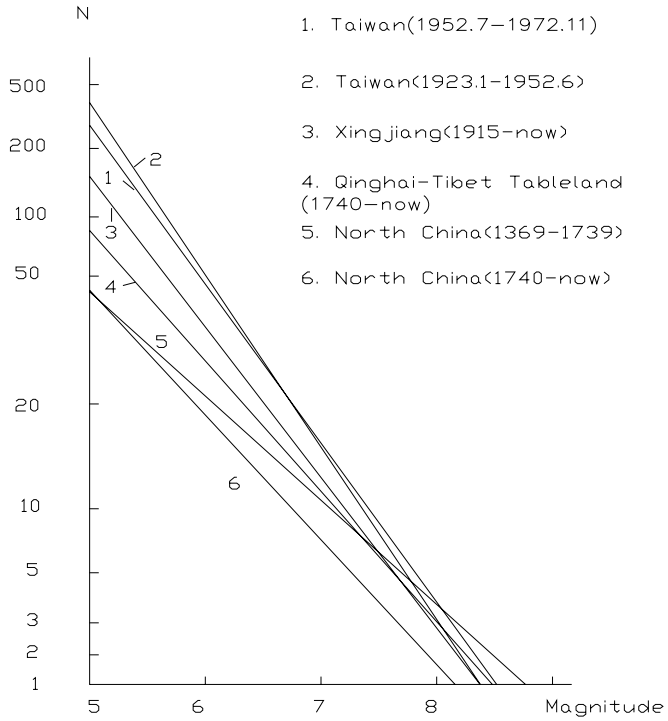

Figure 4 Magnitude-frequency relationship in main seismic regions

Seismic fault model and source depth

Fault model. Table 2 shows percentage of different fault models and maximum magnitude of earthquakes in some seismic regions (Table 2 is a revised table, reference to Huan *et.al*. 1990 (got from the book edited by Hu, 1999)). In North China and Central Qinghai-Tibet Plateau, most of the fault models are strike-slip faults and their percents are 90% and 84%, and the maximum magnitudes are 7.8 and 7.9. But in Southeast China, the percent is only 63% and the maximum magnitude is 7.3. Tangshan earthquake on 28th July1976 is a typical strike-slip fault event, and Jiji earthquake of Ms7.4 on 21 Sept.1999 is a typical reverse fault event.

Fault length. There are many relationships between fault length and magnitude. Table 3 shows one reference relationship of them (Table 3 is a revised table, reference to Huan *et.al*. 1991 **(**got from the book edited by Hu, 1999)). The fault length of Tangshan earthquake Ms7.8 in 1976 is about 100km (Luo and Hu, 1997).

Seismic focus depth. Among the 51 earthquakes with magnitude larger than 7 mentioned above, there are 23 events from which we can collect seismic focus depth data. Except for two earthquakes, which occurred in Northeast China and their focus depths are 595km and 570km, others are shallow focus earthquakes. Their focus depths range from 1 km to 59 km and most of them are between 10km and 30km.

Table 2 Percent of fault model & maximum magnitude of earthquake in some seismic regions

Fault Model	Strike-Slip Fault		Reverse Fault		Normal Fault	
Regions	%	M*max*	%	M*max*	%	M*max*
Vicinage of China	52	8.5	44	7.25	4	6.9
North China	90	7.8	7	4.5	3	7.1
Central of Qinghai-Tibet Plateau	84	7.9	11	7.2	5	6.8
Southeast China	63	7.5	13	3.4	19	4.6

Table 3 relationships between fault length and magnitude

Magnitude	6	6.5	7.0	7.5	8.0
Fault length (km)	About 20	30~40	50~60	80~100	100~200

SEISMIC ZONING MAP

There are four generations of seismic zoning maps in China. The third generation of zoning map was compiled in 1990 and the fourth generation 2001. These two zoning maps are compiled by adopting probabilistic method of the seismic hazard analysis.

Seismic intensity zoning map of China (1990)

It is the first time to compile seismic intensity map of China by using probabilistic seismic hazard analysis method. Based on the analysis of the seismic activity and seismo-tectonic environment, 7 seismic regions are firstly divided into 26 seismic provinces as the statistic elements of the seismicity analysis. Then 733 seismic potential source areas are divided in the seismic provinces. Considering the inhomogeneity of seismicity distribution in both space and time, the seismic intensities with various probabilities of exceedance are calculated at about 30,000 controlling points in the whole country. And then the seismic intensity zoning map (scale with 1:4,000,000) is compiled with 10 percent of probability of exceedance during a period of 50 years. Figure 1 is a revised seismic intensity zoning map. In the original zoning map, the whole country is divided into 5 grades of zones, they are MMI<V, VI, VII, VIII and >IX (CCSZMC, 1992). But in Figure 1 there are only 4 grades, they are MMI<V, VI, VII and >VIII.

Seismic ground motion parameter zonation map of China (2001)

China Seismological Bureau published a new seismic zoning map in 2001 (scale with 1:4,000,000). There are four main characteristics in the new zoning map. Firstly, it is the first seismic ground motion parameter zoning map of China. Peak acceleration and characteristic

period Tg ($Tg=2\pi V/A$) of acceleration response spectrum are used to make zonation. Therefore there are two zoning maps, one peak acceleration zoning map and another characteristic period Tg of response spectrum zoning map. In the acceleration zoning map (Figure 5, Hu, 2002) the whole country is divided into 7 grades of zones, they are A<0.05g, 0.05g, 0.10g, 0.15g, 0.20g, 0.30g and ≥0.40g.

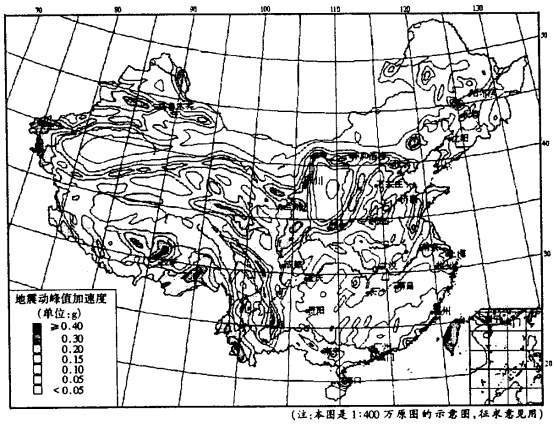

Figure 5 Peak acceleration zonation map of China

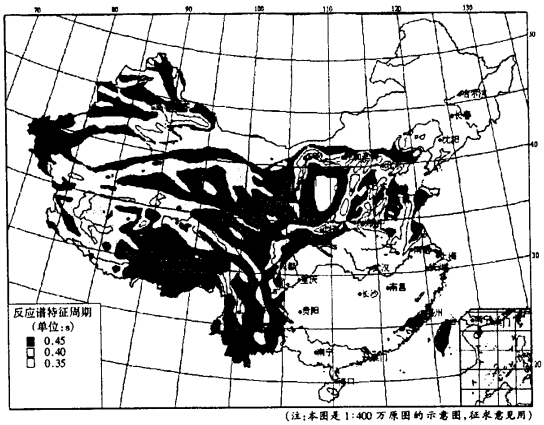

Figure 6 Characteristic period Tg of response spectrum zonation map of China

In Tg zoning map (Figure 6, Hu, 2002) there are 3 grades, they are 0.30s, 0.35s and 0.40s. Secondly, the compile methodology considers the inhomogeneieou characteristics of seismicity in China, which reflects the progress made on seismic activity in strong and weak regions in the past 10 years. Thirdly, the two zoning maps are compiled for type II site soil condition, and they accompany a table that contains some values such as Tg for type I and type III site conditions. Furthermore, considering the uncertainties in some aspects and different opinions of experts in seismology and geology, etc., several schemes are adopted to make hazard analysis. Compared with the seismic intensity zoning map of China, the grades in the new map are changed from 5 to 7. The increased grades are A=0.15g and 0.30g, which equal to MMI=7.5 and 8.5.

ESTIMATION OF GROUND MOTIONS

Attenuation relationship of MMI in China

The ellipse intensity attenuation models of different rigions are adopted in seismic intensity zonation (CCSZMC, 1992). In Eastern China, the attenuation model is as follows.

In long axis:

$$I = 6.046 + 1.480M - 2.081\ln(R + 26) \tag{2a}$$

In short axis:

$$I = 2.617 + 1.435M - 1.441\ln(R + 7) \tag{2b}$$

In Western of China, the attenuation model is as follows

In long axis:

$$I = 5.643 + 1.538M - 2.109\ln(R + 25) \tag{3a}$$

In short axis:

$$I = 2.941 + 1.363M - 1.494\ln(R + 7) \tag{3b}$$

Where I is MMI, M surface magnitude and R epicentral distance in km.

Comparison of attenuation characteristics in North China and in US

Butler et al considered China to be an intra-plate region. They stated in their paper (1979) "it is likely that the intensity fall off characteristics of northeast China are more akin to those of the stable continental eastern United States than the basin and range, tectonic environment of the west".

Four recently developed attenuation models are calibrated by using a very limited amount of strong motion data recorded in North China (Wong, *et al*. 2002). Their research shows that the attenuation characteristics of ground motions in the North China are similar to those in western US. The supporting evidence includes coda and S-wave Q factors, preliminary results of kappa values, stress drop, shear wave velocity profile in the shallow earth crust, and areas enclosed by the isoseismal of Modified Mercalli intensity V etc. From the comparisons between results obtained by using different attenuation models it is recommended that the Crouse and McGuire (1996) spectral attenuation model could be used as a potential attenuation model for the North China (Wong, *et al*., 2002).

Probability-Consistent Scenario Earthquake and its application

Luo proposed a new definition of Probability-Consistent Scenario Earthquake (PCSE) and an evaluation method of its magnitude $M(p_0)$, focal distance $R(p_0)$ and orientation $\varphi(p_0)$ (Luo, 1996, 2000a). The exceeded probability of ground motion $y(p_0)$, which caused

by PCSE $M(p_0)$, is equal to p_0. p_0 is calculated from conventional probability hazard analysis method. PCSE and improved empirical Green's function method can be used to estimate ground motions (Luo and Hu, 1990, 1997, Luo and Dan, 1994a, Luo *et al.*, 1994b, Luo, 2000b). HHT (Hilbert-Huang Transform, Huang *et al*.1998) method is used to analyze strong ground motion (Luo and Shi, 2002). It is a useful tool to separate different frequency components from ground motion records.

DISCUSSION AND CONCLUSION

From the introduction above we can come to the conclusion as follows. Firstly, China is a large country where there were many large earthquakes occurred in the past thousand years, and China is now in active seismic period. Secondly, the seismicity of China is inhomogeneous both in space and time. Thirdly, the seismic zonation maps of China reflect research level of Chinese scientists and engineers in Seismology, Geology and Earthquake Engineering. And it can be applied to aseismic design, programs of national land use, the countermeasure for earthquake disaster mitigation and protection. Fourthly, except for some earthquakes occurred in Taiwan, South China Sea, Northeast regions are inter-plate earthquakes, most of them occurred in China are intra-plate earthquakes. Fifthly, the attenuation characteristics of ground motions in the North China are similar to those in western US. But the attenuation characteristics of whole China should be studied more. Furthermore, PCSE, Empirical Green function method and HHT can be used to analyze and estimate seismic ground motion.

ACKNOWLEDGMENT

This paper is written under the encouragement of Professor Fan Lichu of Tongji University, academism of Academic of Engineering of China and Professor George, C. Lee, director of MCEER, University of Buffalo, United States.

REFERENCES

Butler R, Stewart G S, and Kanamori H (1979), The July 27, 1976 Tangshan, China earthquake – a complex sequence of interpolate events, *Bull. Seism. Soc. Am., Vol.*83, pp1178-1798.

CCSZMC (the compiling committee of seismic zoning map in China), (1992), Seismic intensity zoning map of China (1990), Earthquake Research in China, Vol.8, No.4, pp1-11

Crouse C B and McGuire J W (1996), Site response studies for purpose of revising NEHRP seismic provisions, *Earthquake Spectra*, Vol.12, No.3, pp 407-439

Hu, Y. (1988), Earthquake Engineering, Seismology Press, Beijing, pp114-115.

Hu, Y. (2002), Introduce of seismic ground motion zoning map, *Advances in Modern Earthquake Engineering*, edited by Wang Y., Li A and Cui J., Press of East South University, Nanjing, pp1-7.

Hu. Y. (1999), *Technical book for seismic safety analysis*, edited by Y. Hu, Seismology Press, Beijing, 1999, pp.115-116.

Huang, *et al*. 1998. The empirical mode decomposition and the Hilbert spectrum for nonlinear and non-station time series analysis. *Proc. R. Soc. A*, 454, pp903-995

Luo, Q. and Y. Hu, (1990), An Improved Empirical Green's Function Method and Synthesis of Near-field Accelerograms in Lulong Earthquake, *Earthquake Engineering and Engineering Vibration*, Vol.10, No.3, 1-13.

Luo, Q., Y. Hu and K. Dan, (1994a), Statistical-empirical Green's function method for estimating near-field earthquake ground motions (in Chinese with English abstract), *Journal of Natural Disasters*, Vol.3, No.3, pp.1-10.

Luo, Q. and K. Dan, (1994b), Simulation of Accelerations in Epicentral Region for 1923 Kanto, Japan, Earthquake (M7.9) (in Chinese with English abstract), *Earthquake Engineering and Engineering Vibration*, Vol.14, No.4, 35-43.

Luo, Q., (1996), Probability-Consistent Scenario Earthquake and Its Determination (in Chinese with English abstract), *Earthquake Engineering and Engineering Vibration*, Vol.16, No.3, 22-29.

Luo, Q. and Y. Hu, (1997), Synthesis of Accelerations of the 1976 Tangshan Earthquake *Ms*7.6 in Near- and Far-Field by Using Semi-Empirical Method (in English), *Acta Seismologica Sinica*, Vol.19, No.3, 347-354.

Luo, Q., (2000a), Probability-consistent Scenario Earthquake and Its Application in Estimation of Ground Motions, *Proceedings/12th WCEE*, Auckland, New Zealand, Paper ID.0010.

Luo, Q., (2000b), Estimation of ground motions affecting Shanghai by long distance earthquake, Advances in Structural Dynamics, Proceedings of Conference on Advances in Structural Dynamics, Vol. I, pp.225-232, Dec. 13-15, 2000, Hong Kong, China, edited by J. M. Ko and Y. L. Xu, Elsevier Science Ltd, Oxford.

Luo, Q. and C. Shi, (2002), HHT and its application in analysis of seismic wave spectra, Advances in Modern Earthquake Engineering, edited by Wang Y., Li A and Cui J., Press of East South University, Nanjing, pp.373-376.

Wong Y, Zhao J X and Luo Q (2002), Attenuation characteristics of ground motions in North China, Earthquake Engineering and Engineering Vibration (English edition), Vol.1, No.2 (in printing).

Performance-Based Seismic Design of Highway Systems

Ian G. Buckle[1]

ABSTRACT

In recent years, a major review of performance criteria for bridges has been undertaken in the United States and a move towards performance-based, multi-level seismic design of bridges has begun. In a parallel exercise, a risk-based methodology has been developed for assessing the performance of highway systems taking into account the seismic fragility of bridges and their interconnectivity. These efforts have opened the door to performance-based seismic design of highway systems, in which system-level performance criteria, such as maximum permissible traffic delay times, are targeted for highway systems immediately following earthquakes of varying size. This paper explores the feasibility of such a design approach and potential applications for resource allocation and emergency planning.

BACKGROUND

The seismic performance of highway systems in recent earthquakes has been less than satisfactory. In the last decade, numerous highways have been closed due to earthquakes in California, Costa Rica, Japan, Turkey and Taiwan, and although life-safety was generally preserved, public frustration with closures and restricted access has been widespread.

Just as with many other lifeline and infrastructure systems, highways are rarely designed for seismic loads and there are no known codes or specifications for the seismic design of highway systems. Instead most of the progress that has been made towards reducing the vulnerability of these systems has been directed towards the performance of bridges, essential components of most highway systems. But despite the widespread use of seismic bridge codes and specifications, many of the highway closures in recent earthquakes have been due to bridge damage and collapse.

Historically, the United States and many other countries have used a single-level earthquake to seismically design bridges and other structures. This earthquake, usually called the *design* earthquake, is intended to represent the largest earthquake that could reasonably be expected to occur during the life of the bridge. Inherent in such a statement is the notion of 'uniform risk' since the design level is intended to be an earthquake with the same probability of exceedance from one region to another, rather than using the maximum historical event for each region, which may have a very low probability of occurrence.

The *Standard Specification for Highway Bridges* in the United States (AASHTO 1992) adopted this uniform risk approach following the 1989 Loma Prieta earthquake, and uses a level of hazard that has a 10% probability of exceedance in a 50-year exposure period. This corresponds to an event with a return period of about 500 years (actually 475 years). In more recent years the exposure period has been adjusted to 75 years, corresponding to the assumed life of a normal highway bridge (AASHTO 1994). The probability of exceedance was then raised to 15%, so as to maintain, approximately, the same return period (500 years).

At the same time as adopting this uniform risk approach, a corresponding set of performance expectations were included in the philosophy of the AASHTO specifications (AASHTO 1992). These are given in Art. 1.1 of the specification and summarized below:

- Small to moderate earthquakes should be resisted within the elastic range, without significant damage.
- Realistic seismic ground motion intensities and forces are used in the design procedures.

[1] Professor, Department of Civil Engineering, MS 258, University of Nevada, Reno, 89557, USA

- Exposure to shaking from large earthquakes should not cause collapse of all or part of the bridge. Where possible, damage that does occur should be readily detectable and accessible for inspection and repair.

A set of basic concepts for seismic design was derived from this philosophy (Art. 1.3, AASHTO 1992), and these are summarized below:

- Hazard to life to be minimized.
- Bridges may suffer damage but have a low probability of collapse.
- Function of essential bridges to be maintained.
- Ground motions used in design should have a low probability of being exceeded in the normal lifetime of the bridge.

Characterized by a lack of specificity, these criteria were nevertheless a significant advance over the then prevailing requirements for seismic design.

By contrast, little has been achieved by way of assessing the performance of an inventory of bridges interconnected by a network of roads, and subjected to the same earthquake. Nor have other components of highway systems (retaining walls, slopes, tunnels, culverts and the like) been systematically studied and their contribution to system vulnerability determined. Applications of seismic risk assessment procedures to water supply systems and other utilities have been developed, but until very recently their application to highway systems had not been attempted.

Bridges are critical components of highway systems and with few exceptions are designed to single-level performance criteria. Furthermore, the overall impact of bridge vulnerability on the performance of complete highway systems is not generally known, due to lack of data on the other components of highway systems and a credible methodology for performing such an analysis. Improving the performance of bridges, and the systems of which they are part, is urgently required. Performance-based design and seismic risk assessment procedures appear to offer a way forward.

THE CASE FOR PERFORMANCE-BASED DESIGN OF BRIDGES

The assumption is made in single-level design (and retrofit) that if performance at the design event is satisfactory, it will be satisfactory at all other levels, both smaller and larger. Such an assumption is generally not true, as seen in recent earthquakes in California, Costa Rica, Japan, Turkey and Taiwan. It would be true for smaller events if elastic performance was required at the design event, and it may also be true for larger events, if the design event was sufficiently large and a generous degree of conservatism used in the design. But under the design event, inelastic performance (damage) is explicitly intended (in most bridges), and provided life safety is preserved, the consequential restrictions on access are considered to be tolerable.

However, these restrictions become unacceptable, if they were to occur on a more frequent basis such as during a smaller earthquake. Since this is a nonlinear problem, assurances regarding performance during smaller earthquakes cannot be obtained simply by scaling performance at the design event and thus explicit design (or at least a design check) should be made at this level, to gain this assurance.

Similarly, performance during a larger event cannot be estimated by scaling upwards and relying on reserve strength. Without explicit quantification, this approach is unreliable because it is based on engineering judgment and an experience database that is thin and largely unverified, especially in the central and eastern United States (CEUS).

The argument is thus made, that to avoid adverse performance, such as seen in Loma Prieta, Northridge, Kobe and Taiwan, explicit consideration of bridge performance during at least two levels of earthquake (and perhaps more) should be undertaken. Furthermore, the expected level of performance during these earthquakes should be stated with a greater level of specificity than has been the case in the past, and assurances given that these performance levels will be met. This argument leads to the consideration of performance-based engineering for the seismic design and retrofit of bridges.

Performance based engineering (PBE) has been defined as consisting of the selection of design criteria, structural systems (layout, proportioning and detailing), and the assurance and control of construction quality and long-term maintenance, such that at specified levels of ground motions, and

with defined levels of reliability, *the structure will not be damaged beyond certain limiting states or other usefulness limits.* (SEAOC 1995). This definition has been paraphrased from that developed for buildings in the SEAOC Vision 2000 Project where PBE was explored and its potential for improving the seismic performance of new buildings was clearly demonstrated.

Application of the design phase of PBE requires several fundamental issues be addressed. These include:

- Selecting the ground motions (hazard levels) and corresponding damage states (performance objectives)
- Developing analytical methods for the verification of damage states and performance objectives.

The first of these bullets requires that ground motions be known with a degree of confidence (i.e. the 500-yr seismic design coefficient for a given bridge in a given site class, is known within acceptable limits), and that realistic and meaningful objectives can be defined. The second bullet requires a level of sophistication in analysis that can be implemented with ease and reliability. Further, the relationship between damage states and performance objectives (such as crack width to lane closures) must be not known with a degree of certainty.

HAZARD LEVELS AND PERFORMANCE OBJECTIVES FOR BRIDGES

Factors to be considered when selecting hazard levels and setting performance objectives include:

- How many earthquake levels should be used? Ideally it should be many, but in practice two or three levels should sufficient to assure that the desired range of performance is achieved. These might be *small, moderate and large* if three events are favored, or *small and large* if only two events are considered. In the latter case, they might also be referred to as *frequent and rare* events.
- How many different kinds of bridges should be considered? It is unreasonable to expect that all bridges should have the same performance criteria for the same earthquake. More important bridges for example, might be expected to perform to a higher level than less important bridges. Temporary bridges and those under construction might also have specific criteria. Setting aside these special cases, two or three categories should be again be sufficient, and these might be based solely on *importance,* although it might be preferable to use *expected performance level* as the differentiating parameter.
- How should these performance requirements be specified? It is not a simple matter to measure performance and therefore to be able to specify it. One measure might be the number of days a bridge is closed for repair following an earthquake, or has restricted access (lane reduction or weight reduction or both). Another measure might be the extent of damage as given by residual displacements or offsets, crack widths, extent of spalled concrete and exposed rebar, number of misaligned or unseated bearings, settlement of approach fills, distress to expansion joints and vehicle barriers, and the like. Neither measure is particularly satisfactory and in practice both are used to complement each other. In this case both a performance level (PL) and a damage level (DL) is used to set the performance criteria.

If dual events are considered (rather than three levels) and two bridge types identified, the above performance criteria may be formatted in a 2 x 2 matrix with the rows assigned to the earthquake level and the columns to bridge type. Elements within the matrix are the required performance and damage levels. Table I shows such a performance criteria matrix.

Four performance levels and four damage levels are shown in Table I corresponding to two earthquake levels and two bridge types. If more hazard levels and/or more bridge types are to be considered, the number of performance and damage levels (PL, DL) would, in principle, increase. But in practice duplication among the PLs and DLs is common and the number of separate and distinct levels may not even be as many as shown in Table I.

TABLE I. PERFORMANCE CRITERIA MATRIX FOR HIGHWAY BRIDGES.

EARTHQUAKE	**BRIDGE TYPE 1** (e.g. Standard Bridges)	**BRIDGE TYPE 2** (e.g. Important Bridges)
Frequent Earthquake	PL1 DL1	PL2 DL2
Rare Earthquake	PL3 DL3	PL4 DL4

where PL1 through PL4 is Performance Level 1 through 4
and DL1 through DL4 is Damage Level 1 through 4.

Caltrans Experience

Immediately following the 1989 Loma Prieta earthquake, the California Department of Transportation (Caltrans) moved towards dual-level performance-based design. Endorsed by the Caltrans Advisory Board and an independent review by the Applied Technology Council, these criteria were customized to the seismic hazard in California and Caltrans prevailing practice. Two bridge classes were identified (Ordinary and Important) and the rare and frequent earthquakes identified as the *safety evaluation* earthquake (SEE) and the *functional evaluation* earthquake (FEE) respectively.

The safety evaluation earthquake is determined deterministically by the California Division of Mines and Geology (CDMG) for each site and is identified as the maximum considered earthquake (MCE). In some circumstances this rare earthquake is determined probabilistically, using a 1000 – 2000 year return period. The functional evaluation event (the frequent earthquake) is also a probabilistic event with about a 40% PE in the expected life of the bridge (about a 200-year event). An *important* bridge is one satisfying any of the following:

- required to provide secondary life safety
- would create a major economic impact if closed for restoration of functionality, or
- designated in a local emergency response plan as critical.

An *ordinary* bridge is any bridge not classified as *important.*

It is noted that for *important* bridges, the same performance level is required for both earthquakes, but greater damage is tolerated for the rare earthquake (SEE) than for the frequent event (FEE). For *ordinary* bridges, less stringent performance is required for the SEE than for the FEE and a greater level of damage is also tolerated. There is a similar differential between the performance and damage levels for ordinary and important bridges.

Applications in California

As noted above, Caltrans has been using explicit dual level designs for major bridges for almost a decade, and implicitly for ordinary bridges for about the same period of time. Two examples, where the above criteria have been applied, are the new I-80 crossing over the Carquinez Straits in the North Bay (40 km north of San Francisco), and the new East Bay structure between San Francisco and Oakland. Both bridges are major lifeline structures and of critical importance to the region. As a consequence both are classified as *important* and fall into the right hand column of the performance matrices, where stringent performance is required even for rare events.

For the FEE, it is intended that there be no loss of capacity in the Carquinez Bridge (725m main span), that damage that does occur be minimal and not require immediate repair, and that there be no permanent structure displacements. For the SEE, there again be no loss in capacity, damage that does occur be repairable without disruption, and no permanent structure displacements.

The new East Bay crossing of the San Francisco Oakland Bay Bridge, which will replace the truss spans damaged in the 1989 Loma Prieta earthquake, comprises four separate structures totaling about 3 km in length. The main structure is a single-tower, self-anchored suspension bridge with a 385 m main span. The FEE for this bridge is a 450-year event, and full service is required almost immediately after this event with only minimal damage. Thus essentially elastic performance is required which implies only minor cracking, no apparent permanent deformations and no damage to the expansion joints. The SEE has a return period of 1500 years and again full service is required almost immediately after this earthquake. Any damage that does occur must be repairable with minimal impact on functionality. Such damage must be limited to reinforcement yield, spalling of concrete cover, and minor yielding of structural steel. Despite the relatively high FEE, the design has been governed by the SEE event. It is noted that for wind, the 100-year speed has been used for service load design and that a 10,000-year speed was used to determine the critical flutter velocity threshold.

Much of the above discussion also applies to the retrofit of existing structures. As a third example, the criteria proposed for the retrofit of Golden Gate Bridge in San Francisco are described. Instead of two-level criteria as above, three earthquake levels are defined and performance criteria developed for each. The three levels are: (1) frequent but small earthquakes, (2) moderate earthquakes, and (3) the maximum credible earthquake.

Performance criteria are as follows. For the *frequent but small events*, there should be no loss of capacity, only minimal damage and then only to non-essential elements; no elements requiring immediate repair, and no impact on margins of safety. For *moderate earthquakes*, there should be no loss of capacity, no disruption to regular function, and repairable without disruption. Damage that does occur will be small, and although residual stresses and deformations will be tolerated, they will be confined to non-critical members. For the *maximum credible earthquake*, the bridge will not be closed for more that 48 hours. Nevertheless emergency vehicles must have immediate access; public transportation has access within 'days' and the structure must be fully operational within 'weeks'.

VERIFICATION OF PERFORMANCE OBJECTIVES FOR BRIDGES

Traditional methods of seismic design are force-based using either modified forces from elastic models (including R-factor methods) or nonlinear capacity and demand analyses (including pushover methods). Some of these methods are listed below in order of increasing rigor and complexity (MCEER 2001a):

- *Capacity spectrum method*, in which demand and capacity evaluation are combined in a single procedure. Method is restricted to very regular structures, which can be modeled as single degree-of-freedom systems; is the basis of the AASHTO guide specification for isolated bridges.
- *Elastic response spectrum methods*, in which demands are calculated from response spectrum analysis using elastic spectra and single- or multi-mode techniques depending on the complexity of the structure. R-factors are used to obtain design forces based on assumed capacity of the structure for inelastic action. Design displacements are set equal to elastic displacements.
- *Nonlinear static displacement capacity verification methods* (pushover analysis), in which the displacement capacities of individual bridge substructures are determined from lateral load-displacement analyses taking into account the nonlinear behavior of their components.
- *Nonlinear dynamic analysis methods*, in which force and displacement demands are found from step-by-step time-history analyses using ground motion records and taking into account the nonlinear behavior of various bridge components.

Although the development of capacity-spectrum and capacity-verification methods have greatly improved the analyst's ability to directly address various damage states, and by implication, various performance objectives, they are essentially force-based and appear to be less powerful than the newer *displacement-based methods* which use nonlinear displacement spectra rather than acceleration spectra to characterize the earthquake loads.

In these latter methods, displacements and deformations are calculated directly and forces follow from the displacements. Since many damage states and performance objectives are in fact

displacement states, a displacement-based method allows these damage states to be targeted directly. For regular bridges, that may be modeled as single-degree-of-freedom systems, the method is straightforward and may be summarized in the following nine steps (after Priestley 2000):

Step 1: Develop an equivalent single-degree-of-freedom model of the bridge.
Step 2: Select the damage state (performance objective) for the earthquake under consideration.
Step 3: Determine the displacement of the bridge, Δ_{max}, that is consistent with the selected damage state, using a nonlinear static analysis of the structure (a pushover analysis) or similar.
Step 4: Calculate the corresponding displacement ductility demand, $\tilde{\mu}$
Step 5: Calculate the corresponding equivalent viscous damping ratio, $\tilde{\zeta}$
Step 6: Using Δ_{max} and ζ, obtain the required effective period, T_{eff}, from the displacement spectrum for the earthquake under consideration.
Step 7: From the effective period, calculate the required effective stiffness, K_{eff} and hence the base shear, V_b, from $V_b = K_{eff} * \Delta_{max}$.
Step 8: Check actual K_{eff} against required K_{eff} from (7) and redesign substructure accordingly. Repeat from (3) as necessary.
Step 9: Select new damage state for a new earthquake and repeat from (2).

The main advantage of the method is the transparent manner in which the damage state is used to influence the design and the inclusion of nonlinear static analysis in a logical manner. Disadvantages include relating damage states to performance objectives, the need for displacement spectra, and the complications that arise for bridges that cannot be modeled as single-degree-of-freedom systems. But it is noted that, apart from the need for displacement spectra, these disadvantages also apply to force-based methods.

Damage States and Performance Objectives

In this paper, the term *damage state* has been used to describe, say, the first yield in the vertical reinforcement of a bridge column, or the transverse offset of a girder, or the formation of a sufficient number of fully developed plastic hinges to form a collapse mechanism. On the other hand *performance objective* has been used to describe the serviceability of a bridge after an earthquake usually expressed in such terms as 'no collapse but closed to traffic except emergency vehicles', or 'unrestricted access after 24 hours', or 'no interruption to bridge function at any time'.

The relationship between damage states and performance objectives is ill-defined at best and this is one reason for specifying both in Table I. But they are not independent of each other and inconsistencies can arise if their interdependence is not realized. Attempts to link one with the other have been made based on experience and engineering judgment. For example in the proposed revisions to the AASHTO LRFD specifications for seismic design, (MCEER 2001a), recommendations are made for limiting values of structure displacements and plastic hinge rotations as they might affect serviceability. As noted in the commentary to these recommendations (MCEER 2001b), these values are based on consensus opinions of workshop participants and are subject to review. Some typical values, based primarily on California experience, are shown in Table II.

SEISMIC RISK ASSESSMENT PROCEDURE FOR HIGHWAY SYSTEMS

General Description

An outline of a seismic risk assessment (SRA) procedure for a highway system is shown in Figure 1, where it is seen to involve four main steps. These are: (1) initialization of the SRA; (2) development of system SRA results for each scenario earthquake and simulation specified under Step 1; (3) incrementation of the simulations and the scenario earthquakes and repeat of Step 2; and (4) aggregation of the SRA results for all earthquakes and simulations.

This SRA procedure has several desirable features. First, it may be carried out within a geographical information systems (GIS) framework, which enhances data management, improves the efficiency of the analysis, and enables the immediate display of analysis results. Second, if the GIS

TABLE II. PROPOSED BRIDGE DAMAGE STATES FOR SELECTED PARAMETERS ACCORDING TO REQUIRED PERFORMANCE OBJECTIVE (MCEER 2001a)

PARAMETER	PERFORMANCE OBJECTIVE	
	Bridge Type 1 Life Safety Only Significant Disruption	**Bridge Type 2** Fully Operational Immediate Access
Column plastic hinge rotation	0.035 rad or by analysis	0.01 rad
Vertical offset in girders	0.2 m	0.03 m
Horizontal offset in deck	shoulder width	0.1 m
Longitudinal joint opening or 1.0 m whichever is less	not more than seat width	0.1 m

database is modular, the addition of improved data, procedures, and models as they are developed from future research and development efforts is facilitated. Third, the procedure enables the effects of uncertainties in the earthquake characterization, hazard models, and vulnerability models to be considered, and has the capability of developing aggregate SRA results that could be either deterministic or probabilistic, depending on user needs.

Four modules comprise the SRA procedure as shown in Figure 1. These are noted below:

- *system module*: network inventory, traffic data, origin-destination zones, trip tables, traffic management, network analysis models
- *hazards module*: seismic zones, topography, local soils, ground motion attenuation, geologic hazard models, model uncertainties
- *component module*: structural data, repair costs, repair procedures, traffic states, loss models, fragility models, model uncertainties
- *economic module*: economic sectors (locations, productivity, damageability), stakeholder impacts, economic models

Detailed descriptions of these modules are given by Werner et al (2000).

Demonstration of Seismic Vulnerability Assessment

The above SRA methodology has been applied to the highway system in the City of Memphis (Figure 2) in conjunction with currently available data and models, to demonstrate the application of the procedure and give one example of the type of results that can be obtained.

System

The City of Memphis is located in the southwestern corner of Tennessee, just east of the Mississippi River and just north of the Tennessee-Mississippi border (Figure 2). Because of its proximity to the New Madrid seismic zone, the potential seismic risks to the Memphis area are well recognized and have been studied extensively. The highway system evaluated under this demonstration exercise includes the beltway of interstate highways that surrounds the city, the two crossing of the Mississippi River (at Interstate Highways 40 and 55), major roadways within the beltway, and highways just outside of the beltway that extend to important transportation, residential and commercial centers to the south, east, and north. The system contains a total of 286 bridges.

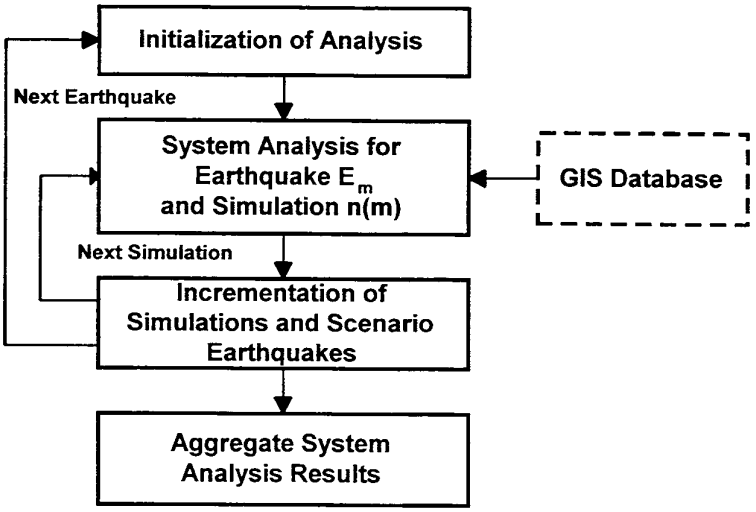

(a) Outline of four-step procedure

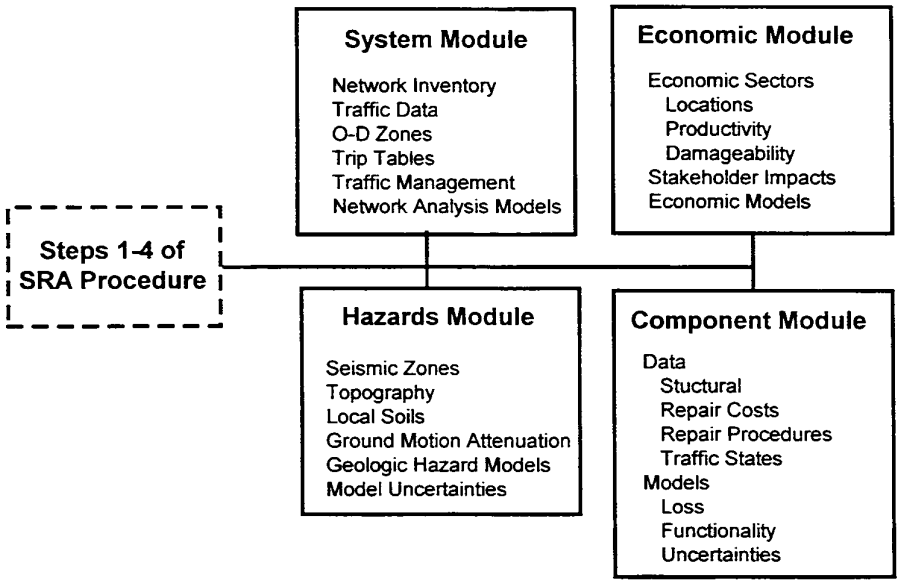

(b) Modules comprising GIS database

Figure 1. Seismic Risk Analysis Procedure for Highway Systems (Werner et al 2000).

Assumptions

As noted earlier, this demonstration SRA is based on currently available data and models only. Because the data and models are very preliminary at this time, it has been necessary to make certain simplifying assumptions in this assessment. These include:

- a scenario earthquake, with a moment magnitude = 5.5, and epicentral distance between 35 and 50 km to the closest and furthest points of the Memphis highway system

- traffic flow and volume data, roadway capacities and O-D zones as provided by the Memphis and Shelby County Office of Planning and Development (OPD); traffic flow data were based on OPD's 1988 traffic forecasting model
- ATC-25 loss models for conventional highway bridges that differentiate between simple span bridges and those with continuous girders but do not consider the influence of other structural attributes on bridge performance (ATC 1991)
- simplified functionality models for estimating closure impacts and restoration times for simple span and continuous girder bridges; post-earthquake traffic management was not considered.
- MINUTP traffic forecasting models for calculating O-D times pre- and post- earthquake

Figure 2. Highway Network for City of Memphis.

Results

Detailed results of this study are given by Werner et al (2000). In this short paper only the overall travel times and distances are presented to illustrate the effect of network redundancy on system response. Implications of these results are further discussed by Buckle et al (1998).

Overview of Seismic Vulnerability Assessment Procedure.

The results of this SRA illustrate the potential impact of earthquake damage on traffic flows in the Memphis area highway system. The analysis consisted of two parts. First, the PGAs estimated for the scenario earthquake were applied to the fragility models after each earthquake in order to estimate the state of the system at times of three days and six months after each earthquake (in terms of the number of available lanes along each roadway in the system). Then, the effects of any reductions in the available lanes (due to earthquake damage) on traffic flows throughout the system were estimated by using the MINUTP transportation forecasting software, together with a regional traffic capacity and flow data base developed at the Memphis and Shelby County OPD. From this, travel times and distances throughout the system after each earthquake were compared to pre-earthquake travel times and distances (in which all travel times and distances are average values for a 24 hour period). Overall travel time and distance for the entire system may be compared, which is computed as the sum of the travel times and distances respectively between all origin-destination (O-D) zones in the

system. This set of comparisons provides an approximate measure of the impacts of the earthquake on overall system performance. Further, a breakdown of these total travel times and distances may be compared for particular key O-D zones. These latter comparisons indicate the spatial distribution of the earthquake impacts through out the system and also show how travel to, and from, critical O-D zones are impacted by the earthquake damage to the highway system. Only the former comparisons are presented below.

Overall System Travel Times.

Table III shows that, as a result of the estimated bridge damage due to the assumed earthquake, overall system travel times three days after the earthquake are nearly 34 percent larger than the pre-earthquake values. Six months after the earthquake, bridge repairs during that time have reduced the overall system travel time; however it is still nearly 20 percent larger than the pre-earthquake value.

TABLE III. EFFECTS OF EARTHQUAKE ON TOTAL SYSTEM TRAVEL TIMES AND DISTANCES.

PARAMETER	Pre-earthquake value	Value @ T=3 days	Increase over pre-earthquake value	Value @ T=6 days	Increase over pre-earthquake value
Total vehicle hours traveled in 24-hr period	3.73×10^5	4.99×10^5	33.8%	4.46×10^4	19.6%
Total travel distance in 24-hr period (miles)	15.5×10^6	15.6×10^6	small	15.6×10^6	small

Overall System Travel Distances.

Table III also shows that overall system travel distances are not sensitive to the estimated bridge damage due to the earthquake, despite the fact that the total number of trips estimated over a 24-hour period by MINUTP (solely on the basis of demographics) was nearly the same for the pre-earthquake system and for the scenario earthquake. This lack of change of travel distances, despite significant increases in travel times, is due to the availability of more direct, but less time-efficient, routes that are taken after the earthquake. For example, if faster but less direct routes along interstate highways and beltways, that would ordinarily be used, are closed because of bridge damage, slower but more direct routes along city streets with no damaged bridges would be used instead.

THE CASE FOR PERFORMANCE-BASED DESIGN OF HIGHWAY SYSTEMS

The methodology described above has opened the door to implementing performance-based seismic design for highway systems. As for highway bridges, the goal of such a design approach is to satisfy certain specified performance criteria following earthquakes of different sizes, but in this case, the objectives are set for a highway network or subset thereof. Following the approach for bridges, successful application will require two issues to be addressed:

- Establishment of realistic and meaningful performance objectives at various hazard levels, and
- Verification of the performance objectives.

Performance objectives for highway systems might simply be related to changes in total system travel times (Table III) for emergency traffic should a small, medium or large earthquake occur in the region. More stringent criteria might be imposed for small and more frequent earthquakes, than for the large and rare events. Alternatively, performance might be measured by system restoration time,

which is the time required to restore a system back to full capacity (or some fraction thereof) following an earthquake. For small earthquakes this might less than a day, but for larger events restoration times might be measured in months. Table IV presents a possible set of criteria based on maximum acceptable restoration times, using two sets of times corresponding to 80 and 100% restoration respectively.

System performance can be verified using the risk assessment methodology described above and illustrated in Figure1. In this way more intelligent allocation of resources can be made with respect to either seismic retrofitting of highway structures, or the deployment of emergency response measures. For example, bridges might be retrofitted in order of their impact on overall system performance, such as the total travel time for emergency vehicles, or the time required to restore 80% of the network capacity. It may be found that retrofitting 10% of the deficient bridges in an inventory may be all that is necessary to get a system back to 80% of its pre-earthquake performance. Such a result could have a profound effect on the allocation of resources to bridge retrofit programs.

TABLE IV. PERFORMANCE CRITERIA MATRIX FOR HIGHWAY SYSTEMS BASED ON RESTORATION TIMES (ILLUSTRATIVE PURPOSES ONLY)

EARTHQUAKE	**HIGHWAY SYSTEM TYPE 1** Standard Operating Requirements	**HIGHWAY SYSTEM TYPE 2** Essential Operating Requirements
Frequent Earthquake (FEE)	$T_{80} \leq 2$ days $T_{100} \leq 7$ days	$T_{80} < 1$ day $T_{100} < 1$ day
Rare Earthquake (SEE)	$T_{80} \leq 30$ days $T_{100} \leq 90$ days	$T_{80} \leq 7$ days $T_{100} \leq 30$ days

NOTES:

1. A 'highway system' may be a subset of a larger highway network, subdivided according to operational requirements.

2. Two classes of operating requirements are defined: standard and essential. 'Essential' requirements are more rigorous than 'standard' requirements.

3. System performance is measured by time required to restore network to given percentage of traffic capacity before earthquake.

4. T_{80} and T_{100} are times required to restore system to 80% and 100% of capacity before earthquake, respectively.

As with the performance-based design of bridges, consequential issues arise when considering application to highway systems. For example, the uncertainty in the ground motion needs to be reduced and the relationship between component damage states (e.g. bridge column crack widths) and overall system performance (e.g. travel times to emergency care facilities) needs to be better understood. Nevertheless the above tools show great promise and deserve further study.

CONCLUSIONS

A major review of performance criteria for bridges has been undertaken in the United States and a move towards performance-based, multi-level seismic design of bridges has begun. In a parallel exercise, a risk-based methodology has been developed for assessing the performance of highway systems taking into account the seismic fragility of bridges and their interconnectivity. These efforts have opened the door to performance-based seismic design of highway systems. The goal of such an approach is to satisfy specified performance levels for highway systems immediately following earthquakes of different size. Such criteria might be minimum delay times for emergency traffic for a

small, medium or large earthquake. More stringent criteria might be imposed for smaller and more frequent earthquakes, than for larger and rare events. Alternatively, performance might be measured by system restoration time, which is the time required following an earthquake to restore the system back to full capacity (or some fraction thereof). For small earthquakes this might less than a day; for large events restoration times might be measured in months.

It is concluded that there are significant benefits to be gained by combining the progress made in performance-based bridge design with risk-based assessment of highway systems. Smarter use of scarce sources in seismic retrofitting can be expected, together with more efficient deployment of emergency services following a damaging earthquake.

ACKNOWLEDGEMENTS

The development of a performance-based seismic design methodology for bridges in the United States has been the work of many people over the last decade. Principally funded by the California Department of Transportation (Caltrans), the American Association of State Highway and Transportation Officials (AASHTO), and the Federal Highway Administration (FHWA), the author is grateful for this support and for the opportunity to contribute to this effort.

The development of a seismic risk assessment procedure for highway systems has been the achievement of Stuart Werner at Seismic Systems and Engineering Consultants, and has also been funded by the Federal Highway Administration. The assistance of the City of Memphis and the State of Tennessee with the analysis of Shelby County is gratefully acknowledged.

REFERENCES

AASHTO (1992), *Standard specifications for highway bridges*, Fifteenth Edition, American Association of State Highway and Transportation Officials, Washington DC.

AASHTO (1994), *LRFD bridge design specifications*, First Edition, American Association of State Highway and Transportation Officials, Washington DC.

ATC (1991), *Seismic vulnerability and impact of disruption of lifelines in the contiguous United States*, Report ATC-25, Applied Technology Council, Redwood City, CA.

Buckle, I.G., Friedland, I.M. and Werner, S.D. (1998), *Seismic retrofitting of highway systems*, Proc Asia-Pacific Workshop Seismic Design & Retrofit of Structures, National Center for Research on Earthquake Engineering, Chinese Taipei.

MCEER (2001a), *Recommended LRFD guidelines for the seismic design of highway bridges*, Part I: Specifications, MCEER Technical Report, Buffalo, NY.

MCEER (2001b), *Recommended LRFD guidelines for the seismic design of highway bridges*, Part II: Commentary and Appendices, MCEER Technical Report, Buffalo, NY.

Priestley M.J.N. (2000), *Performance based seismic design*, Bull NZ Soc Earthquake Eng., Vol 33, No 3, pp325-346.

SEAOC (1995), *Performance based seismic engineering of buildings*, Structural Engineers Association of California, Vol 1, Sacramento, CA.

USGS (1996), *National seismic hazard maps*, http://geohazards.cr.usgs.gov/eqint/cgi-bin/find-ll-l.cgi.

Werner, S.D., Taylor, C.E., Moore III, J.E., Walton, J.S., and Cho, S. (2000), *A risk-based methodology for assessing the seismic performance of highway systems,* Technical Report MCEER-00-0014, Multidisciplinary Center for Earthquake Engineering Research, University at Buffalo, Buffalo NY.

Mitigate Earthquake Hazard & Risk for Highway Bridges Through Planning, Design and Retrofitting

W. Phillip Yen[1] and James D. Cooper[2]

EXTENDED ABSTRACT

An earthquake hazard is an inevitable natural hazard with the potential for large numbers of fatalities and injuries, major property and infrastructure damage and serious disruption of every day life. Our transportation systems, which connect nations, states and cities, are our lifelines delivering daily needs such as food, water, and intra-city communication. Among these systems, highway bridges are the most vulnerable to seismic damages. However, earthquake losses may be reduced to a minimum through an integrated assessment and planning system, and through better techniques and specifications for designing earthquake-resistant bridges and highways. This paper summarizes seismic mitigation measures for bridges and highways through *planning, design* and *retrofitting*.

The *planning*, recognized as part of "Risk Management", is a process of deciding which hazards at what scale should be managed, determining what should be done for a hazard, and in what priority. This planning, called "Seismic Risk Assessment (SRA)", evaluates earthquake risks, and has a systemwide approach. It provides the methods, models, data needs, and procedures for conducting a system-wide analysis of scenarios for earthquake impacts on a highway system or sub-network, e.g. primary and secondary highways within a city, county or other geographic region. This assessment methodology describes expected damage to the highway elements and the resulting effect on vehicular travel between various origins and destinations within the network. Developed to serve as a decision support (guide) tool for bridge owners such as State highway departments. It includes establishment of appropriate levels of seismic design, prioritizing the retrofit of existing bridges and development of post-earthquake response plans. SRA contains procedures that provide a basis for addressing these seismic performance issues and incorporate data and methodology pertaining to engineering issues (structural, geotechnical and transportation), repair and reconstruction factors, system network and risk analysis, and socio-economic effects from damage to the system. It also provides a mechanism for estimating system-wide direct losses (i.e., costs for repair of damaged components) and indirect losses due to reduced traffic flow and/or increased travel time (economic impacts). A trail demonstration of the SRA procedure was performed to calibrate and validate this methodology. This exercise was conducted on the highway system in Memphis, Tennessee. The Memphis was selected because of its proximity to the New Madrid seismic zone. The potential seismic risks to the Memphis area from this fault are well recognized and have been studied extensively.

[1] Research Structural Engineer, Office of Infrastructure, R&D Federal Highway Administration, 6300 Georgetown Pike, McLean, VA 20121
[2] Office of Bridge Technology, Federal Highway Administration, 400 7th Street NW, Washington, D.C. 20590

Design is the first step for equipping bridges to resist earthquakes. Good design details have saved many bridges from collapsing from unseating or shear failure. Design methods evolved over time and produce details that directly affect bridge performance under earthquake and other natural hazard loading. Design methods are steadily improved based on experience with destructive earthquakes and advanced seismic research. The current seismic design specification, adopted as a standard in 1992 by AASHTO, was primarily developed by US highway agencies, including FHWA and CALTRANS. Realistic seismic provisions first entered this code after the 1971 San Fernando earthquake. The fundamental design objective of the current seismic specifications is to prevent collapse in large earthquakes. In small to moderate earthquakes, the intent of the code is to resist these loads within the elastic range without significant damage to structural components. In large earthquakes, no span or part of a span should collapse. However, the AASHTO specs consider some damage acceptable in these circumstances, provided it is limited to flexural hinging in pier columns and that it occurs above ground in regions that are visible and accessible for inspection and repair. The design earthquake is a single level event with a 475-year return period. Design forces are calculated from an elastic analysis of the bridge using response spectra approximating the design quake. As the result of an effort by the National Cooperative Highway Research Program and FHWA, a recommended new seismic design specification was completed in March, 2001. This recommended code contains significant changes in the design approach and criteria to reflect lessons learned from recent earthquakes and research studies. A dual-level design method has now been introduced in the recommended design specification. Bridge design objectives are categorized in two levels of seismic performance. They are "Life Safety" and "Operational". The greatest advantage of the dual-level approach is that it addresses safety and functional performance directly and separately to better assure that performance goals are met. The new code will include *Nonlinear Static Displacement Capacity Verification, (Pushover Analysis)* in the design procedure. This analysis, appearing for the first time in the design specifications, is a displacement-based approach for analyzing dynamic response. The objective is to determine the displacement at which the earthquake-resisting elements achieve their inelastic deformation capacity. Damage states are defined by local deformation limits, such as plastic hinge rotation, footing settlement or lift, and abutment displacement. Displacement may be limited by loss of capacity such as degradation of strength under large inelastic deformation or $\rho - \Delta$ effects.

Retrofitting is an urgent process to upgrade those bridges constructed (usually prior to 1971), with little or no consideration given to seismic forces. These structures are very vulnerable to earthquake strikes, and need to be retrofitted based on site seismicity and structural types. FHWA's *Seismic Retrofitting Guidelines for Highway Bridges* was first issued in 1983 and was followed in 1987 by *Seismic Design and Retrofitting for Highway Bridges*. In 1995, FHWA updated these manuals with more current knowledge and practical technology. This revision, reflecting recent changes in retrofitting philosophy and performance criteria, was adopted by AASHTO shortly after 1995. The fundamental retrofitting philosophy is to prevent unacceptable damage. In general, unacceptable damage includes: 1) Serious injury or loss of life, 2) Collapse of all or part of the bridge, and 3) Loss of use of a vital transportation route. Seismic retrofitting is a planning and design solution for mitigating earthquake hazards to existing bridges. Because not all bridges can be retrofitted simultaneously, the most critical bridges should be retrofitted first. The selection of bridges for retrofitting requires an overall evaluation of the structure and highway system including seismic risk, economics and societal

impacts. Thus, the process for the retrofitting bridges involves the assessment of multiple variables and requires considerable judgment. The retrofitting process is divided into three stages 1) Preliminary Screening, 2) Detailed Evaluation, and 3) Design of Retrofitting Measures. This process ensures a significant improvement in seismic capacity of these older structures that are at risk from earthquakes.

Seismic Safety Evaluation of Large Scale Interchange System in Shanghai

Lichu Fan[1], Jianzhong Li[1], Shide Hu[1], Guiping Bi[1] and Liying Nie[1]

ABSTRACT

The report for the seismic evaluation and retrofit of a large scale interchange system in Shanghai Xin-zhuang has been completed by State Key Laboratory for Disaster Reduction of Civil Engineering (SLDRCE) in Tongji University. In this paper, the important problems of the seismic evaluation procedure and the analysis model were investigated. The suggestions for local models of plate girder bridges and continuous girder bridges in a large scale interchange system were given. Additional studies were conducted to determine pounding effects at the structure interfaces in bridges.

1. State Key Laboratory for Disaster Reduction in Civil Engineering, Tongji University, Shanghai 200092, PRC

INTRODUCTION

Xin-zhuang interchange system is the largest transportation engineering in Shanghai, and it is also the largest interchange system in Asia at present as shown in Figure 1. The interchange site is between the outer ring road's station at the No.1 Subway and the Xin-zhuang's station. The site locates approximately at 1km south west of the Xin-zhuang Town, and is the start-point of the Hu, Hang, Yong's freeway. Xin-zhuang interchange system includes four trunk highways with six entrances and exits. The four layers interchange system with 20 directional bifurcated girders to make a complex cloverleaf interchange. The whole system has 11.1km-long bridges with total plan area of more than 84 thousand square meters. The highest construction at the interchange system is 21 meters. In the original seismic design, according to the China Code for Seismic Design of Highway Engineering (JTJ 041-89)[1], the seismic intensity 7 is considered for the interchange system.

STRUCTURAL CHARACTERISTICS

The superstructure of bridges in Xin-zhuang interchange system includes four kinds of girders:

(1) The concrete hollow plate girders with the depth ranging from 0.95m to 1.05m;
(2) The posttensioned box girders with uniform depth ranging form 1.1m to 1.6m;
(3) The irregular box girders with varied width;
(4) The steel and concrete composite girders.

The heights of columns of the piers range from 2m to 20m. The girders are directly supported on the teflon bearings and the elastomeric bearings without connection between the bearings and girders or cap beams. The teflon bearings are located at expansion joints. For simple girder bridges, the inverse T type cap beams are used as shown in Figure 2. Most piers have a specified concrete compressive strength of 30 Mpa with l**ongitudinal steel reinforcement ratio ranging from 1.4% to 2.5%**. The volumetric ratio of lateral steel reinforcement provided inside the plastic is about 0.3%.

In the bridges in the interchange system, the shear keys and seismic concrete block structures (shown in Figure 3) were widely used to prevent a girder fall.

SEISMIC SAFETY EVALUATION PROCEDURE

According to the characteristics of Xin-zhuang interchange system, seismic evaluation procedures for the overall bridge have evolved as outlined below:

(1) Earthquake safety assessment at site. This includes site-specific information on the expected ground motion that consist of a basic responses spectrum shape, or shapes, with peak ground acceleration related to annual probability, and artificial generated accelerograms that closely match the responded spectrum.

Figure 1. Xin-zhuang interchange system

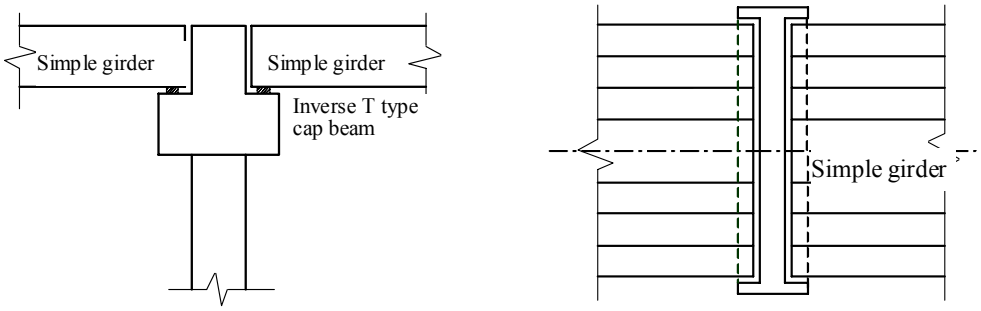

Figure 2. Inverse T type cap beam

Figure 3. Seismic concrete block

(2) Testing of material behavior and investigating of structural component at site. In order to determine the difference between the design and actual bridges, the concrete and reinforcement strength of actual bridges in Xin-zhuang interchange system were tested and were compared with the design values.

(3) Two level dynamic analysis. Linear Level-1 with global model of entire interchange system and linear local models was first performed using three-dimensional elements. The global model focuses on the overall behavior and includes all structural components. The global model analysis is an important first step in the initial assessment of the seismic vulnerabilities of a structure. Such analysis can provide initial indication of "hot spots" to plan an evaluation strategy, categorize members by their demand/capacity ratio, and envelope peak response quantities to a design spectrum. The linear local analysis models were applied to investigate the difference between linear dynamic analysis of global and local models to get simplified model methods. Nonlinear level-2 analysis is defined as nonlinear dynamic time history analysis with considerations of geometrical nonlinearity, nonlinear boundary conditions, other inelastic element (for example, bearings)
and inelastic members. Level-2 analysis is mainly applied to local models. The local models emphasize the localized behavior, especially complex inelastic and nonlinear behavior.

(4) Determination of capacity for piers, bearings and connection elements. Based on material properties for concrete and reinforcement, nominal flexural strength, shear strength of structural components have been determined in accordance with specified code formula.

(5) Capacity/demand ratio analyses. Based on the results of nonlinear dynamic time history analysis, capacity/demand ratio analyses were carried out. Based on the results of capacity/demand ratio analyses, the suggestion plan for retrofit is given.

The flow chart outlining the step in the seismic evaluation procedures for a large scale interchange system is given in Figure 4.

ANALYSIS MODELS

Global Model

The global model focuses on the overall behavior and includes all structural components in interchange system as shown in Figure 5. The superstructure is modeled by three-dimensional linear elastic beam-column elements placed at the geometric centroid of the cross section. At end of each continuous beam or simple beam, the three-node frame ends are connected by rigid elements that extend transversely from the centerline of the superstructure (detail A in Figure 5). For models of the straight bridge, the rigid elements extend perpendicular to the centerline. For skewed models, the rigid elements extend at skew angle. Three-dimensional linear elastic beam- column elements are also used to model the column and cap beam for each of the piers in the bridges in the global model. Each elastomeric bearing in bridges is modeled by a linear spring element as shown in

detail A in Figure 5. Total of 6310 three-dimensional linear elastic beam-elements and 2104 linear spring elements were used in the global model.

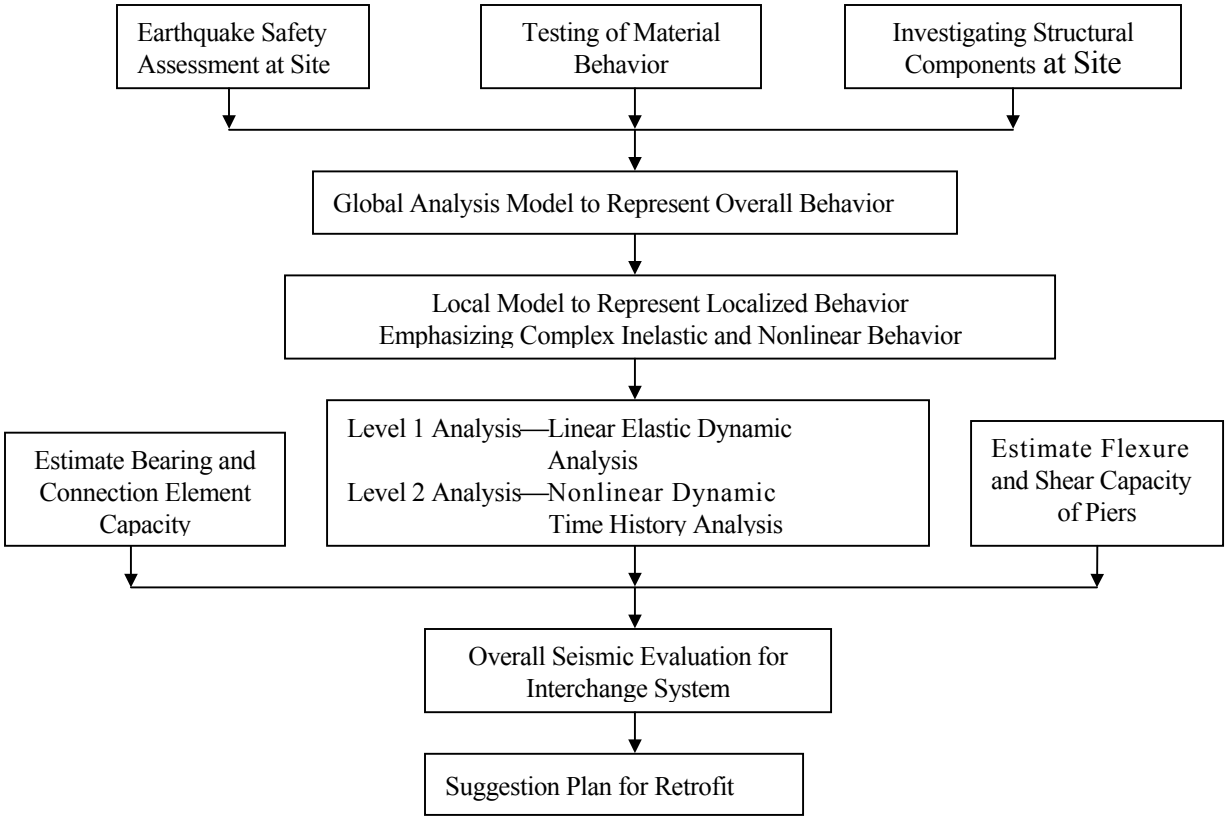

Figure 4. Seismic evaluation procedures

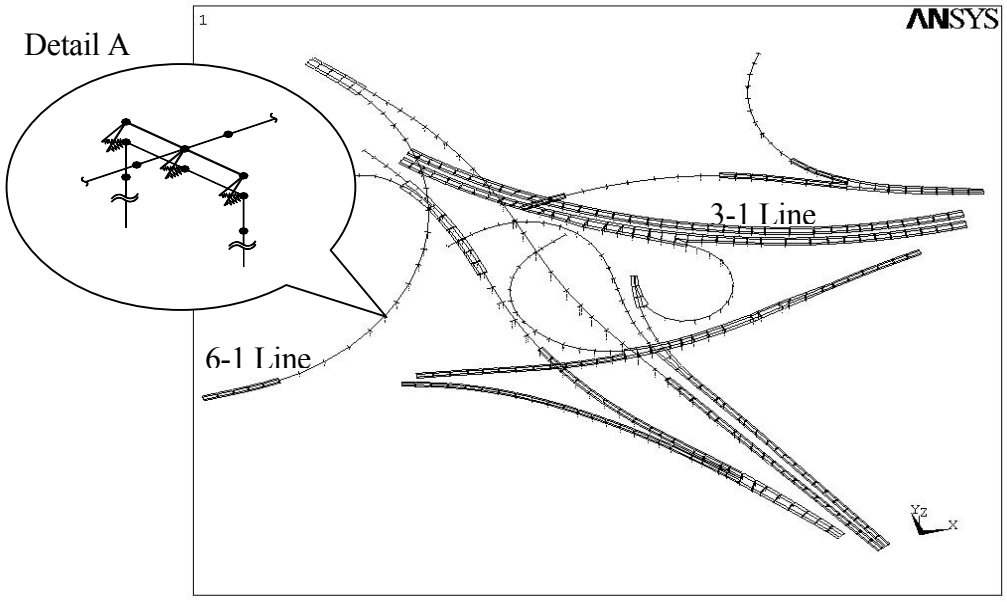

Figure 5. Global model

Nonlinear Elements and Nonlinear Local Models

Based on the analysis results of global model and characteristics of the Xin-zhuang interchange system, the linear and nonlinear analysis local models were established. The detail description of linear local analysis models was presented in the report of the seismic evaluation of Xin-zhuang interchange system [2]. Here, the typical nonlinear elements and nonlinear local models are discussed as following:

Pier columns

The inelastic three-dimensional beam-column element with a fiber model of the cross section [3] was used to model each column of the piers in the bridges. Figure 6 shows the fibers of the section. Each fiber has a specified stress-strain relationship, which can be specified to represent unconfined concrete, confined concrete, and longitudinal steel reinforcement. The distribution of inelastic deformation and forces is simply by specifying cross section slices along the length of the element. The fiber model approach provides versatile modeling of bi–axial moment-axial force interaction with distributed inelastic hinges and can represent the loss of stiffness caused by concrete cracking, yielding of reinforcing steel, and stain hardening. In this study, Mander's model for confined concrete and unconfined concrete [4] were used to represent the stress-strain behavior of concrete as is shown in Figure7.

Bearing

As mentioned above, the girders in the bridges in the Xin-zhuang interchange system are directly supported on the teflon bearings and the elastomeric bearings without connection between the bearings and girders or cap beams. The horizontal sliding behavior of interface between the bearings and girders or cap beams is presented by nonlinear spring elements with bilinear model shown in Figure 8. The value of initial stiffness k_0 for the bilinear model is determined by shear stiffness of a bearing. The frictional force, F_f, at a sliding interface, may be described by following equation (1).

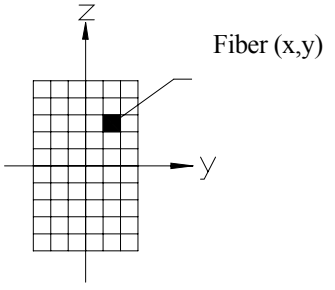

Fig.6 Column elements with fibers

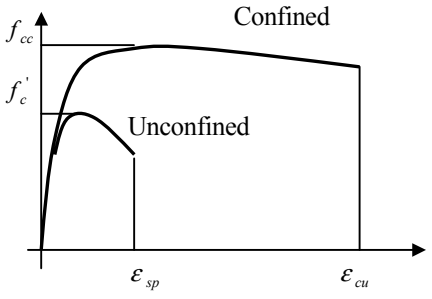

Fig.7 Stress-strain behavior of concrete

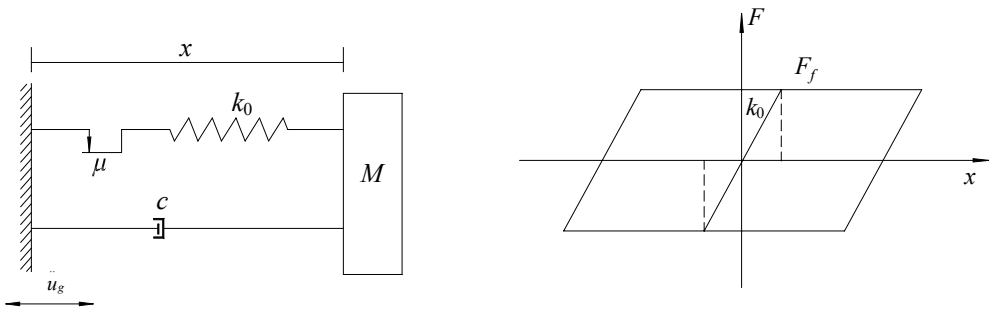

(a) (b)

Figure 8. (a) Nonlinear spring element; (b) Bilinear mode

$$F_y = \mu_d R \tag{1}$$

in which R= the vertical reaction force of a bearing; μ_d =sliding fraction coefficient of interface.

Pounding effects

Based on the characteristics of Xin-zhuang interchange system, the following three kinds of collisions may occur during earthquakes:

(1) Collisions between the simple girders and inverse T type cap beams;
(2) Pounding of adjacent girder segments at expansion joints for the continuous girder;
(3) Collisions between the girders and the seismic concrete block structures;

The collision is modeled by a nonlinear spring element with gas as shown in Figure 9. The nonlinear spring element with gap becomes active when the relative displacement between adjacent structures is smaller than the initial gap D_0. The initial stiffness k_0 and post-yield stiffness k_1 of the spring are used to represent the elastic and plastic behavior of pounding structures.

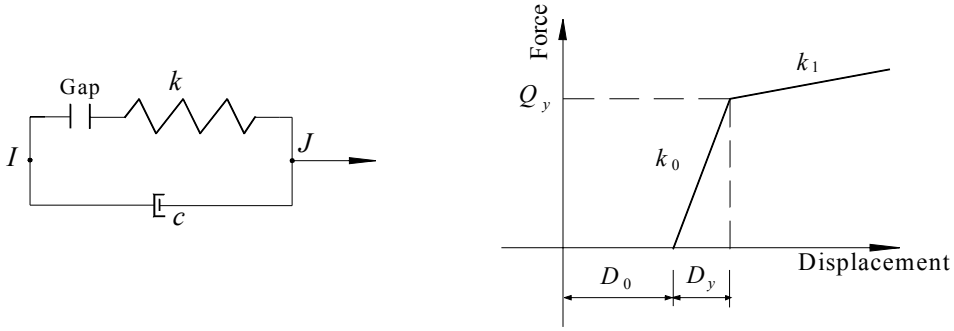

Figure 9. Nonlinear spring element with gap

Nonlinear local models

As mentioned above, in the bridges in the Xin-zhuage interchange system, there are three kinds of bridge, simple girder bridges, curve continuous girder bridges and bifurcated girder bridges. Here the typical nonlinear local models for a simple girder bridge and a curve continuous girder bridge are given as following.

The 3-1 Line in Xin-zhuang interchange is a 36 span bridge with simply supported concrete hollow plate superstructure. Pier10 to pier 12 are two column bents, and other piers are single column bents. The column heights vary considerably over the bridge from 1m to 15m. The 6-1 Line includes simply supported girder and continuously supported girder bridges. The part of continuous bridge is a 13 span bridge with box girder superstructure and single column pier. The expansion joints located at top of pier 5, pier 10, pier 14 and pier 18.

The nonlinear local analysis models for simple the girder bridge in 3-1 Line and the continuous girder bridge in the 6-1 Line are presented in Figure 10 and Figure 11 respectively. The superstructure and the cap beam are modeled by three-dimensional linear elastic beam-column elements. A nonlinear spring element with gap is used to model impact (Detail A in Figure 10 and Figure 11). To be able to capture impact caused by in-plane rotation of the superstructure, three nonlinear springs are used at each end of rigid element. The nonlinear spring element with bilinear was used to model horizontal sliding behavior of interface between the bearings and girders or cap beams. For the interface between the teflon bearing and girder (cap beam), sliding fraction coefficient 0.02 is suggested; for the interface between the elastomeric bearing and girder (cap beam), 0.15 is suggested. Each column of the piers in the bridge is modeled by inelastic three-dimensional beam-column element with a fiber model.

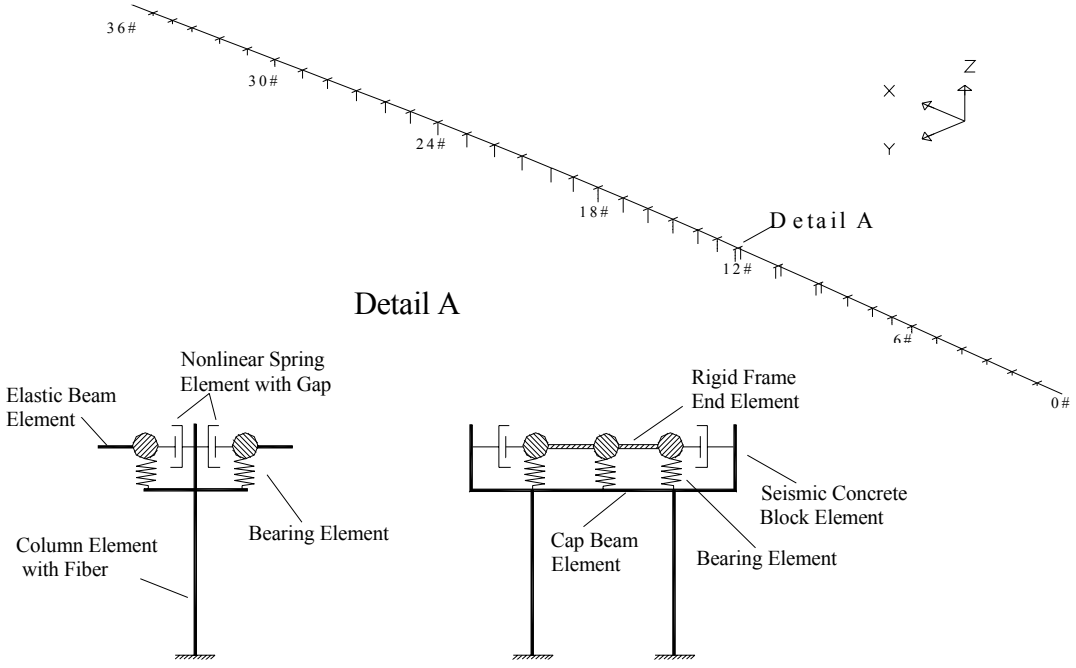

Figure 10. Nonlinear local model of simple girder bridge in 3-1 line

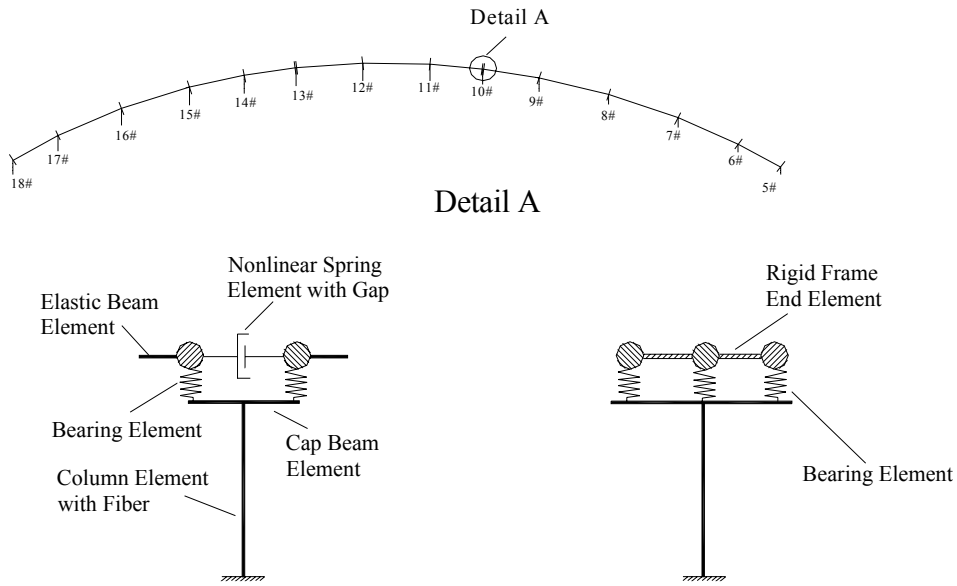

Figure 11. Nonlinear local model of continuous girder bridge in 6-1 line

EARTHQUAKE LOADING

According to earthquake safety assessment at site, site-specific acceleration coefficient (shown in Figure 12) and typical site-specific time histories of input acceleration for a 10% and 2% probability of exceedance in 50 years are provided. The input acceleration for a 10% probability of exceedance in 50 years was used to represent design earthquake and the input acceleration for a 2% probability was used to represent severe earthquake in the seismic safety evaluation of the Xin-zhuang interchange system.

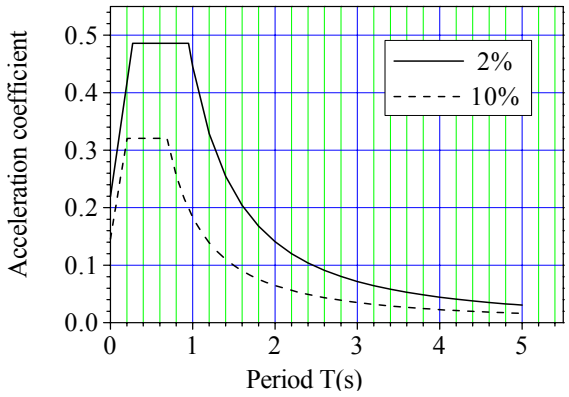

Figure 12. Site- specific acceleration coefficient

ANALYSIS RESULTS

The computer program ANSYS [5] was used to perform linear spectral analysis for the global and linear local model. For the nonlinear dynamic time history analysis, the specific computer program developed by State Key Laboratory for Disaster Reduction of Civil Engineering in Tongji University was adopted.

To assess the response, the maximum relative displacements between the girder and the pier, column displacement, column curvature ductilities, column bent moments, column shear forces and the impact forces for seismic concrete block were calculated with the site-specific input acceleration of a 10% and 2% probability, respectively. The detail analysis results are presented in the report of the seismic evaluation of Xin-zhuang interchange system. Parts of import results are discussed as following:

Under Design Earthquake

The pier columns in the interchange system work generally in the elastic range and the shear capacity of the columns is adequate to resist the design earthquake. Because the girders in the bridges are directly supported on the elastomeric bearings without connection between the bearings and girders or cap beams, the horizontal sliding between the elastomeric bearings and girders or cap beams in simple girder bridges occur. The collisions between the girders and the seismic concrete block structures induce a large impact force in simple girder bridges. The maximum values of impact force between the girders and the seismic concrete block structures in the 3-1 Line are about 9320kN.

Under Severe Earthquake

Parts of pier columns enter to plastic work range and maximum demand/capacity ratio of curvature ductility is about 5.293. The shear capacity of the columns is adequate to resist the severe earthquake according to China Seismic Code for Urban Bridges [6]. The horizontal sliding between the elastomeric bearings and girders or cap beams in simple girder bridges and parts of continuous occur. The typical sliding displacement history between the elastomeric bearing and girder at pier 35 in 3-1 Line is shown in Figure 13.

The collisions at concrete block structures, expansion joints and inverse T cap beams induce a large impact force, and may cause considerable damage or even lead to collapse of colliding structures under severe earthquake. The typical pounding time history between the girder and the seismic concrete block at pier 2 and moment time history at column bottom of pier2 in 3-1 line are presented in Figure 14 and Figure 15. Figure 16 and Figure 17 show the typical pounding time histories between the girder end and inverse T cap beam at pier 35 and moment time history at column bottom of pier35 in 3-1 Line.

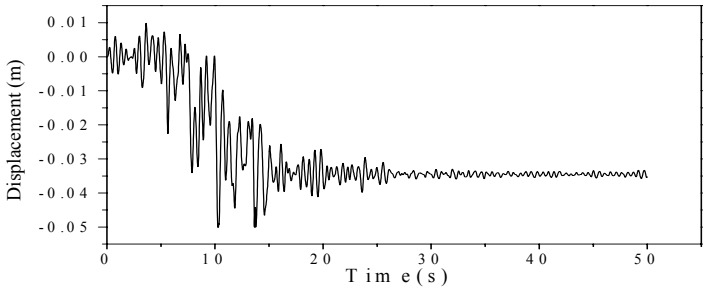

Figure 13. The typical sliding displacement history between the elastomeric bearing and girder

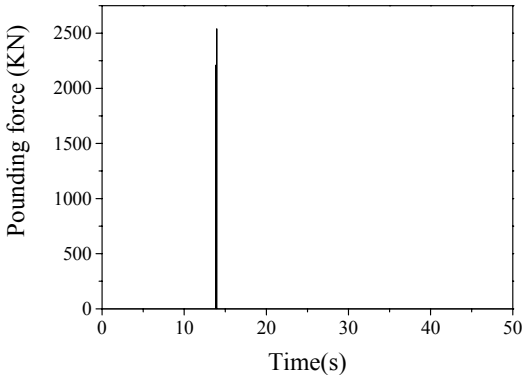

Figure 14. Pounding time histories at the concrete block

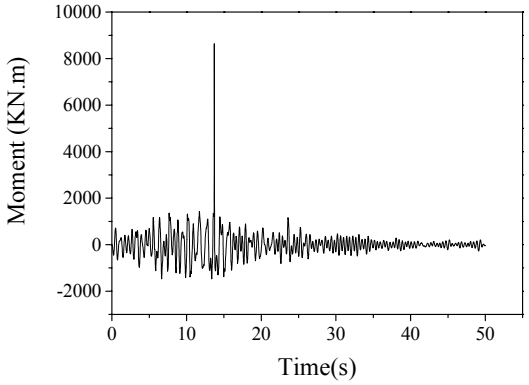

Figure 15. Moment time histories at column bottom

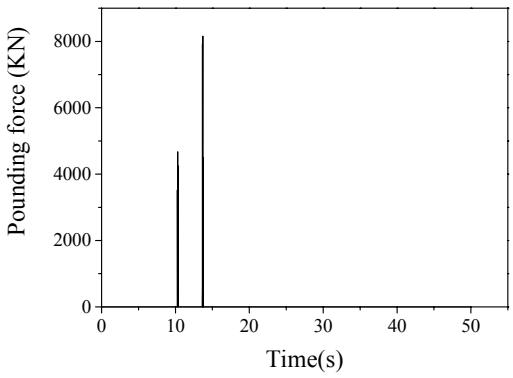

Figure 16. Pounding time histories at inverse T cap beam

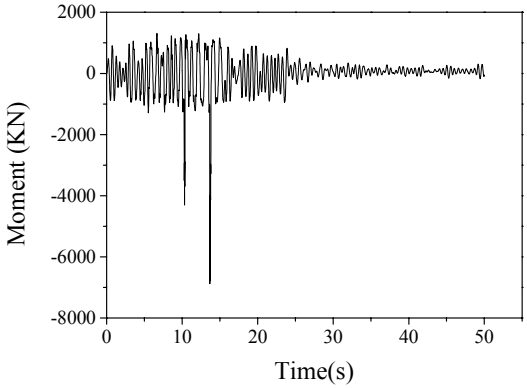

Figure 17. Moment time histories at column bottom

Retrofit Suggestions

Based on the analysis results of the Xin-zhuang interchange system, following suggestions are given for retrofit:

(1) To insure that sliding between the elastomeric bearings and girders or cap beams does not occur under design and severe earthquakes, the bolts should be applied to connect elastomeric bearings with girder or cap beam. The links shall be adequate to resist the design and severe earthquakes.

(2) To reduce pounding effects in the interchange system, the rubber layer should be attach on the inner side of seismic concrete block. A rubber layer on the interface of pounding can reduce the pounding time, than reduce pounding forces.

CONCLUSIONS

Based on the characteristics of the large scale interchange system, the seismic evaluation procedures have been investigated. Three kinds of analysis models, global model, linear local and nonlinear local models are established, and two level dynamic analysis, linear spectral analysis and nonlinear dynamic time history analysis were carried out for Xin-zhuang interchange system.

The analysis results were investigated. The results show that the horizontal sliding between the elastomeric bearings and girders or cap beams occur under design earthquake and severe earthquakes. The collisions at concrete block structures, expansion joints and inverse T cap beams induce a large impact force, and may cause considerable damage or even lead to collapse of colliding structures under severe earthquake. Based on the analysis results, suggestions are given for retrofit.

REFERENCES

Transportation Ministry of P.R.C. 1989. “Code for Seismic Design of Highway Engineering (JTJ 041-89)”

Lichu Fan, Jianzhong Li, Shide Hu, Guiping Bi and Liying Nie. 2001. “Seismic Safety Evaluation of xin-Zhuang interchange system,” Stare Key Laboratory for Disaster Reduction of Civil Engineering in Tongji University.

Enrico Spacone, Filip. C. Filippou and Fabio F. Taucer. 1996. “Fiber Beam-Column Model for Nonlinear Analysis of R/C Frames: Part 1. Formulation,” Earthquake Engineering and Structure Dynamics.25 (4):711-725.

J. B. Mander, M. J. N. Priestley and R. Park. 1988. “Theoretical Stress-Stain Model for Confined Concrete,”ASCE Journal of Structure Engineering. 114 (8):1804-1826.

ANANS, Inc.1997. “ ANASYS Workbook Release 5.4,” Third Edition. SAS, IP Inc.

Stare Key Laboratory for Disaster Reduction of Civil Engineering. “China Seismic Code for Urban Bridges (Draft 2001),” Shanghai, P.R.C.

A New Approach to Analysis of Soil-Pile-Structure Interactions for Long-Span Bridges

Seung-Il Nam[1] and Jamshid Ghaboussi[2]

ABSTRACT

Dynamic soil-structure interaction problems are a major part of the seismic analysis and evaluation of the long-span bridges. The accurate modeling of major bridges with multiple spans for seismic analysis requires that the whole bridge and its foundations be modeled, usually using finite element method. This is specially so when nonlinear behavior is present in both the superstructure and the substructure. However, finite element methods for bridges having multiple spans crossing extended area are difficult to be implemented because of the enormous amount of computations. As a result, simplified models have been proposed for modeling of the foundations of the long span bridges.

The effectiveness of conventional Winkler-type foundation models become questionable for the case of a large number of closely spaced piles, which often form the foundations of long-span bridges. A new approach for developing a discrete parameter models using genetic algorithms is introduced in this paper. This method gives the simplified Winkler-type foundation models with finite-element-method-like accuracy regardless the complexity of the problem. Simple preliminary results are presented. It is shown that the Winkler model constructed from genetic algorithms gives satisfactory result for seismic analysis. Due to the flexibility of the method, the model can be modified and even more simplified without severe loss of accuracy for any given purpose.

1. Doctoral student, Department of Civil and Environmental Engineering, University of Illinois at Urbana-Champaign, Urbana, IL 61801, USA
2. Professor, Department of Civil and Environmental Engineering, University of Illinois at Urbana-Champaign, Urbana, IL 61801, USA

INTRODUCTION

Considerable amount of research has been devoted to the seismic analysis of structures, including the soil-structure interaction effects. For seismic analysis of the combined system of the superstructure, its foundations and surrounding soil medium, various numerical techniques are currently at hand. Most of these methods have been developed for seismic analysis of buildings. Considerably less research effort has gone into developing methods for seismic analysis of major bridges, which are inherently different, and behave differently under seismic loads. In fact most of the methods for seismic analysis of major bridges are the extensions of the methods of analysis that have been developed for buildings.

Soil-structure interactive effects are important in buildings and they can be included in seismic analysis almost routinely. However, soil-structure interaction effects are far more important in major bridges and they are more difficult to model with reasonable accuracy. In fact, the very excitations that the major bridge superstructures experience are the direct result of the foundation-soil-superstructure interaction. Current methods consisting of springs and dashpots that are used in practice do not adequately account for the soil-structure interaction effects in major bridges. Far more research is needed to properly account for these effects.

For the design and retrofit of large structural systems having strong nonlinearity in both structure and soil, such as long-span bridges subjected to strong ground motions, it is imperative to perform three-dimensional nonlinear finite element analysis in time domain in order to extract transient and nonlinear characteristics of dynamic behavior.

Despite the extensive research on this subject, proper modeling of soil-structure interactions in numerical analysis of soil-pile-structure systems is one of the most challenging parts in the seismic analysis of long-span bridges. For finite element analysis of long-span bridges, besides the difficulties in representing absorbing boundaries, extremely large number of elements required to model the soil medium is still frustrating on most pc's and microcomputers. Therefore, representing soil-foundation-structure interactions with satisfactory accuracy and with reasonable computational cost is the key task in numerical analysis of long-span bridges.

As alternatives to the finite element methods, boundary element methods using Green's function are often carried out to reduce the computational cost and to properly represent infinitely large soil medium. Several hybrid models have been introduced (Guin and Banerjee, 1998, Pavlatos and Beskos, 1994) where finite element method is used for structural components and then boundary element method is used for soil medium. However, boundary element method is not suitable for describing the nonlinear behavior of soil. Another alternative method widely accepted is the Winkler-type foundation models. These models easily allow for the nonlinear behavior of soil and significantly reduce computational effort compared to finite element methods (El Naggar and Novak 1666, Nogami et al. 1990). Wang et al. preformed a comparison of various spring-dashpot models and they pointed out that radiation damping and nonlinear p-y curves have significant effect on the response of the systems. Generally, the effectiveness of the Winkler models is mainly controlled by the determination of nonlinear p-y curves of the spring and the representation of radiation energy and the pile-to-pile interaction. Many long-span bridges have foundations with a large number of closely spaced piles in complex arrangements. Although the Winkler models are easily derived for simple single pile systems, the effectiveness of the model becomes questionable for increasingly complex arrangement of pile groups.

In this paper, a new method is introduced to develop Winkler-type foundation models for pile foundations. The method is expected to properly construct Winkler models regardless of the complexity of the geometry of the pile group and to produce the seismic response as accurately as the response of the finite element model. The use of genetic algorithms play an important role in the proposed method.

PROPOSED METHOD FOR NUMERICAL MODELING OF PILE FOUNDATIONS

In conventional Winkler models used in pile foundations, the effect of soil is represented by two elements, the near-field element and the far-field element. Each element consists of masses, springs and dashpot. Various methods have been developed to determine the values and the variation of the masses, springs and dashpots. Near-field elements, representing the effect of soil around the piles, generally are modeled as nonlinear springs, whose behavior is to be determined by empirical formula. On the other hand, far-field elements consist of linear springs and dashpots and they represent radiation of scattering waves from the structure. As far as far-field behavior is concerned, there are analytical solutions in frequency-domain for homogeneous linear halfspace. In the time domain, it is possible to closely represent the radiation of energy in a certain range of frequencies with the proper choice of spring and dashpot constants (Nogami et al. 1990). However, in reality the situation is far more complex. The ground conditions may consist of layered deposits, or even more complex geological formations. For a soil deposit composed of different layers or more complex geological formations applying analytical solutions that cannot be adequately verified are unlikely to model the radiation effects correctly and to produce reliable results.

Most methods for modeling the pile-soil interaction are developed for single piles. An additional complicating factor is the pile-to-pile interaction in pile groups. The behavior of a pile in a pile group can be very different than the behavior a single pile. Consequently, the elements in the Winkler model should account for these differences. The method proposed in this paper accounts for the pile group effects.

In the method proposed here, a conventional two elements Winkler model, where each element has a mass, a spring and a dashpot, are adopted to account for both nonlinear soil reaction around the pile and the effect of radiation damping. However, it has to be noted that different models, with varying degrees of complexity can be used for this purpose. In the proposed model we account for the pile group effects by placing another set of springs and dashpots between the piles to represent pile-to-pile interactions.

The most important part of any pile foundation model is how to determine the values and variation of the various springs and dashpots of the model. At the outset the discrete Winkler parameters, spring and dashpot constants, etc., are treated as unknowns. A reference data set for the same structure-foundation-soil system is needed to determine these parameters. In the proposed method we first perform a detailed nonlinear dynamic finite element analysis of the soil-pile-foundation system. This finite element model would normally contain the foundation, the bridge pier above the foundation, and the pile group and a portion of the soil mass surrounding the pile group, as shown in Figure 1. This finite element model is the subject to the ground shaking and the response of the system is computed. The computed response of the finite element model is then used as the reference data set.

The problem of determination of the discrete Winkler parameters, spring and dashpot constants from this reference data set is a classical problem of system identification and parameter determination. This is accomplished by applying an optimization method. We have chosen to use genetic algorithm for solving the optimization problem. The discrete parameters of the system are the unknowns variables in the genetic algorithm. The values of the discrete parameters evolve during the generations in genetic algorithm in such a way that the results of the discrete Winkler type model matches the results of the finite element analysis. The main steps of this process are schematically illustrated in Figure1.

Genetic algorithms are employed to carry out the optimization process. Genetic algorithms are powerful tools for searching for the optimal solutions. Unlike the conventional calculus based optimization methods, genetic algorithms search solutions in a global manner where the derivatives of the object function are difficult or even impossible to find. In the example presented later in this paper, displacement time histories of the finite element system at certain locations in the pier and the piles are picked as reference data and they are compared to those of the discrete parameter system. The parameters keep evolving such that the difference between displacements of two systems becomes smaller and smaller. There is no way to find the explicit search directions for the optimal values of the parameters with the displacement difference. As discussed later, after evolutions, it is expected that the discrete parameter systems are capable of replacing finite elements around the pile.

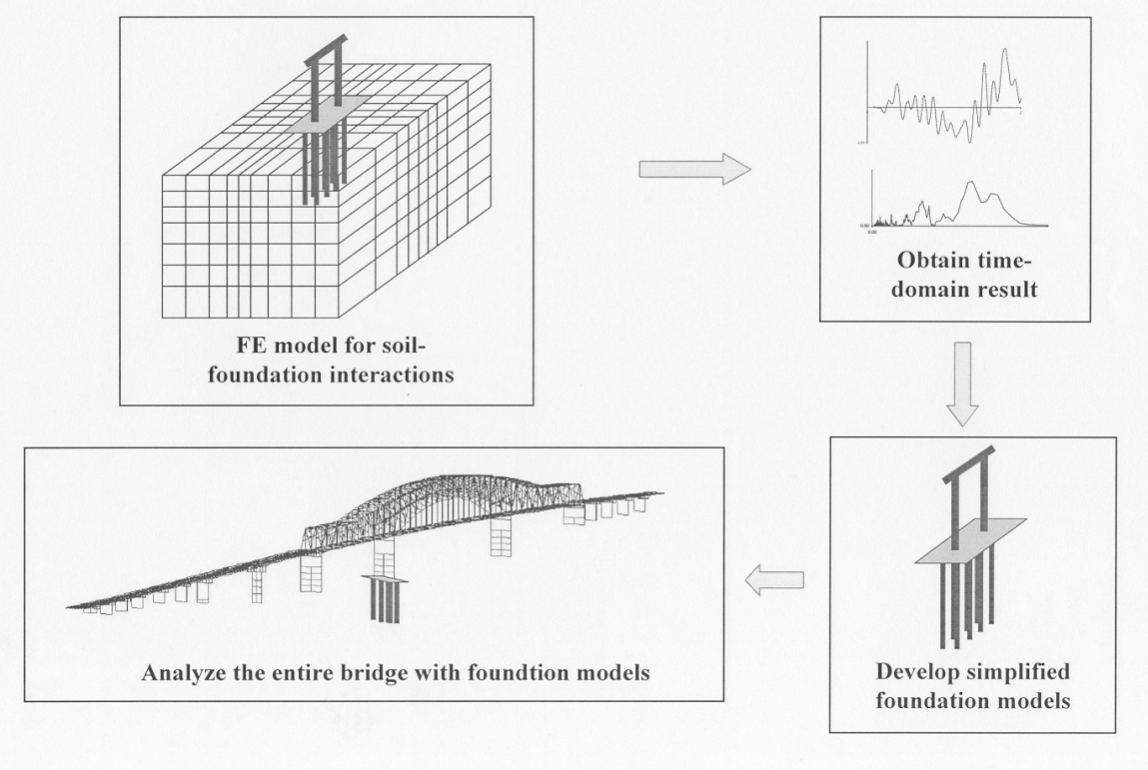

Figure 1. Schematic procedure for the proposed method

CASE STUDY

An I-57 bridge at Cairo across Mississippi River is examined as a case study. The bridge consists of approach spans and a main span (see Figure 2). The soil deposit under the bridge is about 160m thick and consists of 5 layers of sand and clay. In order to examine the dynamic characteristics of the bridge, a three-dimensional finite element models was constructed using SAP2000. Figure 3 shows the finite element model of the superstructure, along with three models of the foundation system. The modal characteristics of the bridge showed that there are two longitudinal modes around the period of 2.15sec, and 47 modes above the period of 1.0sec. It is also noteworthy that it has a significant number of modes associated with the torsion of approach spans. The torsional modes of the approach spans may play an important role in the seismic behavior of the bridge.

The foundations of approach spans consist of a large number of group piles, while the main spans have caissons. For example, a typical pier in the approach spans of the bridge has over 80 piles under the 20m×7m pier base cap. The closely spaced pile groups make the application of conventional Winkler modes nearly impossible. Arbitrary reduction factor can be introduced to Winkler springs or a large number of piles can be replaced with equivalent 2 by 2 pile group. However, the effectiveness of those methods has not been verified for seismic base excitations. The method proposed here is capable of producing the simple discrete parameter model for any complex arrangement of the pile groups.

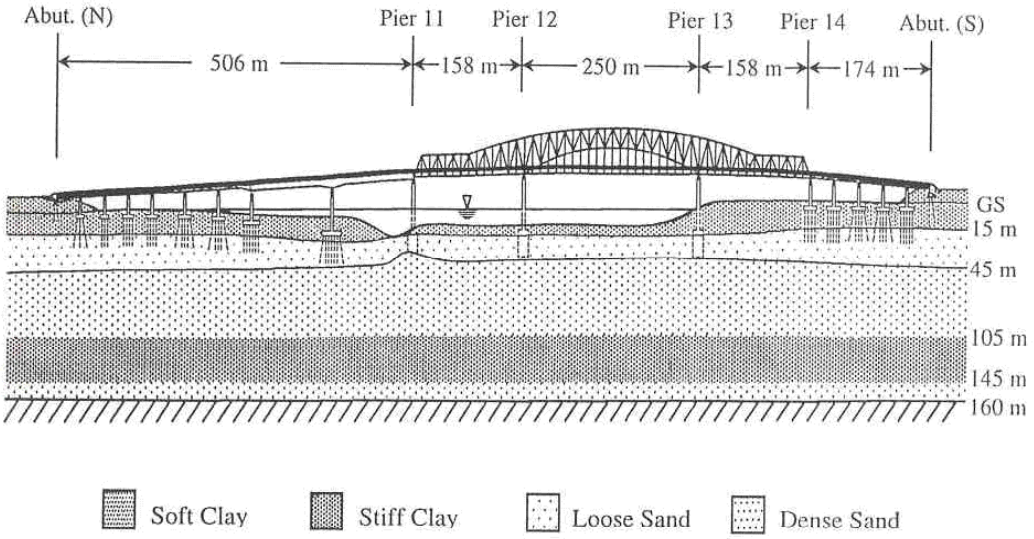

Figure 2. Elevation view of Cairo Bridge

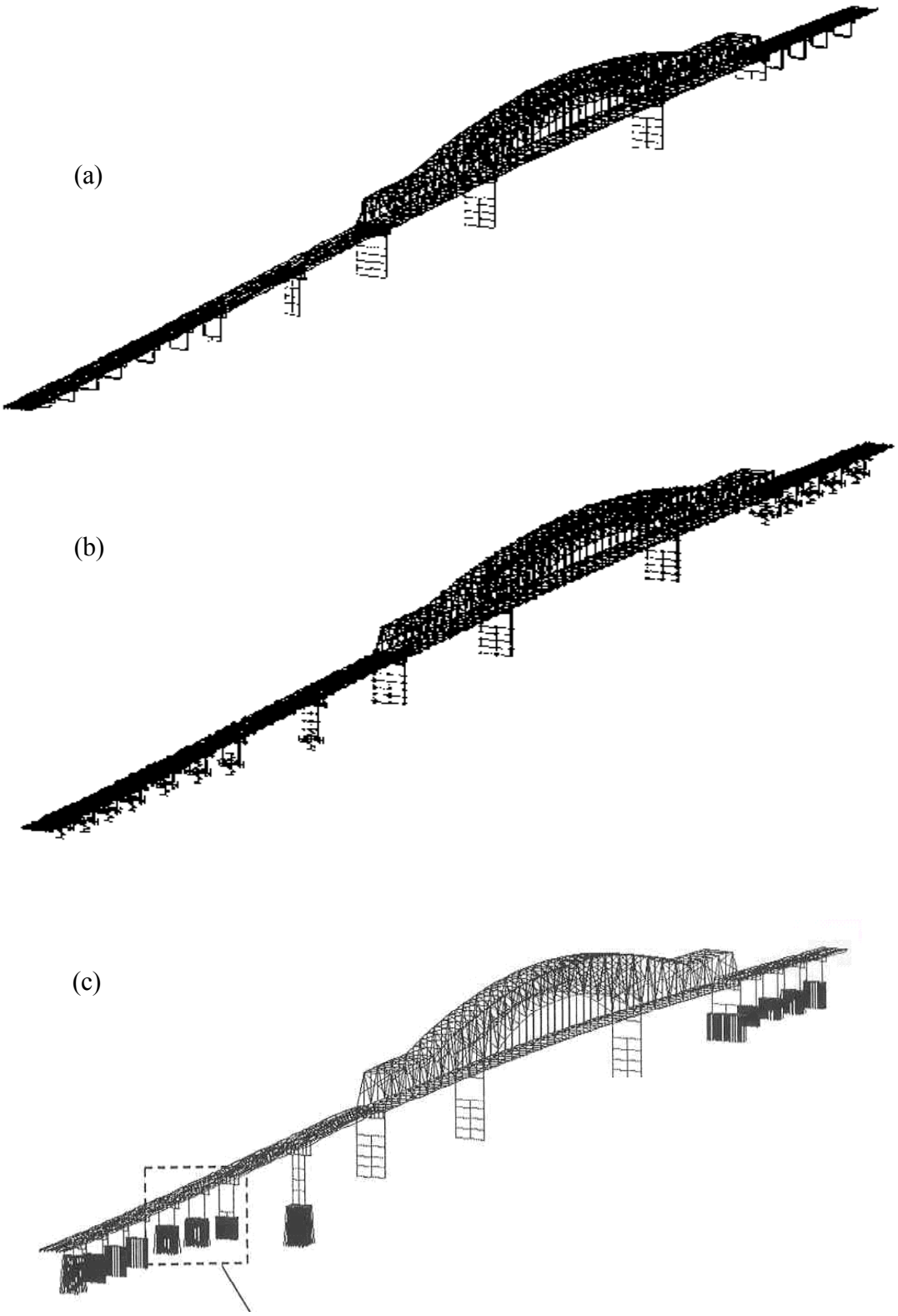

Figure 3. Finite element models using different foundation models: a) fixed base, b) 6 by 6 stiffness matrix, c) nonlinear springs at pile nodes.

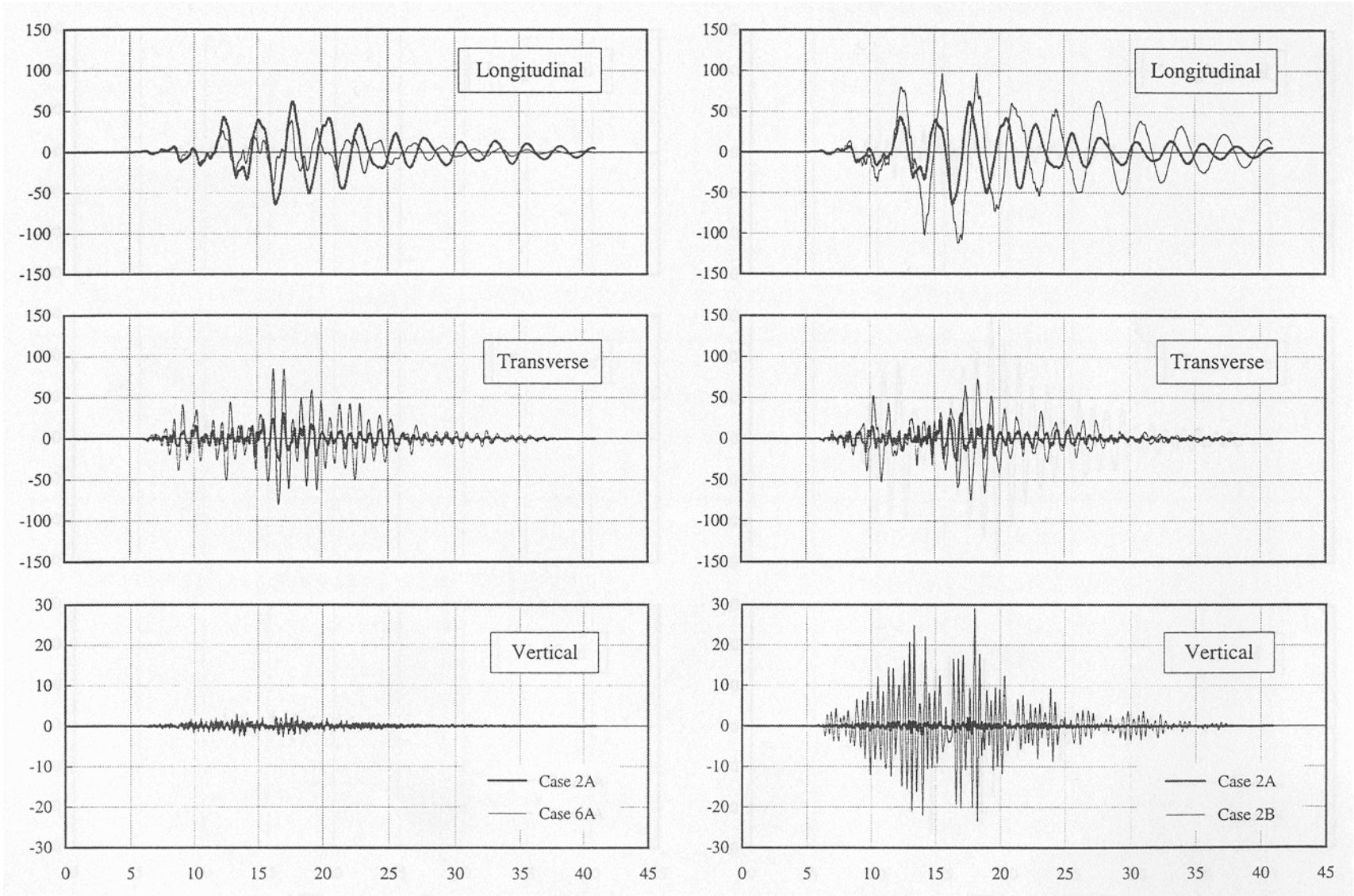

Figure 4. Displacements at the bent cap of pier 1 (after Kornkasem, 2001). Case 2A: 6 by 6 stiffness matrix without pile interaction, Case 2B: 6 by 6 stiffness matrix with pile interaction, Case 6A: nonlinear springs at pile loads.

Artificially generated acceleration time histories developed for the use in the New Madrid seismic zone (Hwang 1998) were applied at the bedrock to obtain ground motions. As a preliminary study, three types of models were used in time-domain analysis. In model, A, the base of each pier is fixed and the model is completely linear, while in model B the base is still fixed but nonlinear behavior in bearings and expansion joints were taken into account. In model C, in addition to the nonlinear behavior in the superstructure, spring elements were attached at the base of each pier to account for the foundation impedance. Absolute values of maximum displacements along the centerline of the deck were given for each model. The results show that there exist significant differences between longitudinal and transverse displacements from model A and C or B and C as shown in see Figure 4. This implies that soil-structure interactions play a more important role in those displacements that in the vertical displacements. Transverse displacements are observed to be so high that they are capable of causing severe damage to bearings. Significant torsion is also present between shear centers and mass centers of the bridge decks and truss sections

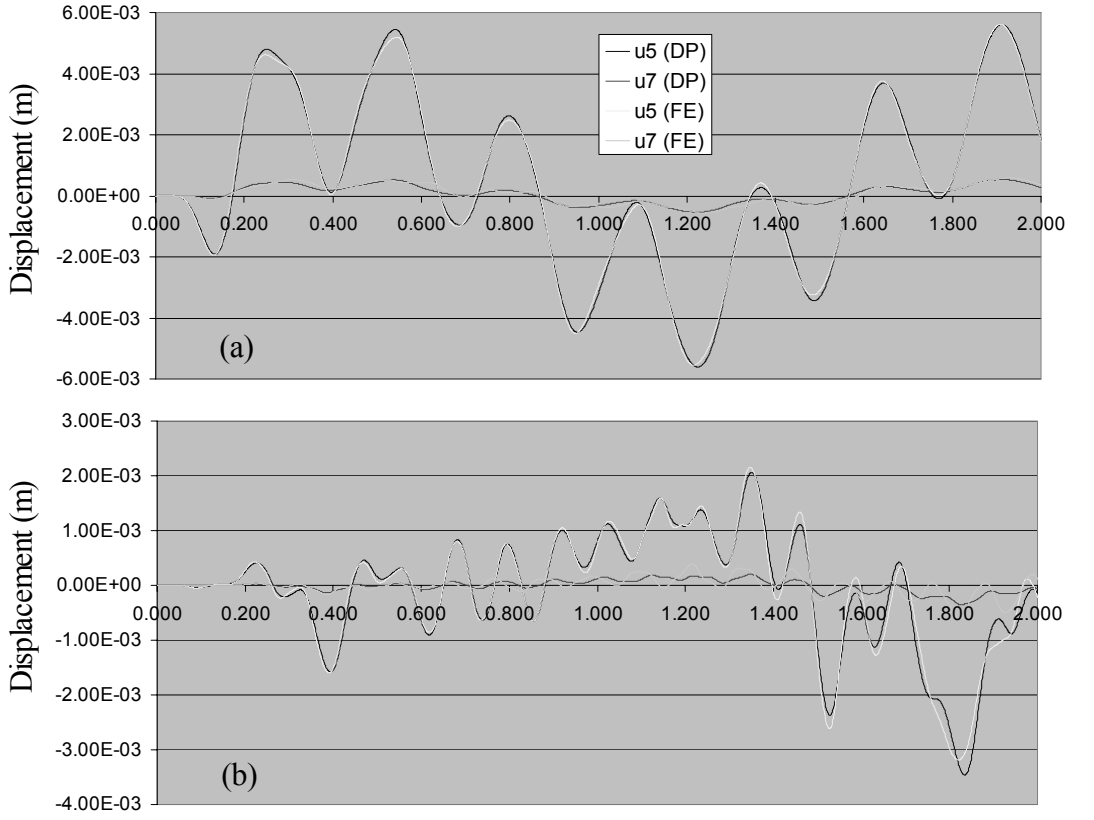

Figure 5. Displacements at selective nodes. a) F(t) = step loading, b) F(t) = banded white noise

The seismic behavior of this bridge has been thoroughly examined with various foundation models (Kornkasem 2001). Cases for a fixed base, linear and nonlinear 6 by 6 stiffness matrices at the base of the bridge pier and nonlinear springs attached at pile nodes are analyzed using SAP2000, as shown in figure 4. Pile-to-pile interaction effects have been taken into account for 6 by 6 stiffness matrices by introducing the static interaction factor. It was pointed out that this interaction factor tends to overestimate stiffness reductions. It was also shown that different foundation models have a significant affect on the dynamic response and the natural periods of the bridge.

PRELIMINARY STUDY WITH THE PROPOSED METHOD

The 2 by 2 pile group has been analyzed with the method described above. Three-dimensional finite element mesh including the bridge pier, pier base, piles and soil medium were constructed. The same pier and piles were constructed for the discrete parameter model, where nonlinear springs were used in near-field elements in order for the response to resemble nonlinear finite element analysis. Two sets of loading time histories, step loading and banded white noise, were applied at the top of the column and the displacement time histories were used to determine the spring and dashpot constants. The frequency content of the banded white noise should span the sufficiently large range to obtain the discrete parameter system that works in any possible loading condition. After the evolution of genetic algorithms, the displacements of the discrete parameter model are shown to be similar to those of the FE model, as shown in figure 5. In the figure, u4, u5 are nodes of the frame above ground and u6 and u7 are nodes of the pile below the ground. To verify the performance of the model, different superstructure geometry with a different loading were analyzed. It can be noted that the Winkler model determined by genetic algorithms closely matches the response of finite elements model, except the high frequency response of the pile.

CONCLUDING REMARKS

As shown in the case study, the soil-structure interaction effects plays an important role and their modeling is one of the most important factors in the seismic analysis of the long-span bridges. The modeling of the whole superstructure and the foundation system, specially the pile group foundation, is very important in computing realistic seismic response of major bridges, as demonstrated in this paper. Moreover, we have also shown the importance of detailed modeling of the foundation and the soil-foundation interaction. More realistic and detailed modeling of the pile foundation lead to the response of the superstructure that is very different than when the simplified models are used.

A new approach to construct computationally efficient, yet relatively accurate discrete parameter model has been proposed for pile foundations. In this approach the parameters of discrete Winkler type models are determined by matching the response of a detailed finite element model that includes the foundation and the pile group. We have proposed using genetic algorithm for the purpose of parameter identification. Genetic algorithm is a powerful tool for this purpose and it is highly flexible. This research is still in progress and we have only presented the results of a preliminary study. A simple 2 by 2 pile group is examined as a preliminary study and it is shown that the proposed method produces the Winkler-type model that performs as well as the nonlinear three-dimensional finite element analysis.

Having the flexibility to modify and simplify the model and not to have to depend upon analytical solutions or empirical formula, the proposed method has advantages over the conventional methods for computing Winkler foundation models for the case of extremely complex arrangement of piles. The future research should be focused on the actual complex pile groups and the verification of the capability of the method to produce simplified and accurate models. The method requires carrying out finite element analysis every time a discrete parameter model is constructed. It is possible to make design curves for constructing Winkler models through extensive parameter study using this method.

ACKNOWLEDGEMENTS

The research reported in this paper was funded by National Research Foundation through a grant from the Mid-America Earthquake Center. The first author was supported by this grant. This support is gratefully acknowledged. The opinions expressed in this paper are solely those of the authors.

REFERENCES

Cai, Y. X., Gould, P. L. and Desai, C. S. 1995. "Investigation of 3-D nonlinear seismic performance of pile-supported structures", *Performance of Deep Foundations under Seismic Loading,* ASCE Geotech. Special Pub. No. 51, 17-31.

Elassaly, M., Ghali, A. and Elbadry, M. M. 1995. "Influence of soil conditions on the seismic behaviour of two cable-stayed bridges", *Canadian J. Civ. Eng.*, **22**, 1021-1040.

El Naggar, M. H. and Novak, M. 1996. "Nonlinear analysis for dynamic lateral pile response.", *Soil Dynamic and Earthquake Engineering*, **15**, 233-244.

Finn, W. D. L., Thavaraj, T. and Wu, G. 1996. "Seismic Analysis of pile foundations: State-of-art", *Proc. 11th WCEE*, paper no. 2073.

Finn, W. D. L. and Wu, G. 1996. "Nonlinear seismic analysis of pile foundations", *Proc. 11th WCEE*, paper no. 1414.

Goldberg, D. E. 1989. *Genetic Algorithms in Search, Optimization, and Machine Learning*, Addison-Wesley.

Guin, J. and Banerjee, P. K. 1998. "Coupled soil-pile-structure interaction analysis under seismic excitation", *J. of Struct. Eng.*, ASCE, **124**, no 4, 434-444.

Hwang, H. M. 1998. *Artificial acceleration time histories*, Center for Earthquake Research and Information, University of Memphis.

Kornkasem, W. et al. 1999. "Seismic analysis of a truss-arch bridge across the Mississippi River", Presented for publication on the 5th U.S. Nat. Conf. Lifeline Earthquake Eng.

Kornkasem, W. 2001. *Seismic Behavior of Pile-Supported Bridges,* Ph. D. Thesis, University of Illinois at Urbana-Champaign.

Nam, S.-I. et al. 2000. " Analysis of soil-structure Interaction of major river-crossing bridges.", *Proceedings of 12WCEE*. Paper no. 0496.

Nogami, T., Otani, J., Konagai, K. and Chen, H.-L. 1992. "Nonlinear soil-pile interaction model for dynamic lateral motion", *J. of Geotech. Eng.*, ASCE, **118**, no 1, 89-106.

Pavlatos, G. D. and Beskos, D. E. 1994. "Dynamic elastoplastic analysis by BEM/FEM.", *Engineering Analysis by Boundary Elements*, **14**. 51-63.

Wang, S. et. al. 1998. "Nonlinear seismic soil-pile structure interaction." *Earthquake Spectra,* EERI, **14**, no 2, 377-396.

Preliminary Study of Hydrodynamic Effects on Seismic Response of Bridges

Jun-jie Wang[1], Wei Lai[1], Ning-yong Zhang[1], Li-min Sun and Li-chu Fan[1]

ABSTRACT

The planning background of sea strait bridges remind engineers paying close attention to the aseismic design of bridges in deep water. In this paper a preliminary study of the water dynamic effects on seismic responses of bridges in deep water has been carried out. The Morison Equation is used to model water dynamic pressure under seismic action, but only the inertia term of Morison Equation is considered. Two types of bridges are analyzed, the first is long span bridge with GBS, and the second is short span bridge with group pile foundation. The maximum water depth is about 280m for the first type of bridge, and the water depth for the second bridge is about 30m. The results show that the seismic hydrodynamic pressure may be important for correctly predicting the responses of bridges in deep water under seismic action in some cases, it may changes the seismic response by 10% to 100%.

[1]State Key Laboratory for Disaster Reduction in Civil Engineering, Tongji University, Shanghai 200092, PRC

INTRODUCTION

Sea straits and sea bays dotted in China have been great obstacles of economy development for regions in a country, such as Hainan Province in China, and archipelago of Zhoushan in China. Recently, a planning was lunched by the government of China (in 1996) to construct a series of sea strait(or sea bay) crossing bridges(or tunnels), one of them is shown in Figure 1. In fact, there are many sea-crossing bridges in planning worldwide. Figure 2 is an example.

To cross these sea bays or sea straits, one of the solutions is to construct bridges, or part of a crossing link consists of bridges. These bridges stand in sea with water depth up to 80-100m, the water might have important effects on seismic response of the bridges. However, engineers have a lack of knowledge about such a problem.

The prediction of seismic response of bridges in deep water requires special consideration due to fluid-structure interaction. In 1965 Hisao Goto and Kenzo[1] Toki[1], Kotsubo[2] investigated the seismic response of bridge pier in water. From 1973-1980, a series of research work had been finished by Liaw, Chopra, Rea, Byrd, and Nilrat[3-6]. The above pioneer research work demonstrated the importance of the fluid-structure interaction in the earthquake response behaviour of tower surrounded by water. The experimental research had also been done by Rea et al[5] and Byrd[6]. The experimental results are used to verify the analytical theory and to find main factors for hydrodynamic forces for tank-type structures.

In 1980, Nilrat[7] proposed a finite element method for determining the hydrodynamic pressure distribution on rigid axisymmetric bodies oscillating in a fluid. The results of the finite element analysis are compared with experimental results showing good comparisons in most cases. In 1986 Tanaka and Hudspeth[8] developed employed an eigenfunction solution to calculate the hydrodynamic forces under sinusoidal horizontal ground motion, and the results from eigenfunction solution was verified by experimental data from a squatty circular column and a slender circular column.

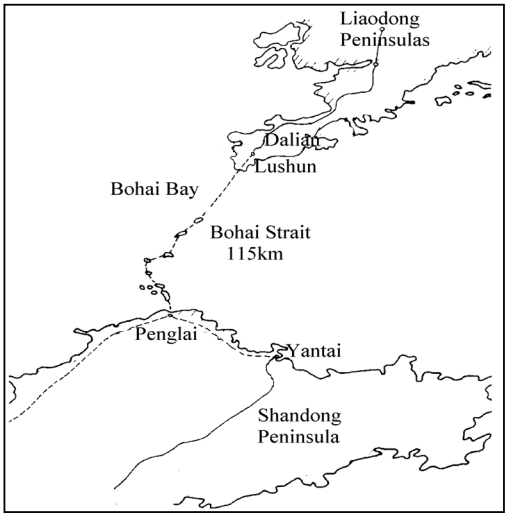

Figure 1. The Bohai Bay.

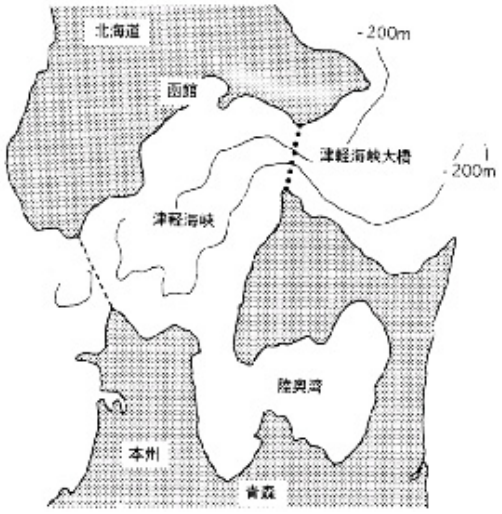

Figure 2. Honshu-Hokkaido Strait in Japan.

So far the research about the importance of hydrodynamic forces to structures in water mainly focuses on three types of structures, marine tanks, intake-outlet towers[3-5,11-13], offshore platforms[14,16,17]. However, few papers contribute to the bridges in deep water, eg. sea strait bridges.

As a preliminary investigation, the Morision equation is employed to consider the water effects on the seismic response of bridges in this paper, and two types of bridges are analyzed, the first is long span bridge, and the second is bridge with group piles foundations.

DYNAMIC EQUATION

Seismic action will produce relative motion between the bridge pier and sea water. This relative motion acts on the bridge pier in two manner, the first is the inertia action because of the change of the water, and the second is the viscosity action of the water. For a slender column (eg. pile) with small diameter, the water dynamic effects on the pier can be expressed by Morision equation:

$$\mathbf{F} = \rho \mathbf{V}\ddot{\mathbf{u}} + (C_M - 1)\rho \mathbf{V}(\ddot{\mathbf{u}} - \ddot{\mathbf{x}} - \ddot{\mathbf{x}}_g) + \frac{1}{2} C_D \rho \mathbf{A}_P [(\dot{\mathbf{u}} - \dot{\mathbf{x}} - \dot{\mathbf{x}}_g) | (\dot{\mathbf{u}} - \dot{\mathbf{x}} - \dot{\mathbf{x}}_g) |] \tag{1}$$

where ρ is the density of the water; $\dot{\mathbf{u}}$、$\ddot{\mathbf{u}}$ are the absolute velocity and acceleration the water respectively; $\mathbf{x}$、$\dot{\mathbf{x}}$ and $\ddot{\mathbf{x}}$ are the relative displacement, velocity and acceleration respectively; $\ddot{\mathbf{x}}_g$ is the seismic ground motion; C_M is the inertia factor, and C_D is the viscosity factor. In this study, C_D is equal to 2，and C_M is equal to 2.0.

In this study, it assumed that the water is still, i.e., $\dot{\mathbf{u}} = \ddot{\mathbf{u}} = 0$, therefore equation (1) can be rewritten as,

$$\mathbf{F} = -(C_M - 1)\rho \mathbf{V}(\ddot{\mathbf{x}} + \ddot{\mathbf{x}}_g) - \frac{1}{2} C_D \rho \mathbf{A}_P [(\dot{\mathbf{x}} + \dot{\mathbf{x}}_g) | (\dot{\mathbf{x}} + \dot{\mathbf{x}}_g) |] \tag{2}$$

then one can obtain the motion equation of a bridge under seismic action with the water effects,

$$\mathbf{M}\ddot{\mathbf{x}} + \mathbf{C}\dot{\mathbf{x}} + \mathbf{K}\mathbf{x} = -\mathbf{M}\ddot{\mathbf{x}}_g - (C_M - 1)\rho \mathbf{V}(\ddot{\mathbf{x}} + \ddot{\mathbf{x}}_g) - \frac{1}{2} C_D \rho \mathbf{A}_P [(\dot{\mathbf{x}} + \dot{\mathbf{x}}_g) | (\dot{\mathbf{x}} + \dot{\mathbf{x}}_g) |] \tag{3}$$

The third term in the right hand is nonlinear one, by adopting the linearization technique[5] to this term, one can obtain the following linearized equation,

$$\mathbf{M}\ddot{\mathbf{x}} + \mathbf{C}\dot{\mathbf{x}} + \mathbf{K}\mathbf{x} = -\mathbf{M}\ddot{\mathbf{x}}_g - (C_M - 1)\rho\mathbf{V}(\ddot{\mathbf{x}} + \ddot{\mathbf{x}}_g) - \frac{1}{2}C_D\rho\mathbf{A}_P\sigma_{\dot{\mathbf{x}}+\dot{\mathbf{x}}_g}\sqrt{\frac{8}{\pi}}(\dot{\mathbf{x}} + \dot{\mathbf{x}}_g) \tag{4}$$

Then,

$$[\mathbf{M} + \mathbf{M}_w]\ddot{\mathbf{x}} + [\mathbf{C} + \mathbf{C}_w]\dot{\mathbf{x}} + \mathbf{K}\mathbf{x} = -[\mathbf{M} + \mathbf{M}_w]\ddot{\mathbf{x}}_g - \mathbf{C}_w\dot{\mathbf{x}}_g \tag{5}$$

$$\mathbf{M}_w = (C_M - 1)\rho\mathbf{V}, \qquad \mathbf{C}_w = \frac{1}{2}C_D\rho\mathbf{A}_P\sigma_{\dot{\mathbf{x}}+\dot{\mathbf{x}}_g}\sqrt{\frac{8}{\pi}} \tag{6}$$

where $\sigma_{\dot{\mathbf{x}}+\dot{\mathbf{x}}_g}$ is the variance response of absolute accelerations of the bridge. $\sigma_{\dot{\mathbf{x}}+\dot{\mathbf{x}}_g}$ is a unknown vector, the computation of sub-matrix of concerns the unknown $\sigma_{\dot{\mathbf{x}}+\dot{\mathbf{x}}_g}$, an iterative procedure is needed.

If the effect of water viscosity is neglected, the motion equation of a bridge under the seismic action can be simplified,

$$[\mathbf{M} + \mathbf{M}_w]\ddot{\mathbf{x}} + \mathbf{C}\dot{\mathbf{x}} + \mathbf{K}\mathbf{x} = -[\mathbf{M} + \mathbf{M}_w]\ddot{\mathbf{x}}_g \tag{7}$$

In this simple case, the effects of the water is equivalent to an additional mass matrix. The additional mass matrix changes the dynamic characteristics of the analyzed bridge, and then changes the seismic responses of the analyzed bridge. In this paper only the inertia effect is taken into account.

WATER EFFECTS ON LONG SPAN BRIDGE

In general, the superstructure of a sea strait bridge take the usual configuration as the long span bridges which go across a river. But a sea strait bridge featured by its type of foundation, an example is shown in Figure 3.

In this paper as an example the planning bridge for Honshu-Hokkaido[18] strait in Japan is analyzed, and the effects of water on the seismic responses long span bridges is investigated.

To verify the effects of the water on the seismic responses of a long span bridge over a sea strait, two structural models are used in computation: (1) the pylon only; (2) the plane bridge model. Six cases of the water depth are considered in the analyses, which are 0, 30, 60, 90, 120 and 150m, and the depth of 150m is the natural situation.

The comparison between the free vibrational frequencies without water and with water of 150m are shown in Figure 4. It can be seen that the hydrodynamic pressure largely changes the he free vibrational frequencies of the bridge, therefore it can be expected that the hydrodynamic pressure would largely changes the seismic response of bridge.

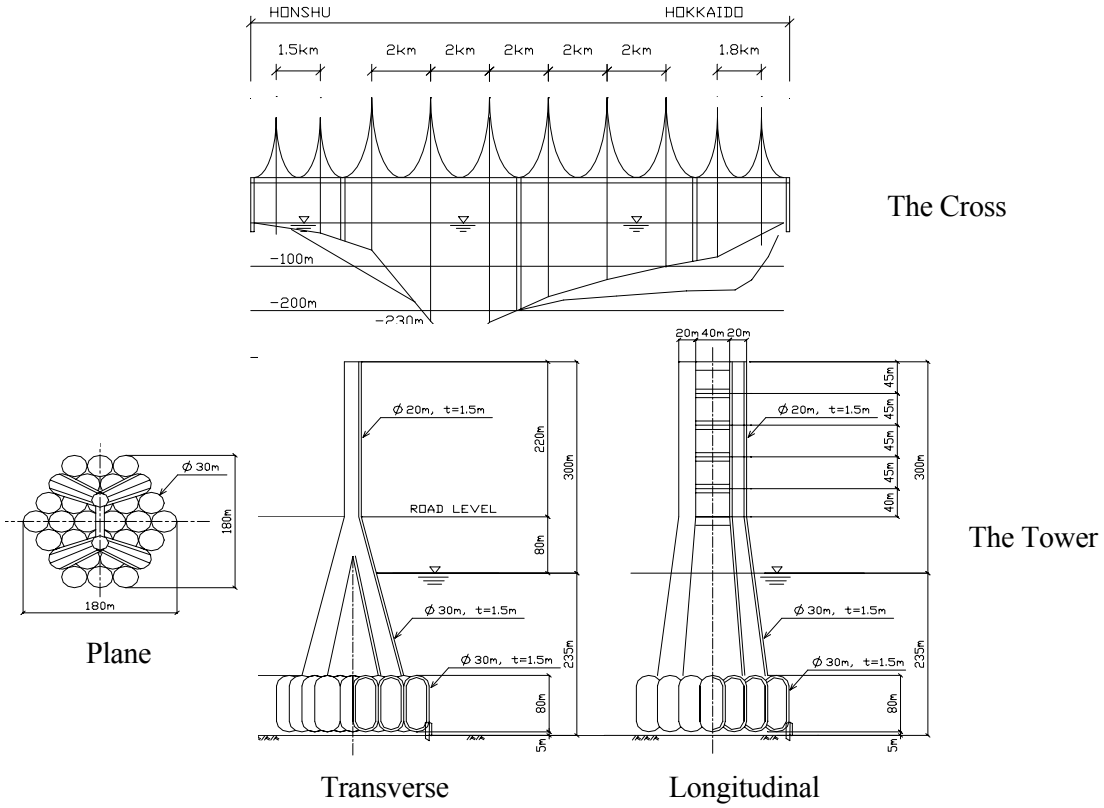

Figure 3. The Planning Bridge Solution For Honshu-Hokkaido Strait in Japan.

Define the ratio:

$$R_w = \frac{RSP - RSP_0}{RSP_0} \times 100 \tag{8}$$

where RSP is the seismic response for case with water, and RSP_0 is the seismic response without water. The results of R_w are shown in Figure5 and 6.

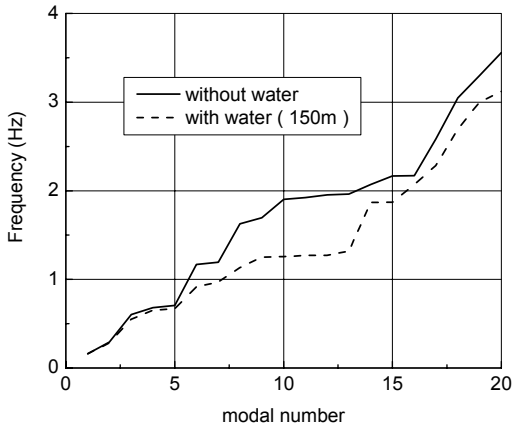

Figure 4. Frequencies of the Analyzed Bridge.

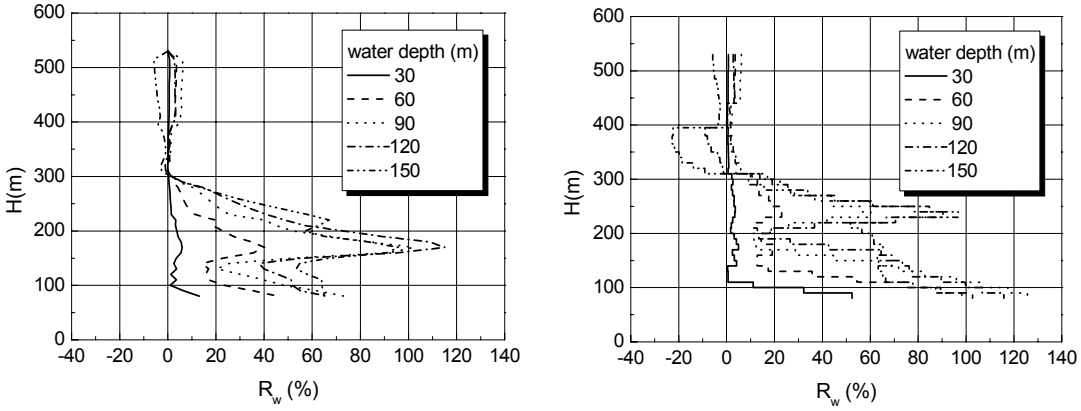

Bending Moment Shear Force

Figure 5. The Water Effects on Seismic response For Tower Model.

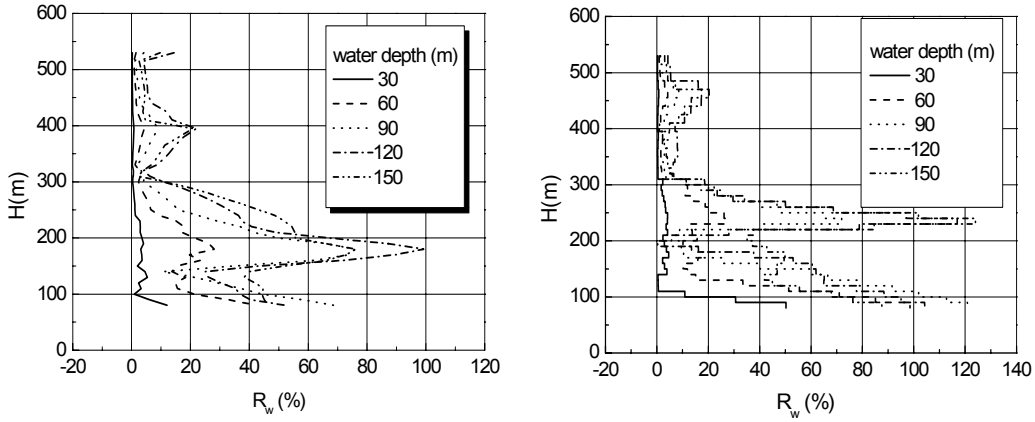

Bending Moment Shear Force

Figure 6. The Water Effects on Seismic response For Plane Bridge model.

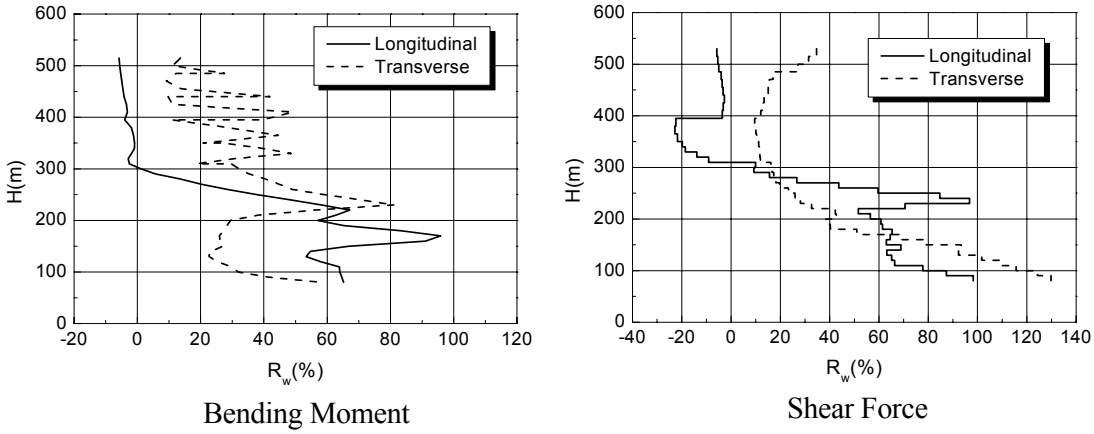

Bending Moment Shear Force

Figure 7. Responses in Both Longitudinal and Transverse Direction For Tower Model.

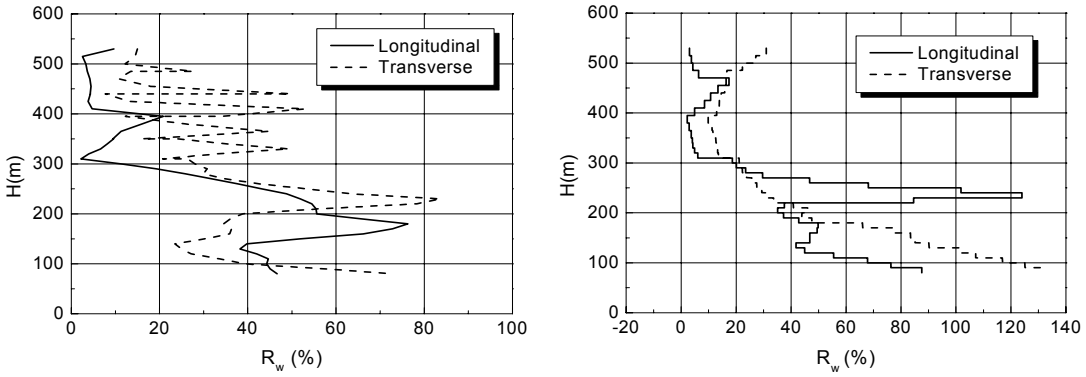

Bending Moment Shear Force

Figure 8. Responses in Both Longitudinal and Transverse Direction For Plane Bridge Model.

At first, with the increase of water depth, the seismic response of the tower simply increase, reach its maximum value at water depth of 120m, but get less at water depth of 150m. In fact the dynamic effect of water is equvalent a additional mass matrix, which change the inertia of the tower, so the dynamic characteristic of free vibration of the tower changes. The effect of this change on the seismic response of the tower depends on the characteristics of the input seismic ground motion. In principle, the tower will obtain its maximum response if the dominate frequency of input seismic ground motion coincides with controlling frequency of free vibration of the tower. For the tower, the water depth that will give maximum response is 120m. Therefore it is not always true that deeper water gives larger seismic response of the tower.

In general, the effect of the water is really important for the correct predict of the seismic response of the tower, and the net increase may reach 100%. The effect of the water on the seismic response of the tower changes with the height of the tower, R_w get its maximum values at the bottom or at some height of the tower, it depends on which response is considered. This shows the complexity of the water effect on the seismic response of the tower.

The results from the tower model and the results from plane bridge model reach the same conclusions.

The Figure 7 and 8 show the comparison of water effect on the seismic response in transverse direction and the longitudinal direction. The same conclusion can be reached for seismic response of the tower in the transverse direction.

Two examples of the time histories of seismic responses for tower model are shown in Figure 9 and 10.

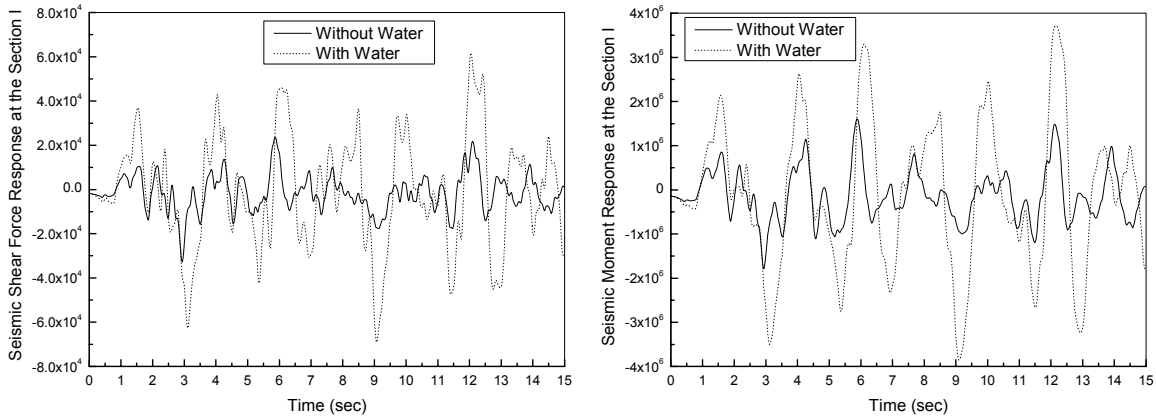

Figure 9. Seismic Responses at the Bottom of the Tower for Tower Model.

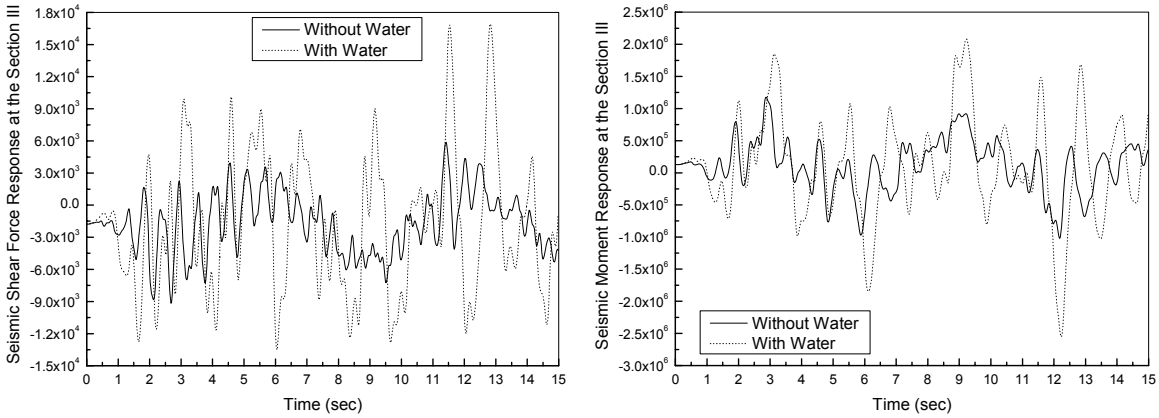

Figure 10. Seismic Responses at the Height of Free Water Surface for Tower Model.

WATER EFFECTS ON BRIDGES WITH GROUP PILES

In China, group piles foundations are widely used in bridge construction, from short span bridges to long span bridges, an example is shown in Figure 9. In this section, Pingtan Bridge[19] is taken as an example to investigate water dynamic effects on the seismic response of bridges with group pile foundations.

Five cases are considered in computation : (1) without water and without the mass of superstructure; (2) with water below the pile-cap and without the mass of superstructure; (3) with water above the pile-cap and without the mass of superstructure; (4) without water and with the mass of superstructure; (5) with water above pile-cap and with the mass of superstructure.

The effect of hydrodynamic pressure on the free vibrational frequencies is shown in Figure 10; the seismic responses are shown in Figure11-16.

It can be seen from Figure 10 that the added mass makes important changes of the free vibrational frequencies of mode 6, 7, 8(the values of frequencies are about 25-35rad/s, i.e., 4.0-5.5Hz). That means the seismic response might be largely changed by the added mass if the dominate spectral area of the seismic excitation is at this frequency phase.

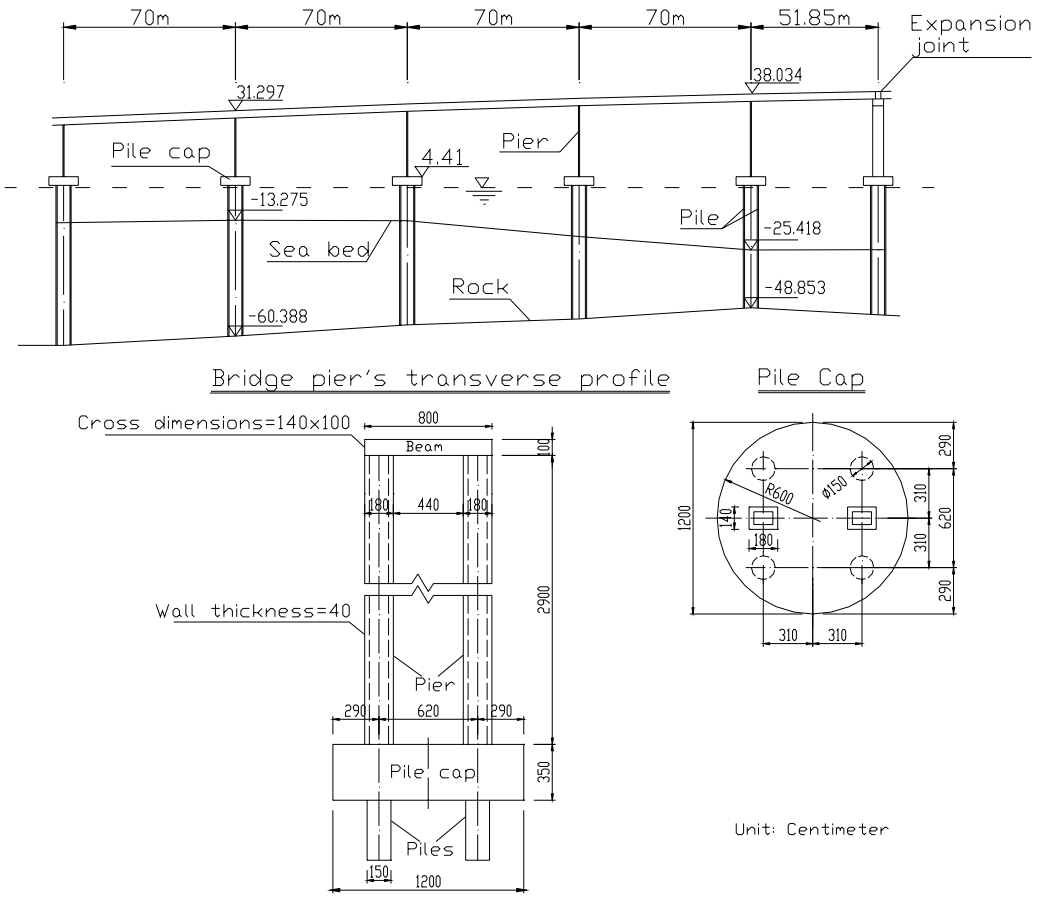

Figure 11. The Pingtan Bridge Over Pingtan Sea Strait.

It can be observed from Figure 11-18 that the effect of the added mass(hydrodynamic pressure) on the seismic response of the bridge depends on several factors: (1) the total mass of the bridge; (2) the added mass; (3) the response that is concerned. To the Pingtan Bridge, the effect of the hydrodynamic pressure on the seismic response the bridge show the following features:

- the added mass enlarges the seismic responses at the first part of time, and then reduce the responses, either for the response displacements, or for the internal force responses.
- The effect of added mass on the response of piles is larger than that of the pier since the added mass is attached to the piles.
- The effect of seismic hydrodynamic pressure of the seismic responses of the bridge is significantly different if or not the pile cap is below the free surface of the water.

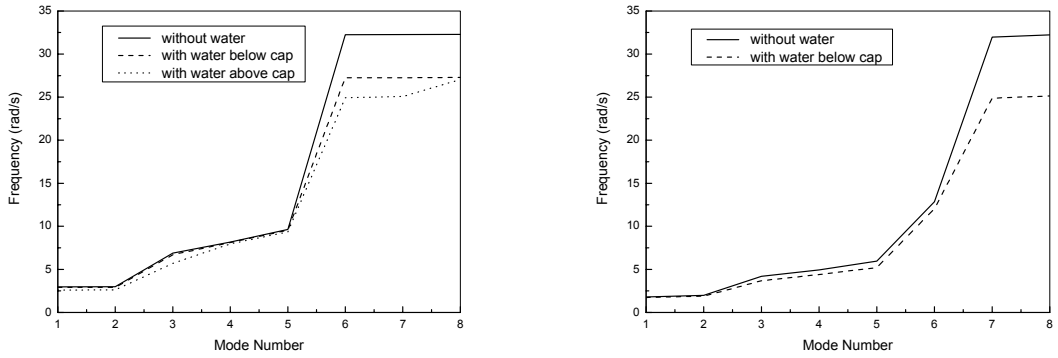

Figure 12. Frequencies of Free Vibration of the Analyzed Bridge.

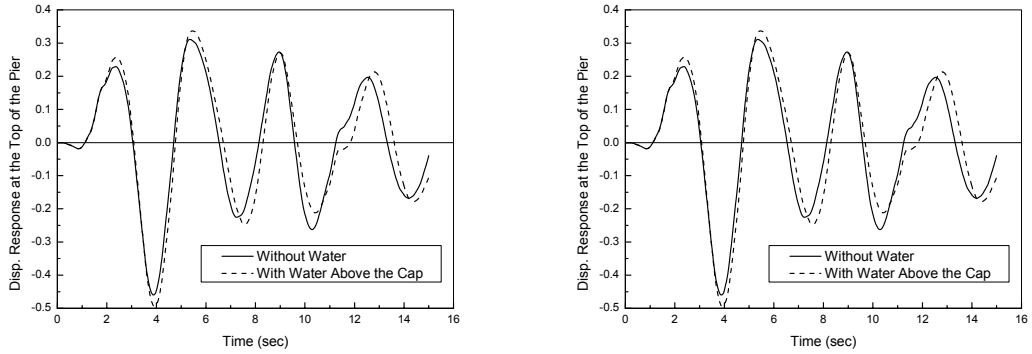

Figure 13. Seismic Displacement Response At the Top of The Pier.

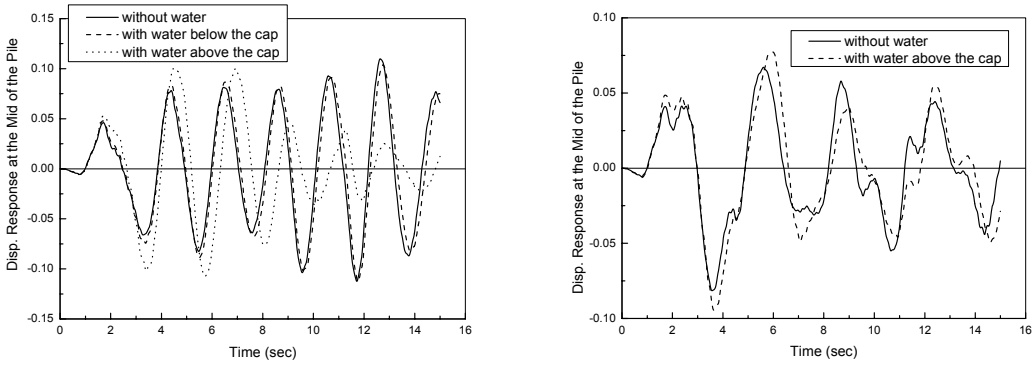

Figure 14. Seismic Displacement Response At the Mid of The Pile.

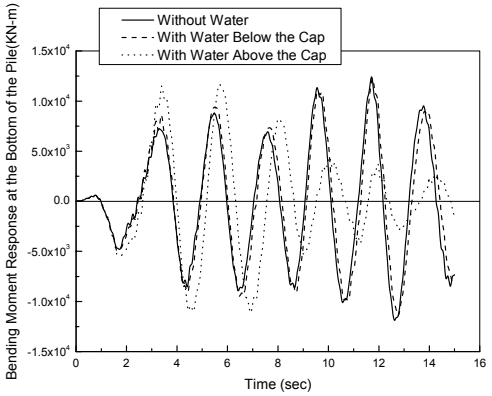

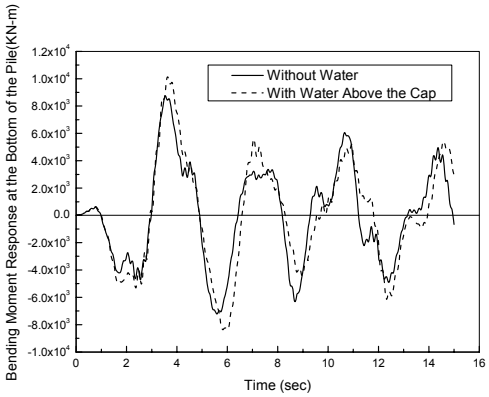

Without the Mass of Superstructure With the Mass of Superstructure

Figure 15. Seismic Bending Moment Response At the Bottom of The Pile.

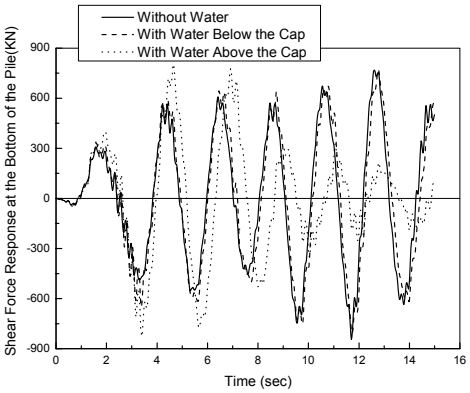

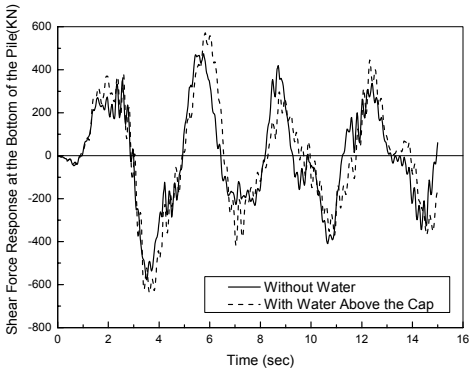

Without the Mass of Superstructure With the Mass of Superstructure

Figure 16. Seismic Shear Force Response At the Bottom of The Pile.

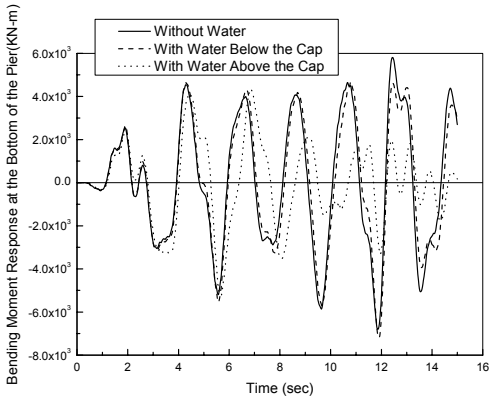

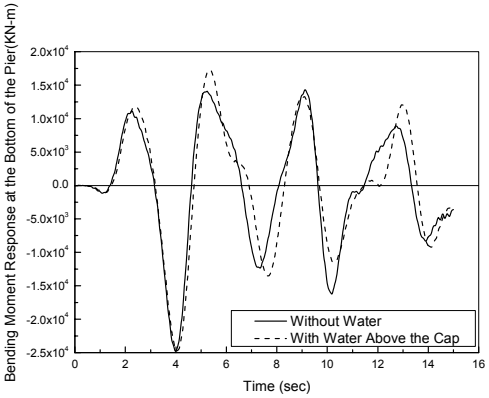

Without the Mass of Superstructure With the Mass of Superstructure

Figure 17. Seismic Bending Moment Response At the Bottom of The Pier.

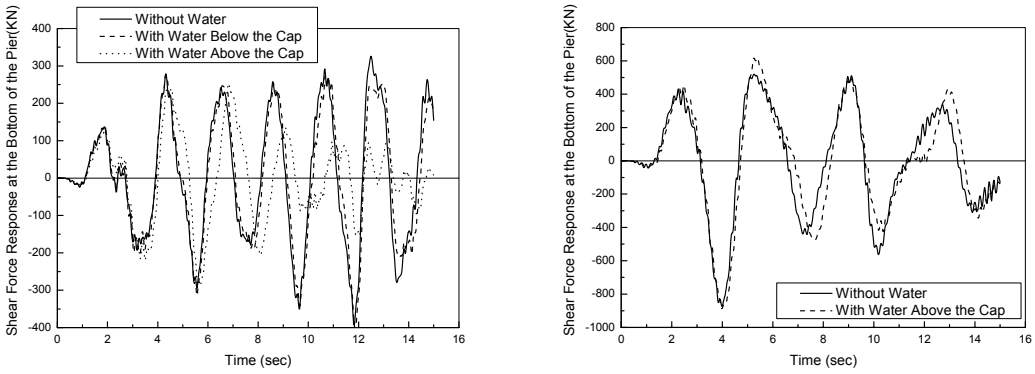

Without the Mass of Superstructure With the Mass of Superstructure

Figure 18. Seismic Shear Force Response At the Bottom of The Pier.

CONCLUSIONS

The planning background of sea strait bridges remind engineers paying close attention to the aseismic design of bridges in deep water. But so far engineers have a lack of knowledge about this problem. In this paper a preliminary study of the water dynamic effects on seismic responses of bridges in deep water has been carried out, and the following conclusions have been reached.

- The hydrodynamic pressure may have important effect on the seismic response of the bridges in deep water, research in details on this effect should be a primary part for aseismic designs of sea strait bridges.
- The effect of hydrodynamic pressure on the seismic response of the bridge depends on several factors, the total mass of the bridge, the added mass, the response that is concerned.
- The hydrodynamic pressure may changes the seismic responses of Honshu-Hokkaido Strait Bridge by 30%-100%, and more than 15% for Pingtan Bridge.

Finally, it should be mentioned that the calculated results presented in this paper are preliminary, it assumed that the Morison equation is suitable for the cases studied, and the hydrodynamic damping is neglected. Because the importance of hydrodynamic effects on the response of bridges suggested by the numerical analysis in this paper, to verify the theoretical method and the conclusions from the numerical computation, a shaking-table test is under preparation and is going to be finished in by the end of 2002.

ACKNOWLEDGEMENT

This research is supported by the National Science Foundation of China at granted No. 40072088.

REFERENCES

H. Goto and K. Toki. 1965. "Vibration Characteristics and Aseismic Design of Submerged Bridge Piers," *Proc. Third World Conf. On Earthq. Eng*, Auckland, Welligton, New Zealand.

S.Kotsubo. 1965. "Seismic force effect on submerged bridge piers with elliptic cross-section," *Proc. Third World Conf. On Earthq. Eng.*, Auckland, Welligton, New Zealand.

C.Y. Liaw and A.K. Chopra. 1973. "Earthquake response of axisymmetric tower structures surrounded by water," Report No. UCB/EERC 73/25, EERC, University of Califirnia, Berkeley, CA.

C.Y. Liaw and A.K. Chopra. 1974. "Dynamics of towers surrounded by water," *Earthquake Engineering & Structural Dynamics*, Vol.3, No.1, 33-49.

D.Rea, C.Y. Liaw and A.K. Chopra. 1975. "Dynamic properties of San Bernardino intake tower," Report No. UCB/EERC 75/05, EERC, University of Califirnia, Berkeley, CA.

R.C.Byrd. 1978. "A laboratory study of the fluid-structure interaction of submerged tanks and caissons in earthquakes," Report No. UCB/EERC 78/08, EERC, University of Califirnia, Berkeley, CA.

F.Nilrat. 1980. "Hydrodynamic pressure and added mass for axismmetric bodies," Report No. UCB/EERC 80/12, EERC, University of Califirnia, Berkeley, CA.

Tanaka Y. And Hudspeth R.T. 1986. "Earthq. Response of Circular Cylindricl Structures in Water," *5th International Symp. on Offshore Mech. And Arctic Eng*., Tokyo, Japan.

Anthony N. Williams. 1986. "Earthq. Response of Submerged Circular Cylinders," *Ocean Eng*., 13(6).

Tanaka Y. And Hudspeth R.T. 1988. "Restoring forces on vertical circular cylinders forced by earthquakes," *Earthquake Engineering & Structural Dynamics*, Vol.16, No.1, pages 99-119.

Goyal, A.; Chopra, A. K. 1989. "Earthquake response spectrum analysis of intake-outlet towers," Journal of Engineering Mechanics, 115, 7, July, pages 1413-1433.

Goyal, A.; Chopra, A. K. 1989. "Simplified evaluation of added hydrodynamic mass for intake towers," Journal of Engineering Mechanics, 115, 7, July, pages 1393-1412.1`

Chopra, A. K.; Goyal, A. 1991. "Simplified earthquake analysis of intake-outlet towers," Journal of Structural Engineering, 117, 3, Mar, pages 767-788.

El Naggar, M. H.; Novak, M. 1996. "Influence of foundation nonlinearity on offshore towers response," Journal of Geotechnical Engineering, 122, 9, Sept., pages 717-724.

Spyrakos, C. C.; Xu, C. 1997. "Soil-structure-water interaction of intake-outlet towers allowed to uplift," Soil Dynamics and Earthquake Engineering, 16, 2, Feb, pages 151-159.

Sun, K.; Nogami, T. 1991. "Earthquake induced hydrodynamic pressure on axisymmetric offshore structures," Earthquake Engineering & Structural Dynamics, 20, 5, May, pages 429-440.

Yamada, Y.; et al. 1989. "Seismic response of offshore structures in random seas," Earthquake Engineering & Structural Dynamics, 18, 7, Oct, pages 965-981.

Bridge and Offshore Engineering Association, *Sea Strait Crossing*, Vol.13, 47-53, 1998.

Fujian Highway Design Institute, The Pre-feasibility Study of Pingtan Bridge, 1999.

Observed Pile and Pipeline Performance in the Full-Scale Lateral Spread Experiment

Scott A. Ashford[1] and Teerawut Juirnarongrit[2]

ABSTRACT

Two full-scale experiments using controlled blasting were conducted in the Port of Tokachi on Hokkaido Island, Japan, to assess the performance of lifeline facilities subjected to lateral spreading. Lifeline specimens in this study included a single pile, a 4-pile group, a 9-pile group, two natural gas pipelines, and one electrical conduit. All of them were extensively instrumented with strain gauges to measure the distribution of moment during lateral spreading. This allowed to compute the loading condition, as well as to conduct the damage and performance assessments on the lifeline facilities. Other instrumentation including pore pressure transducers, GPS units, and slope inclinometers, were also installed to measure the degree of liquefaction as well as the movements of soil and lifelines. This paper presents the test results and provides some discussions on the performance of piles and pipelines observed from the experiments.

Scott A. Ashford, Associate Professor, Department of Structural Engrg., Univ. of California, San Diego, La Jolla, CA 92093-0085

Teerawut Juirnarongrit, Graduate Student Researcher, Department of Structural Engrg., Univ. of California, San Diego, La Jolla, CA 92093-0085.

INTRODUCTION

Lateral spreading, which usually refers to global displacements of gently sloping ground due to liquefaction, is one of the primary earthquake hazards. In past earthquakes, lateral spreading has caused considerable damage to civil infrastructure including port facilities, buildings, bridges, and utilities. Good examples are the damage of quay walls and buildings in the 1995 Kobe earthquake; the damage of pile foundations in the 1964 Niigata earthquake; the damage of over 250 bridges and numerous embankments along the Alaskan Railroad and Highway during the 1964 earthquake; the damages of numerous water and gas lines in the 1906 earthquake; and the significant damage in the San Francisco area in 1989 Loma Prieta earthquake (Bartlett and Youd 1992b; Seed 1987; Youd and Hoose 1976; Bardet and Kapuskar 1993; Clough *et al*. 1994; and O' Rourke and Pease 1992). Therefore, it is extremely essential to understand the behavior of soil as well as structures during lateral spreading in order to improve the current design method for structures and lifeline utilities to prevent the catastrophic failure for future earthquakes. Meanwhile, most lateral spreading research to date has focused on small-scale centrifuge studies (e.g. Abdoun *et al*. 1996), limited area 1-g shake table tests (e.g. Tokida *et al*. 1993), or case histories (e.g. Hamada and O'Rourke 1992; O'Rourke 1996). In addition, some full-scale has been carried out to study the behavior of deep foundations in sand liquefied by controlled blasting (e.g. Ashford et al. 2000), but these tests do not account for the global translations of the lateral spreading soil mass. In light of this, the full-scale instrumented lifeline components in controlled lateral spreading tests were carried out in order to understand the performance of lifelines and be able to implement the test results in engineering practice. The test results will be a valuable source of data for further development of the empirical methods and/or complex numeral models to use to design lifeline facilities subjected to lateral spreading.

Two full-scale experiments using controlled blasting were conducted in November and December 2001 in the Port of Tokachi on Hokkaido Island, Japan, to study the performance of lifeline facilities subjected to lateral spreading. This research project was the joint collaboration between the University of California San Diego (UCSD) and several Japanese organizations. This overall research effort was lead by the Port and Airport Research Institute (PARI). The primary objective of the test was to assess the performance of quay walls subjected to lateral spreading using controlled blasting. One quay wall was of traditional design and new seismic design criteria was applied to the other. Since the test area was so large, it enabled researchers to include additional experiments in the zone of liquefaction and lateral spreading without interfering with the primary objective of the quay wall test. The University of California, San Diego, together with Waseda University (WU) collaborated with other Japanese researchers to install the lifeline specimens in the zone of lateral spreading through the PEER Lifelines Program with support from Caltrans, Pacific Gas & Electric and the California Energy Commission.

In all, UCSD installed 6 test specimens. The pile specimens in the experiment program consisted of a single pile, a 4-pile group, and a 9-pile group. In addition, two natural gas pipelines and one electrical conduit were installed. The objectives of this study is to conduct damage and performance assessments of those lifelines subjected to lateral spreading, as well as to evaluate loading conditions on the structures during lateral spreading.

SITE CHARACTERIZATION

The test site was a recent man-made land that was completed just a few years ago. The land was built by hydraulically placing fill without any ground improvement; therefore, the soil was very loose and highly susceptible to liquefaction.

A subsurface soil exploration program was carried out in many areas throughout the test site to characterize the soil condition. Generally, the soil condition consisted of 7.5 m of hydraulic fill underlain by 1 m of medium dense sand overlying a very dense gravel layer as presented in Figure 1. The hydraulic

fill was comprised of a 4-m layer of very loose silty sand with uncorrected SPT-N values ranging from 1 to 5. This was underlain by a 3.5-m layer of very soft lean to fat clay with sand. Uncorrected SPT blow counts ranged from 0 to 2 blows per foot in this layer. The water table was approximately 1 m below the ground surface. Figure 2 presents the grain size distribution of the hydraulic fill plotted together with the Japanese standard curves for liquefaction potential evaluation. The first 4 m of the soil fell into a zone of highly susceptible to liquefaction. Below this layer, fine contents increased with depth. Only a thin layer of soil at depths between 7.0 and 7.5 m was not liquefiable. Based on the results of grain size analysis and the soil strength characteristic, the soil at the test site was highly susceptible to liquefaction, and therefore appropriate for conducting the full-scale lateral spreading test.

SITE DESCRIPTION AND TEST SETUP

The UCSD experiments were located in a zone of the unapplied seismic design quay wall where the large global translation of the soil was expected. A layout of the test site for the first experiment is shown in Figure 3. The test site was approximately 25 m wide by 100 m long. The front face was bordered by a water way. The water elevation was approximately +2.00 m on the test day. The sheet pile quay wall was driven to the elevation of -8.00 m and was anchored by the tied rods which were fixed to H-piles to prevent the movement of the quay wall. The quay wall retained approximately 7.5 m of hydraulic fill. The ground surface started to gently elevate upwards at 25.2 m away from the quay wall with the embankment slope of 4%. The test site was surrounded by the sheet piles to tip elevations between -5.00 and -8.00 m.

The UCSD pile specimens were located 19.0 m away from the quay wall. The pile specimens consisted of a single pile, a 4-pile group, and a 9-pile group. A group of free head single piles of WU were also located in this region. The pile diameters were 318 mm with wall thickness of 10.5 mm, and a nominal length of 11.5 m. The yield strength of these steel pipe piles was 400 MPa.

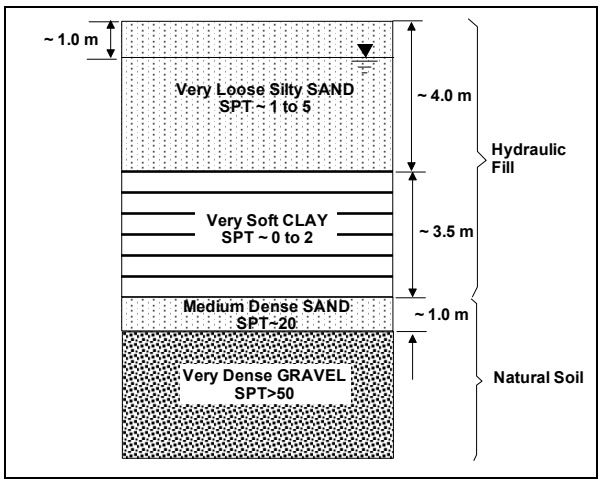

Figure 1. Typical Soil Profile of Test Site.

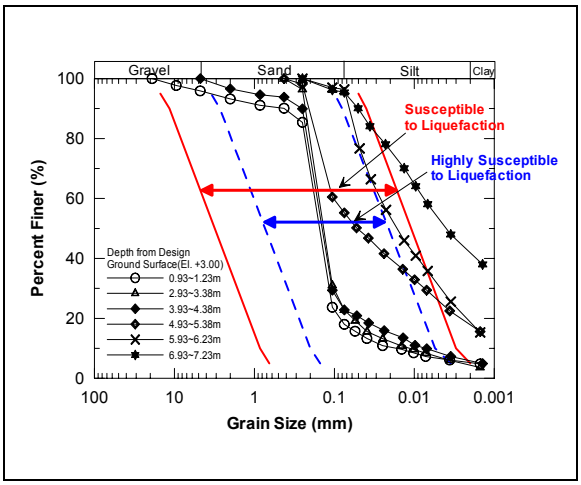

Figure 2. Grain Size Distribution of Soil at Test Site.

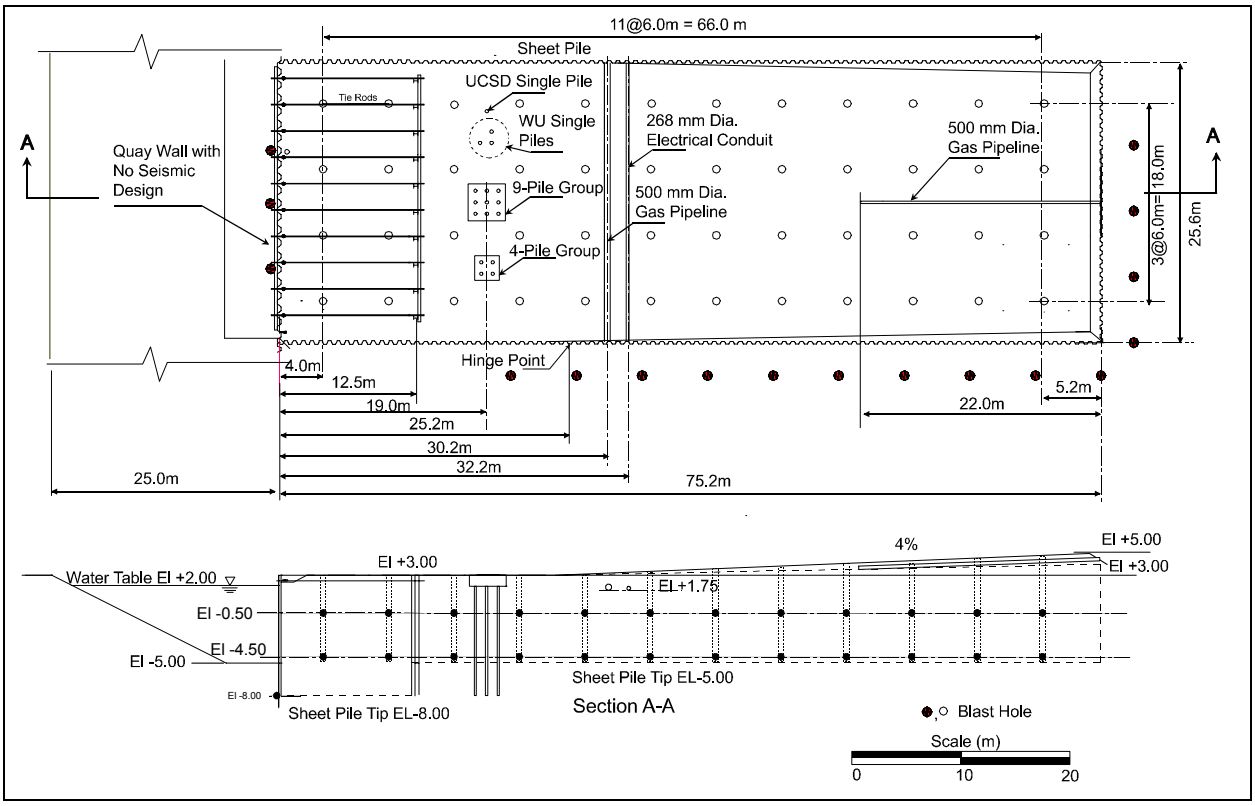

Figure 3. Site Layout of 1st Lateral Spreading Experiment.

In addition, two natural gas pipelines and one electrical conduit were installed. The gas pipeline consisted of a 500 mm diameter pipe with wall thickness of 6 mm and yield strength of 400 MPa. The electrical conduit consisted of a 268 mm diameter with wall thickness of 6 mm and yield strength of 400 MPa. Both pipelines were about 25 m long and located across the test sites at 30 m and 32.2 m away from the quay wall. The bottoms of both pipelines were installed at the elevation of +1.75 m. The other gas pipeline was 22 m long and installed parallel to the direction of the flow. The center of the pipeline was 1 m below the ground surface along its entire length.

Due to the success in using the controlled blast to induce liquefaction of the soil in several tests in Japan as well as the full-scale lateral load tests at Treasure Island (Ashford *et al*. 2000), the same technique was implemented to liquefy the soil at the test site, and thus induce lateral spreading. The blast holes were spaced at 6.0 m on centers in a regular grid pattern. The charges were installed at depths of 3.5 m and 7.5 m below the ground surface. The amount of charges varied from 2 kg nearby the pile specimens to 3-5 kg at other areas. It was done this way so as to prevent damage to a large number of instruments installed in the vicinity of pile specimens. The first experiment was carried out on November 13, 2001. The sequence of the blasting started from the back corner of the embankment and then continued to the next holes of the same rows and proceeded successively towards the quay wall. This was followed by the detonation of the secondary blast holes around the perimeter of the test site. The purpose of these explosives was to loosen the soil in the vicinity of the sheet pile to allow unrestricted flow of the soil in such region. Approximately 20 seconds after the completion of the secondary blasting, the additional explosives were used to break the tie rods of the quay wall and allowed the quay wall to move freely to create additional movement of the soil within the test area.

The second lateral spreading test was performed with an attempt to induce additional ground deformations and further evaluate the performance of lifeline facilities subjected to a higher level of soil deformation. The test site for the second lateral spreading test was significantly modified from the first one as presented in Figure 4. The test site was approximately 30 m wide by 40 m long. The quay wall and sheet piles surrounding the test site were removed to allow the soil to move freely. The waterway was excavated on one end of the test site to an elevation of -1.00 m with the slope of 1:2 and then filled with water to an elevation of +2.00 m. The ground surface was leveled for a distance of 7.5 m away from the edge of the waterway and then started to rise up with an embankment slope of 6% over a distance of 18.0 m. The blast holes were spaced at 6.0 m on centers in a regular grid pattern. Charges were installed at depths of 4.0 m and 8.0 m below the design ground surface (El +3.00m). The amount of charges varied from 2 kg to 4 kg. Two additional rows of blast holes were drilled. One was located on the steep slope adjacent to the waterway with the amount of explosives ranging from 1 to 3 kg. The purpose of these explosives was to loosen the soil at the slope toe prior to the primary blasting sequence such that the embankment soil behind it had a high potential to move freely with larger deformation once the primary blasting initiated. The other was located between the pipelines and piles as denoted as blast holes No. 7 to No. 9. Three kilograms of explosives were installed at El. -3.00 m.

The weather condition for the second lateral spreading experiment was poor as presented in Figure 5 due to a heavy snowfall with a snow thickness of about 0.50 m and a new record of wind speed of 100 kph on the test day. The ground was frozen throughout the test site which would likely impede the global translation of the soil mass. In an attempt to mitigate this, jackhammers were used to break up the frozen ground in the vicinity of test specimens to depths of approximately 20 to 30 cm below the ground surface as presented in Figure 6. The second test was carried out on December 14, 2001. The explosives on the steep slopes were detonated initially from S1 to S5. Approximately 15 second later, the primary sequence of the blasting was started. The primary blast began at blast hole No.1 on the back of the embankment. Then, the blasting proceeded to the next holes of the same rows, and then continued to the next row towards the waterway (i.e., from No.1 to No.17).

INSTRUMENTATION

Piles and pipelines were extensively instrumented with electrical strain gauges. The strain gauges of pile specimens were located at 0.6 m intervals on both upstream and downstream sides of the piles to measure the bending moment along the length of the pile. A series of tiltmeters at various depths were also installed on one pile of each foundation system to use as backup data for strain gauges. Unfortunately, all of them were damaged during the pile installation. The 75x40x5 steel channels with yield strengths of 400 MPa were welded to the steel pipe piles to protect the strain gauges from damage during the pile installation. The strain gauges of the gas pipeline were spaced between 1.0 m and 3.0 m along the top and the side of the pipelines to measure the bending moment along the pipelines in both vertical and horizontal directions, respectively.

Apart from the strain gauges, other instrumentation was also installed to capture behaviors of soil and lifelines in more details. These include pore pressure transducers, soil pressure cells, string-activated linear potentiometers, accelerometers, slope inclinometer casings, and Global Positioning System (GPS) units. A layout of instrumentation for the first experiment is presented in Figure 7. The instrumentation for the second experiment was essentially the same as the first test; therefore, it is not shown in this paper.

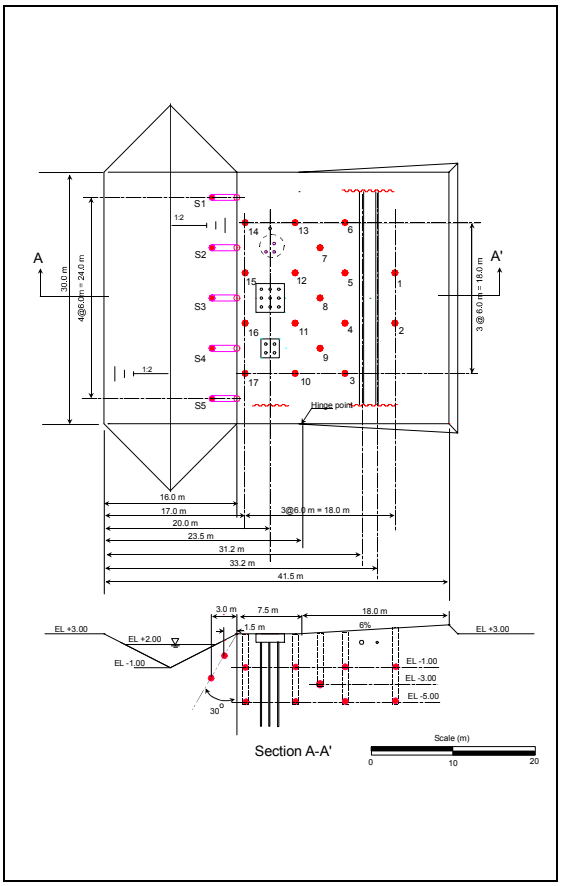

Figure 4. Site Layout of 2nd Lateral Spreading Experiment.

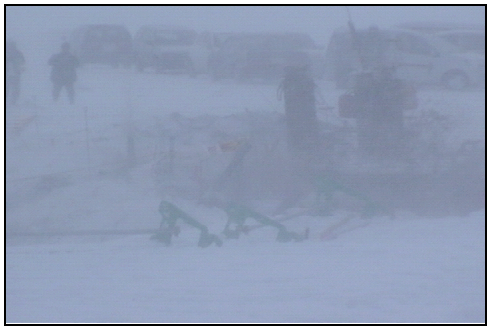

Figure 5. Poor Weather Condition during 2nd Lateral Spreading Experiment.

Figure 6. Breaking up Frozen Ground Surface Using Jack Hammer.

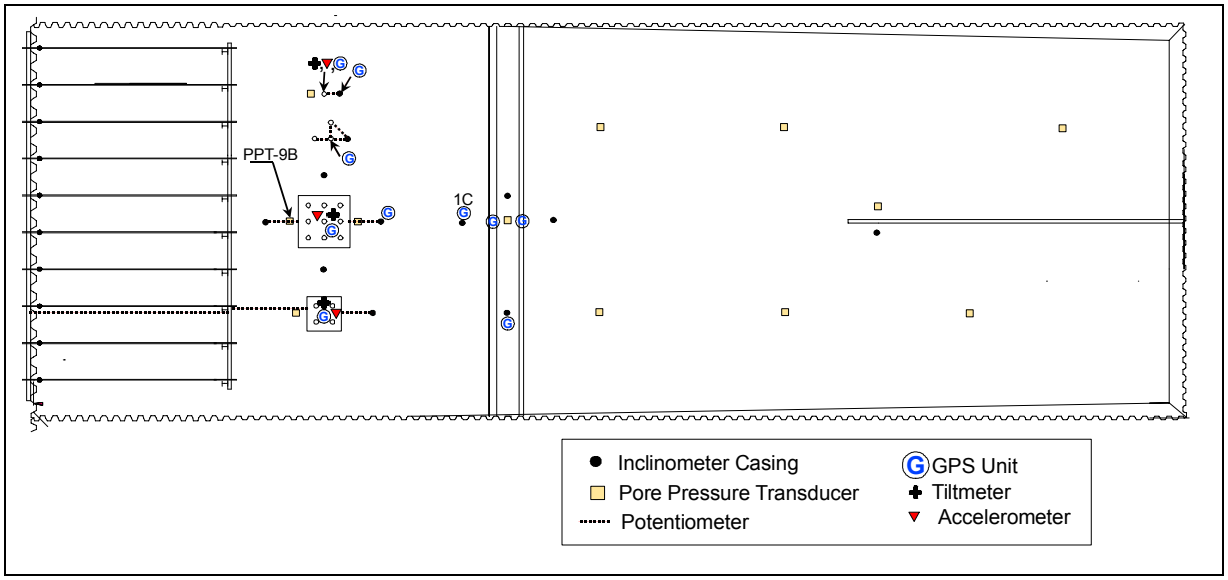

Figure 7. Instrumentation Plan for 1st Lateral Spreading Test.

TEST RESULTS

Excess Pore Water Pressure

An example of excess pore water pressure ratio time-history nearby the 9-pile group at depth of 2 m below the ground surface is presented in Figure 8. The excess pore water pressure ratios built up immediately after the blast though this transducer was located about 50 m away from the first blast hole. The rate of increase in pore water pressure became more rapid as the blast moved closer to the transducers. The increase in pore water pressure ratios proceeded to reach the maximum values at approximately 30 seconds. Fluctuation of pore pressure ratios was obvious as the blasting occurred in the vicinity of the transducer location. The results show that the soil in the vicinity of the 9-pile group was liquefied with the maximum excess pore pressure ratios exceeding 100%. The ratios dropped to about 80% after the blast stopped, then proceeded to dissipate with time. The evidence of increase in excess pore water pressure ratio at times of about 40s and 86s was due to the effect of the secondary blasting of tied rods, respectively. The characteristics of excess pore water pressure ratios in other locations were basically the same as the one presented herein. The excess pore water pressure ratios throughout the entire test site exceeded 70%. Some of them were slightly over 100%. Sand boil was observed following the blasting as presented in Figure 9 confirming that the liquefaction had occurred.

The excess pore pressure ratios in the 2nd test appeared to be much less than those measured during the first test with values ranging between 30% and 80%. No sand boil was observed in the 2nd test. Two possible reasons can be explained regarding the lower excess pore pressure ratios. First, the soil was less susceptible to liquefaction because some settlement took place after the first experiment and caused the soil to become denser. Second, the frozen ground decreased the liquefaction potential due to terrible weather in the second test.

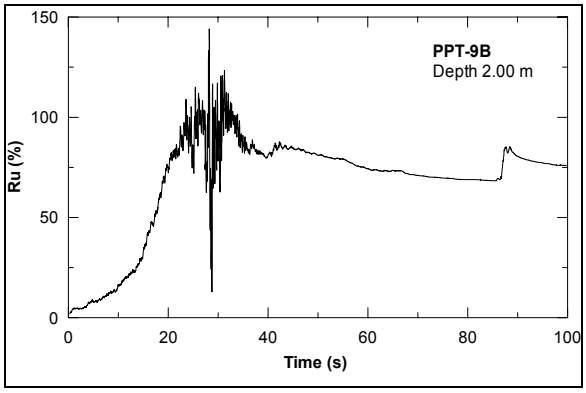

Figure 8. Excess Pore Pressure Ratio vs. Time nearby 9-Pile Group.

Figure 9. Sand Boil after the 1st Experiment.

Deformations of Ground and Lifelines

The GPS units were used to monitor the movements of both ground and lifeline facilities during lateral spreading. The measurements were conducted by a research team from the California Department of Transportation, Caltrans (Turner 2002). An example of time history of soil movements on the downstream side of the gas pipeline (denoted as unit 1C) in longitudinal, transverse, and vertical directions is presented in Figure 10a. The movements of GPS units were observed at about 10 seconds after blasting initiated. As the blasting moved closer to the GPS location, more movements in all directions were observed. The lateral movements between 10 seconds and 27 seconds were due to not only the liquefaction-induced lateral spreading but also the dynamic forces generated by the blasting. With the blasting past the location of GPS units (at about 27 seconds), the effect of dynamic forces from the blasting was not important as indicated by the insignificant movements in transverse and vertical directions. The longitudinal movement observed after 27 seconds was therefore primarily due to liquefaction-induced lateral spreading. Figure 10b presents the displacement path of GPS unit in the horizontal plane of the gravel surface showing that the horizontal movement mainly occurred in the longitudinal direction towards the quay wall.

The vector displacements in the horizontal plane throughout the test site for the first test are presented in Figure 11a. The largest horizontal displacement was about 43 cm occurring at the pile head of the WU pile. The UCSD single pile moved only 32 cm, which was significantly less than the WU piles. This was likely due to the fact that the WU piles were shorter in length and the pile tips were located just above the dense layer; while the UCSD pile was penetrated about 3.5 meters into the dense soils. The WU piles were therefore likely behaved as rigid piles, in which the rotation and movement at the pile tip were expected. In contrast, the UCSD pile acted as a flexible pile where the rotation and the movement at the pile tip was insignificant. As a result, the displacement at the pile head of the UCSD single pile was less than those of the WU piles. The 4-pile group and the 9-pile group moved 21cm and 18 cm, respectively. The data from the GPS units in the vicinity of the pipelines show that the movements of the gas pipeline and electrical conduit were similar with a magnitude of about 38 cm. The average of soil movement was about 35 to 40 cm.

As presented in Figure 11b, the horizontal movements occurred in the second test were generally lower than those occurred in the first test, especially in the vicinity of the pipelines. This was mainly due to the weather condition that decreased the liquefaction potential and thus impeded the global translation. The movement of the gas pipeline was about 50% of that occurred in the first test. The average soil movement in the second test ranged from 10 cm to 23 cm. One GPS unit installed between two pile caps showed the soil movements as high as 45 cm. However, 10 cm of 45 cm attributed to the movement of slope toe due to the effect of initial blasting along the slope edge. The movement of pile groups in the 2nd test ranged from 16 cm to 18 cm, slightly less than that in the first test. The movements of WU and UCSD single piles at the ground surface were 39 cm and 28 cm, respectively.

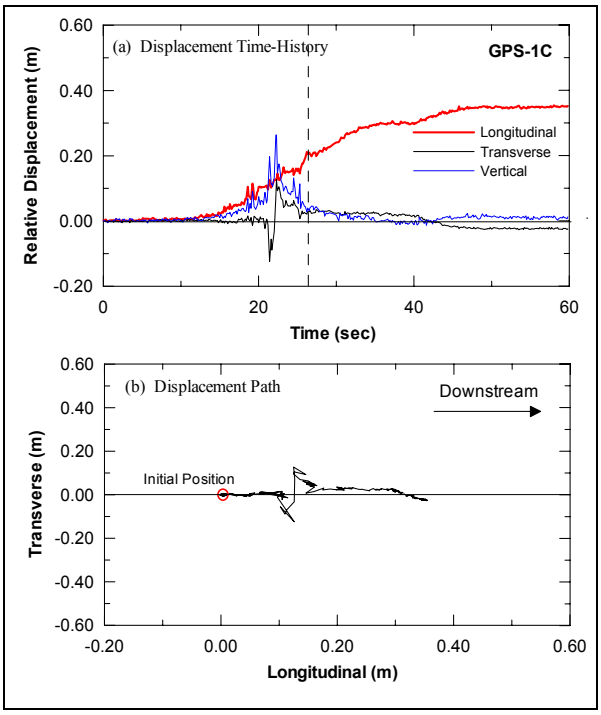

Figure 10. GPS Data (a) Displacement Time-History, and (b) Displacement Path (after Turner 2002).

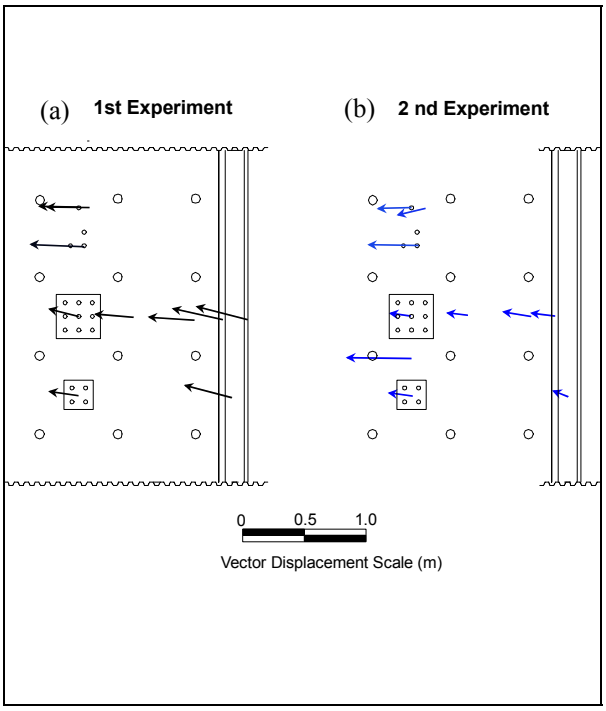

Figure 11. Vector Displacements from GPS Data for 1st and 2nd Experiments (after Turner 2002).

Moment Distribution

Moment distribution along the length of the single pile at the end of the test is presented in Figure 12. The test results indicate that the moments at depths between 0m and 4m were insignificant. One possible explanation for this phenomenon is that after the soil was liquefied, it comes to behave like a viscous fluid material, being able to flow around the pile without significant force acting on the pile. The soil resistance began to increase with depth for the next 3.5 m where a very soft clay layer existed. The maximum moment occurred in a dense soil layer at a depth of about 9 m below the ground surface. The pile was yielded after the second test.

Figure 13 presents the moment distribution of pile No.5 in the 9-pile group. The shape of moment profile from the experiment agreed well with a typical analysis of a pile with fixed head condition showing that the results from the test were reasonable and appropriate for further analysis to estimate the loading distribution of liquefiable soil on the pile. Figure 14 presents the moment profile of each pile in the group after the first experiment. The moment distribution of all piles in the 9-pile group was more or less similar, except for pile No. 2 and No.4 where the moments were smaller than the others. This is likely due to the fact that both piles were shorter in length, and had a smaller degree of fixity into the dense soil layer, resulting in a smaller moment in the piles. It is noted that pile No. 2 and No.4 reached refusal during the pile installation, likely due to the presence of a boulder at that particular depth. The similarity of moment distribution of each pile in the group indicates that a shadowing effect was unimportant in liquefied soil. This conclusion was similar to that of a recent research on the behavior of pile group in liquefied soil conducted at Treasure Island (Ashford and Rollins 2002).

After the second test, all piles in the 4-pile group and the 9-pile group remained elastic with the maximum moment below 70% and 60% of yield moment, respectively. No structural damage was observed on piles to pile cap connections on both pile groups though both pile groups experienced the total movements of nearly 40 cm. In addition, based on the strain gauge data of pipelines (not presented in this paper), all pipelines performed comparatively well without any yielding.

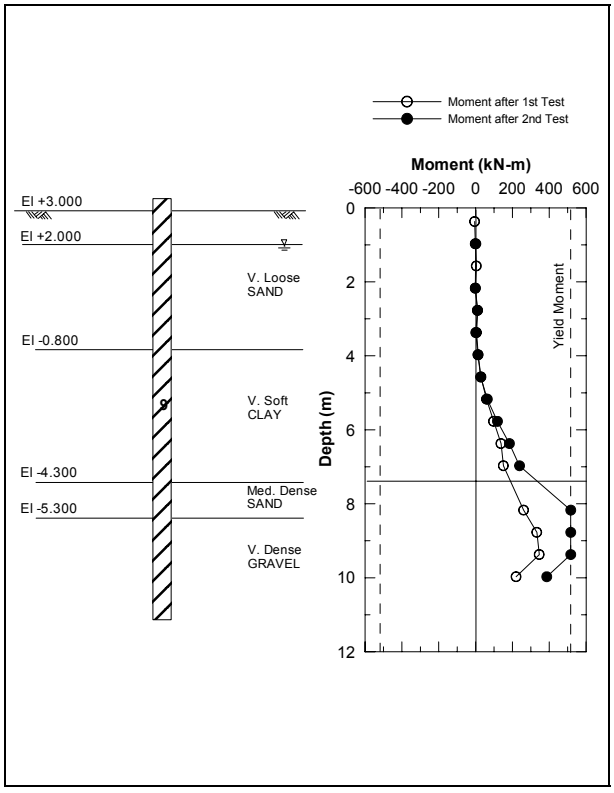

Figure 12. Moment along Single Pile.

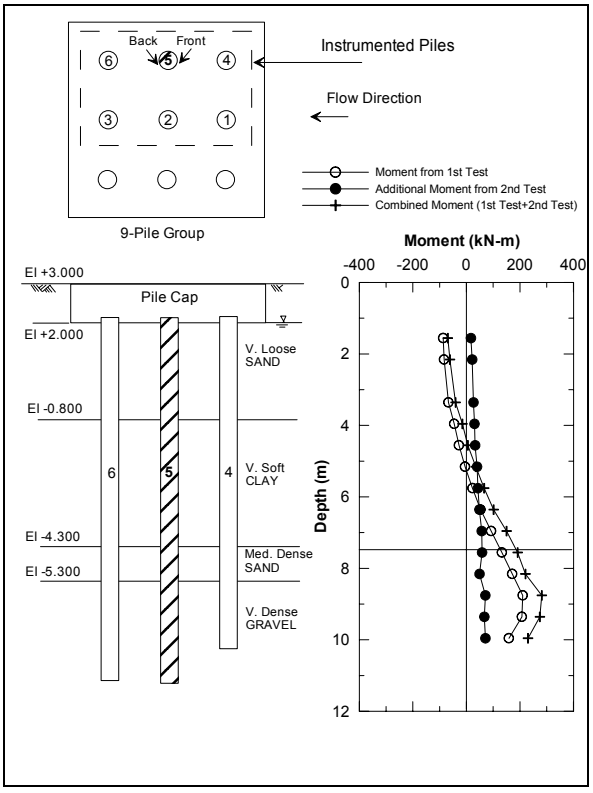

Figure 13. Moment along Pile No.5 of 9-Pile Group.

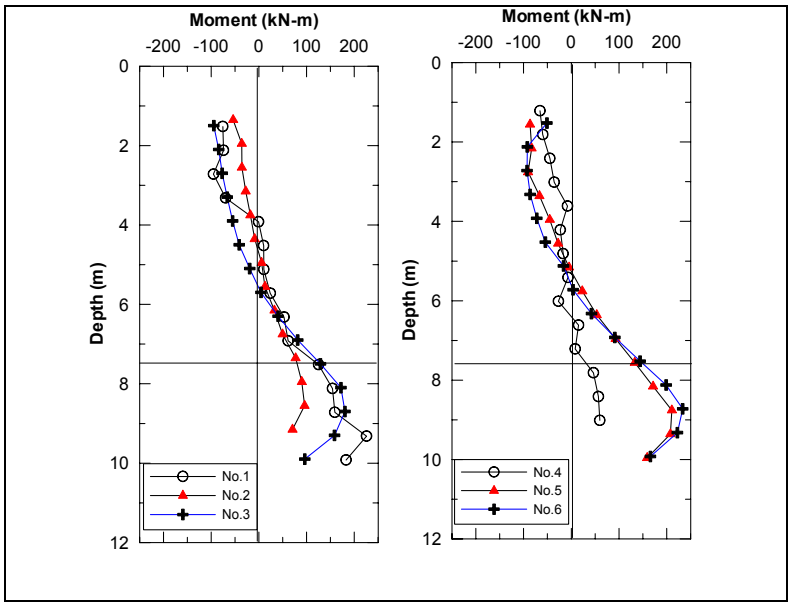

Figure 14. Moment Distribution of Each Pile in the 9-Pile Group (Data Extracted from 1st Experiment).

CONCLUSIONS

Based on the results obtained from two full-scale experiments, the following conclusions can be obtained:

1. Controlled blasting successfully liquefied the soil and induced lateral spreading.
2. The excess pore water pressure ratios exceeded 70% for the first experiment. The degree of liquefaction in the second experiment was much lower than the first one with excess pore pressure ratios ranging between 30% and 80%, likely due to the weather condition.
3. The average soil movements of the first experiment were about 35 cm to 40 cm, while about 9 cm to 22 cm of ground movements were observed in the second test.
4. The total movements of the single pile, 4-pile group, and 9-pile group were 58 cm, 39 cm, and 34 cm, respectively.
5. The total movements at the middle of the gas pipeline and electrical conduit were about 54 cm.
6. Shadowing effect of the 9-pile group in liquefied soil was not observed.
7. The single pile yielded at the end of the second experiment. Both 4-pile and 9-pile groups performed well during both experiments. Piles remained in elastic range with maximum moments of less than 70% of yield moment. No damaged was observed on piles to pile cap connection.
8. All pipelines also performed very well without any yielding.

ACKNOWLEDGEMENT

The authors wish to express their sincere gratitude to the sponsors of the Performance of Lifelines Subjected to Lateral Spreading project, PEER Lifelines Program with support from Caltrans, Pacific Gas & Electric and the California Energy Commission.

The assistance from Dr. Takehiro Sugano of Port and Airport Research Institute (PARI) and Professor Masanori Hamada from Waseda University(WU), the original leaders of this project, in providing a great opportunity for us to participate in this test, as well as effectively managing the project is gratefully acknowledged. Loren Turner, Cliff Roblee and Tom Shantz from Caltrans' Division of New Technology and Research are gratefully acknowledged for their help in monitoring the movements of soil and lifelines using GPS equipments.

We would like to thank Andrea Martinez and Jeremy Allen, the undergraduate students, for their help in analyzing the data and preparing the figures in this paper.

REFERENCES

Abdoun, T. Dobry, R., and O-Rourke, T. D., 1997. "Centrifuge and numerical modeling of soil-pile interaction during earthquake induced soil liquefaction and lateral spreading," *Observation and Modeling in Numerical Analysis and Model Tests in Dynamic Soil-Structure Interaction Problems, Geotechnical Special Publication No. 64*, ASCE, New York, pp.64-70.

Ashford, S. A., Rollins, K. M., 2002. *TILT: Treasure Island Liquefaction Test Final Report, Report No. SSRP-2001/17*, Department of Structural Engineering, UCSD.

Ashford, S. A., Rollins, K. M., Bradford, S. C., Weaver, T. J., and Baez, J. I., 2000. "Liquefaction mitigation using stone columns around deep foundations: fill-scale test results," *Soil Mechanics 2000, Transportation Research Record No. 1736*, TRB, Washington D.C., pp.110-118.

Bardet, J. P., and Kapusker, M., 1993. "Liquefaction sand boils in San Francisco during 1989 Loma Prieta earthquake." *J. Geotech. Engrg.,* ASCE, Vol. 119, No.3, March, pp. 543-562.

Bartlett, S. F. and Youd, T. L., 1992b. "Empirical analysis of horizontal ground displacement generated by liquefaction-induced lateral spreads." *Tech. Rep. NCEER-92-0021*, National Center for Earthquake Engineering Research, Buffalo, N.Y., M. Hamada and T.D. O'Rourke (eds.), August 17.

Clough, G. W., Martin, J. R., II, and Chameau, J. L., 1994. "The geotechnical aspects." *Practical Lessons from the Loma Prieta Earthquake*, National Research Council, National Academy Press, Washington, D.C., pp. 29-63.

Hamada, M., and O'Rourke, T., Editors., 1992. *Case Studies of Liquefaction and Lifeline Performance During Past Earthquakes, Report No. NCEER-92-0001, Vol.1*, National Center for Earthquake Engineering Research, Buffalo, N.Y.

O'Rouke, T. D., 1996. "Lessons learned for lifeline engineering from major urban earthquakes," *Proceedings, Eleventh World Conference on Earthquake Engineering, Elsevier Science Ltd*., 18 p.

O'Rouke, M. J., and Pease, J. W., 1992. "Large ground deformations and their effects on lifeline facilities: 1989 Loma Prieta earthquake." *Case Studies of Liquefaction and Lifeline Performance During Past Earthquakes, Volume 2: United States Case Studies, Tech. Rep. NCEER-92-0002*, M. Hamada and T.D. O'Rourke (eds.), February 17, 85 pages.

Seed, H. B., 1987. "Design problems in soil liquefaction." *J. Geotech. Engrg.,* ASCE, Vol. 113, No. 8, August, pp. 827-845.

Tokida, K., Iwasaki, H., Matsumoto, H., and Hamasa, T., 1993. "Liquefaction potential and drag force acting on piles in flowing soils," *Soil Dynamic and Earthquake Engineering*, Computational Mechanics, South Hampton, England, pp. 349-364.

Turner, L. L., 2002. *Measurements of Lateral Spread Using a Real Time Kinematic Global Positioning System*, California Department of Transportation Division of New Technology &Research, April 2002, 94 pages..

Youd, T. L., and Hoose, S. N., 1976. "Liquefaction during 1906 San Francisco Earthquake." *J. Geotech. Engrg. Div.*, ASCE, Vol. 102, No. GT5, May, pp. 425-439.

Seismic Response of Railway Bridges Considering TRACK Restriction

Guiping Yan[1], Yan Huang[1] and Guanyuan Zhao[1]

ABSTRACT

A simplified model is introduced to describe the dynamic interaction between track and bridge spans. With the model a track-beam model is established and the nonlinear dynamic FEM program is developed to analyze the effects of track restriction to the seismic response of railway bridges. Through the numerical analysis, it is shown that the existence of track is helpful for the piers with lower stiffness to resist earthquake, otherwise for the stiffer piers it may be harmful. By considering the variant track resistance, number of bridge spans, and pier stiffness distribution, the effects of track on the seismic response of railway bridges are discussed.

[1] College of Civil Engineering and Architecture, Northern Jiaotong University, Beijing, 100044, PRC

INTRODUCTION

Bridges play an important role in the railway transportation system. With the use of long rail track, a much stronger connection between bridge spans is provided. How to consider the effects of long rail track on earthquake properties of bridges is still a problem to be studied. The existence of stronger track restriction can cause the variation of the bridge dynamic characteristics, change the internal force distribution, and therefore affect the behavior of bridge during earthquakes. Some research works show that the existence of track can provide an additional restriction to transfer the seismic loads to the roadbed. Thus, the structural elements of the bridge can be partly relieved from the demand to carry all of the seismic loads[1]-[3]. Maragakis has measured the frequencies and damping properties of the Strawberry Park Railway Bridge, and investigated the effects of the rails on the dynamic response of the bridge[1]. The experimental results shows that with the existence of track, the vibration transferred to the adjacent roadbed is obvious. When the rails are cut, the fundamental frequencies of bridges in different directions are decreased. The full-scale experiments by Luo on the simply supported railway bridges also show that the track has the considerable restriction on railway bridges along the longitudinal direction, but they had few function in the transverse direction[3].

So far, no systematical research works have been done about the effects of track restriction on the seismic response of railway bridges. The effects of track are usually neglected in the seismic analysis of railway bridges; therefore the influence of the track on the seismic response of bridges can not be exactly evaluated. CWRs (Continuously Welded Rails) have been used on high-speed railway bridges in many countries. In China, CWRs are also used on some long bridges. With the wide use of CWRs on railway bridges, the effects of track on the seismic response of railway bridges should be further studied.

In this paper, a simplified method of describing the interaction between rails and bridge is developed, in which the beam, rails and roadbed are regarded as a hybrid beam-track element. The beam-track element is consisted of segments of beam-track element. The elasto-plastic relation in the roadbed for each segment is determined according to the real states. The DOF reduction method is used to form the stiffness matrix of the hybrid beam-track element. Based on this, the earthquake response is solved.

ANALYSIS MODEL

Basic Assumption

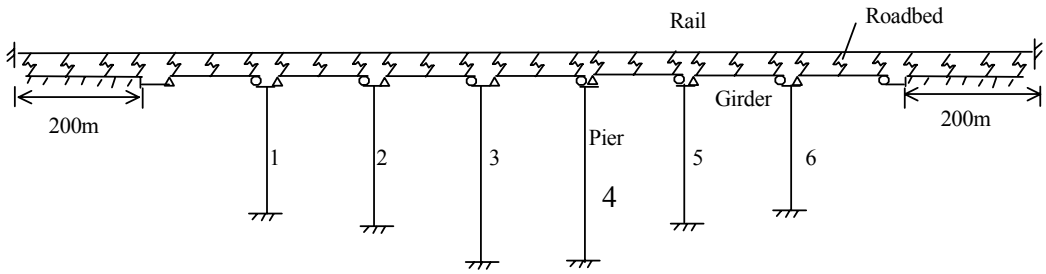

Figure 1 Structural model

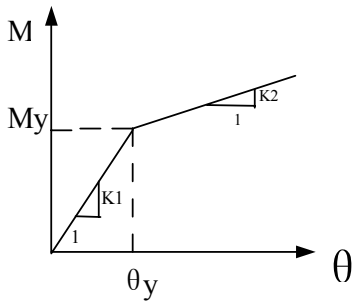

Figure 2 Bilinear model of piers

For the structural system shown in Figure 1, the motion equation of the structure can be expressed as:

$$M\ddot{x} + C\dot{x} + Kx = MI\{\ddot{x}_g\} \tag{1}$$

where M , K , and C are the mass, stiffness, and damping matrixes, $\ddot{x}, \dot{x}, x$ and $\ddot{x}_g$ are the vectors of acceleration, velocity, displacement, and ground acceleration, respectively.

Rails and beams are modeled as linear beam elements and the nonlinear properties are considered about the interaction between track and beams. The non-linear characteristics of piers are defined as the bilinear institute relation as shown in Figure 2. The tracks outside the bridge will share the deformation and longitudinal forces. In the analysis, the length of the rails outside the bridge is selected as 200m.

Nonlinear Properties of Piers

Following conditions are assumed in the analysis. (1) The pier bottom is fixed to the foundation and the interaction between the foundation and soil is ignored. (2) The relationship between the moment (m) at pier bottom and the rotation angle at pier top (θ) is given by:

$$m = \frac{3EI}{l} \cdot \theta \tag{2}$$

where *EI /l* is the linear stiffness of piers. The yielding moment is defined as the moment that the outside reinforcements of pier section begin to yield. The pier stiffness after yield (k_2) is assumed as 10% of the initial one (k_1) .

Interaction Between Track and Beams

Under an intense earthquake, the relative displacements between beam and track will occur. Because of the roadbed resistance, the longitudinal forces will be applied to the rails and beams. The relationship between relative deformation and longitudinal forces are shown in Figure 3.

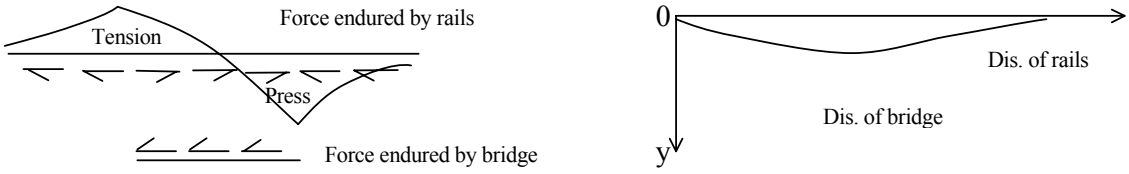

(a) Longitudinal forces (b) Deformation

Figure 3 Deformation and longitudinal forces in the rails and bridge

In order to simulate the interaction correctly, an elasto-plastic model is used to represent the force-displacement relationship of the roadbed, as shown in Figure 4[4][5].

A series of nonlinear springs are used to model the function of track resistance. Only when the space between two adjacent spring elements is small enough the model can have enough accuracy. Therefore the beam, rails, and roadbed are divided into many small segments and nonlinear spring elements. To simplify the data preparation and input works, all sub-elements within one span are combined to form a hybrid beam-track element. The stiffness matrix and its nonlinear characteristics of the hybrid element is calculate by a subroutine and formed by DOF reduced technique.

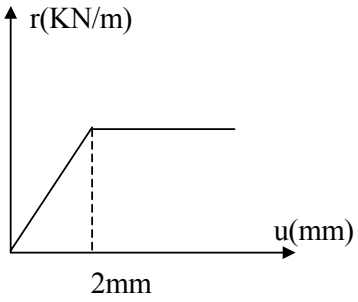

Figure 4 Model of roadbed

The mesh of beam-track element is shown in Fig5, where I, J, K, L are the nodes of the hybrid element. The interaction between the roadbed and the rail is modeled in a similar way.

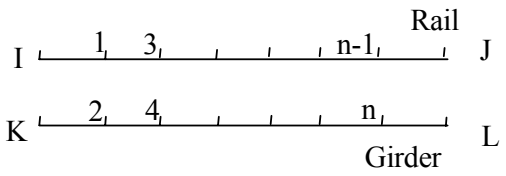

Figure 5 Beam-track element

DEDUCTION OF THE STIFFNESS MATRIX OF THE BEAM-TRACK ELEMENT

Distributed Resistance of Roadbed at Linear Stage

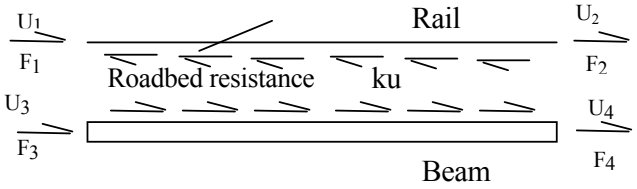

Figure 6 The beam-track element

In Figure 6, u_1, u_2, F_1, F_2 are the displacements and forces at rail ends, u_3, u_4, F_3, F_4 are the displacements and forces at beam ends, respectively. u_r and u_b are the displacements along rail and beam. u_0 is the displacement corresponding to the position where the roadbed begin to yield. When $-u_0 < u_r - u_b < u_0$, resistance of roadbed is a linear function of $u=u_r - u_b$ and distributed resistance in roadbed is ku. Let Young's module and section area for rail are E and A for beam are E_b and A_b respectively. Assuming that the resistance has no effects on the deformation of beam, the displacement of beam is linear one, that is $u_b = u_3 + \frac{x}{L}(u_4 - u_3)$.

The differential equation of the rail is:

$$AE \frac{d^2 u_r}{dx^2} - ku = 0 \tag{3}$$

Assume $\lambda^2 = \frac{k}{EA}$

The solution of the differential equation is

$$u_r = c_1 e^{\lambda x} + c_2 e^{-\lambda x} + \frac{u_4 - u_3}{L} x + u_3 \tag{4}$$

According to the boundary conditions, with the linear assumption of roadbed resistance the element stiffness matrix can be given as:

$$\begin{pmatrix} F_1 \\ F_2 \\ F_3 \\ F_4 \end{pmatrix} = \begin{bmatrix} EA\frac{\lambda\gamma}{\alpha} & EA\frac{-2\lambda}{\alpha} & EA\frac{\beta}{L\alpha} & EA\frac{2\lambda L-\alpha}{L\alpha} \\ EA\frac{-2\lambda}{\alpha} & EA\frac{\lambda\gamma}{\alpha} & EA\frac{2\lambda L-\alpha}{L\alpha} & EA\frac{\beta}{L\alpha} \\ EA\frac{\beta}{L\alpha} & EA\frac{2\lambda L-\alpha}{L\alpha} & \frac{E_b A_b}{L} - EA\frac{\beta}{L\alpha} & -\frac{E_b A_b}{L} - EA\frac{2\lambda L-\alpha}{L\alpha} \\ EA\frac{2\lambda L-\alpha}{L\alpha} & EA\frac{\beta}{L\alpha} & -\frac{E_b A_b}{L} - EA\frac{2\lambda L-\alpha}{L\alpha} & \frac{E_b A_b}{L} - EA\frac{\beta}{L\alpha} \end{bmatrix} \begin{pmatrix} u_1 \\ u_2 \\ u_3 \\ u_4 \end{pmatrix} \tag{5}$$

where $\begin{cases} \alpha = e^{\lambda L} - e^{-\lambda L} \\ \gamma = e^{\lambda L} + e^{-\lambda L} \\ \beta = (1-\lambda L)e^{\lambda L} - (1+\lambda L)e^{-\lambda L} \end{cases}$

Resistance of Roadbed at Nonlinear Stage

When the relative displacement between rail and beam $u_r - u_b$ is greater than u_0, the maximum resistance of roadbed is m, and the equilibrium differential equation of the rail is $AE\frac{d^2 u_r}{dx^2} = m$. When $u_r - u_b$ is less than $-u_0$, $AE\frac{d^2 u_r}{dx^2} = -m$.

Assuming that $u_r - u_b$ is greater than u_0, we have

$$\frac{d^2 u_r}{dx^2} = \frac{m}{AE} \tag{6}$$

The solution of the differential equation is

$$u_r = \frac{1}{2}\left(\frac{m}{EA}\right)x^2 + c_1 x + c_2 \tag{7}$$

According to the boundary conditions, the element stiffness matrix can be developed can be given as when the resistance of the roadbed is linear:

$$\begin{Bmatrix} F_1 - \frac{1}{2}mL \\ F_2 - \frac{1}{2}mL \\ F_3 + \frac{1}{2}mL \\ F_4 + \frac{1}{2}mL \end{Bmatrix} = \begin{bmatrix} \frac{EA}{L} & -\frac{EA}{L} & & \\ -\frac{EA}{L} & \frac{EA}{L} & & \\ & & \frac{E_bA_b}{L} & -\frac{E_bA_b}{L} \\ & & -\frac{E_bA_b}{L} & \frac{E_bA_b}{L} \end{bmatrix} \begin{Bmatrix} u_1 \\ u_2 \\ u_3 \\ u_4 \end{Bmatrix} \tag{8}$$

DOF Reduction

To reduce the element input work, the DOFS of each beam and rail segment should be eliminated and only the DOFS of beam and rail nodes at span ends are left.

To establish the system equation, the relation of stiffness matrix and nodal displacement vector can be written as:

$$\begin{bmatrix} K_{bb} & K_{bi} \\ K_{ib} & K_{ii} \end{bmatrix} \begin{Bmatrix} a_b \\ a_i \end{Bmatrix} = \begin{Bmatrix} P_b \\ P_i \end{Bmatrix} \tag{9}$$

Where a_b and a_i are displacement vectors at boundary and inner nodes respectively.

From equation (9):

$$a_i = K_{ii}^{-1}(P_i - K_{ib}a_b) \tag{10}$$

Substitute equation (10) into equation (9), we have:

$$(K_{bb} - K_{bi}K_{ii}^{-1}K_{ib})a_b = P_b - K_{bi}K_{ii}^{-1}P_i \tag{11}$$

or simply: $$K_{bb}^{*}a_b = P_b^{*} \tag{12}$$

where $$K_{bb}^{*} = K_{bb} - K_{bi}K_{ii}^{-1}K_{ib}$$

$$P_b^{*} = P_b - K_{bi}K_{ii}^{-1}P_i \tag{13}$$

If a_i is a vector with k element, equation (12) can be got by using Gauss-Jordan elimination k times to equation (9). That is to get the result:

$$\begin{bmatrix} K_{bb}^{*} & 0 \\ K_{ib}^{*} & I \end{bmatrix} \begin{Bmatrix} a_b \\ a_i \end{Bmatrix} = \begin{Bmatrix} P_b^{*} \\ P_i^{*} \end{Bmatrix} \tag{14}$$

where K_{bb}^{*}, P_b^{*} are the stiffness matrix and load vector of the substructure after eliminating, and K_{ib}^{*}, P_i^{*} are the corresponding matrix related to inner nodes.

$$\begin{aligned} P_i^{*} &= K_{ii}^{-1} P_i \\ K_{ib}^{*} &= K_{ii}^{-1} K_{ib} \end{aligned} \tag{15}$$

Verification of the Program

With the results given above, the nonlinear dynamic program is developed based on Wilson-θ method. The following 3-span bridge with the same piers is selected to check the reliability of the program. The height, section size, and reinforcement ratio of the piers are 10m, 1.75m×1.75m and 1%, for the spans, the span length and section area are 32m, 2.32m^2, and the roadbed resistance factor is 10KN/m. By inputting the El Centro ground motion, the result given by the program is compared with that given by ANSYS program. In the analysis later, the discrete nonlinear spring models are used. The pier displacements from both analysis are shown in Figure 7. It gives the good consistent.

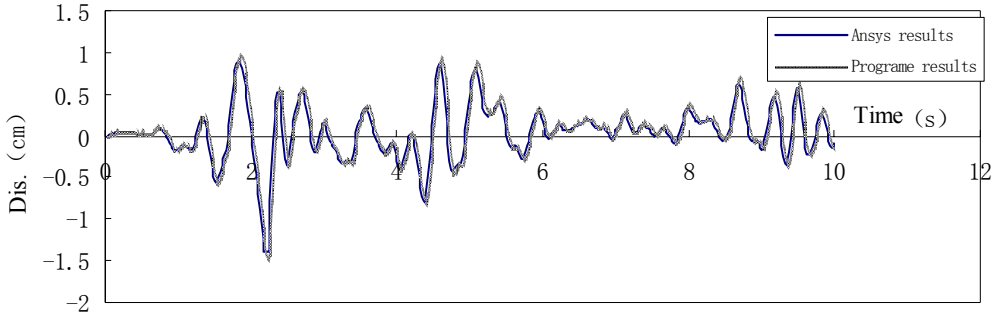

Figure 7 Comparison of results

EFFECTS OF TRACK RESTRICTION ON THE SEISMIC RESPONSE OF BRIDGES WITH THE SAME PIERS

The effects of track on the seismic response of a railway bridge is also affected by other factors, such as the characteristics of piers, the roadbed conditions, and the span numbers, etc. Therefore the discussion will be given according to different cases.

A simply supported railway bridges with piers of equal heights and section are used to seismic response analysis. The bridges have the pre-reinforced concrete T-shaped superstructures with the reinforced concrete substructures. The span length is 32m.

The longitudinal roadbed resistance coefficient is 10KN/m. In following table, the main parameters of the piers are listed for various cases.

TABLE I PARAMETERS OF PIERS

Heights (m)	6	10	14	18	22	26
Section size （m×m）	1.5×1.5	1.75×1.75	2.0×2.0	2.25×2.25	2.5×2.5	2.75×2.75
Stiffness （MN/m）	96	39	25	19	16	14
Yielding moment (KN-m)	6020	9760	14790	21300	29490	39560

Under the excitation of EL Centro ground motion record, the displacements of the left pier tops with and without track restriction are shown in Figure 8.

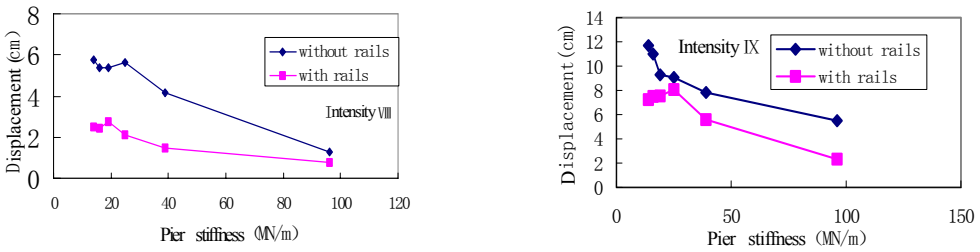

(a) Displacements for intensity Ⅷ (b) Displacements for intensity Ⅸ

Figure 8 Seismic response of bridges

It can be seen that the displacements of the pier tops are reduced when the rails are taken into account. Fore this bridge the displacements are reduced by 10%~50%. The degree of reduction relates to the structure, the site, and the seismic parameters.

Influence of Roadbed Resistance

According to the real track resistance, 3 resistance coefficients of roadbed, i.e. 10kN/m, 15kN/m, 20kN/m are chosen, to study how the change of the roadbed resistance affects the seismic response of bridge. Two ground motion records, the EL Centro S00E and Los Angeles N00W are used in the analysis. With different roadbed resistance, the displacements of the pier top under intensity Ⅷ and Ⅸ are shown in Figure 9 (a) and Figure 9 (b), respectively.

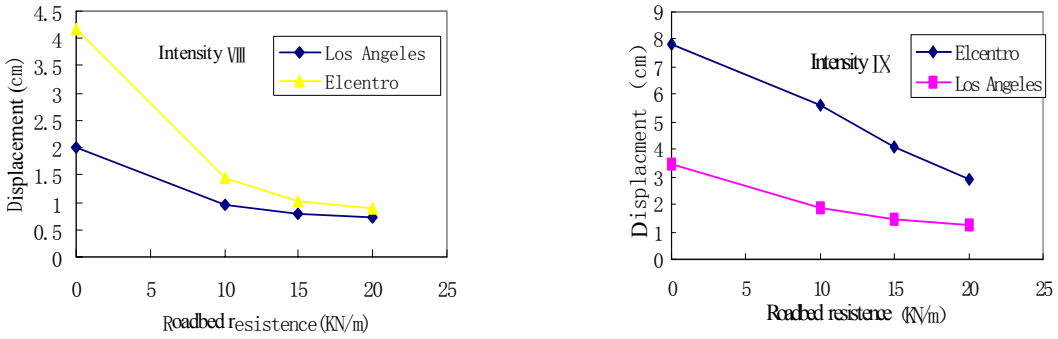

(a) Displacements for intensity Ⅷ (b) Displacements for intensity Ⅸ

Figure 9 Influence of roadbed resistance on the seismic response of bridge

The results show that with the increase of the roadbed resistance, the responses of the bridge are reduced, but for different earthquake intensity the reduction have different features.

Influence of Span Numbers

By considering different span number of bridge, the effects of the track restriction are further discussed. With the same conditions and excitations the seismic response of bridge for various span number are given in Figure 10 (a) and Figure 10 (b).

(a) Displacements for intensity Ⅷ (b) Displacements for intensity Ⅸ

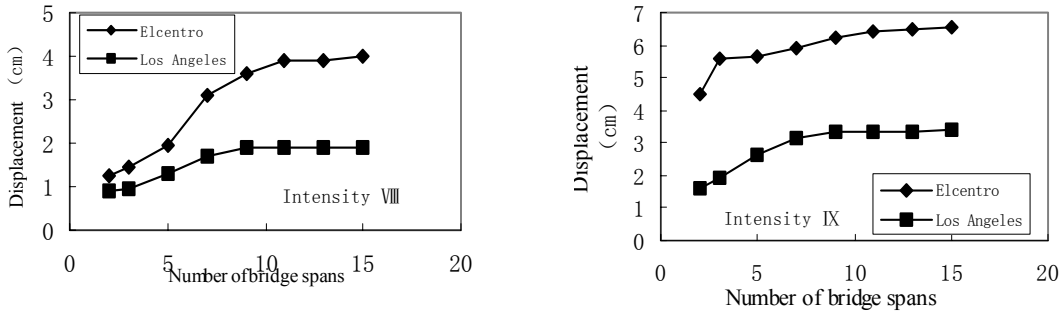

Figure 10 Influence of span number

It can be seen that with the increase of the span number, the seismic response of the pier in the middle increases, but it is not larger than the response of the pier without considering the track restriction.

EFFECTS OF TRACK RESTRICTION ON SEISMIC RESPONSE OF BRIDGES WITH DIFFERENT PIERS

A 7-span railway bridge is taken as the example. The height of No.1 pier on the left side is 6m and the heights of rest piers are 26m. The roadbed resistance coefficient is 10KN/m. By inputting the EL Centro ground motion, the displacements of pier No.1 with and without considering track restriction are shown in Figure 11.

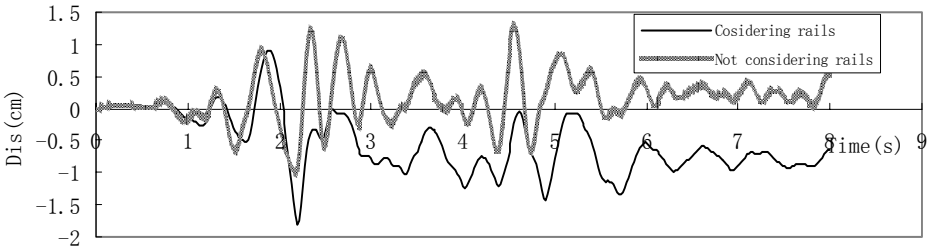

Figure 11 Displacements of pier No. 1

It is can be seen that for stiffer pier the response is obvious higher than that without the track restriction. At the same time, other piers show lower responses when track restriction is considered. That is to say, if the track effect is neglected the safe result can be given for more flexible piers and the not safe one can be given for stiffer piers.

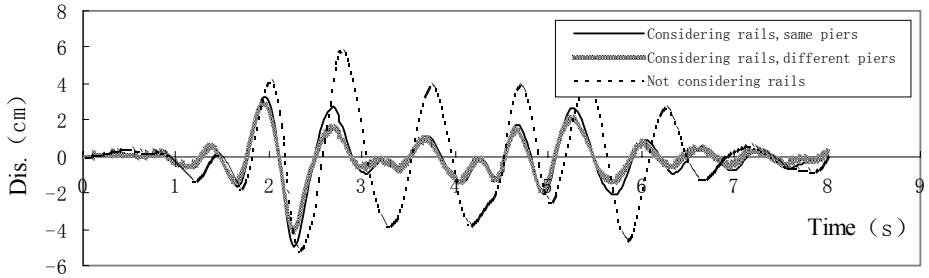

Figure 12 Displacements of pier No. 2

For other flexible piers, the effects of track shoe the same features as that discussed above. In Figure 12 the response of pier No.2 (adjacent to the stiffer pier) is given.

Influence of Roadbed Resistance

With the same 7-span simply supported railway bridge and 3 different roadbed resistant coefficients 10kN/m, 15kN/m, 20kN/m, the seismic responses are compared under the action of EL Centro S00E, Imperial Valley, and Los Angeles N00Wground motion records. The results of pier No.1 and pier No.2 are shown in Figure 13.

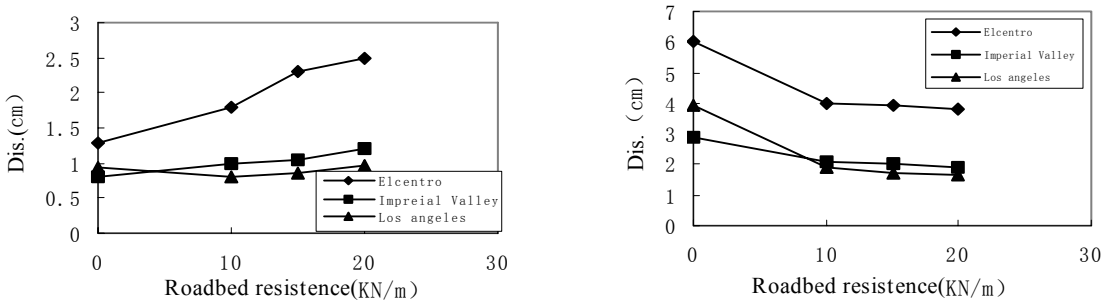

（a）Displacements of pier No.1　　（b）Displacements of pier No.2

Figure 13 Influence of roadbed resistance

With the increase of roadbed resistance, the response of pier No.1 become obvious bigger for the EL Centro earthquake. But the response for other two earthquake waves keep at the same level approximately. Displacement of pier No.2 is reduced as roadbed resistance increase, which shows track restriction to be helpful to flexible pier adjacent to a stiffer pier with increase of roadbed resistance.

Influence of Span Number

By considering different span number, the effects of track restriction are discussed. The seismic response of the pier No.1 and Pier No.2 are given in Figure 14.

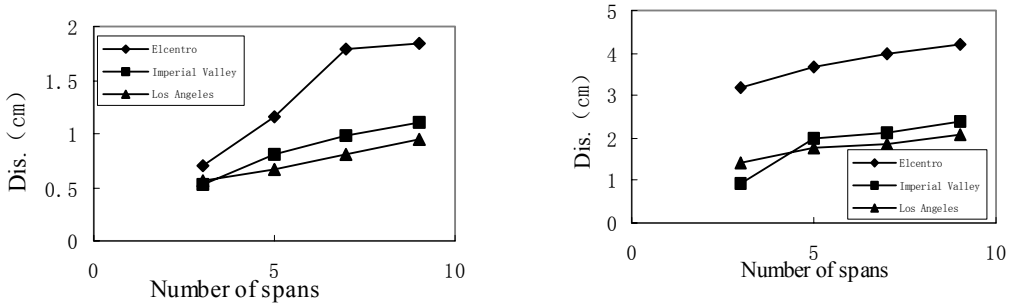

（a）Displacements of pier No.1　　（b）Displacements of pier No.2

Figure 14 Influence of span number

The displacement of pier No.1 increase as number of span increase. The track restriction is not beneficial to this pier as the span number increase. The displacement of pier No.2 becomes bigger with more spans.

CONCLUSIONS

The effects of track restriction on the seismic response of railway bridges are analyzed above. From the discussion, following conclusion can be drawn:

(1) For most flexible pier, the tract restriction can reduce the seismic response of bridges. This function is more obvious with the increase of roadbed resistance.

(2) With the even distribution of pier stiffness, the response of middle pier become

larger with the increase of span number, but it would not be larger than that without the track effect.

(3) For different pier stiffness, track restriction has different effects for stiffer and flexible piers. Especially for stiffer piers, the effect may be negative and should be take into account.

REFERENCES

E.Maragakis, et al, Full-scale Resonance Tests of a Railway Bridge, Structures Congress - Proceedings 1, 1996

Duane E.Otter, et al, Seismic Performance of Railway Bridges, Railway Track & Structure, 1996.5

Luo Xuehai, et al, A Simplified Method for the Dynamic Analysis of Railway Piers, Earthquake Engineering and Engineering Vibration, 1992.6

Jiang Jinzhou, Additional Longitudinal Forces in Continuously Welded Rails and Their Transmission on Railway Bridges, China Railway Science, 1998,6

Guang Zhongyan, et al, Long Welded Railway Tracks, China Railway Press, 1995.7

Seismic Design And Retrofit Guidelines For Bridges In New Jersey, A Low-To-Moderate Seismic Hazard Area

Harry Allen Capers, Jr., PE

ABSTRACT

This paper provides a description of the methodology prescribed for the design and retrofit of bridges for the State of New Jersey, which is located in a low-to-moderate Seismic Hazard Area of the United States. Considering designing structures to meet published seismic design and retrofit requirements of the AASHTO bridge codes has long been a concern of many bridge engineers in the central and eastern states of the United States. To date, most US standards have been based on experiences gained from events occurring in the western states and on codes written in Japan, New Zealand and Europe. Bridge owners outside of the high seismic zones of the United States have either experienced or perceive an increase in the design effort and construction costs associated with meeting these requirements. While no bridge owner will knowingly design a bridge that would put the traveling public at risk, they must also attempt to tailor the requirements of the AASHTO Specification and FHWA to meet the resources available to them and a level of risk acceptable to the jurisdiction in which they work. This paper outlines the approach that New Jersey has taken to address seismic design and retrofit of our structures to meet the level of capital investment it can make at a level of risk that is acceptable to the state by providing modifications to Adopted AASHTO standards. The paper assumes that the reader has a basic understanding of the AASHTO Bridge Design Specifications.

Harry A. Capers, Jr., PE, Manager, Structural Engineering (State Bridge Engineer), New Jersey Department of Transportation, PO Box 615, Trenton, New Jersey, 08625-0615, USA

INTRODUCTION

This paper provides a description of the methodology prescribed for the design and retrofit of bridges for the State of New Jersey, which is located in a low-to-moderate Seismic Hazard Area of the United States. The methodology described herein was first prepared and released in the New Jersey Department of Transportation's (NJDOT) Design Manual for Bridges and Structures, Third Edition, 1998 for use by all designers engaged by agencies within the state to provide highway structure designs in state and federally funded projects. At this time, New Jersey was using the American Association of State Highway and Transportation Officials (AASHTO) Standard Specifications for Highway Bridges, 16th edition with certain state directed modifications as its design specification. Since that time, NJDOT has adopted the AASHTO LRFD Bridge Design Specifications, 2nd Edition with certain state directed modifications, as it's current design specification. The material presented herein is based on that specification.

New Jersey is located in the northeastern portion of the United States, a region that has not in recorded history experienced damaging earthquakes. While not uncommon in the region, earthquakes that occur are usually low intensity events as can be in Table 1.

Location	**Date**	**Intensity MM Scale**	**Magnitude Richter Scale**
Newark	September 1, 1895	VI	5.00
Asbury Park	June 1, 1927	VII	5.00
Trenton	January 24, 1933	V	4.00
Central NJ	August 22, 1922	V	4.00
Salem County	November 14, 1939	V	4.00
West-Central NJ	March 23, 1957	VI	5.00
NJ-PA border	December 27, 1961	V	4.00
Southern NJ	December 10, 1968	V	4.00

Table 1

As one can see, experience with earthquakes in this part of the country is much different than that of western or central areas of the United States where most of the earthquakes have occurred in this country. Consequently until recently the AASHTO Seismic Design codes were largely based on these experiences that focused on larger events and not the magnitudes or risks that could be expected in lower seismic zones. The effect of this has been that many owners were experiencing cost increases in their designs as much as 10% due to seismic design requirements when applying the AASHTO Design specifications without modification.

As can be seen from the above table, for most in New Jersey earthquakes are less than a reality. Further this being typical, seismic design of bridges has always been a difficult issue for bridge owners to accept as a necessary consideration when designing or rebuilding bridges within their jurisdiction especially as the potential exists to draw down as much as 10% of the capital dollars available to them in attempting to meet a low risk requirement of the code. As such, in New Jersey, we have assessed what we feel to be the owner's risks and modified the AASHTO LRFD Bridge Design Specifications, 2nd Edition to, in our opinion, to more realistically represent our state's needs.

SEISMIC DESIGN OF HIGHWAY BRIDGES IN NEW JERSEY

Our current design manual, Design Manual for Bridges and Structures, Third Edition, 1998 directs that seismic design of new highway structures shall follow the requirements of Division 1-A of the AASHTO Standard Specifications for Highway Bridges, 16th edition. In our new manual, we will be directing that the Seismic design of new highway structures shall follow the requirements of Subsection 3.10 of the AASHTO LRFD Bridge Design Specifications. For the designer, this is consistent in that in general seismic design provisions contained in the AASHTO LRFD Specification were based on the code contained in the 16th Edition of the Standard Specification. In view of the fact that our new Design Manual will be issued shortly, this paper will reference the final draft of our LRFD version, Design Manual for Bridges and Structures, Fourth Edition.

Our modifications to the AASHTO Specification are intended to apply to bridge spans not greater than 500 feet and to superstructures of slab bridges, steel girders, concrete girders, box girders or truss bridges as does the AASHTO Specification itself. We require that any structure not meeting these requirements be designed using the results of a site-specific seismic analysis and on occasion, have also required site-specific analysis on unusual structure configurations.

Under either code, the first considerations of an owner is to determine for the Standard Specification which seismic performance category or for the LRFD code which seismic performance zone is to be used for the design of the structure. To make this determination, two characteristics of the bridge must be known. The first is the importance category of the structure. Under the Standard specification this became a non-issue as classifying the bridge as either an essential bridge or other did not change the seismic performance category. However, this classification becomes more significant in the LRFD specification as it segregates post event use of the structure into critical, meaning immediate use by all traffic or designing for no damage, and essential, use by emergency vehicles only which allows accepting some damage to the structure. Both specifications only require no collapse of the superstructure for the lowest importance category. Because of the significant redundancy in the roadway system of the State it was decided that classifying our bridges as essential would provide an acceptable level of risk.

The second characteristic is the ground acceleration coefficient at the location of the bridge. This is found by referencing contour maps of horizontal acceleration prepared for the whole country by the US Geological Survey. For the State of New Jersey ranges from a high of .18 just to the west of the New York metropolitan area to a low of .075 at the very southern end of the state are provided in the USGS maps. For the sake of uniformity of design, to determine the seismic performance category or seismic performance zone throughout the state we have specified that the minimum seismic performance shall be Zone 2 for the entire State of New Jersey. The guidance provided in Subsection 3.10.9.3 of the AASHTO LRFD Bridge Design Specifications should be referred to for clarification on the use of this designation.

The acceleration coefficient for horizontal force effects for use in the design and retrofit of bridge structures is specified in our guidance to designers. It is given on a county-to-county basis as shown in Table 2.

Acceleration Coefficient	County
A = 0.10	Atlantic, Cape May, Cumberland, Salem
A = 0.15	Burlington, Camden, Gloucester, Monmouth, Ocean
A = 0.18	Bergen, Essex, Hudson, Hunterton, Mercer, Middlesex, Morris, Passaic, Somerset, Sussex, Union, Warren

Table 2

For a bridge structure that is located on the border between two counties with different acceleration coefficients, the larger value shall be used. We also direct that vertical components of acceleration shall be neglected.

METHODS OF ANALYSIS

With respect to specific guidance that is provided to designers we direct that the magnitude of seismic forces be determined by considering several factors. These include dead weight of the structure, ground motion (acceleration coefficient), type of soil, fundamental period of vibration, and the Importance classification of the bridge. Other specific guidance provided includes the following items

Single Span Bridges

Due to the higher relative stiffness of abutments when compared to piers, with a single span, the ability to resist earthquakes is increased. Accordingly, for single span design, no formal analysis is required for seismic forces. Designers are directed to consider minimum force requirements as provided in the AASHTO LRFD Bridge Design Specifications for connection of the superstructure to the substructure and to satisfy minimum seat width requirements.

The abutments shall be designed for the effects of static earth pressure and the additional seismic induced earth pressure forces, using the Mononobe-Okabe method. This method is an extension of Coulomb's method for analyzing soil pressure on retaining walls. With the use of this method, we direct that the backfill be assumed to be unsaturated so that liquefaction effects are negligible, the backfill is assumed cohesion-less and that seismically induced active and passive pressures is considered.

Single Span Bridges with Integral Abutments

NJDOT directs that the abutments be designed for seismic forces from the superstructure in addition to the static earth pressure and seismic induced forces using the Mononoke-Okabe method. Both active and passive pressures are to be considered.

Multi-Span Regular Bridges

The Uniform load (Equivalent static load) method or the single mode spectral method is acceptable methods of design. The Uniform load method will require hand calculations, while

the single mode spectral method will require the use of computer software. Also, in using the uniform load method the specific guidance provided by the AASHTO LRFD Bridge Design Specifications are to be followed.

Multi-Span Irregular Bridges

For such bridges, a multi-mode spectral analysis method is required for the analysis of substructures.

Load Combinations

We specify that the AASHTO LRFD Extreme Event-I load combinations be applicable for a seismic analysis. As directed in the AASHTO LRFD Bridge Design Specifications, Dead Load and Live Load forces are to be combined with the forces from a single or multi-mode analysis as follows:

- 100% of longitudinal seismic forces + 30% of transverse seismic forces
- 100% of transverse seismic forces + 30% of longitudinal seismic forces

Site Coefficients and Site Effects

Due to large variations in the values of site coefficients, soil profiles will be based on soil composition at the specific bridge site. A geotechnical investigation is to be performed at all proposed bridge locations to determine the soil conditions, whether cohesive or cohesionless, the type of rock, sand, gravel, and stiff clay, soft clay or silt.

Liquefaction

The potential for soil liquefaction and liquefaction related ground instability is to be investigated at relevant locations along proposed project alignments. Effects of settlement of footings, loss in bearing capacity and increased lateral earth pressures is to be considered in the design of abutments, walls and footings.

Seismic Slope Instability and Landslide

The potential for seismic induced slope movements and landslides along the proposed alignment must be investigated for all projects. Mitigation measures are to be incorporated in the design of abutments, walls and footings.

Response Modification Factors

The LRFD Bridge Design Specifications recognize that it is uneconomical to design a bridge to resist large earthquakes elastically and therefore are assumed to deform inelastically once they exceed their design level. According to the provisions of the AASHTO LRFD Specifications, Response Modification Factors or R-factors shall be used to reduce the moments and forces due to the ability of a member to develop a plastic hinge. Moments and forces for member and connection designs are to be computed by dividing the forces and moments obtained from load

combinations by the appropriate Response Modification Factors. This is the design level of the member.

Abutment Analysis

For all multi-span bridges, regular, irregular or with integral abutments, earthquake forces from the superstructure shall be considered. Abutments need to be analyzed for seismic forces from the superstructure, in addition to the static earth pressure and seismic induced forces using the Mononobe-Okabe method. Both active and passive pressures shall be considered.

Miscellaneous Guidance

Seismic ductility design at locations where plastic hinges will form shall be accounted for on all new structures. Seismic effect considerations are not required for buried structures or culvert structures. In addition to the AASHTO LRFD Bridge Design Specifications, we also recognize the FHWA Geotechnical Engineering Circular No. 3 titled, "Design Guidance: Geotechnical Earthquake Engineering for Highways" as a reference on seismic design.

Alternate Design Criteria

As an alternative to the use of the AASHTO LRFD Specifications, NCHRP Report 472, "Comprehensive Specification for the Seismic Design of Bridges" may be used. Designers may submit a request to the Manager, Bureau of Structural Engineering for the use of the NCHRP Report. A comparison of the effects on the design of a project between the two documents should be made to validate the request.

This specification was the result of an AASHTO sponsored National Cooperative Highway Research Project initiated in 1998 to develop a state of the art seismic specification compatible with the AASHTO LRFD Bridge Design Specification. The proposed specification was intended to replace the current specifications by incorporating experiences gained around the world in all areas of seismic design in a nationally acceptable specification. As was previously stated the existing provisions are based on data that is now considered 10 to 20 years out of date.

The project was completed by a joint venture of the Applied Technology Council and MCEER last spring and was considered by the AASHTO Subcommittee on Bridges and Structures at it's annual meeting this past May. Apparently due to concerns raised over the new USGS seismic hazard mapping the new specifications were not adopted to replace the existing provisions at this meeting.

The specification is available for use and does provide certain benefits to bridge owners in low to moderate seismic risk areas by focusing on proper detailing for seismic events rather than analysis. In the two trail designs performed for the project by New Jersey designers, significant reductions in seismic forces were noted. Other benefits include treatment of new seismic load resistant systems, improved soils information, it forces the designer to identify the seismic load path and it provides a state of the art, performance based method of designing bridges for seismic loading.

SEISMIC RETROFIT OF EXISTING HIGHWAY BRIDGES IN NEW JERSEY

An even greater challenge to us over time has been how to address existing bridges in our inventory that were designed to less than today's standards. New Jersey has approximately 6500 highway carrying bridges within their jurisdictions of which all but about 1250 are over 25 years old. Needless to say, seismic loading was not considered in their design.

Further, in that resistance to seismic loads has not been considered at all in their design, retrofitting these structures would be a very difficult and costly task to undertake. To minimize the impact to our available budget New Jersey has chosen to address this issue, as it affects our existing inventory, as our structures are programmed for rehabilitation or replacement. Typically, preventing collapse of the superstructure is targeted.

NJDOT specifies that the seismic retrofit design of existing highway structures shall follow the guidelines of the FHWA publication titled "Seismic Retrofitting Manual for Highway Bridges" currently numbered as, FHWA-RD-94-052, May 1995. We also specify that highway structures shall be retrofitted for a Zone 2 earthquake, which is consistent with our criteria for new bridges.

However, prior to proceeding with retrofit design, we require a Seismic Retrofit Report to be prepared to provide a determination as to a bridge structure's eligibility for a seismic retrofit. A flow chart to provide guidance in determining if a bridge structure qualifies as a seismic retrofit candidate is included herein as Figure 1. The results of the analysis, performed in accordance with .the flow chart, shall be provided in the Seismic Retrofit Report.

In preparing the Seismic Retrofit Report, the following guidance shall be followed. Initially, seismic retrofitting of a bridge structure shall only be considered under the following conditions:

a. The planned work will involve widening of a deck by more than 30% of its deck area; or,
b. The planned work will involve an entire deck replacement; or,
c. The planned work will involve superstructure rehabilitation or replacement, major abutment or pier repairs to bearing seat areas or bearing repairs or replacement.

Figure 1 - Additional Analysis Required for Existing Bridges Found in Planned Projects

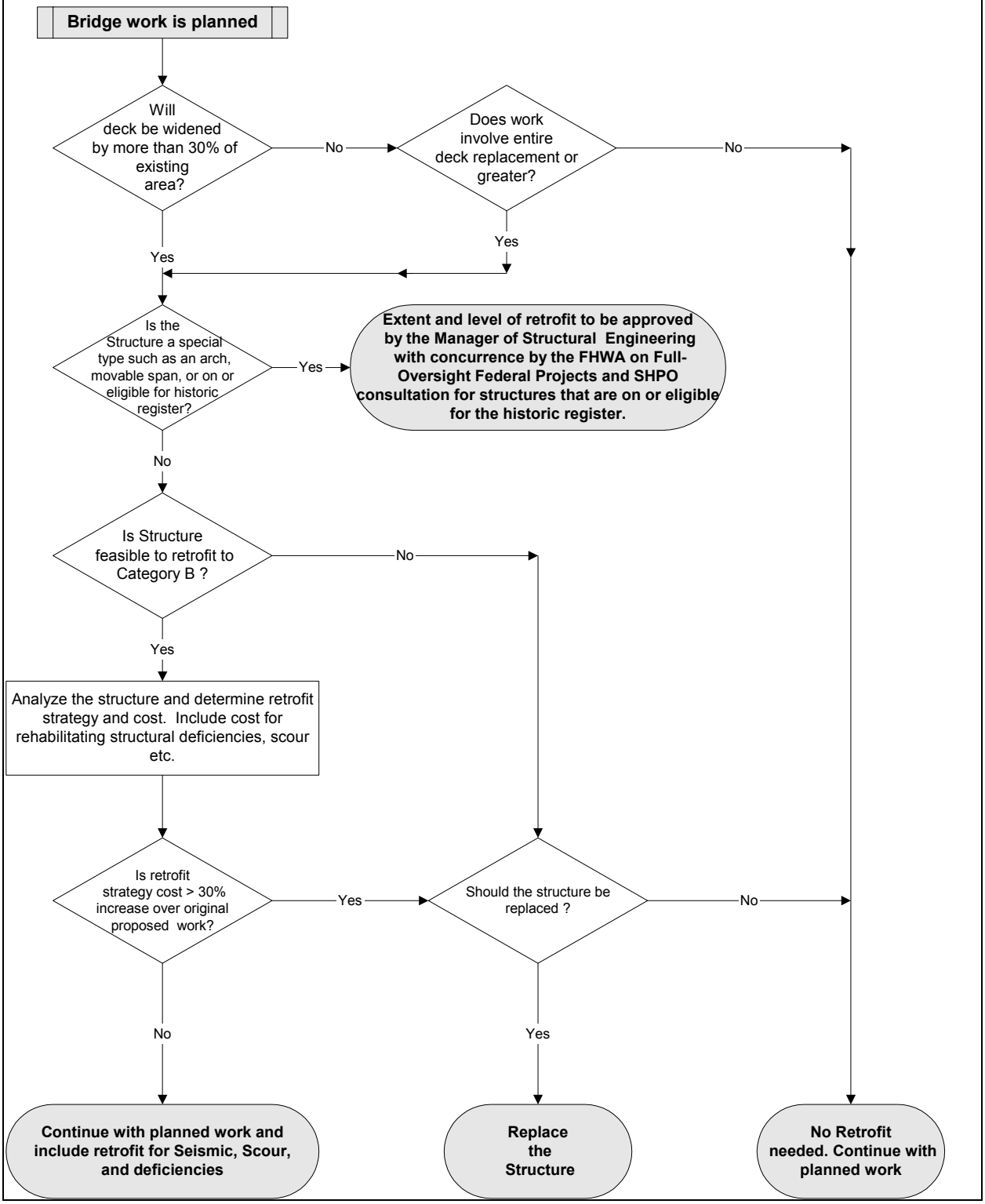

The Report should also include a study of the proposed project to determine if retrofitting a bridge is a cost-effective measure. At a minimum, we direct that two things be done. First, an investigation to determine the extent of retrofitting which may be required must be performed and documented. Second, prior to making a detailed evaluation of the seismic capacity of the bridge structure, the relationship of the bridge structure to other bridge structures on neighboring routes that may also be damaged during an earthquake, be considered. Consider two bridge structures that have similar functions, such as bridge structures A and B as detailed in Figure 2. Assume that bridge structure B is currently in a project and being considered for seismic retrofit. It is possible, that retrofitting bridge structure A would be more economical or that bridge structure A is more seismically adequate than bridge structure B. Accordingly, even though bridge structure A is not in the project scope and bridge structure B is, it would be more rational to retrofit bridge structure A than bridge structure B. If so, not seismically retrofitting the bridge structure may be justified.

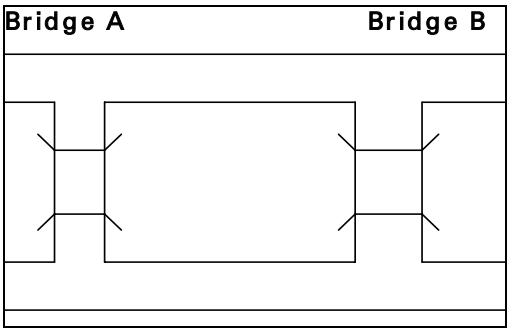

Figure 2
Parallel Bridges

Seismic Retrofit of Bearings

Several methods of seismic retrofit are outlined for bearings and expansion joints within the FHWA Retrofit Manual that is referenced above. Of these methods NJDOT design guidance suggests the following for consideration in order of preference. If applicable, a recommendation as to the proposed treatment of a bridge structure should be included in the Seismic Retrofit Report.

a. Modify existing bearings to resist seismic loads or to prevent toppling of existing bearings by installing longitudinal displacement stoppers.
b. Use of longitudinal joint restraints as outlined in the FHWA Retrofit Manual.
c. Bearing replacement with those type bearings identified in the NJDOT Design Manual for Bridges and Structures. If conventional steel and elastomeric bearings, are proposed to remain, typical modifications to these bearings to withstand the specified design earthquake loadings would include the following:

Modifications To Steel Bearings

a. Increase size, number or embedment of anchor bolts.
b. Increase the outer diameter of the pinhead.
c. Increase the width of the expansion rocker.

d. Increase the top and bottom dimension of the pintle detail for increased movement.

Modifications to Elastomeric Bearings

a. Secure bearing against horizontal and vertical movement.
b. Modify the plan area and/or thickness of the elastomeric bearing to reduce seismic forces to the substructure.

The methods outlined above are recommended procedures and are not intended to restrict the ingenuity and creativity of the Design Engineer. Each bridge is different; therefore, the owner will approve retrofit procedures on a project-to-project basis.

If it is found through a seismic analysis that the substructure is in need of seismic retrofit, it will probably be economically advantageous to study bearing replacement as part of a retrofit.

In evaluating a bridge structure's history, a significant traffic count should warrant an increase to the Seismic Load Extreme Event load combination. As such, the 0.50 live load factor, listed in the AASHTO LRFD Bridge Design Specifications as an Extreme Event II load combination, shall be combined with the Extreme Event I Earthquake load factor. A Designer should use his engineering judgment in assessing the traffic count in applying the increase.

CONCLUSION

Considering designing structures to meet published seismic design and retrofit requirements of the AASHTO bridge codes has long been a concern of many bridge engineers in the central and eastern states of the United States. To date, most US standards have been based on experiences gained from events occurring in the western states and on codes written in Japan, New Zealand and Europe. Bridge owners outside of the high seismic zones of the United States have either experienced or perceive an increase in the design effort and construction costs associated with meeting these requirements. While no bridge owner will knowingly design a bridge that would put the traveling public at risk, they must also attempt to tailor the requirements of the AASHTO Specification and FHWA to meet the financial resources available to them and a level of risk acceptable to the jurisdiction in which they work. In this paper, I have outlined the approach that New Jersey has taken to address seismic design and retrofit of our structures to meet the level of capital investment we can make at a level of risk that is acceptable to the state.

The AASHTO Subcommittee on Bridges and Structures continues to work to find a reasonable solution to this issue through the issuance of a nationally acceptable seismic design specification. The recent work completed by the ATC/MCEER joint venture published as NCHRP Report 472 promises to provide the solution. Hopefully, the remaining concerns expressed by the states at the last annual meeting will be addressed shortly and a state of the art specification addressing all geographic areas of the country will be adopted.

ACKNOWLEDGEMENT

A special thanks to Jack Mansfield, PE Manager, Geotechnical Engineering, NJDOT, Jose Lopez, Project Engineer, Shirish Patel, Principal Engineer, and Sharon Harrison, Administrative Assistant, all of Structural Engineering, NJDOT for their tremendous support in editing and formatting this paper. Finally, thanks to Dr. Mohiuddin (Ali) Khan, PE of STV, Inc. for his tremendous assistance in developing our modifications described herein.

REFERENCES

AASHTO 2002, "AASHTO LRFD Bridge Design Specifications", Second Edition, American Association of State Highway and Transportation Officials, Inc., 444 North Capital Street, NW, Suite 249, Washington, DC, 20001

AASHTO 2002, "Standard Specifications for Highway Bridges", Sixteenth Edition, American Association of State Highway and Transportation Officials, Inc., 444 North Capital Street, NW, Suite 249, Washington, DC, 20001

ATC/MCEER Joint Venture, 2002 "NCHRP Report 472 – Comprehensive Specification for the Seismic Design of Bridges", Transportation Research Board, National Research Council, 2101 Constitution Avenue, NW, Washington, DC 20418

Dombroski, Daniel R., Jr., 1977 "Earthquakes in New Jersey", New Jersey Department of Environmental Protection, Bureau of Geology and Topography, PO Box 2809, Trenton, NJ 08625-2809

FHWA 1995, Report No. FHWA-RD-94-052 "Seismic Retrofit Manual for Highway Bridges", Buckle, Ian G. and Friedland, Ian M (Editors), Office of Engineering and Highway Operations, R&D, Federal Highway Administration, 6300 Georgetown Pike, McLean, Va 22101-2296

NJDOT 2002, Final Draft of "Bridges and Structures Design Manual-LRFD", Fourth Edition, New Jersey Department of Transportation, Bureau of Structural Engineering, PO Box 615, Trenton, NJ 08625-0615

NJDOT 1998, "Bridges and Structures Design Manual", Third Edition, New Jersey Department of Transportation, Bureau of Structural Engineering, PO Box 615, Trenton, NJ 08625-0615

Generation of Response Spectrum Compatible Non-stationary Ground Motions Based on Phase Difference Spectra

Qing-shan Yang[1] Hai-peng Jiang[1]

ABSTRACT

A numerical method is presented for computing artificial earthquake records consistent with a specified target response spectrum or power spectral density. The phase angle spectrum in the proposed algorithm is not an independent random variable distributed in [0, 2π] uniformly, but rather is generated on the basis of the statistical characteristics and the distribution law of phase different spectrum, which controls the nonstationarity of the generated ground motions. The efficiency of the algorithm and the accuracy of the fitting process are substantially improved by applying the component-by-component modulating approach. The proposed procedures are validated by examples.

[1] College of Civil Engineering and Architecture, Northern Jiaotong University, Beijing, 100044, PRC

INTRODUCTION

Response spectrum has been applied in many seismic codes over the world and used as the target spectrum in generating the artificial ground motions which has been studied by a number of authors through various methods (Kaul, 1978a; Preumont, 1984; Ghosh, 1993).

For artificial ground motion, nonstationarity in time and frequency domains is one of the most concerns (Deodatis, 1996; Sabetta, 1996; Shrikhande, 1996). After systematic studies (Yang, 200; Zhao, 1992; Nigam, 1982; Ohsaki, 1979), it is concluded that it is the phase difference spectrum, which mainly controls the nonstationarity of the artificial ground motions. This conclusion is applied in this proposed algorithm. The design response spectrum specified in Code for Seismic Design of Building of China (GB11-89, China) is applied in the presented paper. To improve the matching efficiency, the component-by-component modulating technique is applied, in which the modulating ratios of amplitude spectra for different components are different according to their contribution to the responses.

GENERATION ALGORITHMS

Among various procedures for ground motion simulation, the method relying on trigonometric approximations (Shinozuka, 1967; Mignolet, 1996) is generally applied and written as:

$$a(t) = \sum_{k=1}^{n} A_k \cos(\omega t + \phi_k) \tag{1}$$

Eq.1 may be rewritten in the discrete Fourier transformation as:

$$a(t) = a(m\Delta t) = \mathrm{Re}[\sum_{k=0}^{N-1} F(\omega_k) e^{i\omega_k m}] = \mathrm{Re}[\sum_{k=0}^{N-1} \left(|F(\omega_k)| e^{-i\varphi_k}\right) e^{i\omega_k m}] \qquad \Delta t = T_d / N \tag{2}$$

where T_d is the time length of the generated time history; ϕ_k is the phase angle spectrum; N is the sample number and should be an exponential function of 2 to use Fast Fourier Transformation technique; and $|F(\omega_k)|$ is the two-sided Fourier amplitude spectrum, which may be derived from the one-sided Fourier amplitude spectrum $|F_1(\omega_k)|$:

$$|F(\omega_k)| = \begin{cases} |F_1(\omega_k)| & k = 0, N/2 \\ |F_1(\omega_k)|/2 & k = 1,2,\cdots,N/2-1 \end{cases} \tag{3}$$

and one-sided Fourier amplitude spectrum $|F_1(\omega_k)|$ may be determined from energy considerations as

$$|F_1(\omega_k)| = [4G(\omega_k)\Delta\omega]^{1/2} \tag{4}$$

So, the two-sided Fourier amplitude spectrum may be denoted directly

$$|F(\omega_k)| = \begin{cases} [4G(\omega_k)\Delta\omega]^{1/2} & k = 0, N/2 \\ [G(\omega_k)\Delta\omega]^{1/2} & k = 1,2,\cdots, N/2-1 \end{cases} \tag{5}$$

where $G(\omega_k)$ is the one-sided power spectral density. To establish the relation between the Fourier amplitude spectrum and the response spectrum, the approximate relation between response spectrum and power spectrum was developed (Kaul, 1978b):

$$G(\omega) = \frac{\xi}{\pi\omega}[S_a^T(\omega)]^2 \Bigg/ \left\{ -\ln\left[\frac{-\pi}{\omega T_d}\ln(1-r)\right]\right\} \tag{6}$$

in which T_d is the time length of the recording, r is exceeding probability, equals 5~10% usually, ξ is the damping ratio of the linear oscillator which is used to calculate the response spectrum $S_a^T(\omega)$.

Parameters ϕ_k for ground motion are usually selected to be independent random variables uniformly distributed in $[0, 2\pi]$(Kaul, 1978a; Ohsaki, 1979; Preumont, 1984). While after systematic studies, it is concluded that the phase angle should be obtained according to the following procedures (Yang, 2001; Zhao, 1992; Nigam, 1982; Ohsaki, 1979):

$$\phi_{k+1}(f) = \phi_k(f) + \Delta\phi_k(f)_k \qquad \phi_k \in [0, 2\pi] \qquad k = 0, \quad 1, \cdots n-1 \tag{7}$$

$$\Delta\phi_k(f) = \Delta\bar{\phi}_k(f) + \varepsilon_k \qquad \Delta\phi_k(f) \in [-2\pi, \quad 0] \qquad k = 0, \quad 1, \cdots n-1 \tag{8}$$

and any value in $[0, 2\pi]$ may be specified as the initial phase angle ϕ_0. In Eq.7 $f = \omega/2\pi$ is the linear frequency; $\Delta\phi_k(f)$ is the phase difference spectrum, $\Delta\bar{\phi}_k(f)$ the mean function of phase difference spectrum and ε_k the fluctuating part of the phase difference spectrum about the mean function. The empirical relation of $\Delta\bar{\phi}_k(f)$ to its influence factors is:

$$\log_{10}\left|\Delta\bar{\varphi}(f)\right| = a_1(f) + a_2(f)\cdot M + a_3(f)\log_{10}(R + R_0) \tag{9}$$

and

$$\Delta\bar{\varphi}(f) = -\left|\Delta\bar{\varphi}(f)\right| < 0 \tag{10}$$

where M is the earthquake magnitude; R (Km) is the epicenter distance; R_0=15 is a constant. $a_1(f)$, $a_2(f)$, $a_3(f)$ are regressive coefficients as functions of frequency and their values for bedrock site are listed in Yang (2001) and Zhao (1992).

ε_k is the fluctuating part of the phase difference spectrum about the mean function and can be obtained from:

$$\varepsilon_k = -(\varepsilon_{bk} - 2\pi) \qquad \text{and} \qquad \varepsilon_{bk} = e^{\varepsilon_{ck}} \tag{11}$$

and ε_{ck} is a random variable satisfying the normal distribution law with mean value m_c and

standard deviation σ_c which can be calculated from:

$$m_c = \ln 2\pi - \frac{1}{2}\ln(1+(\frac{\sigma_\varepsilon}{2\pi})^2) \qquad \sigma_c = \ln(1+(\frac{\sigma_\varepsilon}{2\pi})^2) \tag{12}$$

and σ_ε is the standard deviation of random variable ε_k and may be obtained from:

$$\log_{10}\sigma_\varepsilon = d_1 + d_2 \cdot M + d_3 \log_{10}(R+R_0) \tag{13}$$

where d_1, d_2, d_3 are coefficients; the other symbols are the same as that in Eq.9. $d_1 = -1.124$, $d_2 = 0.089$, $d_3 = 0.316$ for bedrock site (Yang, 2001; Zhao, 1992).

Substitute Eqs.5~7 into IFFT (Eq.2), the ground motion compatible to response spectrum $S_a^T(\omega)$ may be obtained. While, as Eq.6 is an approximate relation, the obtained ground motion may be not compatible to target response spectrum accurately enough, it is necessary to modulate the obtained ground motion to improve the accuracy. Let the target response spectrum be noted as $S_a^T(\omega)$, the response spectrum of the obtained ground motion as $S_a(\omega)$, if $S_a(\omega)$ is not close enough to $S_a^T(\omega)$, at any fitting point $\omega = \omega_i$, i.e.,

$$\left|R(\omega_i) - 1\right| > \varepsilon \quad (\varepsilon \text{ is the tolerant error}) \tag{14}$$

where

$$R(\omega_i) = S_a^T(\omega_i) \big/ S_a(\omega_i) \tag{15}$$

then iterative matching is needed and the fitting technique generally used to modulate the Fourier amplitude spectrum (Shaw, 1975, Kaul,1978a) is:

$$|F^{I+1}(\omega_k)| = |F^I(\omega_k)| \cdot R(\omega_i) \tag{16}$$

I is the iteration number and ω_k is the frequencies near the fitting point ω_i.

and substitute the modulated Fourier amplitude spectrum into IFFT (Eq.2), then obtained the renewed ground motion. The convergence criteria should be satisfied following the above iteration.

COMPONENT-BY-COMPONENT MODULATING TECHNIQUE

Though the above fitting technique is applied broadly, what should be noted is its convergence speed is not fast, and sometimes the needed accuracy was not able to be reached at some fitting frequencies. Many works has been done on this problem, and we believe component-by -component modulating technique (Hu, 1986) is a good idea, which will be illustrated by the following example.

It is assumed that there is an oscillator with damping ratio ξ=0.05 and natural circular frequency ω=10.466 rad/s. Its absolute acceleration response $x(t)$ under the S00E component of EL Centro Wave $a(t)$ (Figure1) may be obtained by numerical integration (Figure2). Its maximum absolute value, i.e., the response spectrum S_a is $|x(t)|_{\max} = 8.33 m/s^2$ which occurs at 2.22s, noted this time as $t_{\max}$ (Figure2).

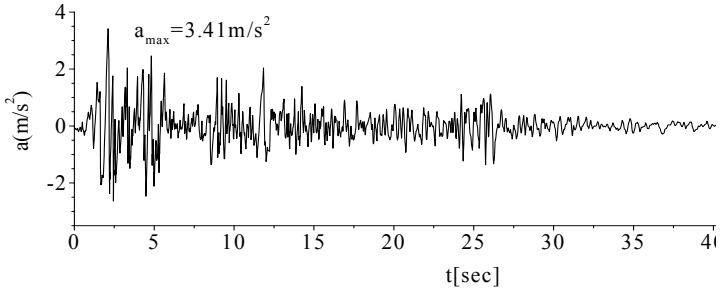

Figure1 S00E component of the time history recorded at EL Centro station in the Imperial Valley earthquake, 1940

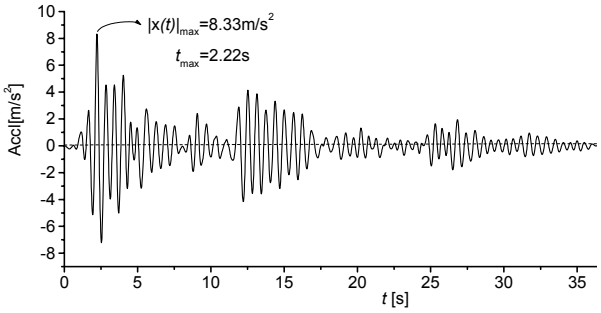

Figure 2 Absolute acceleration response of the EL Centro wave

Meanwhile the S00E component of EL Centro wave may be decomposed to be a real Fourier series:

$$a(t) = \sum_{k=1}^{n} A_k \cos(\omega_k t + \varphi_k) = \sum_{k=1}^{n} a_k(t) \tag{17}$$

The absolute response of the oscillator under each component of the EL Centro Wave $a_k(t)$, $x_k(t)$, may also be obtained by numerical integration (part of them shown in Figure3).

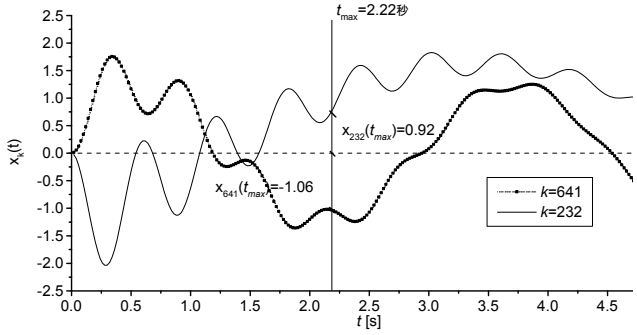

Figure 3 Components of the absolute acceleration

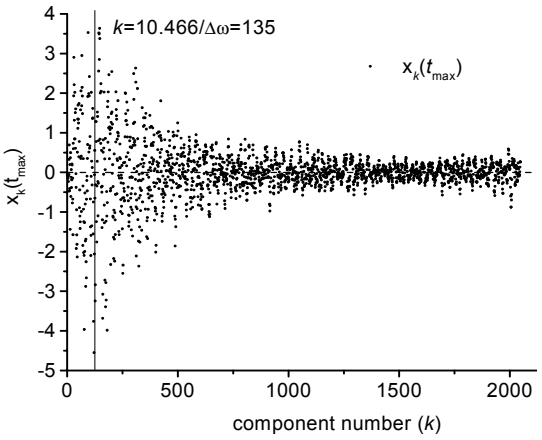

Figure 4 Absolute acceleration response values of each component at $t = t_{max}$

It is apparent that:

$$S_a = |x(t)|_{\max} = |x(t = t_{\max})| = |\sum_k x_k(t = t_{\max})| \quad (18)$$

Response of the oscillator and the distribution of $x_k(t = t_{\max})$ $(k = 1,2,3....n)$ is shown in Figure4.

Figure4 and 3 indicate that though the total response $x(t)$ gets its maximum absolute value at $t = t_{\max}$, the component response $x_k(t)$ at $t = t_{\max}$ may not be its maximum value, even its sign may be also different with that of $x(t_{\max})$. We may group the response components $x_k(t)$ based on their sign at $t = t_{\max}$ as:

Group A: the sign of $x_k(t_{\max})$ is same as that of $x(t_{\max})$

Group B: the sign of $x_k(t_{\max})$ is contrary to that of $x(t_{\max})$

and apply different modulating strategy to them:

If $S_a = |x(t_{\max})|$ is less than the target response spectrum $S_a^T(\omega)$, the amplitude spectrum $F(\omega_k)$ corresponding to Group A will be increased, and that corresponding to Group B decreased. If $S_a = |x(t_{\max})|$ is bigger than $S_a^T(\omega)$, the modulating direction is contrary to the previous. This modulating technique, named as component-by-component fitting technique, will generally be more efficient than Eq.16 and may be formulated as:

$$\text{For Group A: } |F^{I+1}(\omega_k)| = |F^I(\omega_k)| \cdot R(\omega_i) \quad (19a)$$

$$\text{For Group B: } |F^{I+1}(\omega_k)| = |F^I(\omega_k)| / R(\omega_i) \quad (19b)$$

and unified as:

$$\left|F^{I+1}(\omega_k)\right| = \left|F_k^I(\omega_k)\right| \cdot (R(\omega_k))^{sign[x_k(t_{\max})x\ (t_{\max})]} \quad (20)$$

It is should be noted that the total response is practically contributed by a few components with frequencies ω_k close to the natural frequency of the oscillator ω_i, named as effective components (Figure4), and only the effective components need to be modulated for each oscillator with different natural frequencies.

GENERATION OF RESPONSE-SPECTRUM-COMPATIBLE GROUND MOTIONS

Based on the ground motion generation procedures (Sect.2) and the modulating technique (Sect.3), the procedures of generating fully nonstationary and response-spectrum-compatible ground motions may be summarized as:

1. Determine the possible earthquake magnitude *M*, epicenter distance R(Km), and target response spectrum, including parameters, such as the characteristic period of the site, the maximum value of the response spectrum.
2. Obtain the power spectral density $G(\omega)$ from the target response spectrum $S_a^T(\omega)$ at the fitting points $\omega = \omega_i$ $(i = 1,2,\ldots j$, j is the number of the points) based on Eq.6.
3. Obtain the amplitude spectrum of complex Fourier transformation from power spectral

density at the fitting points $\omega_i\,(i=1,2,\ldots j)$:

$$\left|F(\omega_i)\right| = [G(\omega_i)\Delta\omega]^{1/2} \qquad \Delta\omega = 2\pi / T_d \tag{21}$$

then obtain the amplitude spectrum at each calculating frequency by linear interpolation:

$$|F(\omega_k)| = 0 \qquad \omega_k < \omega_{i=1} \tag{22a}$$

$$|F(\omega_k)| = |F(\omega_i)| + \frac{|F(\omega_{i+1})| - |F(\omega_i)|}{\omega_{i+1} - \omega_i}(\omega_k - \omega_i) \tag{22b}$$

$$\omega_i \le \omega_k = k\Delta\omega \le \omega_{i+1} \qquad i = 1,2,\ldots j-1 \quad k = 1,2,\cdots, N/2-1$$

$$|F(\omega_{N/2})| = 2(|F(\omega_{j-1})| + \frac{|F(\omega_j)| - |F(\omega_{j-1})|}{\omega_j - \omega_{j-1}}(\omega_{N/2} - \omega_{j-1})) \tag{22c}$$

Where N is the sample number which should be the exponential function of 2 for using Fast Fourier Transformation.

4. Obtain the phase different spectrum based on the field condition, magnitude and epicenter distance from Eqs.8~13.
5. Specify the initial phase angle and obtain the phase spectrum following Eq.7.
6. Obtain the complex Fourier Spectrum

$$F(\omega_k) = \left|F(\omega_k)\right| e^{-i\varphi(\omega_k)} \qquad k = 0,1,2\ldots N/2 \tag{23a}$$

$$F(\omega_k) = F^*(\omega_{N-k}) \qquad k = N/2+1,\ldots N-1; \tag{23b}$$

where * denotes conjugate complex.

7. Obtain the initial ground motion from Inverse Fast Fourier Transformation (Eq.2).
8. Check the fitting accuracy and modulate the ground motion. Calculating the absolute acceleration response $x(t)$ of the oscillators with natural frequencies $\omega = \omega_i\,(i=1,2,\ldots j)$ under the generated ground motion and determine the absolute maximum value $|x(t)|_{\max}$, its occurring time $t_{\max}$, the algebra value of $x(t_{\max})$, then check the accuracy.

If $\left|R(\omega_i)-1\right| \le \varepsilon$ for each $i=1,2,\ldots j$ (ε is the specified tolerant error), it is indicated that the generated ground motion satisfies the fitting accuracy, and stop the iteration. Otherwise, modulate the generated ground motion following the procedures:

i). Calculate absolute acceleration response $x_k(t_{\max})$ of each oscillator with frequency $\omega = \omega_i\,(i=1,2,\ldots J$, J is the number of the fitting points where the generated ground motion do not satisfied the accuracy) under each component of the generated ground motion $A_k(\omega_k t + \varphi_k)$ at $t_{\max}$.

ii). Determine the contribution of each component,

$$\beta_k = \left|x_k(t_{\max})\right| / \left|x(t_{\max})\right| \tag{24}$$

$\beta_k > \varepsilon_1$ (ε_1 is the specified contribution level, for example, ε_1=0.1) indicates this component gives an important contribution to the total response, i.e., it is effective component, and should be modulated.

iii). Modulate the amplitude spectrum of every effective component for each controlling

frequency following Eq.23 and re-substitute the modulated amplitude spectrum into Eq.2. to obtain the renewed ground motion. Checking the fitting accuracy till the tolerant error is reached at each fitting point.

EXAMPLES

It is assumed the soil of the researched field is bedrock, i.e., site category I; the earthquake intensity is VII; the earthquake risk analysis shows the maximum magnitude of the possible earthquake is 6.5 and the epicenter distance is 150km. It is needed to generate the possible earthquake ground motions compatible to the response spectrum specified by the Code for Seismic Design of Buildings of China (GBJ 11-89) with the above far-earthquake risk parameters.

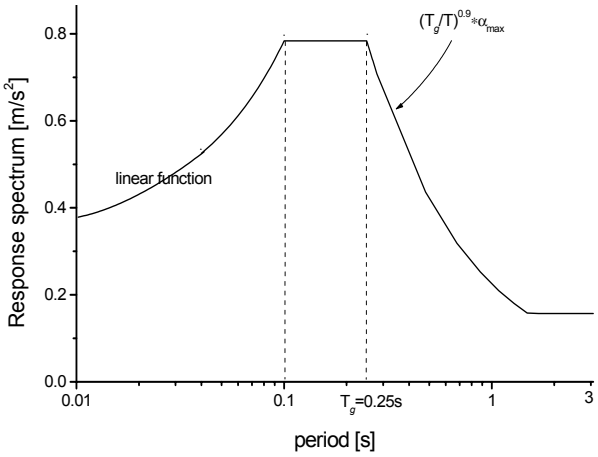

Figure 5 Target response spectrum

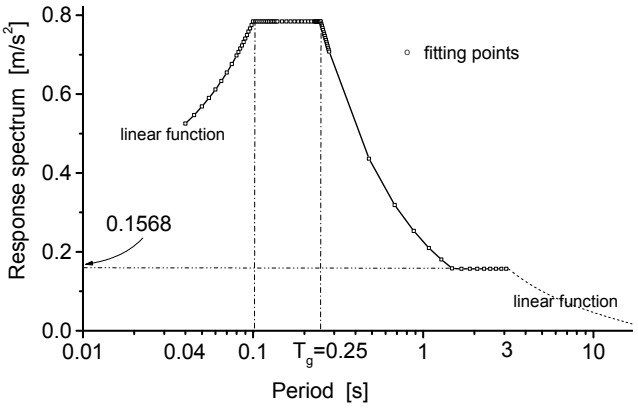

Figure 6 Modified response spectrum

1. Parameters of the target response spectrum. The response spectrum curve specified by Code for Seismic Design of Buildings of China (GBJ 11-89) is shown in Figure5 where the characteristic period is 0.25s for site category I and far-earthquake, the maximum value of response spectrum $S_{a\max}$ is 0.08g for intensity VII (g is the gravity acceleration). The response spectrum curve may be divided into three parts according to the natural period, from T=0s to T=0.1s, the response spectrum varies from $0.45\,S_{a\max}$=0.036g to $S_{a\max}$=0.08g; from T=0.1s to $T = T_g$=0.25s, it maintains its maximum value $S_{a\max}$=0.08g; from $T = T_g$=0.25s to T=3s, it varies following function $S_a = (T_g/T)^{0.9} S_{a\max}$, but if $(T_g/T)^{0.9} < 0.2$, $S_a = 0.2 S_{a\max} = 0.016g$.
2. Some pre-specified parameters of the target ground motions. Specify the sample number N=2^{12}=4096 and the time step as 0.02s, then the time length of the ground motion is T_d = 80.92s; the frequency step $\Delta\omega = 2\pi/T_d$ =0.07765 and the highest frequency in Fourier

transform is $\omega_{N/2} = \frac{2\pi}{N\Delta t} \cdot \frac{N}{2} = 50\pi$, i.e., the frequency scope of the Fourier spectrum is $[0, 50\pi]$, the corresponding period scope is $[0.04s, \infty]$. The definition domain of the target response spectrum should also be $[0.04s, \infty]$ in determining the Fourier amplitude spectrum from Eqs.5 and 6. The period domain of response spectrum in Code for Seismic Design of Buildings of China (GBJ 11-89) should be extended to be that the response spectrum is zero when the period is bigger than 20s and the response spectrum for periods within $[3s, 20s]$ are interpolated linearly between $S_a(3)$=0.016g and $S_a(20)$=0. Based on these parameters, the modified response spectrum is shown as Figure6.

3. Specify the fitting points. Within period $T \in [0.04, 0.08]$, period step $\Delta T = 0.005$, the number of fitting points j_1=8; $\Delta T = 0.009$, j_2=10 in $T \in [0.139, 0.229]$; $\Delta T = 0.002$, j_3=24 and j_4=25 in $T \in [0.082, 0.130]$ and $T \in [0.232, 0.28]$, respectively, where the spectrum function changes from one to another; $\Delta T = 0.2$, j_5=14 in $T \in [0.48, 3.08]$. The total number of the fitting points is $j = j_1 + j_2 + j_3 + j_4 + j_5$=81 (Figure 6).
4. Obtain the power spectrum at these fitting points based on Eq.6 and show it in Figure7.
5. Calculate the complex Fourier amplitude spectrum following Eqs.21 and 22, and present it in Figure8.

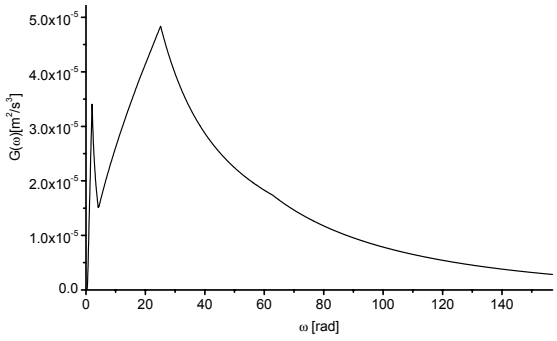

Figure 7 Initial power spectral density

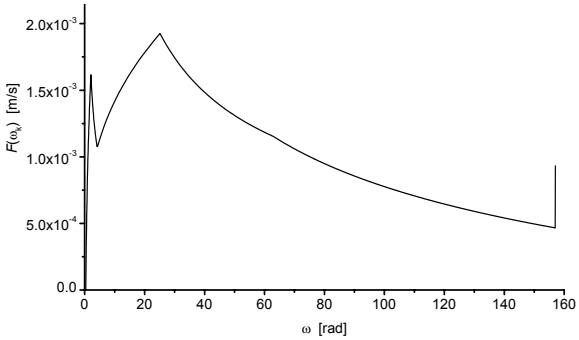

Figure 8 Initial amplitude spectrum

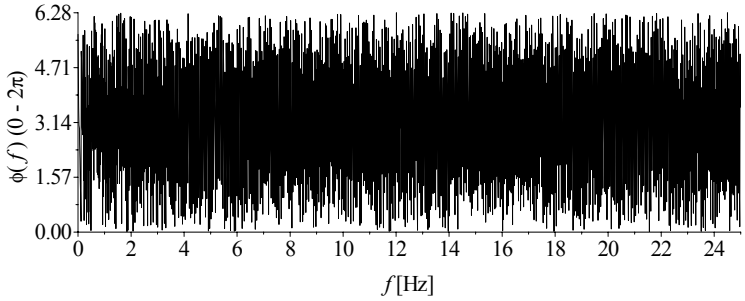

Figure 9 Generated phase angle spectrum for $\phi_0 = 0$

6. Obtain the phase spectrum (Figure9) following the procedures presented in Eqs.7-13.
7. Operate IFFT to the obtained amplitude spectrum (Figure8) and phase spectrum (Figure9) to generate the ground motion (Figure10).

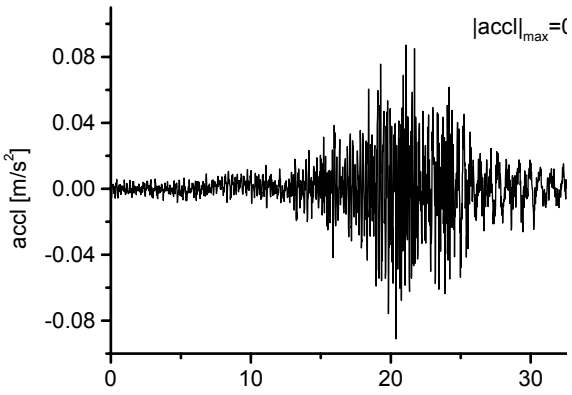

Figure 10 Initial ground motion

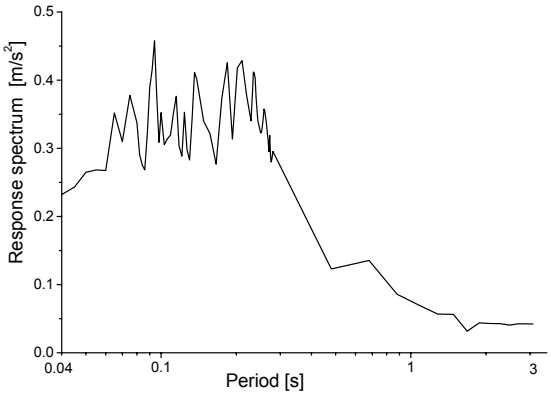

Figure 11 Response spectrum of the initial ground

Checking the response spectrum of the generated ground motion at the fitting points (Figure11).

8. Modulate the Fourier amplitude and the generated ground motion following the procedures presented in Sect.4. As there is a big difference between Figure11 and the target spectrum (Figure5), iteration calculation is needed. After a few times (no more than six) iteration, the ground motion satisfying the tolerant error (5% in this example) is obtained (Figure12). The comparison of the response spectrum of the generated ground motion to the target response spectrum is presented in Figure13.

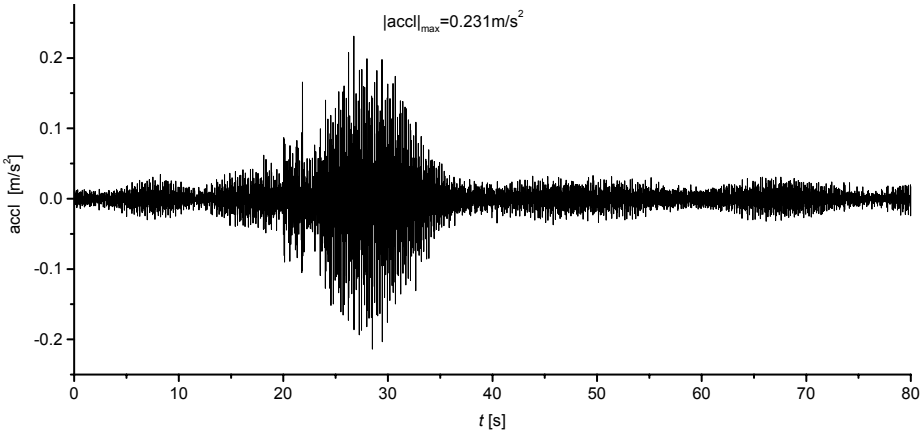

Figure 12 Generated ground motion

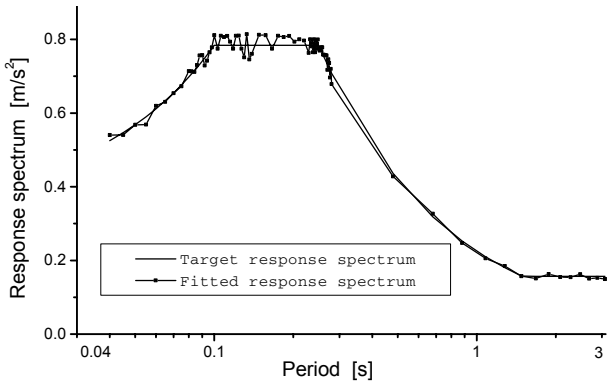

Figure 13 Comparison of the fitted and the target response spectrum on the fitting points points

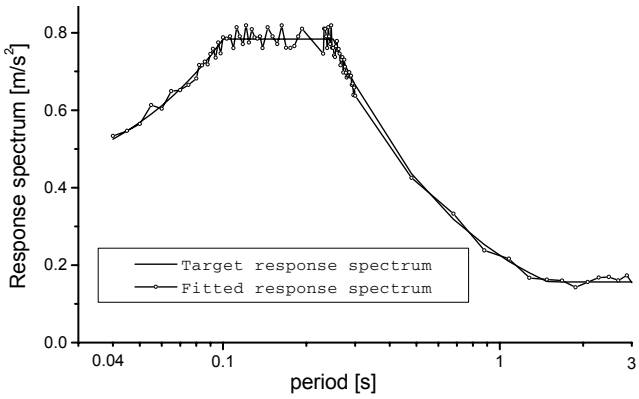

Figure 14 Comparison of the fitted and the target response spectrum on other

The fitting accuracy of the generated ground motion (Figure12) about another set of fitting points is also investigated and it is shown that tolerant error may be not satisfied at a few points but the error is not big, just about 7% (Figure14). It is believed that this error may satisfy the engineering applications, higher accuracy can be reached by increasing the iteration steps if it is needed. The further comparison of the fitting efficiency between Eq.20 and Eq.16 verifies that Eq.23 is more efficient than Eq.16 as the generating procedure in the above example will be divergent if Eq.16 is applied.

CONCLUSIONS

A new integrated algorithm is presented for the generation of artificial records which comply with any target response spectrum and/or target power spectral density requirement and possess the time and frequency nonstationarity typical of the real earthquake recordings. The algorithm proposed in this work, in contrast to most of previous publications, applies the component-by-component fitting technique which makes the response spectrum fitting procedure more efficient and with high convergence speed.

ACKNOWLEDGEMENTS

This study was supported by the National Science Foundation of China under the Grant No. 59708007 and the Teaching and Research Award Fund for Outstanding Young Teachers in Higher Education Institute of MOE, PRC. The authors wish to thank Prof. Chen Yingjun for his constructive comments on this work.

REFERENCES

Deodatis, G., 1996, "Generation of Ground Motion Time Histories as Non-stationary Vector Process: Response Spectrum Compatible Seismograms", *Probabilistic Mechanics and Structural and Geotechnical Reliability, Proceedings of the 7th Specialty Conference on Probabilistic Mechanics and Structural Reliability*, Aug. 7-9, Worcester, MA, USA, pp616-619.

Ghosh, A. K., 1993, "On the Generation of Ground Motion Accelerogram Compatible with a Specified Response Spectrum and a Fourier Amplitude Spectrum", *Transactions of the 11th International Conference on Structural Mechanics in Reactor Technology*, 08/18-08/23/91, Tokyo.

Hu Y., He X., 1986, "Phase Angle Consideration in Generating Response Spectrum-Compatible Ground Motions", *Earthquake Engineering and Engineering Vibration* (in Chinese), **6**(2), 37-51.

Karabalis, D. L., Cokkinides, G. J., Rizos, D. C., Mulliken, J. S., 2000, "Simulation of Earthquake Ground Motions by a Deterministic Approach", *Advances in Engineering Software*, **31**(5), 328-338.

Kaul, M. K., 1978, "Spectrum-consistent Time History generation", *J. of Engineering Mechanics*, ASCE, **104**(4), 781-788.

Kaul, M. K., 1978, "Stochastic Characterization of Earthquakes Through Their Response Spectrum", *Earthquake Engineering & Structural Dynamics,* **6**(5), 497-509.

Mignolet, M. P., Harish, M. V., 1996, Comparison of Some Simulation Algorithms on Basis of Distribution, *Journal of Engineering Mechanics*, 122(2), 172-176.

Nigam, N. C., 1982, "Phase Properties of a Class of Random Processes", *Earthquake Engineering & Structural Dynamics*, **10**(6), 711-717.

Preumont, A., 1984, "The Generation of Spectrum Compatible Accelerograms for the Design of Nuclear Power Plants", *Earthquake Engineering & Structural Dynamics*, **12**(4), 481-497.

Sabetta, F., Pugliese, A., 1996, "Estimation of Response Spectra and Simulation of Nonstationary Earthquake Ground Motions", *Bulletin of the Seismological Society of America*, **86**(2), 337.

Shinozuka, M., Sato, Y., 1967, "Simulation of Nonstationary Random Process", *J. of Engineering Mechanics Division*, ASCE, **93**(1), 11-40.

Shrikhande, M., Gupta, V. K., 1996, "On Generating Ensemble of Design Spectrum Compatible Accelerograms", *European Earthquake Engineering,* Bolona, Italy, X(3), 49-56(1996).

Shaw, D. E., Rizzo, P. C., Shukla, D. C., 1975, "Proposed Guideline for Synthetic Accelerogram Generation Method", *Proceed*ngs of the 2nd International Conference on Structural Mechanics in Reactor Technology, American Nuclear Society, Berlin Germany.

Yang Qingshan, Jiang Haipeng, 2001, "Generation of Fully Nonstaionary Ground Motions Based on Phase Difference Spectra", *Earthquake Engineering and Engineering Vibration* (in Chinese), **21**(3), 10-16.

Zhao Fengxin, 1992, "The Phase Difference Spectrum of Time Histories and the Generation of the Design Ground Motions", Ph.D. *Dissertation* (in Chinese), Institute of Geophysics, China Seismology Bureau.

The Seismic Retrofit of the Golden Gate Bridge

Charles Seim P.E.

ABSTRACT

The construction of record-breaking suspension bridges in the 1920's and 1930's led up to the construction of the Golden Gate Bridge that opened to traffic on May 28, 1937. The bridge is owned, operated, and maintained by the Golden Gate Bridge Highway and Transportation District (GGBHTD). The District has kept the bridge in first-class condition and has upgraded the bridge on several occasions to improve its performance, to reduce maintenance costs, and to provide longer bridge-life.

The bridge had served the City of San Francisco for over 50 years when the Loma Prieta Earthquake struck in 1989. This seismic event jolted the public's attention into awareness of the seismic vulnerability of the San Francisco Bay Area bridges. The damage to other San Francisco Bay Area bridges and structures, however, prompted the State of California to call for rigorous seismic evaluation and retrofit of all transportation structures, including the five long-span bridges crossing San Francisco Bay, and the Golden Gate Bridge.

The GGBHTD acted within a week after the Loma Prieta earthquake by engaging T. Y. Lin International, San Francisco, to evaluate the seismic vulnerability of the Golden Gate Bridge. An interim report produced in 1990 stated that the main suspension span was vulnerable to damage, some of which could be irreparable, and that the approach structures were vulnerable to severe damage with the possibility of collapse.

This paper presents the seismic retrofit design of the Golden Gate Bridge, providing a case study in engineering methodology that can be applied to the seismic retrofit of other major long span suspension bridges. The methodology begins with an owner-developed performance criteria followed by an engineer-developed design criteria to match the performance criteria. The next steps are performing a seismic hazard analysis and developing a site-specific response spectrum and at least three independent ground motions, for short return-period events as well as for long-return period events. The last steps, which take the most time and are the most difficult, are performing elastic and inelastic analyses; developing, designing, preparing plans; and the writing of the construction specifications for the seismic retrofit measures.

Vice President, T. Y. Lin International, 825 Battery St., San Francisco, CA., and 94111, USA
Phone 415 291 3771, Fax 415 433 0807, cseim@tylin.com

INTRODUCTION

One of the most famous, historic, and enduring structural achievements in the world, the Golden Gate Bridge stands as a symbol of the City of San Francisco, California, and as a monument to the achievement of the bridge engineering profession. The start of its construction in January, 1933, culminated nearly a decade of bridge construction in the United States that extended the world record for suspension bridge span lengths four times.

In 1924 the Bear Mountain Suspension Bridge across the Hudson River near West Point, with a main span of 497.6 m (1632 ft), was completed and took the world record away from the Williamsburg Bridge (487.8 m, 1903) in New York City by only 9.8 m (32ft). The Ben Franklin Suspension Bridge, spanning the Delaware River at 533.5 m (1750 ft) near Philadelphia, Pennsylvania took the record two years later in 1926. In 1929, the Ambassador Suspension Bridge at Detroit, Michigan took the record for suspension bridge span-length and at 564 m (1850 ft) it surpassed the 548.8 m (1800 ft) Quebec steel cantilever truss to take the record as the longest span in the world.

However, the George Washington Suspension Bridge in New York City smashed all of these records by almost doubling the Ambassador span-length with a 1,067 m (3500 ft) leap of the Hudson River in 1931.

The Golden Gate Bridge opened to traffic on May 28, 1937 with a modest 213 m (700 ft) increase in span-length (to 1280 m) over the George Washington Bridge. The Golden Gate Bridge then held the title of the world's longest bridge for 27 years, when it lost the record by only 18 m to the Verrazzano-Narrows Bridge in New York. Today the Golden Gate Bridge has slipped into seventh place behind the now-longest span in the World, the Akashi-Kaikyo Bridge in Japan and the third place Jiangyin Bridge in China. China is now embarking on its own record-span setting explosion.

Fig. 1 The Golden Gate Bridge in 1937

The bridge is owned, operated, and maintained by the Golden Gate Bridge Highway and Transportation District (GGBHTD). The District has kept the bridge in first-class condition and has upgraded the bridge on several occasions to improve its performance, to reduce maintenance costs, and to provide longer bridge life. In 1954, a bottom lateral-bracing system was added to the bridge to improve its performance during high winds. In the mid 1970s, all of the corroding vertical hanger cables were replaced. In 1985, a lightweight orthotropic steel deck, paved with epoxy asphalt, replaced the original concrete deck, which was beginning to suffer chloride ion corrosion. The need for maintenance and upgrading of the bridge continues as new challenges to its structural integrity are discovered.

The public's attention was jolted into awareness of the seismic vulnerability of the San Francisco Bay Area bridges by the October 18, 1989 *Loma Prieta* earthquake. This moderate Magnitude 7.1 and 100-km distant earthquake on the San Andreas Fault did not damage the Golden Gate Bridge. The nearest seismograph indicated a peak ground-acceleration of 0.24 g, about three times the value of 0.075 g, used for the original 1930 design.

The damage to other San Francisco Bay Area bridges and structures, however, prompted the State of California to call for rigorous seismic evaluation and retrofit of all transportation structures including five long-span bridges crossing San Francisco Bay. These included: the San Mateo-Hayward Bridge steel box girder (228.7 m, 1967); the San Francisco-Oakland Bay Bridge suspension spans (2 at 704 m, 1936); the Richmond-San Rafael Bridge steel cantilever truss (2 at 326 m, 1956); the Carquinez Strait Bridge steel cantilever trusses (335.4 m, 1927 and 1958); and the Benica-Matrtinez Bridge continuous steel truss (190.5 m, 1963).

Seismic evaluation and retrofit of two bridges outside of the San Francisco Bay Area were also completed. These were the San Pedro-Terminal Island Suspension Bridge near Los Angeles (457 m, 1961) and the San Diego-Coronado Bay Bridge steel box girder (201 m, 1969).

The GGBHTD acted within a week after the Loma Prieta earthquake by engaging T. Y. Lin International, San Francisco, to evaluate the seismic vulnerability of the Golden Gate Bridge. An interim report produced in 1990 stated that the main suspension span was vulnerable to damage, some of which could be irreparable, and that the approach structures were vulnerable to severe damage with the possibility of collapse. In 1993 The GGBHTD engaged T. Y. Lin International in Joint Venture with Imbsen & Associates, Inc., to design the seismic retrofit of the main suspension span and the North approach structures. Another consultant was engaged to design the seismic retrofit of the South approaches.

This paper will focus on the development of the design for the seismic retrofit of the suspension span, which was the first seismic retrofit design of a major long span bridge in the world. This unprecedented achievement is an excellent Case Study in applying the existing technology in earthquake engineering and the technology developed since the earthquake. The technologies used included performing seismic hazard analysis and developing ground motions; adapting computer nonlinear-structural programming for modeling the suspension bridge; and developing innovative seismic retrofitting concepts and devices to strengthen or modify the response of the structure. Perhaps this interesting story may help others in some small way in

their quest of the seismic retrofitting of suspension bridges. These retrofit principles can and should also be applied to the design of new long-span bridges.

BRIDGE DESCRIPTION

Although most people see the Golden Gate Bridge as a single structure, the 2790 m overall length of the bridge actually consists of five different structure types. The bridge's major components are the North and South steel-truss approach viaducts, the Fort Point steel arch, the arch's flanking concrete pylons that are purely architectural motifs, the two concrete cable-anchorages housings, and the main-span steel suspension bridge. All of the foundations for these structures are supported directly on rock, except for the northern viaduct, which is founded on spread-footing bearings on competent soil.

The three-span 1,966-m suspension bridge has a 1280-m center span and two 343-m side spans. The 227-m high towers, each with two shafts of multicellular steel plate configuration, are tapered in steps from the base to the top, which supports cast-steel saddles. Above the roadway the shafts are connected together with four struts forming portals. Below the roadway they are braced together with two sets of cross bracing. At their bases, the tower shafts do not have anchor bolts but depend on their own weight and the restraint provided by the cables for anchorage.

The 0.92-m diameter cables are spaced 27.44- m apart with a cable sag-to-span ration of 1-to-9. At the shoreward end of each side span, the cables pass through concrete pylons, where the cables are restrained vertically at the roadway level by steel cable tie-downs. The stiffening trusses are 7.7-m deep and are spaced 27.44- m apart in the same plane as the cables. The trusses are connected at the top with lateral cross bracing, which was part of the original design. A lightweight bottom lateral cross bracing was added as a wind retrofit in 1954 after the bridge suffered damage from strong winds. This cross bracing was designed for extreme lightness to keep the added stress in the cable to the lowest amount possible.

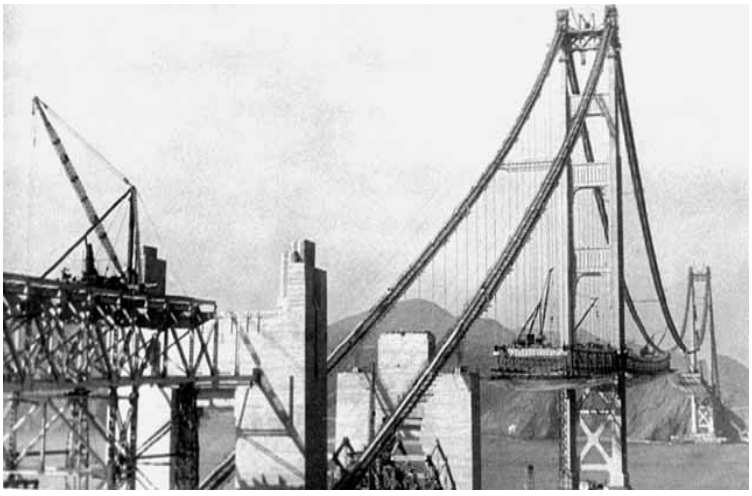

Fig. 2 The Golden Gate Bridge under construction in 1936

The originally 6-lane, 18.29-m wide concrete upper deck was replaced in 1985 with an 18.90-m lightweight orthotropic steel deck because of corroding deck-reinforcing bars. The lighter weight orthotropic steel deck lowered the stress in the cables back to about the original stress level before the addition of the lower lateral cross bracing.

The performance of a long-span bridge during, and the condition of that bridge, after a predicted earthquake, is primarily the owner's responsibility to determine in conjunction with the design engineer. The GGBHTD determined that the GGB is a non-redundant bridge, as there is no alternative route from San Francisco to the North. The Bridge is on a designated lifeline corridor and the bridge should be opened immediately after an earthquake to emergency vehicles.

In California, the performance of bridges is generally specified for two levels of earthquakes that are based on the return periods of the seismic events. A return period from 100 to 475 years is generally specified for an FEE, a functional-evaluation earthquake. For these smaller FEE events, the seismic performance should be nearly full-use of the facility with little damage requiring repairs after the event.

A return period of 1000 to 2000 years is generally used for a SEE, a safety-evaluation earthquake. For these large SEE events, the specified performance can range from no-collapse with non-repairable damage (complete replacement of the bridge required), to repairable damage, or as for the GGB, to nearly full-function of the bridge.

For the GGB, the lifeline determination required that the Bridge performance in a SEE be essentially elastic with either no- or quickly-repairable damage. The bridge should be open to emergency vehicles within hours and to traffic within days. At this high performance level for the SEE event, the GGB will perform with no damage in an FEE event.

According to the United States Historic Preservation Act of 1966 and the Secretary of the Interior's Standards for Rehabilitation, special consideration must be given to any changes to an older bridge that may affect the defining characteristics of the structure. For the GGB, the seismic retrofit measures developed to upgrade the seismic performance of the Bridge followed hierarchical guidelines. The first priority is to meet the seismic retrofit design criteria for the safety of the structure and the traveling public. The next lower priority is to maintain the architectural appearance of the bridge and to follow, as much as possible, the guidelines of the U.S. Historic Preservation Act. Finally, the seismic retrofit measures should retain as much of the original material that formed the structure as possible.

SEISMIC HAZARD AND GROUND MOTIONS

The Golden Gate Bridge spans the mouth of the San Francisco Bay, which was formed by down-cutting rivers during a previous glacial period. The foundation material consists of sandstone, shale, greenstone, and chert under the North Tower, and serpentine and melange under the South Tower. Shear-wave velocities have been measured in the shale, greenstone, and chert, ranging from 1500 m/sec to 2400 m/sec, and in the serpentine, about 1200 m/sec.

The San Andreas Fault lies 10 km West of and parallel to the Bridge and the fault became famous when it caused the San Francisco Earthquake of 1906. The 1000-2000 year return period on the San Andreas Fault's is a Magnitude 8.3 event, comparable to the 1906 San Francisco earthquake. The Hayward Fault is about 16 km East and is also in a direction parallel to the Bridge. The 1000 to 2000-year event on the Hayward Fault is a Magnitude 7.0 event. However, ground motions from this fault did not control any of the seismic retrofit decisions**.**

A site-specific target response spectrum was developed based on an 84 percentile, equal probability, 5% damped spectrum and is representative of a 2,000-year return period earthquake on the San Andreas Fault. Three independent design-ground motions were developed, based on recorded events, and were made compatible with the target spectrum by adjustment of their Fourier amplitudes. The compatible ground motions have peak ground-accelerations of about 0.65 g, peak velocities of about 115 cm/sec, peak displacements of about 60 cm, and durations of 60 to 90 seconds**.** The ground motions were developed by including possible fault-rupture scenarios, wave-passage effects, extended-source effects, and the effect of ray-path incoherency.

A study was made of the response of the bridge to multiple-support excitation versus the response to rigid base excitation. The only systematic trend observed in the study was that vertical displacements of the stiffening trusses were larger for multiple-support excitation, probably because differential movement between the bridge supports straightens the cables and lifts the spans. In other respects, the differences in the response to multiple-support and rigid base excitation were small and somewhat random over the three design earthquakes.

DESIGN CRITERIA

At the start of design, no design documents existed for the seismic retrofit design of long span bridges so the design team had to develop a Design Criteria. It was developed as a guide for the designers and was printed in loose-leaf notebooks so that revisions could easily be inserted. The technical issues that the Design Criteria addressed are based on meeting the Performance Criteria noted above. The seismic retrofit design is based on inelastic analysis of the bridge. Therefore the criteria limit the displacement ductility demands on bridge members. Limited repairable-damage that does not threaten structural safety and that can be repaired without interrupting traffic is acceptable. These Criteria will allow portions of the bridge to respond to limited inelastic action, but the primary response is to be essentially elastic wherever possible.

Compression members carrying gravity loads are required to remain elastic. Width-to-thickness ratios of steel plates in new members are limited to insure compactness and local ductility. Bracing for buckling is required for most existing members to obtain global ductility. The nominal strength of bolts or rivets in joints must be at least 25 percent greater than the nominal strength of the member. For members that respond elastically to ground motions, the member must be designed to ensure good ductility. Where inelastic response is permitted, the member must be part of a redundant system and the member must be designed for large ductile response values. Because of the non-redundancy of the cable system, inelastic deformations are

prohibited. Fortunately, the cable system responded elastically without any retrofitting measures.

STRUCTURAL MODELING

The computer structural modeling was performed in incremental steps, each step adding to the engineers' understanding of how the bridge would respond in a large earthquake. The first step was to determine the dead-load state starting with the geometry and dead load at the completion of the original construction, which determined the initial stresses. To this step was superimposed the addition of the bottom lateral-bracing system and the removal and replacement of the deck. The deformations and stresses of this dead-load state were computed by geometrically nonlinear-analysis, with large displacement theory, and served as the initial condition for subsequent dynamic analysis.

Performing a modal analysis was the next step for determining vibration properties. The natural frequencies and modal shapes were compared with values obtained from ambient vibration tests on the bridge. The good agreement with the first eight modes verified the computer model. It is always a good idea, in the dynamic analysis of existing bridges, to have measured vibration frequencies with which to compare calculated values. The next step was to perform a linear-response spectrum analysis using the site-specific target response spectrum. This analysis gave the engineers an initial insight into the magnitudes of seismic forces and displacements and pointed out problem areas and components for detailed modeling and study.

The last step was performed after these learning stages gave the engineers a good understanding of how the bridge was responding linearly. That last step used a dynamic nonlinear finite element computer program that solved the integrated coupled equations of motion in the time domain with multi-support excitation inputs. The ground motions at the six primary supports were applied as a time-varying displacement boundary condition. Large displacement effects were considered by establishing static or dynamic equilibrium of the structure in its deformed configuration. The effects of limited displacement capacity at expansion joints and tower uplift were modeled by gap elements.

Detailed three-dimensional finite element local models were used to study the stress distribution, relative displacements, uplift, and moment-rotational relationships. These local models were use for detailed study of the tower base uplift behavior, tower struts, and the stiffening truss-tower interaction.

SEISMIC RETROFIT MEASURES

The design teams developed seismic retrofit measures for all of the vulnerable components in the bridge that either would suffer damage or would not develop ductile action. The seismic retrofits of these areas are presented below.

Tower Piers

The towers of the bridge are supported on reinforced concrete piers extending down to bedrock. Although the piers are massive and very stable, they will be severely loaded when the unanchored steel towers rock during an earthquake.

The retrofit of the piers is to drill in, grout, and post-tension high-strength threaded bars from the surface of the pier and under the footprint of the tower base. These bars will prevent a shear failure along the critical failure plane in the pier, which is beneath the loaded edge of the tower.

Tower Bases

The towers are of multi-cellular construction and consist of plates riveted together with corner angles. At the base, the cross-section consists of 103 cells, each 1.07 m×1.07m square that are just large enough to work inside. The plates are 22 mm thick, giving a width-to-thickness ratio of 48. Plates of this shape will buckle shortly after yielding. A finite-element analysis of a cell showed the corner angles to be only minimally effective in restraining buckling of the plates.

The towers will rock during an earthquake; the magnitude of the uplift is about 60 mm at the extreme fibers of the base. Fixing the bases of the towers caused higher stresses than allowing uplift of the towers, and anchoring the tower bases would be very difficult. The uplift causes concentrations of stress both at the base and above the first setback in the tower. The peak-strains were about four times the yield-strain, assuming elastic-plastic behavior**.** Strains of this magnitude can be accommodated by compact sections, but not by the non-compact sections used in the original construction of the tower bases. The ductile behavior of the tower base will be improved by adding retrofit stiffeners along the vertical centerlines of the plates at the base between the horizontal diaphragms. The added stiffeners will prevent buckling of the plates until after a displacement ductility of four is reached.

Hydraulic Dampers

Hydraulic viscous dampers will be will be installed between the stiffening trusses and the towers to absorb energy, to reduce seismic forces of the stiffening truss impacting the tower, and to control displacements at this critical location. These dampers are used because they will not restrain the thermal and traffic-induced movements of the bridge, and because they can be built with the large capacity needed. T he damper design is simply a piston moving in a cylinder that displaces a viscous fluid passing through an orifice from one side of the piston to the other.

Based on an optimization study, dampers were chosen for the retrofit with a force-relationship of:

$$F = (350 \text{ to } 800 \text{ kip} \cdot \sec^{1/2} / \text{in}^{1/2}) \cdot V^{1/2} \quad \text{(English Units)}$$

At a peak velocity of 180 cm/sec, the dampers will produce a control-peak force of 26,000 kN between the stiffening trusses and the towers.

The dampers dramatically reduce the displacement demands on the bridge wind-locks and expansion joints, and eliminate actual impact between the stiffening trusses and the towers. They also reduce the peak stresses in the stiffening truss chords and the towers, and reduce the tower base shear-forces and uplift. The retrofit design also includes modifications to the bridge wind-locks to increase their displacement capacity, in order to eliminate impact within the wind-locks.

Lateral Bracing

The top and bottom lateral-bracing systems are over-stressed by about 50% in both tension and compression. Because of the contribution of higher modes of vibration to the response of the bridge, the overstress occurs over a large proportion of the length of the bridge, and for a large percentage of members. The existing braces are of non-ductile construction; consisting of four angles laced together into a box configuration. A finite-element analysis of a typical lateral brace showed that the corner angles of the brace buckled locally at an overall ductility-demand of only 1.15, which is the limit of usefulness of the member. Rapid degradation of the strength and stiffness occur after the local buckling. An inelastic time-history analysis showed that the deformation demands on the lateral braces were concentrated into those members, which yielded or buckled first. The peak ductility demands from the inelastic analysis were more than five times in excess of the design criteria limit of two.

The retrofit consists of replacing one-half of the top lateral braces with new members. These will be ductile, compact members of tubular cross-section. The lateral bracing systems are the primary means of resistance of the bridge, both to aftershocks and to wind, and these loads must be provided for as part of the retrofit design.

CONCLUSIONS

The seismic retrofit design of the Golden Gate Bridge has provided a Case Study in engineering methodology that can be applied to the seismic retrofit of other major long span suspension bridges. The methodology begins with an owner-developed performance criteria followed by an engineer-developed design criteria to match the performance criteria. The next steps are performing a seismic hazard analysis and developing a site-specific response spectrum and at least three independent ground motions, for short return-period events as well as for long-return period events. The last steps, which take the most time and are the most difficult, are the performing elastic and inelastic analyses, developing, designing, preparing plans, and the writing of the construction specifications for the seismic retrofit measures.

Acknowledgments

The authors wish to acknowledge the Bridge Owner, the Golden Gate Bridge, Highway and Transportation District; the General Manager, Celia G. Kuppersmith; the current District Engineer, Denis Mulligan; and District Staff Engineer, Jerry Kao who acted as liaison for the

Project. Also acknowledged is the help of former District Engineers Dan Mohn, who started the evaluation and seismic retrofit process, and Merv Giacomini, who continued the work. Also Tim Ingham PhD., PE, Associate with T. Y. Lin International, who directed the analyses and seismic retrofit design reported in this paper.

References

T. Y. Lin International, 1990, "Golden Gate Bridge Seismic Evaluation," Golden Gate Bridge, Highway and Transportation District, San Francisco, CA, November.

T. Y. Lin International, 1991, "Golden Gate Bridge Seismic Retrofit Studies," Golden Gate Bridge, Highway and Transportation District, San Francisco, CA, July.

Geospectra Incorporated, 1992, "Geological, Geotechnical and Ground Motion Studies for Seismic Retrofit of the Golden Gate Bridge," Golden Gate Bridge, Highway and Transportation District, San Francisco, CA, July.

T. Y. Lin International, 1992, "Golden Gate Bridge Design Criteria for Seismic Retrofit Measures," Golden Gate Bridge, Highway and Transportation District, San Francisco, CA, November.

Rodriguez, S., Seim, C., and Ingham, T. J., 1994, "Earthquake Protective Systems for the Seismic Upgrade of the Golden Gate Bridge," Proceedings of the Third U.S.-Japan Workshop on Earthquake Protective Systems for Bridges, NCEER-94-0009, March.

Ingham, T., Rodriguez, S., Nader, M., Taucer, F., and Seim, C., 1994, "Golden Gate Bridge Seismic Retrofit Design, Suspension Bridge Strategy Report," Golden Gate Bridge, Highway and Transportation District, San Francisco, CA, April.

Nader, M.N., and Ingham, T.J., 1995, "Seismic Retrofit of the Towers of the Golden Gate Bridge," Proceedings of the National Seismic Conference on Bridges and Highways, San Diego, CA, December.

Rodriguez, S., and Ingham, T.J., 1995, "Seismic Protective Systems for the Stiffening Truss of the Golden Gate Bridge," Proceedings of the National Seismic Conference on Bridges and Highways, San Diego, CA, December.

Response of Seismic Isolated Bridges Using M-DOF Model and 2D Excitation

George C. Lee and Zach Liang

ABSTRACT

This paper discusses two important issues in modeling the seismic responses of structures: the number of degree of freedom and the directions of excitation. By using a simple M-DOF bridge model with two directional excitations, it is showing that the currently used design spectrum method cannot always provide sufficiently accurate results for seismic design of bridges. Rather, further studies should be carried out to develop or to refine design guidelines based on dynamic analysis with multiple directional excitations, particularly for those bridges with added response modification devices/systems.

The paper is prepared for discussion by the workshop participants. It is essentially a progress report of an on-going research task at MCEER sponsored by the U.S. Federal Highway Administration on development of retrofit strategies for special highway bridges.

INTRODUCTION

Maximum peak responses of structures subjected to earthquake ground motion are important information in aseismic design, especially when seismic response modification technologies are used to improve the structural performance. For M-DOF bridges with cross effects introduced by geometrical and modal coupling as well as multidirectional ground excitations, the response can be quite different from the results based on the currently used design spectrum method, which strictly speaking applies only to bridges that can be approximately by S-DOF models. In the latter cases, the response level can be obtained deterministically by a mathematical model with given ground motion record using time history analysis.

When the bridge is equipped with seismic isolation bearing or other types of response reduction devices, the peak value of responses under random excitation cannot be adequately estimated for the bridge-device systems that should be represented by M-DOF systems.

The basic approach to modify earthquake responses of a structure is to increase the dynamic stiffness of the system (combined structure-device system). Increasing the dynamic stiffness, however, is much more complex than increasing the static stiffness. The generic concept of increasing dynamic stiffness is the reduction of a given structural response under a given level of excitation. The responses can be acceleration, displacement, base shear, or other parameters. When the dynamic stiffness is increased for acceleration reduction, the dynamic

George C. Lee, Multidisciplinary Center for Earthquake Engineering, University at Buffalo, Red Jacket Quad, Buffalo, NY 14261, USA
Zach Liang, Multidisciplinary Center for Earthquake Engineering, University at Buffalo, Ketter Hall, Buffalo, NY 14261, USA

stiffness for displacement may be decreased. Further, the dynamic stiffness of acceleration reduction achieved in a certain frequency range may not necessarily mean the reduction of acceleration will take place in all the other frequency ranges (Clough and Penzien, 1993).

Traditionally, the main goal of bridge seismic isolation design is to reduce the acceleration of the deck or the superstructure. This concept can be shown in figure 1. In this figure, the required acceleration level is represented by the dotted line. Originally, a given bridge has a period T_1 with small damping (with damping ratio ξ_s) and an acceleration level of A_1, which is greater than the required level. By adding seismic isolation, the period is shifted to T_2, but then the acceleration level is still greater than the required value. Thus, additional damping is used with damping ratio ξ_l , so that the acceleration level is reduced to A_3 and the design parameters of T_2 and ξ_l are determined (AASHTO, 2001; ICBO, 2000; UBC, 1997).

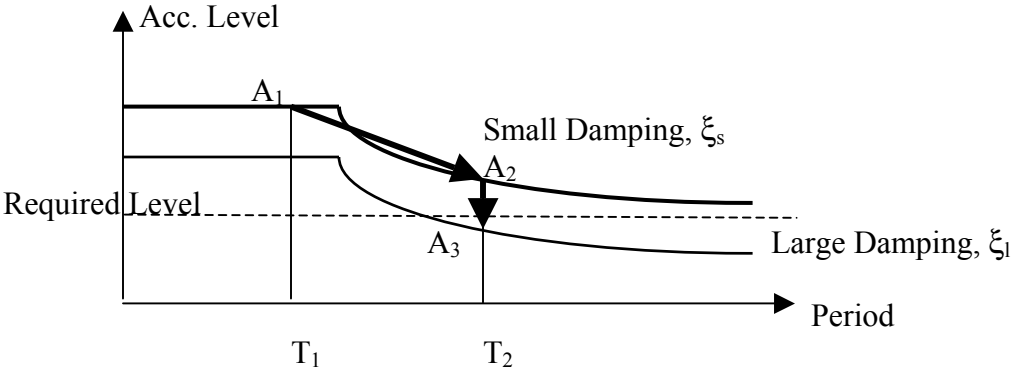

Figure 1. Seismic Isolation Design Concept

In this approach, the corresponding dynamic stiffness of the structure is increased. However, this is achieved by reducing the static stiffness of the bearing and resulting in a drastic reduction of the dynamic stiffness of the displacement. The dilemma is that in order to increase the dynamic stiffness for acceleration reduction, the bearing stiffness has to be very small; but the smaller the bearing stiffness is, the weaker the dynamic stiffness for the displacement will be. This logic further leads to adding damping to reduce the bearing displacement. The concept described in Figure 1 implies that increasing damping can be beneficial for both acceleration and displacement reduction.

This logic can be validated by using time history analysis. Consider the following numerical example:

Suppose the supper structure of a bridge can be modeled by a single mass of 1,000,000 kg and the stiffness of the bearing is 10,000 kN/m, shown in Figure 2(a). The damping ratio is 16.4 % in direction X and 19.1% in direction Y. The isolation system then has the natural period 1.99 seconds in both directions. An earthquake recorded in Llollelo, Chile on March 3, 1985 will be used for the analysis. In a latter section, the reason for choosing this special record will be given.

The Llollelo earthquake was recoded at 100 degree, whose maximum level is 0.71g, as the X directional input and recorded at 10 degree, whose maximum level is 0.45g, as the Y directional input. The results of the time history analysis show that the maximum bearing displacements are about 10.09 cm and 5.50 cm in the X and Y directions, respectively. The

accelerations of the deck are 0.13g and 0.06g in the X and Y directions, respectively. When the damping ratio is doubled, the results are also obtained. They are given in Table 1.

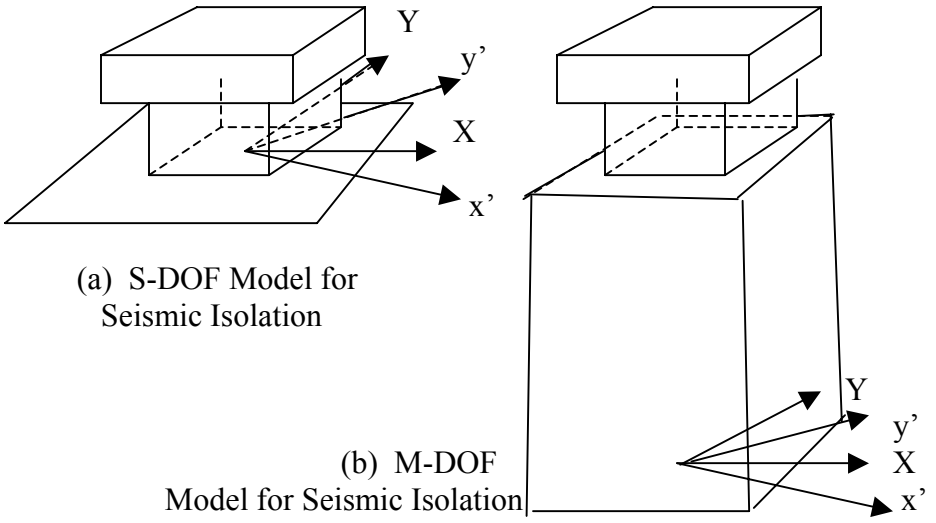

Figure 2. Conceptual Models for Seismic Isolation of a Bridge

TABLE I. COMPARISON OF RESPONSES OF SDOF MODELS WITH DIFFERENT DAMPING

	X disp. (cm)	**X acc. (g)**	**Y disp. (cm)**	**Y acc. (g)**
Original damping ratio	10.09	0.135	5.50	0.06
Damping ratio doubled	7.89	0.144	4.3	0.08
Change	-27.6%	6.9%	-21.7%	18.7%

These results show that, when the damping ratio is doubled, the bearing displacements are reduced. However, the deck accelerations are increased, instead of reduced. The above only illustrates a problem in response estimation using the S-DOF approach. The fundamental aspects in this process are being investigated currently at MCEER under the research contract of the US Federal Highway Administration. Two aspects of this current research will be briefly described in the sections that follow.

EARTHQUAKE GROUND MOTIONS

A 3D ground motion time-history can be completely represented by any 3D Cartesian coordinates. In practice, ground motions are often measured in three fixed directions: north-south, east-west and up-down. For a given structure, a ground motion represented by different coordinates will result in different peak value of the responses. The original record picked up by instruments oriented in the fixed directions therefore may not yield the maximum responses. In order words, the earthquake incident angle is an important parameter that affects the seismic ground records. This issue therefore is how to select the coordinate that can provide the peak value of the response.

Penzien and Watabe (1975) defined the principal axes of ground motions as a set of mutually perpendicular axes about which cross-correlation along such axes are zero-valued. Their original idea is to identify the direction of the direction from the recording location to the epicenter. However, this concept was subsequently used by many researchers, as a reference to select the earthquake incident in the horizontal plan. If a pair of principal axes is in the horizontal plan, then the vertical direction automatically defines the third axis. It is noted that, if only the horizontal plane is considered, such pair of axes always exists. Therefore, the definition of principal axes in the horizontal is legitimate.

In many of the existing earthquake records, the vertical component is relatively small. In this case, the cross correlation between the horizontal components and the vertical one can be quite small. Therefore, the above-mentioned horizontal principal axes can automatically become a 3D set of principal axes under the definition of Penzien and Watabe. However, there are other records that have large vertical components and the correlation function of the horizontal and vertical signals may not be taken as zero.

Let x, y and z denote the two arbitrary horizontal and the vertical directions (see figure 2) and R_{xy} denote the correlation function of the signal along x and y axes. We can establish a 2D and a 3D covariance matrix as follows:

$$h = \begin{bmatrix} R_{xx} & R_{yx} \\ R_{xy} & R_{yy} \end{bmatrix} \quad \text{and} \tag{1a}$$

$$H = \begin{bmatrix} R_{xx} & R_{yx} & R_{zx} \\ R_{xy} & R_{yy} & R_{zy} \\ R_{xz} & R_{yz} & R_{zz} \end{bmatrix} \tag{1b}$$

Where R_{xy} is the correlation function of signals measured from x and y directions, at time zero, and so on. Both h and H are symmetric. Orthogonal eigenvectors are available to decouple the symmetric matrices. For the 2D matrix, its eigenvector matrix can always be written in the following form:

$$\begin{bmatrix} \cos(\theta) & -\sin(\theta) \\ \sin(\theta) & \cos(\theta) \end{bmatrix} \tag{2a}$$

that indicates that turning an angle θ from the original Cartesian coordinates, the newly formed correlation matrix h' will have its off-diagonal entry equal to zero. This is the definition of the principal direction.

Returning now to the numerical example of the M-DOF bridge model and examine the concept of the principal axes of ground motion. First of all, the cross-correlation function of the accelerations is equal to –7.66. Recall the maximum values of the Llollelo earthquake ground acceleration are 0.71g and 0.45g. The correlation function seems to have a large value and not close to zero. From equation (2a), if the angle θ is chosen to be 4.02^0, zero-valued correlation functions can be obtained. Denoting the new direction as x' and y' as shown in Figure 1, the new excitations yield the responses as shown in Table II

TABLE II. COMPARISON OF RESPONSES OF A S-DOF MODEL WITH DIFFERENT SEISMIC INCIDENT

	X disp. (cm)	**X acc. (g)**	**Y disp. (cm)**	**Y acc. (g)**
Original incident	10.09	0.135	5.50	0.062
Principal axes	10.73	0.131	5.28	0.064
Change	-1.6%	-4.0%	-1.5%	-4.1%

Table II shows that the input along the principal axes does not produce larger responses. Instead, the responses become smaller. This fact motivated us to examine further the details about the covariance matrix.

In order to decouple the 3D correlation matrix and to force the two horizontal correlation functions zero-valued, the corresponding eigenvector matrix must have the following form:

$$\begin{bmatrix} \cos(\theta) & -\sin(\theta) & 0 \\ \sin(\theta) & \cos(\theta) & 0 \\ 0 & 0 & 1 \end{bmatrix}$$

This requirement may not be satisfied by many earthquake records. Therefore, to use 3D ground motions, the first problem is how to define the principal axes in the horizontal plan.

Consider the Llollelo earthquake, without the vertical acceleration, the 2x2 matrix is given by

$$h = 10^8 \begin{bmatrix} 1.9007 & -0.0767 \\ -0.0767 & 0.8643 \end{bmatrix} \text{ with its eigenvector matrix equal to } \begin{bmatrix} 0.9973 & 0.0734 \\ -0.0734 & 0.9973 \end{bmatrix}$$

With the vertical data, however, the 3x3 matrix is

$$H = 10^8 \begin{bmatrix} 1.9007 & -0.0767 & 0.4551 \\ -0.0767 & 0.8643 & -0.1117 \\ 0.4551 & -0.1117 & 1.2460 \end{bmatrix}, \text{ with its eigenvector matrix equal to}$$

$$\begin{bmatrix} 0.8836 & 0.4621 & -0.0752 \\ -0.0929 & 0.3305 & 0.9392 \\ 0.4589 & -0.8229 & 0.3350 \end{bmatrix}$$

From the above matrix, we can no longer extract the angle 4.02^0 corresponding to zero-valued correlation functions. The corresponding angle for this case actually will be much larger than $4^{0.}$

López and his coworkers (1997, 2002) have shown that, even in a horizontal plan, seismic incident along the above-defined principal axes will not yield the maximum peak value. In their study, existence of critical incident angle is pointed out, which is measured from the

above-mentioned principal axes. Because their formulation is based on the design spectrum, no information is provided about the variation of peak responses under different excitations with varying seismic incident. The current MCEER study to-date using time history analysis has shown that such a exact variation can be quite large (Yang, 2002; Lee and Liang, 2002 in print). The maximum peak values can be several times larger than the minimum values. This implies that, if a bridge is designed based on the original records or the record projections along the principal axes defined by Penzein and Watabe (1975), the responses of the bridge may be several times smaller than the actual maximum values.

To substantiate this point, results of the time history analysis using the S-DOF model of the same example are given in Table III.

TABLE III. COMPARISONS OF RESPONSES UNDER EXCITATIONS WITH DIFFERENT SEISMIC INCIDENCE

	X disp. (cm)	**X acc. (g)**	**Y disp. (cm)**	**Y acc. (g)**
Critical incident	12.18	0.142	11.28	0.141
Principal axes	10.73	0.133	5.28	0.062
Change	5.16%	5.8%	130.4%	128.8%

It is seen that more than 100% error exists.

The important conclusion of the above analysis is that the dynamic stiffness is differently related to various response parameters. These response parameters can have their maximum values at different incident angles. In other words, a given structure under a given earthquake may have many critical seismic incidents.

In the next section, the effect of seismic incident angle will be given by using the same numerical example.

DIRECTIONAL CROSS EFFECT AND MODAL COUPLING OF DYNAMICALLY LOADED STRUCTURES

If a structure can be completely decoupled in individual modes, then using model superposition (the S-DOF approach) will not introduce errors. If a structure does not has responses due to perpendicular excitations, then we can compute the response in the two individual directions. To classify the responses in three or two mutually perpendicular directions is a useful approach, because seismic ground motion along a single direction of a building causes responses at different floors of the building along the same direction. However, such idealized consideration does not exist in real structures. It is, therefore, important to understand the cross effects on the responses and to determine their magnitude.

To understand cross effects, the first question to consider is whether a given structure has principal axes under dynamic load. If not, then a load acting along one axis will cause responses in the perpendicular directions. In this case, directly estimate of the peak response by superposition method is difficult because the relationship between the amplitude of excitation and the peak response is non-linear.

The nonexistence of principal axes for dynamic loaded structures has been shown by the authors (Lee and Liang, 1998). Assume that a structure consists two sub-structures and each of them has its own principal axes. If these two pairs of principal axes are not in the identical directions, then the total structure will not have principal axes. Experimentally, the authors have

quantitatively validated the theory with the shaking table using a 3 story steel frame structure. The ground motion is single directional. The structure was tested in many positions, by turning it from 0^0 to 100^0 around a vertical axis. The experimentally observed cross effects are the responses in the perpendicular direction of the single direction excitation (Liang and Lee, 2002; Yang et al, 2002).

This cross effect is not only caused by structural rotation (torsional effect). Both theoretical and experimental studies show that, without rotation, cross effect still exists and our experimental results show that more than 50% enlargement of the responses can be easily realized due to cross effect without detectable rotating of the test structure.

To substantiate the above, the previous numerical example will be again utilized. Figure 2(b) shows the possibility of adding more DOFs to the model if the column is flexible.

Suppose, two more DOFs in each directions are added with the corresponding modal parameters listed in Table IV.

TABLE IV. MODAL PARAMETERS OF MDOF MODEL BRIDGE

Mode	**6**	**5**	**4**	**3**	**2**	**1**
Natural Frequency (HZ)	46.6156	37.8707	22.5061	27.4108	0.5585	0.4486
Damping Ratio	0.0160	0.0556	0.0678	0.0356	0.3438	0.3656

Recall in our numerical example when the isolation system is modeled by S-DOF in each direction, with the same damping coefficient, the damping ratios are 32.8 % in X direction and 38.2% in Y direction. If we have a more flexible pier and add more DOFs, the corresponding damping ratios change slightly and have the values of 34.4% and 36.6%, respectively.

First, by ignoring the cross effect and by inputting the excitation in the X and Y direction independently, the difference of results between M-DOF and S-DOF models are listed in Table V.

Next, we consider the cross effect. In this case, the input contains the two perpendicular excitations. The results are also given in Table V for the purpose of comparison.

TABLE V. COMPARISON BETWEEN SDOF AND MDOF MODEL

	X disp. (cm)	**X acc. (g)**	**Y disp. (cm)**	**Y acc. (g)**	**X bases hear (kN)**	**Y base shear (kN)**
SDOF (principal axes)	4.54	0.144	7.72	0.081	454	772
SDOF (critical incident)	8.47	0.145	9.09	0.145	847	909
MDO (single excitation)	8.06	0.146	9.12	0.141	1,016	884
MDOF (with cross effect)	7.83	0.147	9.43	0.151	1,007	900

From Table V, it is seen that different models can yield quite different results. Bearing displacement is one of the most critical parameters. By means of the MOF model with the consideration of slight cross effect as well as the critical seismic incident, we can compute the largest bearing displacement as large as 9.4 cm.

More detailed comparisons can be made by examining Figure 3, where the comparison of the base shear by using the S-DOF and M-DOF models is shown. The seismic incident angles

are chosen from 0^0 and 180^0. It is seen that, different models and different directions will have their own critical incident angles. The maximum and minimum values changes drastically. For example, the maximum base shear of the M-DOF model in the X and Y direction are 68% and 91%, respectively, larger than that of the minimum value, whereas the factors of S-DOF model are different.

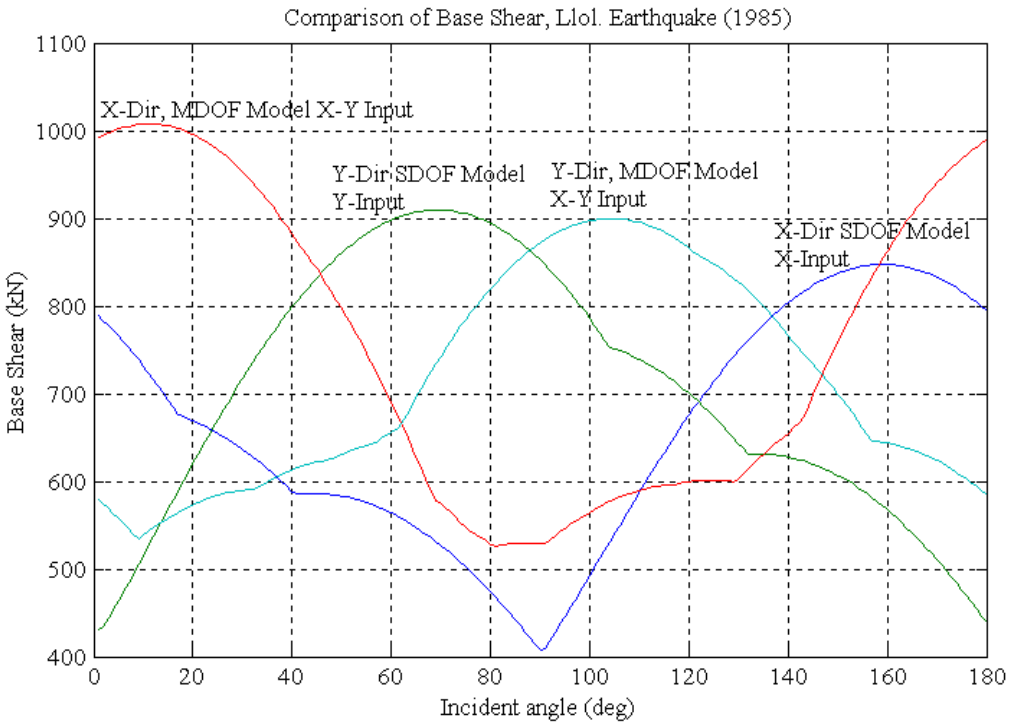

Figure 3. Comparisons of the base shear M-DOF vs. S-DOF

The results of bearing displacement by using single and 2D excitations are shown in Figure 4. The differences are measures of the cross effect. It is seen that the critical incident angles between the single and 2D excitations are different. The maximum of the bearing displacement with concern with the cross effect is 130% larger than that of the minimum value in the X direction. Without consider the cross effect, it is 100% larger that value in Y directions. About 30% different is visualized. It is noted that, in the example and with the Llollelo earthquake, the different of the amplitude of the bearing displacement is not significant. However, results using other earthquake records have shown that, with the same model bridge, a much larger difference in the bearing displacement can result.

In Figure 5, the deck accelerations by using the M-DOF and S-DOF models are compared. Again, it is seen that, the critical incident angles between these two models are different. In addition, the maximum deck acceleration is more than 90% larger than that of the minimum value in the X direction, and in the Y direction it is about 90% larger.

Figure 6 shows the comparison of the deck acceleration by using the single and 2D excitations. Once again, the critical incident angles are different in these two cases. In addition, Table VI lists the results of the critical angles for the M-DOF model under 2D excitations. It can

be seen that, first of all, different parameters do have different incident angles. In addition, the incident angles for identical parameter along perpendicular axes are rarely perpendicular.

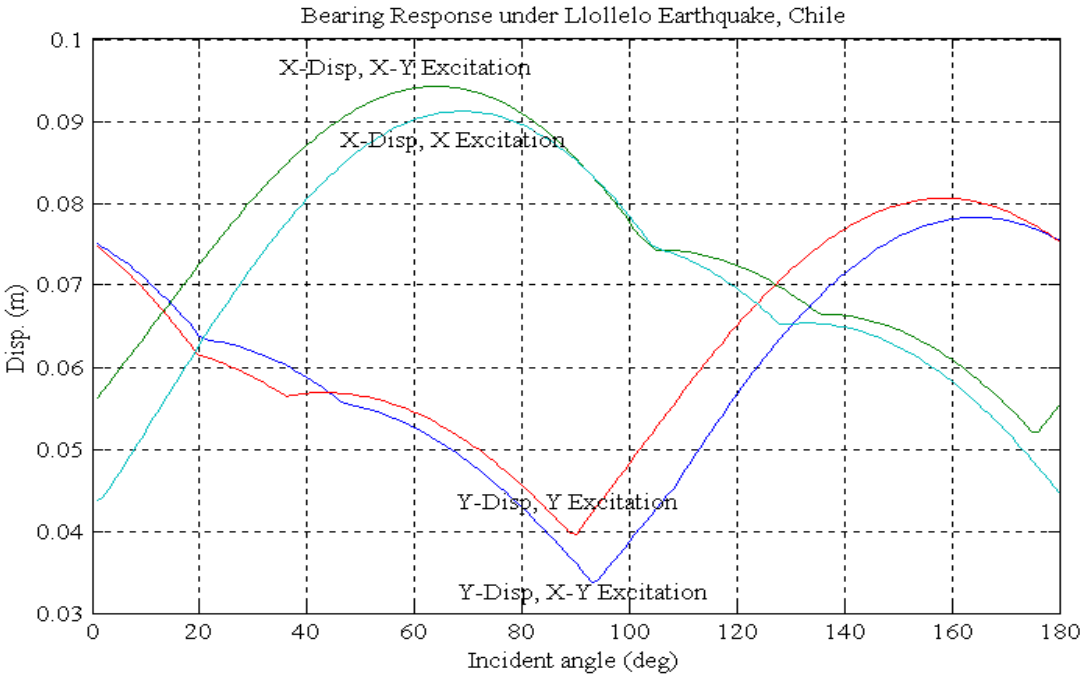

Figure 4. Comparisons of the bearing displacement, single and double excitations

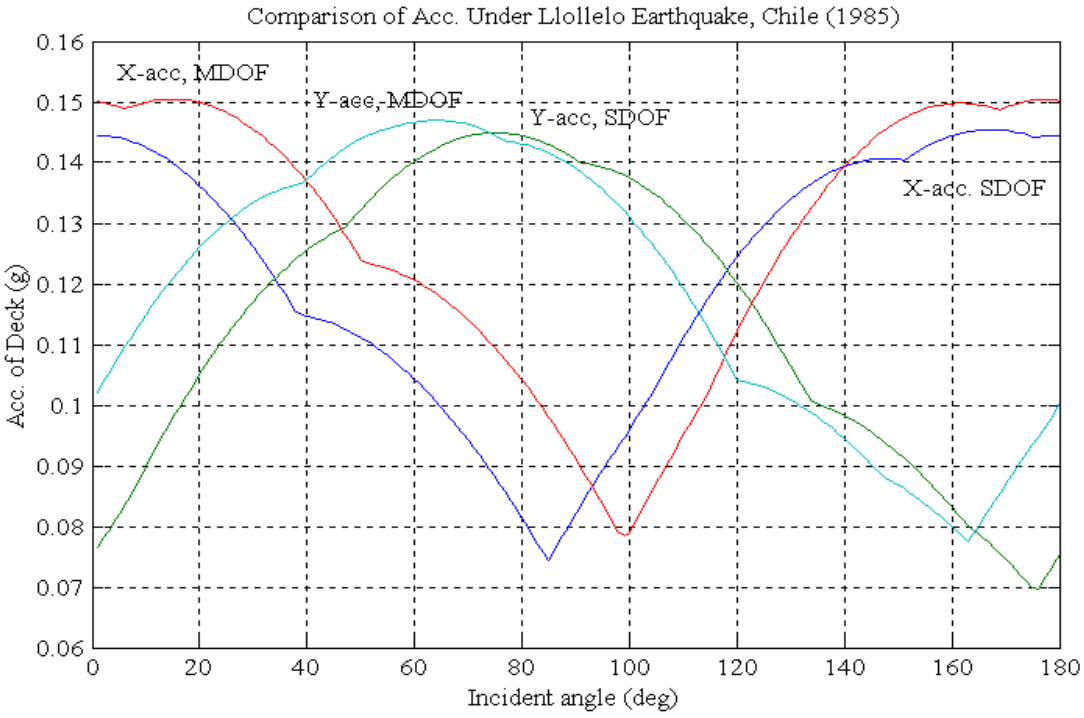

Figure 5. Comparison of deck accelerations, M-DOF. vs S-DOF

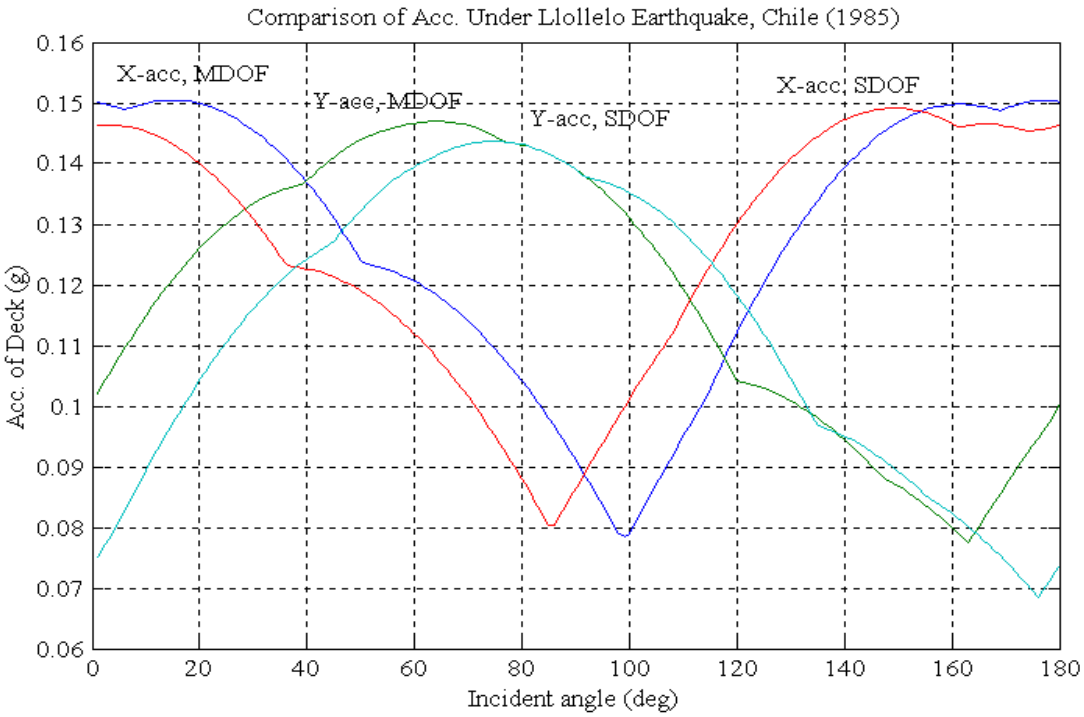

Figure 6. Comparison of deck accelerations, single and double excitations

TABLE VI. CRITICAL INCIDENT ANGLE (DEGREE)

	X direction	**Y direction**
Acc. of deck	15	64
Bearing disp	164	64
Base Shear	11	104

SUMMARY

One of the major difficulties in seismic response estimation of structures is to properly handle the nonlinear relationship between the maximum response and the amplitude of the ground excitation. The design response spectrum is a simple approach. However, it has its limit in applications. This paper presents a numerical example on the responses of a seismic isolated bridge by using M-DOF model and two directional excitations to illustrate the applicability of the design response spectrum. Two major issues influencing the seismic responses are discussed: (1) the choice of input ground motions, and (2) the geometrical and modal coupling effect.

It is expected that time history analyses will be more and more intensively used as computer technology improves to gradually replace the spectrum analysis in bridge design. Accurate modeling and correctly selecting the forcing functions are critical in time history analysis. This paper is prepared as a progress report of the current MCEER research on the subject, for the purpose of inviting discussions and comments from the workshop participants. Hopefully, future cooperative research projects can be developed with PRC researchers interested in formulating design guidelines for seismic response modification of bridges.

REFERENCES

AASHTO Guide Specifications for Seismic Isolation Design. 2001.

Clough, R.W. and Penzien, J. 1993. *Dynamics of Structures*. Second Edition, New York: McGraw-Hill.

Hernández, J. J. and López, O. A. 2002. Response to Three-Component Seismic Motion of Arbitrary Direction. *Earthquake Engineering and Structural Dynamics*, 31:55-77.

International Conference of Building Officials. 2000.

Lee, G. C. and Liang, Z. 1998. "On Cross Effects of Seismic Response of Structures," *Engineering Structures*, 20(4-6): 503-509.

Lee, G. C. and Liang, Z. to appear 2002. "Towards next generation seismic isolation technology." Proceedings International Conference on Advances in Building Technology, Hong Kong, Elsevier Science Ltd.

Liang, Z. and Lee, G. C. to appear 2002. Principal Axes of M-DOF Structures under Dynamic Loading, Part I: Theoretical Considerations, MCEER Technical Report.

López, O. A. and Torres, R. 1997. "The Critical Angle of Seismic Incidence and the Maximum Structural Response." *Earthquake Engineering and Structural Dynamics*, 26:881-894.

Penzien, J. and Watabe, M. 1975. "Characteristics of 3-dimensional earthquake ground motions." *Earthquake Engineering and Structural Dynamics,* 3: 365-374.

Uniform Building Code (UBC), (1997)

Yang, T. 2002. Investigation of Principal Axes of M-DOF Structures under Dynamic Loadings, M.S. Thesis, University at Buffalo, State University of New York, Buffalo, NY, June 2002.

Yang, T., Liang, Z. and Lee, G. C. to appear 2002 . Principal Axes of M-DOF Structures under Dynamic Loading, Part II: Experimental Observations, MCEER Technical Report.

Seismic Conceptual Design

for Bridge Tower of a Long-span Cable-stayed Bridge

Ai-jun Ye[1],Shi-de Hu[1] and Li-chu Fan[1]

ABSTRACT

The performance of a long-span cable-stayed bridge is highly dependent on the choice of tower type. In this paper, three types of tower (inverted Y shape, diamond shape and A shape) was compared from a seismic design viewpoint, the results indicate that tower of inverted Y shape or A shape has better seismic behavior than that of diamond shape. Further, for the inverted Y shape tower, the influence of height variation of the crossbeam section on seismic behavior was analyzed, and the results indicate that the influence is light within a certain variation range.

[1]State Key Laboratory for Disaster Reduction in Civil Engineering, Tongji University, Shanghai 200092, PRC

INTRODUCTION

The tower of a cable-stayed bridge is one of the key components of the whole structure. The type and dimension of the tower determine the dynamic characteristics and seismic behavior of the bridge to a great extent. Therefore, seismic conceptual design for bridge towers is discussed herein.

The cable-stayed bridge under investigation has a steel box girder deck of 40.6m wide overall and 2088m's long. The layout of spans is 100+100+300+1088+300+100+100m. Figure1, Figure 2 shows the elevation of the bridge and the cross-section of deck respectively. Three types of concrete tower were designed, i.e. inverted Y shape, diamond shape and A shape, see Figure 3. There is a little difference in the cross-section dimension between inverted Y shape, diamond shape and A shape tower. Each tower of the bridge is founded on a caisson of about 80m's deep. The deck is supported by sliding bearings sitting on top of each auxiliary pier and anchored pier, and there is no bearing between deck and crossbeam of each tower. The sectional area of the first cable away from tower is 0.01134 m^2, and that near the tower is 0.00518m^2.

The emphasis of dynamic analysis was put on two aspects:

(1) The comparison of dynamic characteristics and seismic behavior between inverted Y shape, diamond shape and A shape tower;

(2) The influence of height variation of the crossbeam section on seismic behavior of the tower.

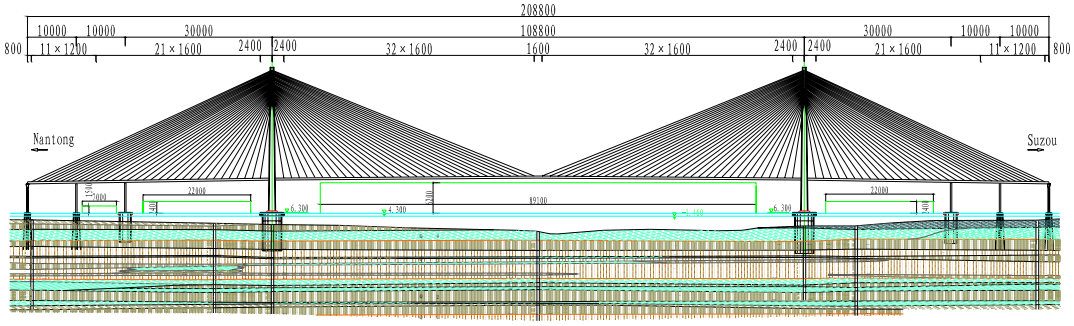

Figure 1. Elevation of the cable-stayed bridge

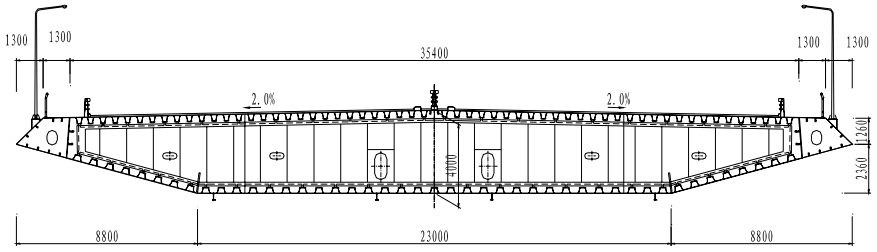

Figure 2. Cross-section of the deck

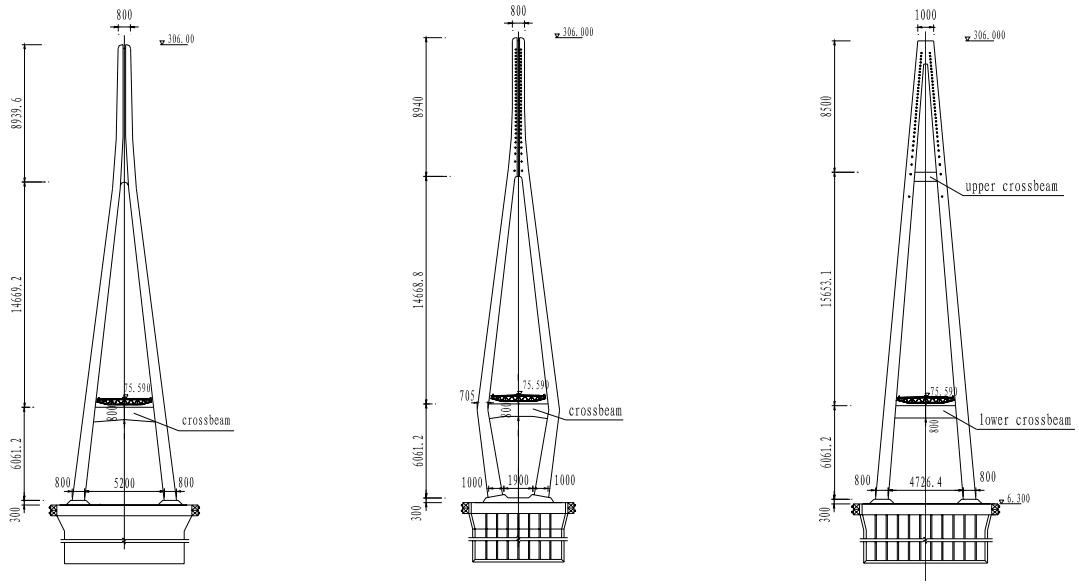

(a) inverted Y shape tower (b) diamond shape tower (c) A shape tower

Figure 3. Three types of tower

CONSTRUCTING OF DYNAMIC ANALYSIS MODEL

Based on the design drawings of the cable-stayed bridge, three 3-dimension finite element models were constructed to make the dynamic characteristics and seismic response analysis. Model 1 is for inverted shape tower (see Figure 4.), Model 2 is for diamond shape tower, and Model 3 is for A shape tower.

In each FE model, the deck, towers and side piers were represented by beam elements with six degrees of freedom (DOFs) for each node. The bridge deck was simplified using a single spine passing through the shear center of the deck cross section. The stiffness and mass properties of the deck were calculated and assigned to the spine. The cables and the deck spine were linked with master-slave relation. Each tower was modeled using a 3-D frame. The cables were represented by linear elastic truss elements with three DOFs for each node, considering the influence of cable's sag and dead load on the geometric stiffness. The nonlinear stiffness characteristic of the cables due to sag was approximated by linearizing the cable stiffness using the concept of an equivalent modulus of elasticity, such as the Ernst equation.

The deck and each tower were linked with master-slave relation only in transverse, while the deck and each side pier (anchored pier or auxiliary pier) were linked with master-slave relation in transverse and vertical. Each tower and side pier was fixed at the bases.

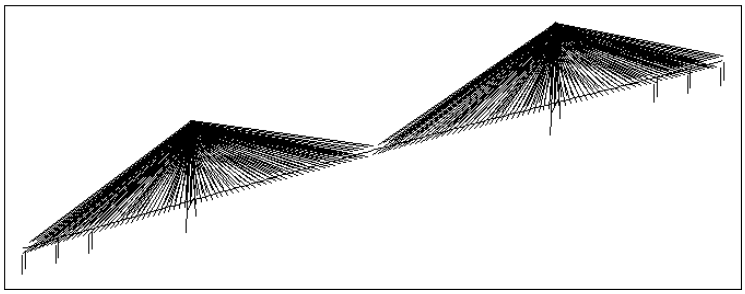

Figure 4. Dynamic model of the cable-stayed bridge (inverted Y shape)

ANALYSIS OF DYNAMIC CHARACTERISTICS

Analyzing and understanding the dynamic characteristics of bridge is the base of making seismic behavior analysis. Therefore, in this part, three FE models (mentioned above) were used to achieve the dynamic characteristics of the bridge.

Assuming that the bridge vibrates around its dead-load static equilibrium position, the natural modal properties were computed. Table I shows the results. One can see from the table, the dynamic characteristics of the bridge with three types of tower are almost the same except the transverse vibration of the tower its own. For the first tower-dominate lateral vibration mode, frequency of diamond shape tower is 27% lower than that of inverted Y shape tower, and frequency of A shape tower is 31% lower than that of inverted Y shape tower. Furthermore, the torsional vibration frequency of A shape tower is also about 3% lower than that of the other two types of tower.

In addition, the first vibration mode of the bridge is floating longitudinally, and the corresponding period approaches 15s. Therefore, the response spectra and time history curves used to carry out seismic response computation must include the information of a long period of 15s.

TABLE I. COMPARISION ON DYNAMIC CHARACTERISTICS OF THREE TYPES OF TOWER

Order	Inverted Y shape tower		Diamond shape tower		A shape tower	
	Frequency (Hz)	Mode characteristics	Frequency (Hz)	Mode characteristics	Frequency (Hz)	Mode characteristics
1	0.0680	Floating longitudinally	0.0688	Floating longitudinally	0.0677	Floating longitudinally
2	0.1044	Lateral bending symmetrically	0.1040	Lateral bending symmetrically	0.1043	Lateral bending symmetrically
3	0.1801	Vertical bending symmetrically	0.1803	Vertical bending symmetrically	0.1787	Vertical bending symmetrically
4	0.2227	Vertical bending anti-symmetrically	0.2230	Vertical bending anti-symmetrically	0.2213	Vertical bending anti-symmetrically
5	0.2779	Lateral bending anti-symmetrically	0.2718	Lateral bending anti-symmetrically	0.2741	Lateral bending anti-symmetrically
6	0.3150	Vertical bending symmetrically	0.3109	Tower lateral bending in same direction	0.2920	Tower lateral bending in same direction
7	0.3819	Vertical bending anti-symmetrically	0.3156	Vertical bending symmetrically	0.2958	Tower lateral bending in reverse direction

8	0.4258	Vertical bending	0.3185	Tower lateral bending in reverse direction	0.3130	Vertical bending
9	0.4281	Tower lateral bending in same direction	0.3830	Vertical bending	0.3805	Vertical bending
10	0.4291	Tower lateral bending in reverse direction	0.4277	Vertical bending	0.4220	Vertical bending
16	0.5406	Torsional bending symmetrically	0.5398	Torsional bending symmetrically	0.5223(14)	Torsional bending symmetrically
27	0.7804	Torsional bending anti-symmetrically	0.7806	Torsional bending anti-symmetrically	0.7591	Torsional bending anti-symmetrically

SELECTING OF INPUT EARTHQUAKE MOTION AND ANALYSIS METHOD

Response spectrum method is selected in the seismic response computation, so two ground response spectra (longitudinal and vertical respectively) from the site earthquake risk analysis were selected as the input earthquake motion, see Figure 5. The corresponding damping ratio for the two response spectra is 5%. The peak value of acceleration on ground surface is 0.194g in horizontal, and 0.135g in vertical.

The first 300 modes of the bridge were included and combined with CQC method in the analysis. A damping ration of 5% is used for all modes.

The structural responses under seismic inputs in longitudinal-vertical and in transverse-vertical were computed respectively.

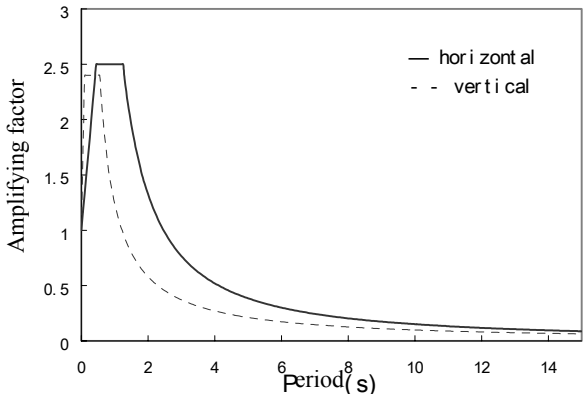

Figure 5. Response spectrum curves

SEISMIC BEHAVIOR ANALYSIS OF THE CABLE-STAYED BRIDGE WITH DIFFERENT TYPES OF TOWER

Based on the three models and earthquake input mentioned above, the seismic response was predicted. Seismic response of the bridge with the three types of tower was analyzed with comparison, as shown in Table II, Table III and Table IV. From which we can see, the difference

on longitudinal seismic response among three types of tower is small, while the difference is big on transverse direction. Among which, as for inner forces, there is little difference between tower of inverted Y shape and A shape; but for displacements on the top of the tower, A shape tower is 55% larger than the inverted Y shape tower. In particular, both inner forces and displacements of diamond shape tower are very large, the bending moment on the bottom of the tower and the displacement on the top of the tower are twice as large as that of inverted Y shape tower.

Table V shows the transverse inner forces on side piers. For the bending moment at the bottom of 1# auxiliary pier, which controls the design, result of inverted Y shape tower is 6% less than that of diamond shape tower, 7% more than that of A shape tower. So, the difference is small.

As a whole, inverted Y shape tower and A shape tower have a better aseismic behavior than diamond shape tower.

TABLE II. MAXIMUM VALUES OF INNER-FORCE ON CONTROL SECTION OF MAIN TOWER (LONGITUDINAL-VERTICAL INPUT)

Tower shape	Section location of tower	Axial force P (kN)	Shear Force Q_3 (kN)	Bending Moment M_2 (kN.m)
Inverted Y shape	Bottom of tower	7.503E4	2.699E4	2.250E6
	Above the crossbeam	6.669E4	1.809E4	1.241E6
	Below the intersection	3.255E4	9.564E3	5.193E5
Diamond shape	Bottom of tower	7.426E4	2.805E4	2.310E6
	Above the crossbeam	6.546E4	1.876E4	1.249E6
	Below the intersection	3.211E4	9.651E3	5.278E5
A shape	Bottom of tower	7.646E4	2.941E4	2.362E6
	Above the lower crossbeam	6.815E4	1.922E4	1.302E6
	Below the upper crossbeam	3.587E4	1.020E4	5.874E5

where subscript 3 indicates the longitudinal direction , subscript 2 indicates the transverse direction

TABLE.III MAXIMUM VALUES OF INNER-FORCE ON CONTROL SECTION OF MAIN TOWER (TRANSVERSE-VERTICAL INPUT)

Tower shape	Section location of tower	Axial force P (kN)	Shear Force Q_2 (kN)	Bending Moment M_3 (kN.m)
Inverted Y shape	Bottom of tower	2.612E5	3.996E4	1.462E6
	Above the crossbeam	2.047E5	3.777E4	1.235E6
	Below the intersection	1.939E5	9.114E3	5.118E5
	End of the crossbeam	1.018E4	7.507E4	1.720E6
Diamond shape	Bottom of the tower	2.322E5	6.711E4	2.956E6
	Above the crossbeam	1.822E5	3.095E4	7.410E5
	Below the intersection	1.710E5	7.321E3	3.438E5
	End of the crossbeam	1.622E4	7.114E4	1.628E6
A shape	Bottom of tower	1.974E5	4.179E4	1.488E6
	Above the lower crossbeam	1.431E5	3.888E4	1.118E6
	Below the upper crossbeam	1.298E5	1.019E4	7.784E5
	End of the lower crossbeam	1.933E4	6.829E4	1.560E6

where for tower column: subscript 3 shows the longitudinal direction, subscript 2 shows the transverse direction; for crossbeam: subscript 2 shows the vertical direction, subscript 3 shows the longitudinal direction

TABLE IV. MAX. DISPLACEMENT ON KEYPOINTS **(m)**

Tower shape	Location	Longitudinal-vertical input		Transverse-vertical input	
		Longitudinal	Vertical	Transverse	Vertical
Inverted Y shape	Top of tower	1.292	/	0.222	/
	End of deck	1.198	/	0.118	/
	Mid-span	1.201	0.246	0.955	0.246
Diamond shape	Top of tower	1.260	/	0.488	/
	End of deck	1.168	/	0.132	/
	Mid-span	1.171	0.247	1.002	0.246
A shape	Top of tower	1.309	/	0.345	/
	End of deck	1.213	/	0.113	/
	Mid-span	1.216	0.241	0.983	0.241

TABLE V MAX. INNER-FORCE OF CONTROL SECTION OF SIDE PIERS

(TRANSVERSE-VERTICAL INPUT)

Tower shape	Section location	Axial Force P (kN)	Shear Force Q_2 (kN)	Bending Moment M_3 (kN.m)
Inverted Y shape	Bottom of 1# auxiliary pier	6.415E3	1.024E4	5.339E5
	Bottom of 2# auxiliary pier	4.869E3	8.543E3	4.261E5
	Bottom of the anchored pier	2.113E3	7.723E3	3.639E5
Diamond shape	Bottom of 1# auxiliary pier	7.083E3	9.708E3	5.040E5
	Bottom of 2# auxiliary pier	4.978E3	8.400E3	4.152E5
	Bottom of the anchored pier	2.336E3	8.813E3	4.086E5
A shape	Bottom of 1# auxiliary pier	5.248E3	1.094E4	5.713E5
	Bottom of 2# auxiliary pier	4.913E3	8.808E3	4.418E5
	Bottom of the anchored pier	2.116E3	7.417E3	3.477E5

where axial 3 shows the longitudinal direction, axial 2 shows the transverse direction.

Numeral order is from tower to the anchored pier.

INFLUENCE ANAYLSIS OF THE HEIGHT VARIATION OF CROSSBEAM SECTION ON THE SEISMIC RESPONSE

Since the inner forces due to earthquake are greatly more than that of the static load, so it will control the design. Section checking shows that: when the earthquake motion is input in transverse-vertical direction, bending moment of the crossbeam is considerably large, which makes the design of section with 8m high very difficult. So herein we try to analyze the sensitivity of seismic response of inverted Y shape tower by modifying the height of the section from7.0m up to 10.0m.

Table VI and Table VII show the inner forces of control section of inverted shape tower under longitudinal-vertical input and transverse-vertical input respectively.

Table VI shows that as section height of the crossbeam increase from 7.0m up to 10.0m, so do the inner forces of tower column, however, the variation ratio is small, not more than 1%.

Table VII shows that seismic response of sections along the bridge tower varies inconsistently under transverse-vertical input: results of column section above the crossbeam, and section at the end of crossbeam have the trend to increase, while results of column section at the

bottom of the tower and below the intersection decreases. When the height of crossbeam varies from 8.0m to 9.0m, the seismic responses of the four control sections mentioned above vary slightly, the increase ratio of crossbeam bending moment is within 6%, while the section strength can be greatly improved. Therefore, it is beneficial to the seismic behavior of the tower.

TABLE VI. THE INFLUENCE OF HEIGHT VARIATION OF CROSSBEAM SECTION ON THE INNER FORCES OF TOWER (LONGITUDINAL-VERTICAL INPUT)

Height of crossbeam (m)	Section location	Axial Force P (kN)	Shear Force Q_3 (kN)	Bending Moment M_2 (kN.m)	Variation ratio
7.0	Bottom of tower	7.490E4	2.676E4	2.243E6	-0.3%
	Above the crossbeam	6.670E4	1.808E4	1.240E6	-0.1%
	Below the intersection	3.253E4	9.545E3	5.176E5	-0.3%
8.0	Bottom of tower	7.503E4	2.699E4	2.250E6	0
	Above the crossbeam	6.669E4	1.809E4	1.241E6	0
	Below the intersection	3.255E4	9.564E3	5.193E5	0
9.0	Bottom of tower	7.519E4	2.726E4	2.258E6	0.3%
	Above the crossbeam	6.669E4	1.812E4	1.243E6	0.2%
	Below the intersection	3.257E4	9.583E3	5.214E5	0.4%
10.0	Bottom of tower	7.537E4	2.753E4	2.266E6	0.7%
	Above the crossbeam	6.672E4	1.815E4	1.244E6	0.2%
	Below the intersection	3.260E4	9.602E3	5.236E5	0.8%

where 3 shows the longitudinal direction,2 shows the transverse direction; the variation ratio is based on 8.0m,"+"means increasing,"-" means decreasing.

TABLE VII. THE INFLUENCE OF HEIGHT VARIATION OF CROSSBEAM SECTION ON THE INNER FORCES OF TOWER (TRANSVERSE-VERTICAL INPUT)

Height of crossbeam (m)	Section location	Axial Force P (kN)	Shear Force Q_2 (kN)	Bending Moment M_3(kN.m)	Variation ratio
7.0	Bottom of tower	2.435E5	3.876E4	1.496E6	2.3%
	Above the crossbeam	1.897E5	3.629E4	1.185E6	4.0%
	Below the intersection	1.784E5	9.089E3	5.181E5	1.2%
	End of the crossbeam	9.556E3	6.872E4	1.574E6	-8.5%
8.0	Bottom of tower	2.612E5	3.996E4	1.462E6	0
	Above the crossbeam	2.047E5	3.777E4	1.235E6	0
	Below the intersection	1.939E5	9.114E3	5.118E5	0
	End of the crossbeam	1.018E4	7.507E4	1.720E6	0
9.0	Bottom of tower	2.736E5	4.076E4	1.433E6	-2.0%
	Above the crossbeam	2.162E5	3.891E4	1.265E6	2.4%
	Below the intersection	2.057E5	9.121E3	5.050E5	-1.3%
	End of the crossbeam	1.084E4	7.945E4	1.821E6	5.9%

10.0	Bottom of tower	2.819E5	4.131E4	1.409E6	-3.6%
	Above the crossbeam	2.245E5	3.976E4	1.283E6	3.9%
	Below the intersection	2.143E5	9.116E3	4.987E5	-2.6%
	End of the crossbeam	1.146E4	8.252E4	1.891E6	9.9%

where 3 shows the longitudinal direction , 2 shows the transverse direction; the variation ratio is based on 8.0m,"+"means increasing,"-" means decreasing.

CONCLUSION

Based on the above discussion, conclusions can be made as follows:

- The difference on longitudinal seismic response among the three types of tower is small, while the difference is big in transverse direction. Among which, diamond shape tower has the disadvantage of particular large bending moment on the bottom of tower and displacement on the top of tower, while for inverted Y shape and A shape tower, the bending moment and displacement are comparatively small. Therefore, tower of inverted Y shape or A shape has better seismic behavior than that of diamond shape
- Since the influence of height variation of crossbeam section on seismic behavior is small, increasing the section height (1m) could be an alternative to achieve sufficient section strength for the crossbeam, where reinforcing bars is difficult to be set.

REFERENCES

Li-chu Fan, Shi-de Hu and Ai-jun Ye. 2001. "Seismic Design For Long Span Bridge," People's Communication Publishing House (in Chinese)

Li-chu Fan.1997. "Seismic Design Of Highway Bridge", Huajie International Publishing Co. limited

Analytical Investigation of the Response of Lu-Pu Bridge with Added Viscous Dampers

Shi-de Hu[1] , Zhi-qiang Wang[1] and Li-chu Fan[1]

ABSTRACT

Energy dissipation devices have been widely used in the world since 1970s for the seismic protection of bridges. Viscous passive damping devices have lately emerged as one of the alternative technology devices that are available for using in the seismic design of bridge structures. Different bridge structure types and site conditions may result in significantly different strategy in applying the seismic protection concept with viscous dampers. The present study examines the seismic response of LuPu bridge, with the arch span length of 550m long, using supplemental viscous damping devices and some testing results of viscous damper property are presented. For LuPu bridge, the use of large damping elements only at a few locations within the supuerstructure to reduction local response of the bridge.

The series of analysis provided an understanding of the sensitivity of the bridge response to different parameters. These included the effect of the damper non-linearity, such as velocity exponent and damping constant on the response reduction.

[1]State Key Laboratory for Disaster Reduction in Civil Engineering, Tongji University, Shanghai 200092, PRC

INTRODUCTION

LuPu bridge provides the direct highway link between PuDong and PuXi. With a 550m main span and 2×100m side span the arch bridge is the longest span in the world at the moment. It is a new symbol of shanghai city. The major components of the arch bridge are the steel arch rib, steel bridge deck, as shown in figure 1.

Nonlinear time history analysis of LuPu bridge reveals that relative displacements at expansion joints are large. Impact might take place under earthquake. Therefore, longitudinal viscous dampers will be installed to limit relative displacements at expansion joints.

MODELING PARAMETERS

The present investigation use non-linear transient 3D dynamic analysis to determine the response of LuPu arch bridge with varying damper parameters subjected to earthquake ground motions.

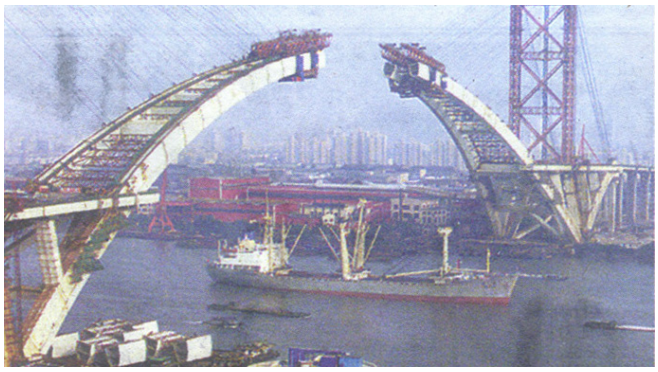

Figure 1. Main span of LuPu bridge

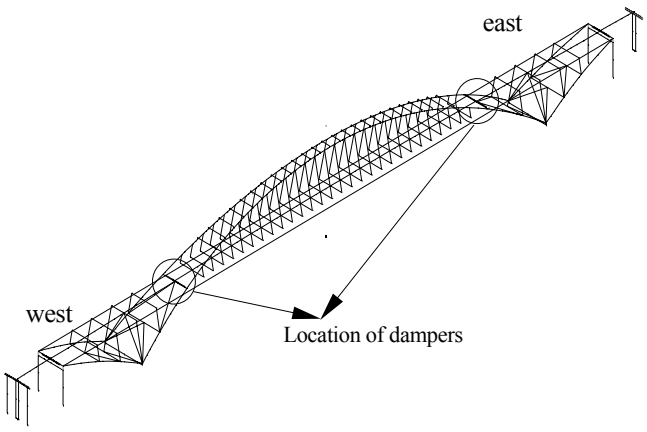

Figure 2. Damping element locations

Bridge analysis model

Longitudinal dampers will be installed at locations as shown in Figure 2. Two viscous dampers will be installed at each of the expansion joints between the main span deck and transverse girder of arch rib.

The main objective is to reduce the relative displacements at the expansion joints, thus eliminate the possibility of impact forces and a reduction of arch rib stress due to longitudinal displacements. At the same time, viscous damper can accommodate slow temperature displacements without forces at the dampers.

Ground motion

Some spectrum compatible acceleration time histories were created, one of such time history is used in this investigation. It was used to represent the site motions of LuPu bridge. Figure 3 shows the pseudo acceleration response spectrum of the time history.

Damping devices

In this investigation, viscous dampers were utilized. The devices modeled were based on those available commercially from SRIM. These are the damping devices currently being used in some other bridges. They are fluid viscous devices that dissipate energy by forcing a silicon fluid through orifices at high velocity. The behavior of the devices can be described by the following equation:

$$F = C|V|^{\xi} \operatorname{sgn}(V) \qquad (1)$$

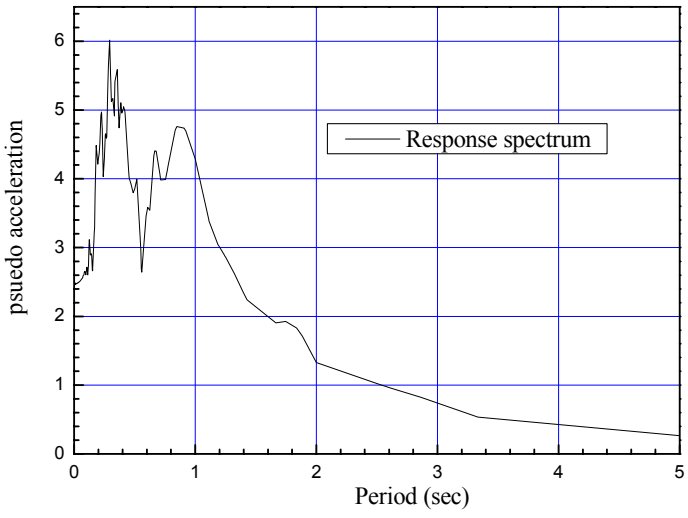

Figure 3. Response spectra of ground motion

where F is the damping force, V is the velocity across the device; C is a damping coefficient and ξ is an velocity exponent in the range of 0.1 to 2.0. These damping devices can be manufactured with a wide range of C and ξ value. The cost of the devices is generally proportional to the maximum damping force required. Figure 4 gives the diagram of the damping force-displacement relationship for the case of harmonic motion, keeps the coefficient C constant and varies the exponent ξ from 0.15 to 1.0, the normal range of practical devices. As ξ reduce from 1.0 to 0.15 the damping force reduces and the damping force-displacement relationship trends from an elliptical toward a more rectangle form.

The result from a transient dynamic analysis can be quite voluminous. It is important to identify relatively few parameters that will still represent the total behavior of the structure. For these analyses, the maximum and minimum axial forces in a representative number of elements were monitored.

Baseline analysis

The LuPu bridge in its existing configuration without dampers was subjected to the ground motions to obtain a benchmark for evaluating the effectiveness of the damping elements. table 1 show the response of LuPu bridge to the artificial wave. Both are plots the maximum and minimumo0 axial force in the arch rib during the earthquake.

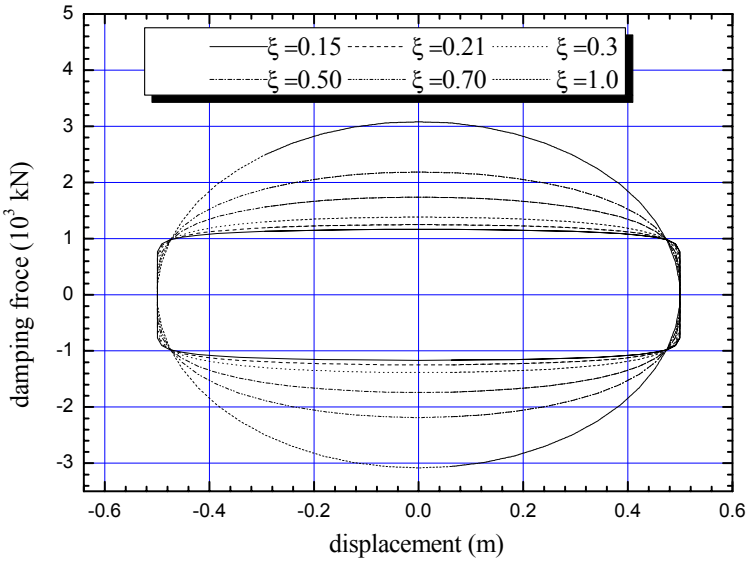

Figure 4. Harmonic damping force-displacement relationship

Analyses with dampers

The properties of the dampers were optimized to achieve an appropriate reduction of the relative displacements and stresses, keeping the damper force within reasonable limits. Different values for the exponent ξ were evaluated. Exponents ξ from 0.15 to 1.0 were considered. For each of these exponents, several values of C were examined in a parametric study aimed identifying the optimum dampers. This study was carried out by calculating the seismic response to one of the ground motions with three-dimensional elastic models of the bridge. The same damper properties were assumed for all dampers. Thirty different configurations of the damping devices were utilized. The dampers were located at the same positions in the bridge for all cases, but the parameters of the dampers themselves were varied. See table 2.

TABLE I ANALYSIS RESULT WITHOUT DAMPER

Position of sections	P4 (longitudinal+vertical)					
	Axial force（kN×10^4）		Shear force （kN×10^3 ）		Moment（kN.m×10^4）	
	west	east	west	east	west	east
Section of arch springing of Side span	3.949	4.266	8.967	11.06	25.32	20.61
Section of arch springing of Main span	2.963	2.960	9.578	10.75	17.61	27.04
Displacement of expansion joints（mm）	160.7	169.1				

TABLE II CASES OF PARAMETERS ANALYSIS

Cases of analysis	C	230	330	460	560	660	Ground motion level
ξ		0.15	0.15	0.15	0.15	0.15	P4
		0.21	0.21	0.21	0.21	0.21	
		0.3	0.3	0.3	0.3	0.3	
		0.5	0.5	0.5	0.5	0.5	
		0.7	0.7	0.7	0.7	0.7	
		1.0	1.0	1.0	1.0	1.0	

Damper parameters variations

Variation of velocity exponent ξ

The value of ξ in equation 1 was varied to determine its effect on response and on maximum damper force. Figure 5, 6 and 7 show the change in the response parameters of structure with changing ξ value.

Figure 5, 6 and 7 display a reduction of the maximum relative displacement at the expansion joint and damper force by increasing ξ, but axial force of arch bridge increases.

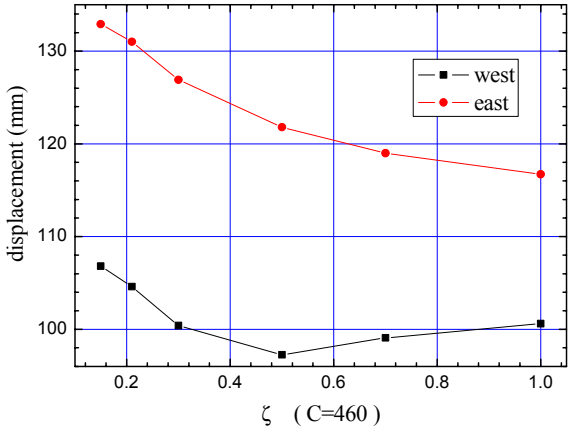

Figure 5. Relative displacement of expansion joint

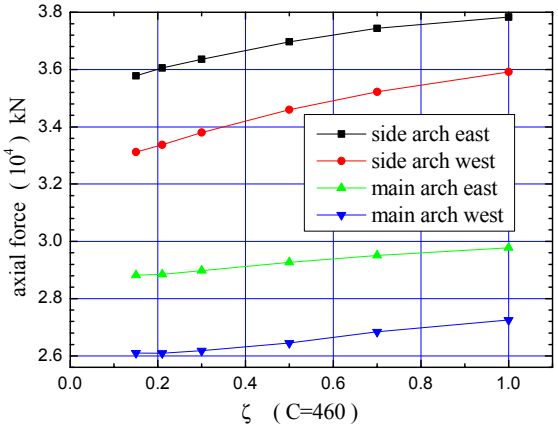

Figure 6. Arch rib axial force

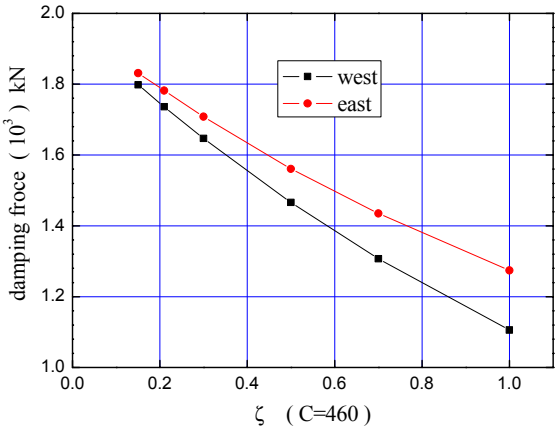

Figure 7. Damping force of damper

Variation of damping coefficient *C*

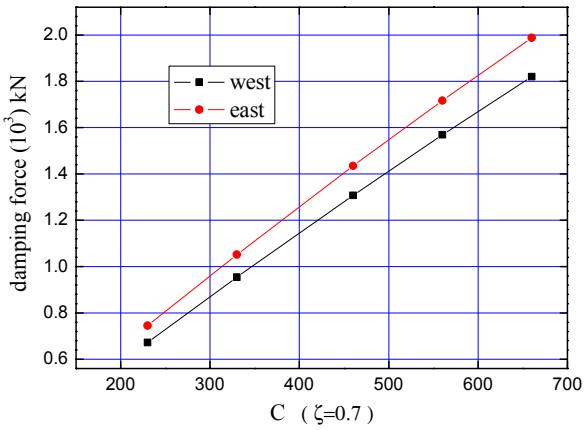

Figure 8. Damping force of damper

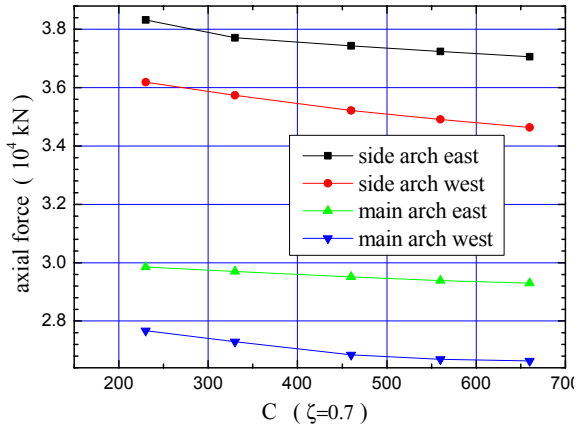

Figure 9. Arch rib axial force

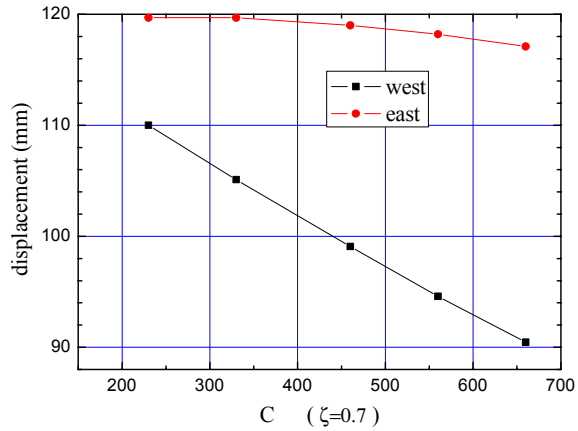

Figure 10. Relative displacement of expansion joint

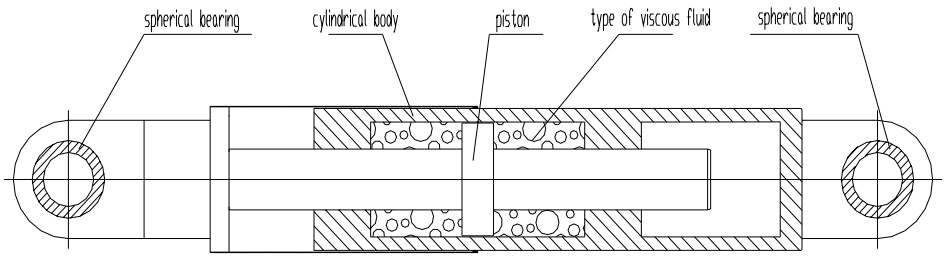

Figure 11. Fluid damper

The value of C in equation 1 was varied to determine its effect on response and on maximum damper force. Figure 8, 9 and 10 show the change in the response parameters of structure with changing C.

Figure 8 9 and 10 show a reduction of the maximum relative displacement at the expansion joint and axial force of arch bridge with increasing C. But damping force increases.

DAMPER TESTS

Fluid viscous dampers were identified as the type of energy dissipator that was most able to meet the demanding load and displacement requirements for the earthquake. In the design process, it was recognized that there is little precendent for the use of viscous damping devices in the seismic design of LuPu bridge, at least in china, and that a comprehensive testing program would be required to verify that fluid viscous dampers could provided the desired performance.

The damper test program of dynamic performance described in this paper was undertaken at State Key Laboratory for Disaster Reduction in Civil Engineering of Tongji University specifically to validate the assumed mechanical characteristics of reduced-scale viscous dampers.

The damper in the testing program is unaxial fluid viscous damper. It is essentially cylindrically-shaped units, see Figure 11 ,with a piston and piston rod moving relative to the main body of the damper. The test damper is reduced-scale with respect to the full-size units that will be used in the LuPu bridge. The damper needed to be scaled down to achieve a reasonable size of device for the testing program.

The damper tested is designed for a force-velocity relationship of

$$F = 92 \cdot V^{0.21} \quad \text{kN} \tag{2}$$

The test damper is designed to produce approximately 200kN at a velocity of 200mm/s, and to have a displacement range of ± 70 mm. These values represent scale factors of 1:10 for force, 1:2.857 for displacement, and 1:3.2 for velocity.

In total, about 29 tests were performed on the damper. Some results for the damper are presented and discussed here. A typical damper force-displacement plot for a constant-velocity test is shown in Figure 12. The plot is for a five-cycle test with a target constant velocity of

35.2mm/s. It can be seen that the damper force output was very stable and repeatable in this test. Note that because the damper force is a function of velocity and that the applied velocity was approximately constant, the damper force is therefore also approximately constant across the test displacement range. For each of the constant velocity tests, an "average" value of damper force as a function of velocity was determined, and then compared against the target force-velocity

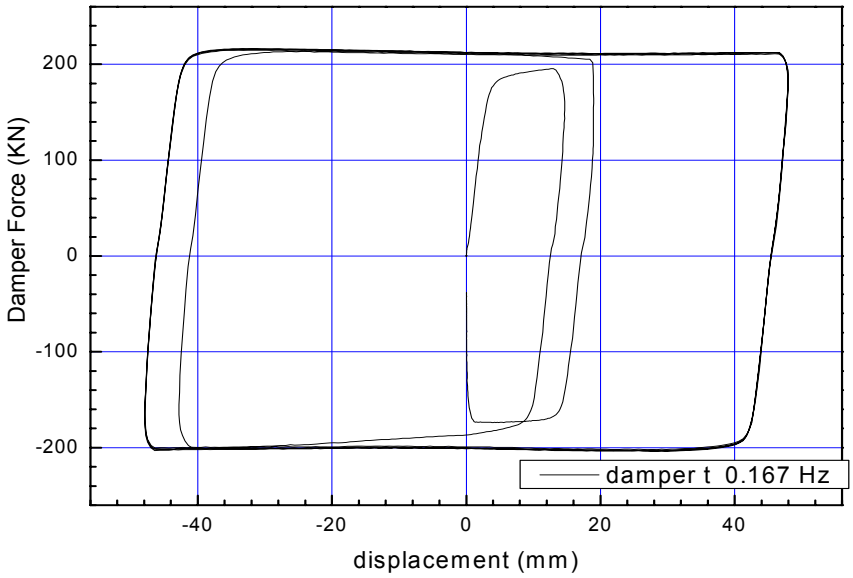

Figure 12. Typical damper force verus displacement plot for a cyclic constant-velocity test

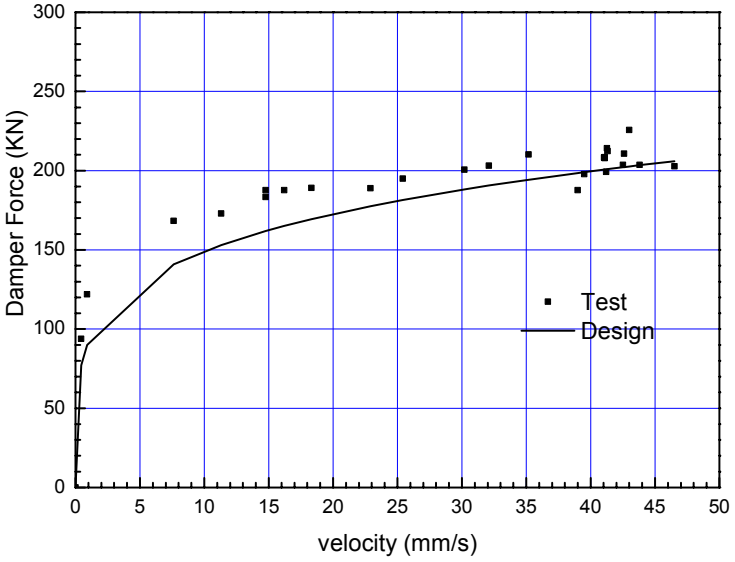

Figure 13. Damper force verus velocity for all cyclic constant-velocity tests

relationship. Figure 13 summarizes all of the constant-velocity tests. The solid line shown in the figure is the target force-velocity law (Eq.2). It can be seen that in general, there is good agreement between the actual and target damper behavior.

Other damper characteristics that were evaluated in the test program include: the predictability of the damper behavior under seismic loading, sinusoidal Tests.

CONCLUSIONS

Although this investigation has been far from thorough, the following conclusions can be drawn:

Placing dampers in LuPu arch bridge can reduce the response of the bridge to earthquake excitations.

The response sensitivity analysis that was performed to obtain the optimum design and understand the behavior of the bridge with damper can be generally applied to other structures.

It shows that the importance that the velocity exponent and damping coefficient can have on the optimum seismic design, the force , relative displacements, and on the damping force. Considering these results, exponent ξ range from 0.2～0.5 was selected, damping coefficient is about 500kN.mm/s.

Besides seismic excitation, the damper will be subjected to thermal movements, wind excitation and small amplitude, high frequency vibrations caused by traffic on the bridge. The final damper design must be able to perform well under all these environments.

REFERENCES

Lichu, Fan, 1997, Seismic Design for Highway Bridge, Huajie International Publishing Co. Limited, Hong Kong.

Priestley, M.J.N., Seible, F., and Calvi, G.M. 1996. *Seismic Design and Retrofit of Bridges.* John Wiley & Sons, Inc., New York.

Aiken, I.D. and Kelly, J.M., 1996, " Cyclic Dynamic Testing of Fluid Viscous Dampers," Proceedings, Caltrans; Fourth Seismic Research Workshop, California Department of Transportation, Sacramento, California, July.

Parvin, A. and Ma, Z., 2001, " the Use of Helical Spring and fluid Damper Isolation Systems for Bridge Structures Subjected to Vertical Ground Acceleration," Electronic Journal of structural Engineering, (2),98-110.

Seismic Performance and Retrofit of a 24-Span Freeway Bridge

M. Saiidi[1], A. Itani[1], Q. Yang[2], and T. Isakovic[3]

ABSTRACT

Seismic retrofit screening of highway bridges in Nevada, USA has identified a major viaduct in downtown Las Vegas as a structure with highest priority for retrofit. The bridge has 24 spans and 110 columns of various shapes. The seismic performance, vulnerability, and retrofit details of the bridge and its adjacent ramps are being evaluated. Five major aspects of study are in progress. The focus of this article is on the effects of incoherent ground motion on the viaduct, detailed nonlinear dynamic analysis of the bridge, and shake table studies of single column piers. It is shown in the paper that combination of geometric incoherency, wave passage, and site characteristics effects can increase the base shears considerably. The columns in the main bridge are found particularly vulnerable to the longitudinal motion of the bridge. The shake table tests of the as-built octagonal columns have shown that the pedestals are unable to work with the columns and separate from the column under large drifts.

INTRODUCTION

New concepts and issues have emerged in the past few years in seismic evaluation and retrofit of structures. The underlying principle in utilizing new concepts is to ensure a reliable, economical, and intelligent design that makes optimal use of innovative materials and information technology tools. Some of the new tools, while may be well developed in the arena of their origin require further research and development before they can be adopted in civil engineering projects. It may be hard to justify the development work for specific projects of relatively small magnitude. However, the potential benefit of such research can be significant for large projects and hence undertaking the so-called "high risk" studies may be warranted.

In planning the seismic retrofit of major bridges, it is inevitable that the solution will involve both conventional and non-conventional strategies. This article presents some of the results of an on-going study to develop retrofit plans for a major freeway viaduct in Las Vegas, Nevada. This bridge has been identified as the most critical bridge for retrofit in Nevada due to its high average daily traffic. Several aspects of the structural response and retrofit methods are being studied. The article will present a summary of the study of three of the critical issues.

[1] Civil Engineering Department, University of Nevada, Reno, NV 89557, USA
[2] Civil Engineering Department, Northern Jiaotong University, Beijing, CHINA
[3] Civil Engineering Department, University of Ljubljana, Ljubljana, SLOVENIA

Figure 1. Bridge aerial view.

DESCRIPTION OF THE VIADUCT

The aerial view of the freeway and the bridge is shown in Fig. 1. The viaduct consists of two main 22-span continuous structures for the westbound and eastbound traffic on Interstate 95 in North Las Vegas (Fig. 2). In addition a 7-span on ramp and two off ramp bridges, one with two spans and the other with three spans are connected to the viaduct. The superstructure is cast-in-place multicell box girder in all the structures and has seven in-span hinges in the main structure. The main bridges are supported on multi-column piers with two to four diamond shape columns and the ramp bridges are supported on irregular octagonal single-column piers some with a pedestal. Figures 3 and 4 show the cross section of the columns. Single columns

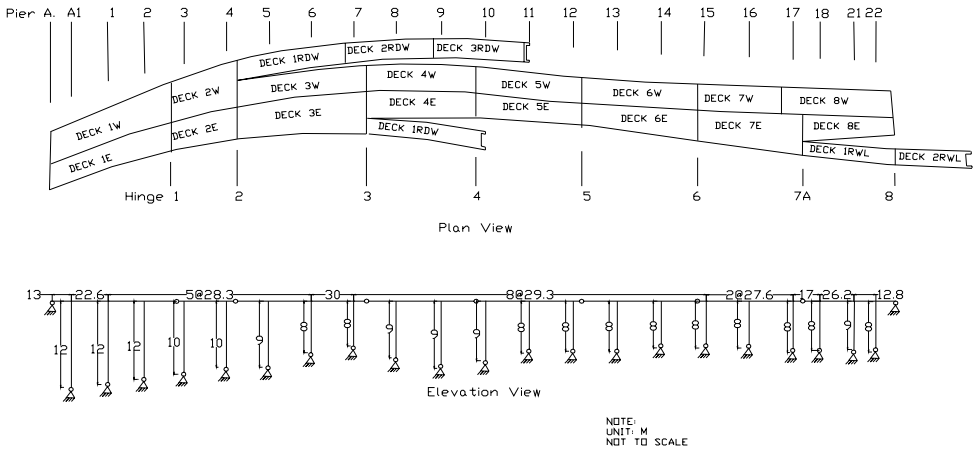

Figure 2. Dimensions of the viaduct.

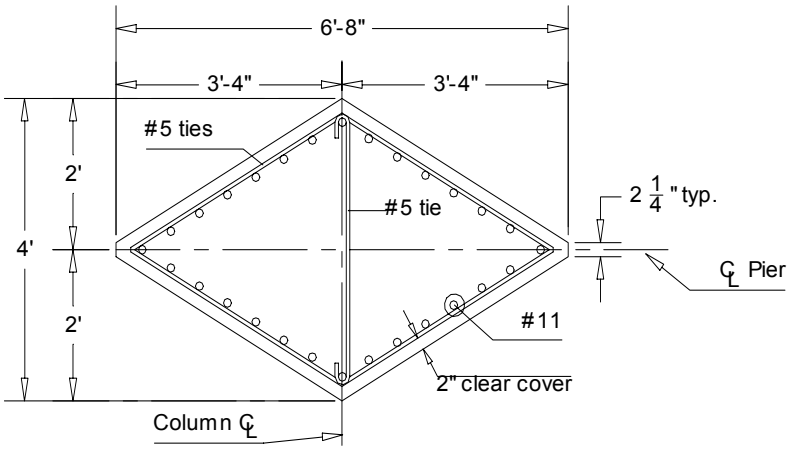

Figure 3. Typical column cross section in multi-column piers (1 in.= 25.4 mm)

are detailed with a one-way hinge at connection to the footing and columns of the multi-column bents are detailed with two-way hinges at the base.

The viaduct was constructed in 1969 and was widened in 1984 by adding one row of columns and a new box cell on the north side with little seismic load and detailing consideration. The columns are supported on spread footings. Based on the soil blow counts at the site of the bridge, approximately the west third of the bridge is on a relatively soft soil while the rest of the structure is on medium firm soil.

Seismic codes place Las Vegas in areas of moderate seismicity category. To determine how critical a bridge is with respect to the need to upgrade its seismic performance, however, the average daily traffic (ADT) is also factored in. As a result the Nevada Department of Transportation has identified the viaduct as the most critical bridge in Nevada with respect to priority for seismic retrofit because of its high ADT in addition to having seismic deficiencies. Seismological studies of the Las Vegas area have pointed out the possibility of strong ground motion due to soil amplification despite the fact that the area is categorized as having only a moderate probability of experiencing high seismic forces (Su et al. 1998).

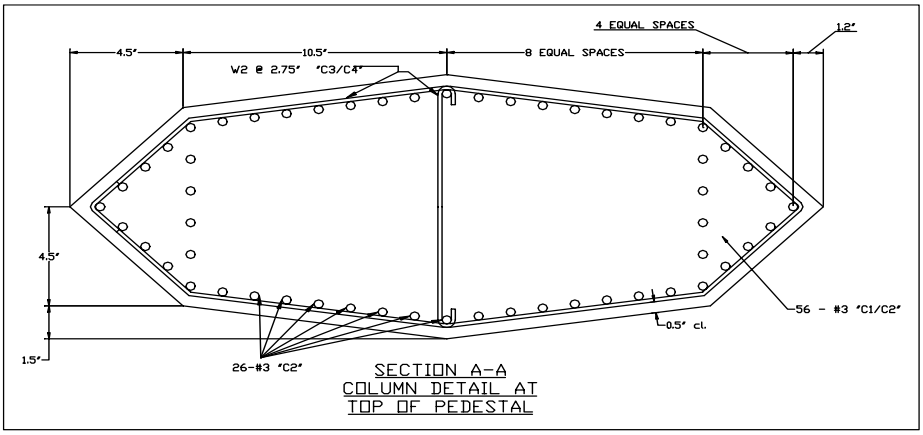

Figure 4. Typical column cross section in single-column piers (1 in. =25.4 mm)

CRITICAL ISSUES

The original structure and the subsequent expansion were not designed to resist significant seismic forces. As a result there are many deficiencies in the bridge with respect to seismic detailing. These include inadequate lateral steel in the columns (Fig. 3 and 4), short anchorage length for longitudinal bars, insufficient shear steel in the beams, very low amount of bottom steel in the beams at connections to columns, a lack of top mat of steel in footings, short seat widths at hinges, and a lack of shear steel at beam column connections. Considering the length of the viaduct and variation in soil properties, there is also uncertainty about the performance of the bridge under incoherent ground motions at different supports.

The study to address these deficiencies include (1) a reduced linear modeling of the bridge to study the effect of incoherent ground motions, (2) a three-dimensional detailed nonlinear modeling of the viaduct subjected to earthquakes to determine the performance level under different loading scenarios, (3) shake table studies of the as-built and retrofitted models of single-column bents, (4) shake table studies of the as-built and retrofitted models of multi-column bents, and (5) an exploratory study of the application of innovative materials for retrofit. Due to space limitation only a summary of the research in Tasks 1, 2 and 3 is presented in this article.

INCOHERENT GROUND MOTION EFFECTS

Although commonly assumed to be uniform, ground motion at different supports of a structure may vary from one support to the next. Variation in support excitation may be due to three causes: (1) geometric incoherency, (2) wave-passage, and (3) local site geotechnical characteristics. The first effect is due to randomness of the earthquake motion even at a given site with practically the same distance from the earthquake source. The second effect is caused by delay in the motion from one support to the next as the earthquake wave passes through the site. Finally the third source of variation is that, for the same bedrock motion, soils of different properties and depth transfer the motion to the surface differently. The first two factors can be particularly important for relatively long structures, whereas the third factor can be important even for short structures with supports located on soils layers that are different from one another.

The total length of the bridge is 552.7 m. Furthermore soil investigation of the site prior to construction have shown that the soil type over the western third of the bridge may be categorized as soft, while the soil for the rest of the bridge is in the category of medium firm. Considering the length and the variation in the soil type it was decided to include all three sources of deficiencies in the study. No site-specific seismic studies and detailed soil investigations have been conducted for the viaduct. As a result it was felt that the study of the incoherency effects would have to be approximate. A reduced linear model of the viaduct was used to determine the trends in the response relative to the response for uniform ground motions. The structure was treated as a planar system subjected to in-plane ground motion loading in the longitudinal direction of the bridge. Details of the study are presented by Yang et al. 2002.

Figure 5 shows the elevation of the reduced model of the viaduct. To develop the model, each segment of the structure between adjacent hinges was represented by a single mass supported on a column that had the same lateral stiffness as that of the bridge segment. Bridge hinges were modeled as pinned connections. The coherency function was adopted from a

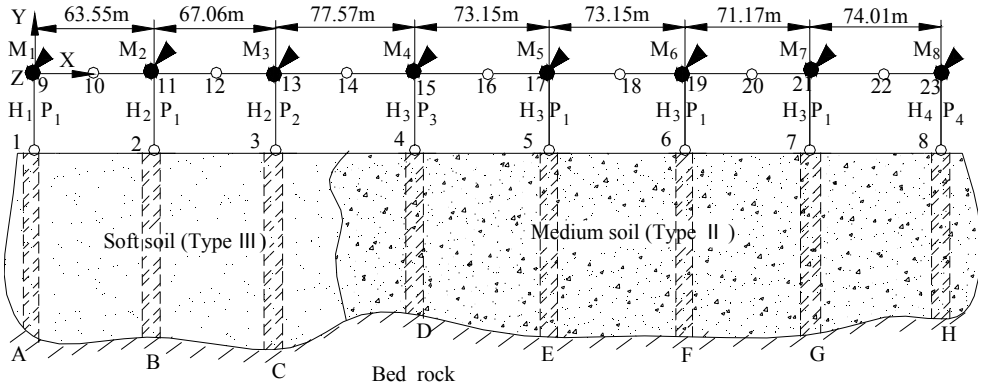

Figure 5. Reduced model of viaduct.

previous study that was based on random processes principles developed by Yang and Chen (2000). Eight acceleration records were generated at bedrock with slightly different peaks in a range of 0.38 to 0.41g. These motions were used to determine the displacement and acceleration histories at the ground level of the soil column under each support of the reduced model. To study the effect of wave passage, a wave velocity of 600 m/sec. was used for the entire viaduct even though the soil varied from the west to the east. This was done because blow counts of the

western and eastern parts, although placed the soils in different categories, were not drastically different.

The effect of different combinations of incoherency parameters were studied by focusing on the "column" base shears in the reduced model. An artificial acceleration record generated for a magnitude 7.4 at 40 km distance from the epicenter was used. To establish a benchmark, the model was analyzed for two uniform ground motions obtained by combining the bedrock motion near the middle of the viaduct one with amplification due to soft soil and the other with

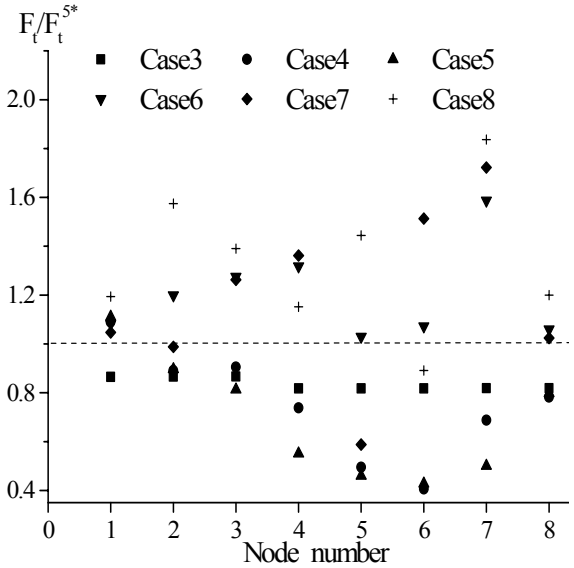

Figure 6. Effect of incoherent motion.

amplification with medium firm soil. The average of the two responses was used as the representative response for uniform ground motion.

The ratios of base shear at different column base nodes for the non-uniform and uniform motions are shown in Fig. 6. In case 3 only the effect of site characteristics was included. Cases 4 and 5 included the wave passage effect in addition to the local site effect, one for waves traveling from east to west and the other traveling in the opposite direction. In case 6 the combination of local site effect and geometric incoherency was included. Finally cases 7 and 8 accounted for all three parameters, for waves traveling from east to west and west to east, respectively. A ratio exceeding one on the vertical axis indicates an increase in force due to incoherent ground motion. It can be seen in Fig. 6 that cases 3, 4 and 5 were not generally critical. However, for cases 6 to 8 the base shear ratios exceeded 1 in many piers. The maximum ratio occurred in Pier 7 with ratios being 1.59, 1.72, and 1.84 for case 6, 7, and 8, respectively. It was concluded that the inclusion of all three incoherency effects can be the most critical combination and even eliminating the wave passage effect (case 6) led to force ratios that exceeded one in one-half of the piers.

NONLINEAR DYNAMIC ANALYSIS OF COMPLETE SYSTEM

The study of possible effects of incoherent ground motion described in the previous section was conducted on a reduced, 2-dimensional, linear version of the structure to keep the model manageable and to allow for the study of combination of several parameters. In the part described in this section a comprehensive model of the bridge was developed for analysis on program Drain-3DX (Prakash, et al., 1993). This part of the study is still in progress, but preliminary results have been obtained and are presented. The essential features used in the model were nonlinear fiber elements for the columns, hinges, shear keys, restrainers, and abutments. A three-dimensional model of the bridge was developed for analysis subjected to uniform support excitation in two horizontal orthogonal directions.

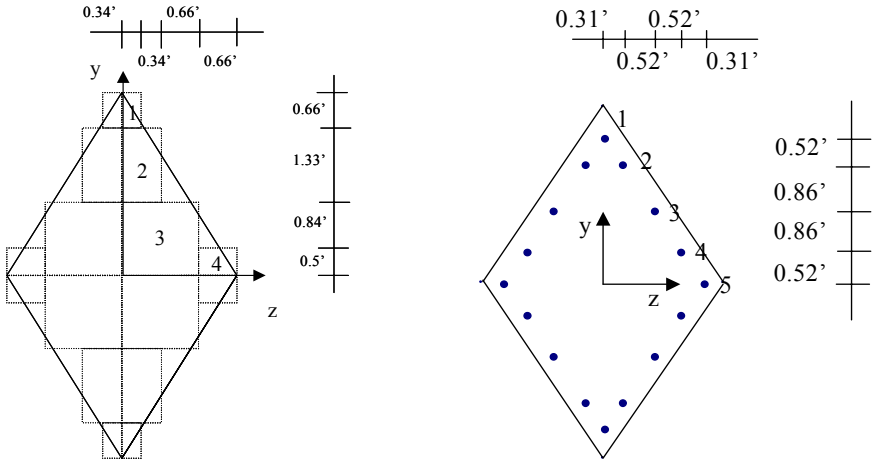

(a) Concrete (b)

Figure 7. Fiber elements for diamond columns.

Nonlinear Elements

The columns in the bridge are of two general types, diamond shape sections used in multi-column bents and irregular octagonal sections used in single column bents. There is considerable variation in the longitudinal steel ratio in diamond shape columns ranging from 2.2 to 5.6 percent. As can be seen in Figs. 3 and 4, the longitudinal steel is distributed around the section. In developing the fiber elements for plastic hinges, the bars were lumped as shown in Figs. 7 for the diamond shape columns. Similar simplifications were made in octagonal columns. A trilinear curve with properties based on the average measured properties was used for concrete and steel fibers.

Several nonlinear components had to be included at the hinges. Figure 8 shows the nonlinear hinge model that included unidirectional springs for shear keys, restrainers, and impact effect. The impact and restrainer springs are activated in the longitudinal direction after closure of a gap (in the case of the impact spring) or tightening of the restrainer rods (in the case of the restrainers springs). The shear key elements act in the transverse direction of the bridge after the initial gap between the edge of the shear key and the superstructure is closed. At connections between the ramps and the main structure, the hinge element is more complicated but has the same spring types as those shown in Fig. 8.

The eastbound and westbound structures in the main bridge are connected at a longitudinal hinge. This hinge was modeled only with compression springs. Therefore, the two structures were allowed to separate during the earthquake without resistance.

Dynamic Analyses and Results

Two acceleration records were used in the analysis, the 1941 El Centro record and an artificial earthquake based on Eurocode 8. The peak ground acceleration for the former was 0.35g and for the latter was 0.2g. The spectra for the two records are shown in Fig. 9. The peak accelerations are varied for different runs to simulate the effect of earthquakes with different intensities.

A modal analysis of the structure was first conducted. Because of the hinges and the nonlinearity they introduce two sets of vibration modes were calculated with two different boundary conditions, one with hinges disconnected and the other with hinges fully connected.

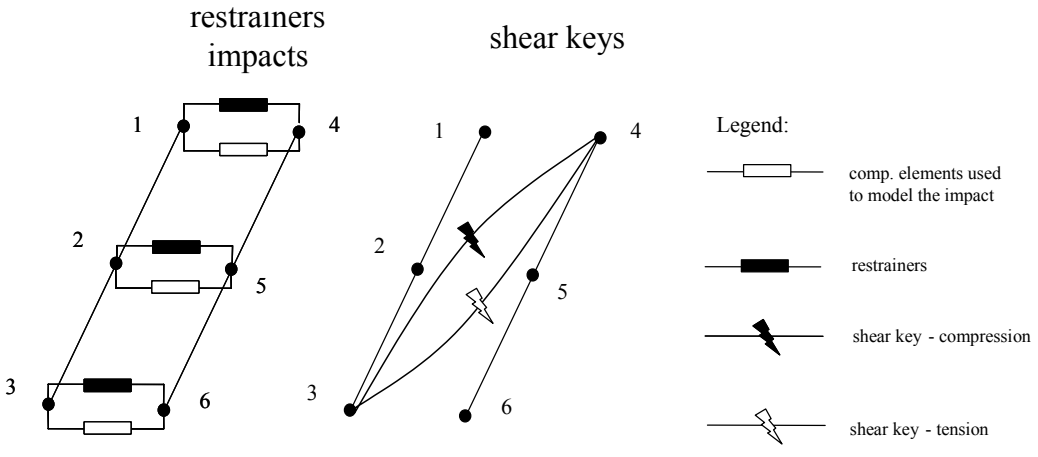

Figure 8. Hinge components.

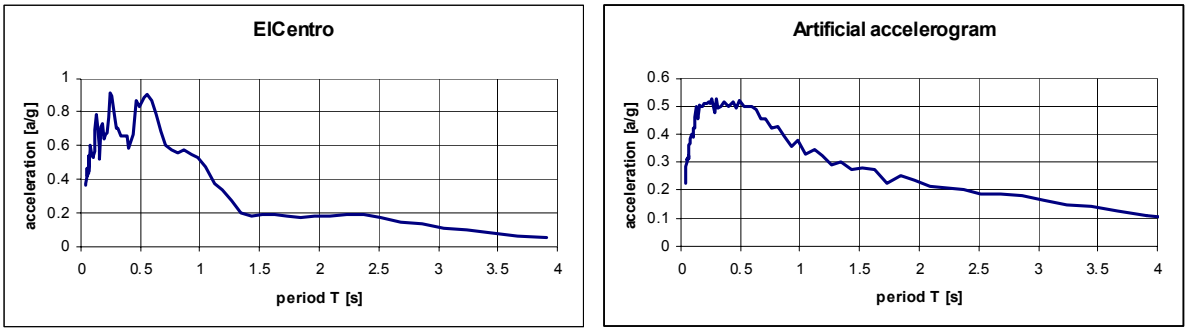

Figure 9. Acceleration spectra for 5% damping.

The former led to 61 important modes with period ranging from 0.12 to 1.77 sec., and the latter lead to 17 important modes with a period range of 0.14 to 0.62 sec. The actual behavior of the bridge is in between these two sets of boundary conditions and depends on the ground motion characteristics and the response amplitude. Because of differences in column heights and pier stiffnesses, the model with disconnected joints had a particularly large contribution from in-plane rotational modes. The results of the modal analysis were used to estimate the mass and stiffness proportional damping coefficients used in the response history analyses. A damping ratio of 5 percent was used.

Figure 10 shows the longitudinal displacement envelopes for analysis in the longitudinal direction of the bridge subjected to the El Centro record amplified by a factor of two (PGA= 0.7g). The maximum displacement was 101 mm (3.96 in.), corresponding to a column drift ratio of 1 percent. This level of drift led to yielding of the columns and the development of plastic hinges with relatively low ductility demand. Given the low level of confinement in the columns, however, they are expected to have a ductility capacity of approximately 1.5 and are likely to be damaged under this motion. Considering the uncertainty in the abutment capacity, the analysis was repeated with abutments removed. Because of the low flexibility of the diamond shape

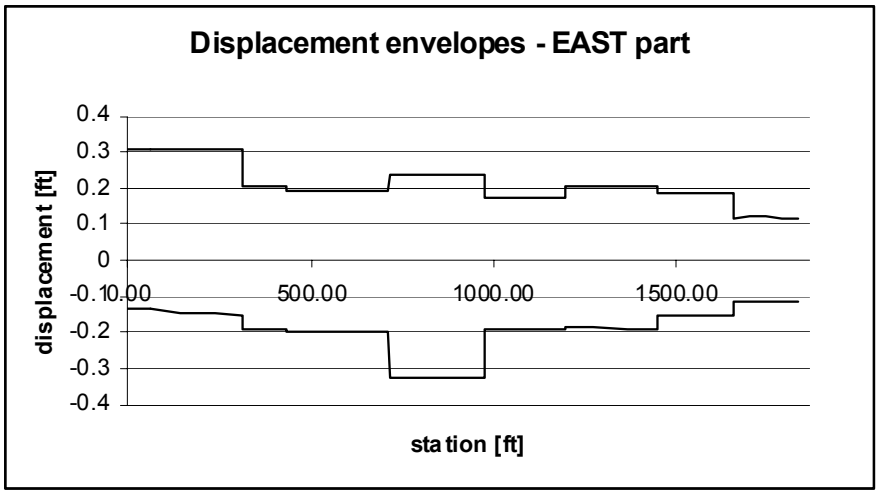

Figure 10. Maximum longitudinal displacements for 2x El Centro (1 ft.=305mm).

Figure 11. Shake table setup.

columns in the longitudinal direction of the bridge the maximum displacement increased to 244 mm (9.6 in.) with a column drift ratio of 2.6 percent. It was concluded that if the abutments fail during the earthquake, the high deformation demand on the columns would lead to column failure and collapse of the structure.

SHAKE TABLE PERFORMANCE OF OCTOGONAL SINGLE COLUMNS

As-Built Specimen

Three, quarter-scale models of the octagonal single column piers were constructed for shake testing in the strong direction. One specimen has been tested in the as-built condition and the other two will be retrofitted and tested to determine the effectiveness of different retrofit techniques. The models represented the most critical single columns in the ramp structure with respect to the shear demand.

Shake Table Testing

Figure 11 shows the shake table set up for the as-built specimen. Preliminary nonlinear dynamic analysis of the column for a variety of earthquakes indicated that the most demanding motion would be the Sylmar record of the 1994 Northridge earthquake. This motion was simulated on the table with increasing amplitudes in successive runs until the column failed. The envelope of the measured load-displacement hysteresis relationships is shown in Fig. 12. The primary damage occurred in the pedestal. Vertical cracking of the pedestal began at relatively small motions. As the intensity of the motion increased, the pedestal cracks widened and led to separation of the pedestal from the column (Fig. 13). Several important observations were made. Figure 12 shows that the overall load-displacement response is ductile. The measured displacement ductility capacity exceeded 6. The longitudinal bar strain data indicated substantial strains without bar pullout despite the fact that the bar anchorage lengths do not meet the current code requirements. The early cracking of the pedestal at a displacement ductility of approximately 0.5 is of concern because the pedestals are buried and their damage after moderate

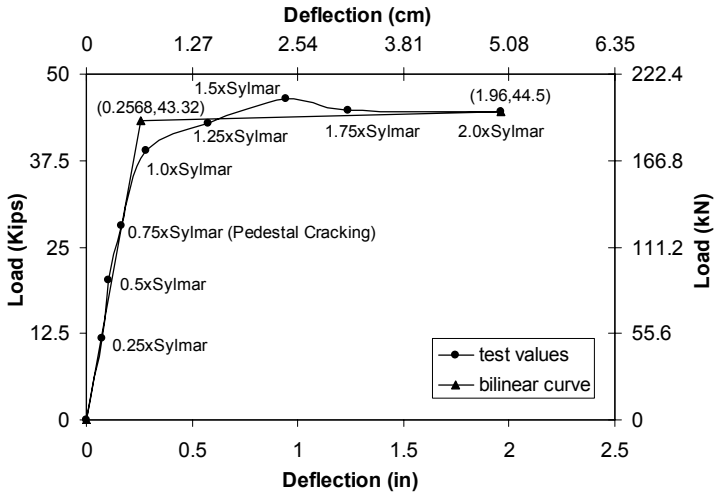

Figure 12. Load-deflection envelope.

earthquakes may go undetected. The damage in the column above the pedestal was minimal as can be observed in Fig. 13.

Retrofit Details

The bottom of the pedestal is detailed with one-way hinges. The present and past studies of one-way hinges have indicated a relatively low level of energy dissipation even when the dowels are properly anchored. In the course of designing the retrofit for the pedestal it was decided to enlarge and strengthen the pedestal to the point that plastic hinging would shift from the bottom of the pedestal to the column immediately above the pedestal. The retrofit work is currently in progress on the second as-built column. Additional steel bars are being placed to enlarge the pedestal while maintaining one-way hinge action according to the design shown in Fig. 14. The ends are rounded so that fiber-reinforced plastic composite jackets can be placed to

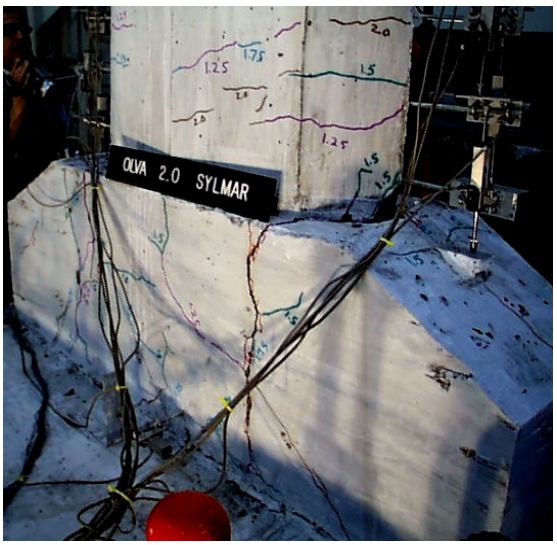

Figure 13. Damage to octagonal column after the test.

improved the connectivity between the column and pedestal in the horizontal direction. The column above the pedestal will be kept as-is. Shake table testing of the retrofitted model will reveal the adequacy of the column and the necessary level of retrofit for the column. The retrofit details for the third as-built column will be designed after testing of the second column.

CONCLUSIONS

Several aspects of the behavior and retrofit of a major viaduct are being studied. The results of the study of the incoherent ground motion effects suggest that internal forces can be significantly higher than those based on uniform ground motion when all three parameters, namely, geometric incoherency, soil characteristics under different supports, and the wave passage effects are included. The increase in the force even for earthquakes with peak ground acceleration (PGA) of approximately 0.4g exceeded 80 percent. The nonlinear dynamic analysis of the entire bridge has revealed that severe column damage for response in the longitudinal direction of the bridge could occur in an earthquake with PGA of 0.7g. Should the abutments suffer significant damage, the severe column damage could lead to collapse. The study of single column bents showed that, contrary to the assumed behavior, the pedestal damage can be the main source of nonlinearity and that the damage could initiate under relatively small motions (with PGA of 0.3g). The nonlinear dynamic analysis of the bridge, retrofit of single columns, and study of multi-column bents are in progress.

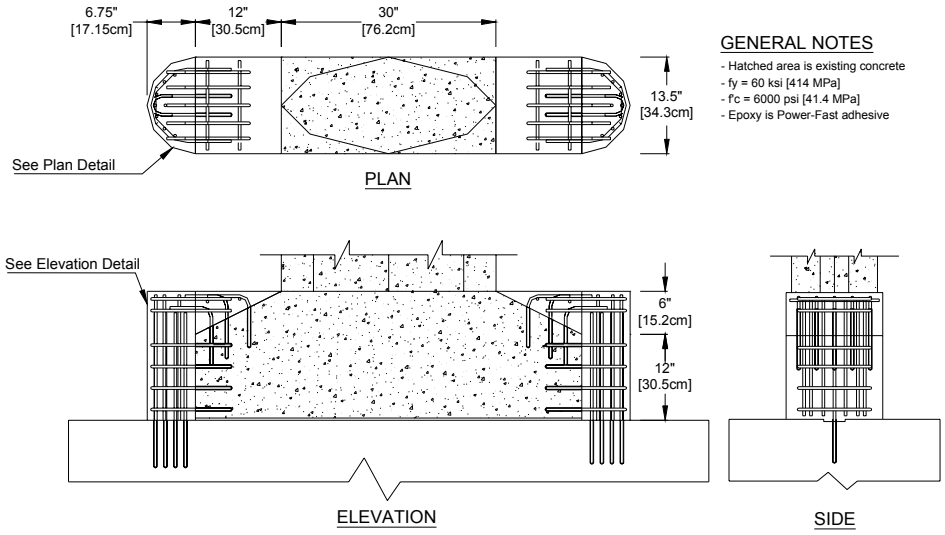

Figure 14. Retrofit details for the pedestal.

ACKNOWLEDGEMENT

The study reported in this article is funded by the US Federal Highway Administration and the Nevada Department of Transportation (NDOT). The advice of Messrs Bill Crawford and Troy Martin of NDOT is much appreciated. Several graduate students have been working on different aspects of the project and they are thanked for their dedication. The students involved in the parts of the study presented in this article are: C. Ayoub, D. Gang, N. Johnson, S. Kandasamy, H. Wang, and H. Mohamad.

REFERENCES

Prakash, V., G.H. Powell, and S. Cambell, (1993) "Drain-3DX, Base Program Users Guide Version 1.0," Earthquake Engineering Research Center, University of California, Berkeley, November.

Su, F., J. Anderson, S. Ni, and Y. Zeng, (1998) "Effect of Site Amplification and Basin Response on Strong Motion in Las Vegas, Nevada," Earthquake Spectra, V. 14, N. 2, pp. 357-376.

Yang, Q., M. Saiidi, H. Wang, and A. Itani, (2002) "Influence of Ground Motion Incoherency on Earthquake Response of Multi-Support Structures," Civil Engineering Department, University of Nevada, Reno, Report No. CCEER 02-2.

Yang Q., and Y. Chen, (2000) "A Practical Coherency Model for Spatially Varying Ground Motions", *Structural Engineering and Mechanics*, **9**(2), pp. 141-152.

Nonlinear Seismic Response Analysis of Effects of Sliding and Pounding of Urban Interchange Bridges with Rubber Bearing

Li-ying Nie[1], Jian-zhong Li[1], Li-chu Fan[1]

ABSTRACT

In design and construction of urban interchange bridges, the rubber bearing is usually placed on the top of pier directly and the shear force transmitting from superstructure depends on friction between the interfaces. The slide might occur on the interfaces between rubber bearing and girder bottom or pier top under an earthquake. The excessive bearing displacement caused by sliding might induce pounding between adjacent components. In this paper, the effects of sliding for rubber bearing and pounding between adjacent components are investigated.

[1] State Key Laboratory for Disaster Reduction in Civil Engineering , Tongji University, Shanghai 200092, PRC

INTRODUCTION

Rubber bearing is commonly adopted in bridge construction. In design and construction of urban interchange bridges the rubber bearings are placed on the top of pier directly and the shear force transmitting from superstructures depends on friction between the interfaces. The slide might occur on the interfaces between rubber bearing and girder bottom or pier top under an earthquake. The slide occur on the interfaces between rubber bearing and girder bottom or pier top is called rubber bearing sliding in the latter in brief.

The effects of rubber bearing sliding in the former seismic analysis were usually not considered [1,2]. Bearing's sliding might induce not only excessive displacement but also pounding between adjacent components. In this paper, the effects of sliding of rubber bearing and pounding between adjacent components are investigated.

FINITE ELEMENT MODEL

Finite element model of sliding bearing

To simulate the sliding behavior of a bearing, a three-dimensional sliding bearing element which is assumed to be lateral isotropy based on the bilinear restoring force characteristics has been used. The three-dimensional sliding bearing element with three translation degrees is depicted in Figure 1(a). The element vertical deformation is assumed to exhibit linear elastic behavior and horizontal restoring force characteristics is depicted in Figure 1(b).

In Figure1(b), the bearing force F is the horizontal resultant force ,and the displacement d is the horizontal resultant displacement corresponding to F . The k_1 is stiffness of bearing before sliding , k_2 is stiffness of bearing after sliding , F_{cr} is the critical frictional force which is expressed as

$$F_{cr} = N\mu \qquad (1)$$

In which N is the vertical resistant force of bearing include dynamic and dead vertical resistant force ; μ is the frictional coefficent of sliding interface.

In three-dimensional sliding bearing element, the frictional coefficent of sliding interface μ is assumed to be constant ,so the critical frictional force is dominated by the vertical resistant force of bearing N .

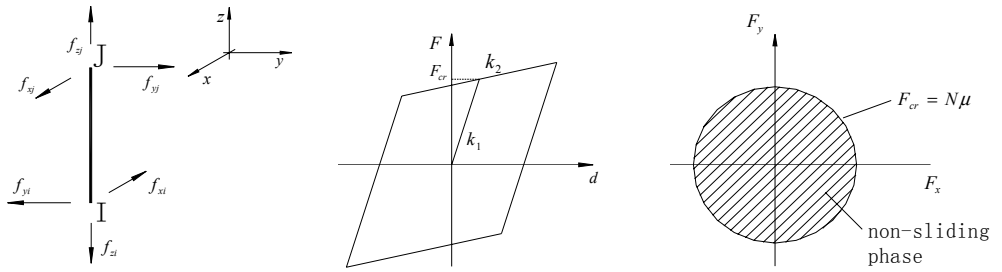

a. Sliding bearing element model b. Restoring force characteristics c. Criteria for sliding and non-sliding phases

Figure 1 Analytical element model of three-dimensional sliding bearing

The criteria for sliding and non-sliding phases[3] which is depicted in Figure.1.(c) is used to judge the sliding phase of element .The resultant of the frictional forces F is expressed as:

$$F = \sqrt{F_x^2 + F_y^2} \tag{2}$$

where F_x、F_y is frictional force of bearing in x- and y-direction.

In non-sliding phase the resultant of the frictional forces which mobilized at the sliding interface is less than the critical frictional force, i.e. $F < F_{cr}$, The system will start sliding as soon as this resultant exceeds the critical frictional force. Thus, the sliding phase of the system will take place if $F = F_{cr}$.

Contact element model

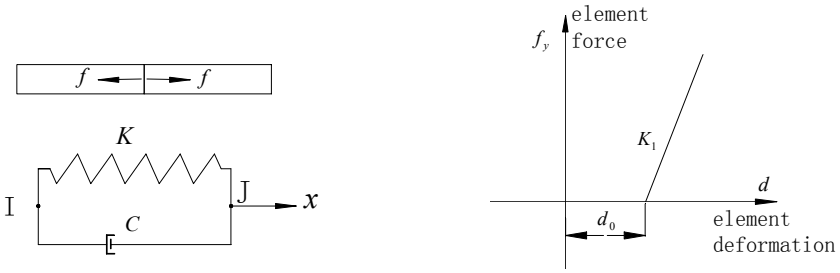

a. Contact element model b. Restoring characteristics

Figure 2 Analytical model of contact element

The contact element is used to simulate the pounding which is the boundary nonlinear phenomenon by changing from one stage to the other[4,5] as depicted in Figure 2a. The two segments moving independently at first and the element become active if the relative displacement between adjacent components is smaller than the initial gap. So incremental equation of contact element can be expressed as

$$\{\Delta f_s\} = k \cdot \Delta(d_i - d_j) \tag{3}$$

where $\{\Delta f_s\}$ is the incremental element force, $k = \begin{cases} 0 & d_i - d_j < d_0 \\ K_1 & d_0 < d_i - d_j \end{cases}$, k is stiffness of element , d_0 is initial gap and K_1 is impact stiffness.

NONLINEAR SEISMIC ANALYSIS FOR BRIDGE WITH RUBBER BEARING

Outline of analysis

Rubber bearings for bridges have been widely used in china for more than 30 years. The sliding might occur on interface if there isn't any connection between rubber bearing and top surface of pier or bottom surface of slab.

To analyze the effects of rubber bearing sliding in urban interchange bridges, dynamic analysis of multi-span simple supported girder bridge has been carried out under minor, design and severe earthquake. The minor, design and severe earthquake are defined as ground motion with 63%,10% and 2% probabilities of exceedance in 50 years, respectively.

To analyze the dynamic behavior, which considered effects of rubber bearing sliding and the pounding of bridge structure, two analytical models are established, i.e.:

Model I: the analytical model without considering the effects of pounding.

Model II: the analytical model with considering the effects of pounding.

The multi-span simple supported girder bridge consisted of 36 spans, in which 0#, 36# are abutment and expansion joints are set on the top of 0#, 6#, 12#, 18#, 24#, 30# piers. In addition, the bearings are adopted rubber bearings or PTFE. The important aspects of analytical model is given as following:

(1) All the bottoms of pier were assumed fixed ends.

(2) The inelastic characteristics of piers were represented by the fiber beam-column element.

(3) Rubber bearings and PTFES were simulated by three-dimensional sliding bearing element introduced in this paper respectively, in which the frictional coefficient between rubber bearing and concrete is 0.15 and frictional coefficient between PTEF and concrete is 0.02.

(4) Girders of superstructure were simulated by the elastic beam element.

(5) The masses of structure system were discrete as lumped-mass.

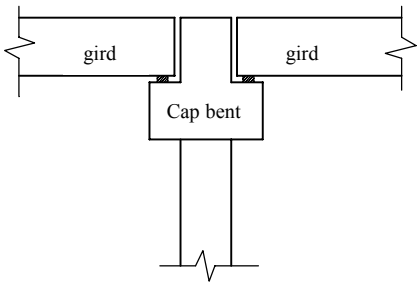

Figure 3 Convex cap bent

(6) In multi-span simple supported girder bridge, all cap bents which are depicted in Figure 3 are convex and have retaining block on each transversal side. There are gaps between ends of girder and bent caps or retaining blocks. Pounding might occur under an earthquake in this situation. In analytical model II with considering effects of pounding, the

pounding was represented by contact element .The width of initial gap between cap bents and girders end are 0.08m at extension joint and 0.05m where extension joint don't exist. The width of gaps between retaining blocks and girders end are 0.05m in the same way.

The analytical model of multi-span simple supported girder described above is depicted in Figure 4.

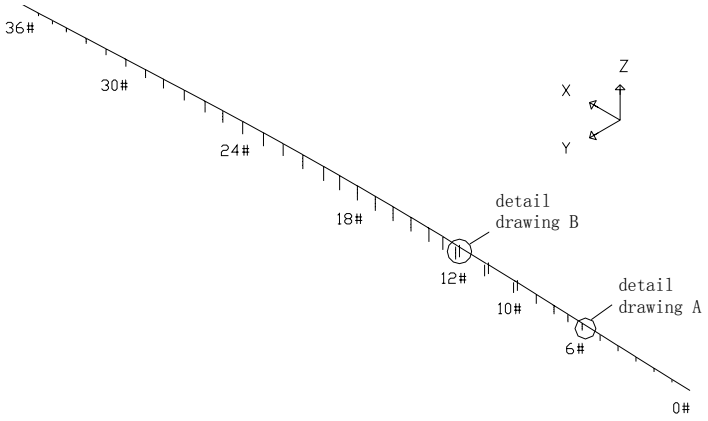

a. Dynamic analytical model of multi-span simple supported girder

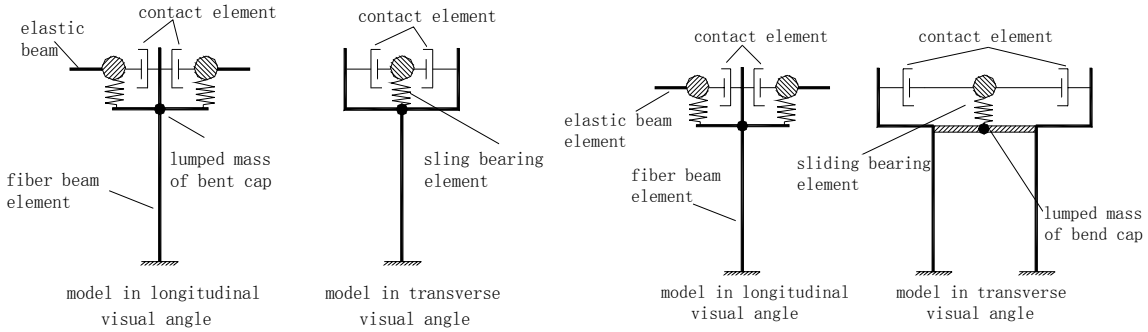

b. Detail drawing A of single column c. Detail drawing B of double column

Figure 4. Analytical model of multi-span simple supported girder

There are two cases for seismic wave exciting during analysis:

Case I: Combine the response resulting from 100% of the transverse input acceleration with the corresponding response from 30% of the longitudinal input acceleration.

Case II: Combine the response resulting from 100% of the longitudinal input acceleration with the corresponding response from 30% of the transverse input acceleration.

The typical site-specific time histories of input acceleration are provided.

Analysis results

Seismic response for analytical model I—without consideration of pounding

(1) Bearing displacement under minor, design and severe earthquake

- Acceleration history time input along transverse axis

The rubber bearings of entire bridge don't slide under minor earthquake. The maximum displacement for rubber bearing which occurred at top of 33# pier is 0.7263cm.

The rubber bearings of entire bridge have slid under design earthquake. The maximum displacement for rubber bearing which occurred at top of 9# pier is 2.995cm. Because the maximum displacement for rubber bearing is smaller than initial gap between girder end and retaining block, pounding will not occur.

The rubber bearings of entire bridge have slid under severe earthquake. The maximum displacement for rubber bearing which occurred at top of 9# pier is 13.76cm. Because the displacements for rubber bearings are larger than initial gap between girder end and retaining block, pounding will occur.

- Acceleration history time input along longitudinal axis

The rubber bearings of entire bridge don't slide under minor earthquake. The maximum displacement for rubber bearing which occurred at top of 1# pier is 0.6696cm.

The parts of rubber bearings on the each end of bridge have slid under design earthquake. The maximum displacement for rubber bearing which occurred on top of 1# pier is 2.194cm. Because the maximum displacement for rubber bearing is smaller than initial gap between girder end and convex bent cap, pounding will not occur.

The parts of rubber bearings on the each end of bridges have slid under severe earthquake. The maximum displacement for rubber bearing which occurred on top of 1# pier is 10.95cm. Because the displacements for rubber bearings are larger than initial gap between girder end and convex bent cap, pounding will occur.

(2) Peak seismic force response for piers

If the pier is under the elastic range, the ratio of the maximum moment to yield moment at pier bottom is used to reflect on the force response behavior. The calculating results is shown in Table I, Table II.

TABLE I. PEAK SEISMIC RESPONSE UNDER DESIGN EARTHQUAKE

Seismic wave excite in transverse				Seismic wave excite in longitude			
NO. Pier	Transverse shear (KN)	Transverse moment (KN-m)	Ratio of moment	NO. Pier	Longitudinal shear (KN)	Longitudinal moment (KN-m)	Ratio of moment
16#	5.080E+02	6.595E+03	0.2558	7#	4.424E+02	3.105E+03	0.6677
17#	5.017E+02	6.589E+03	0.2595	8#	3.947E+02	3.010E+03	0.6259
21#	5.817E+02	7.453E+03	0.2901	29#	3.924E+02	2.874E+03	0.5471

TABLE II. PEAK SEISMIC RESPONSE UNDER SEVERE EARTHQUAKE

Seismic wave excite in transverse				Seismic wave excite in longitude			
NO. Pier	Transverse shear (KN)	Transverse moment (KN-m)	Ratio of moment	NO. Pier	Longitudinal shear (KN)	Longitudinal moment (KN-m)	Ratio of moment
16#	6.230E+02	7.951E+03	0.3728	7#	6.007E+02	4.181E+03	0.9573
17#	6.175E+02	7.966E+03	0.3785	27#	5.138E+02	4.668E+03	0.9243
21#	6.615E+02	8.380E+03	0.4012	28#	6.016E+02	4.917E+03	0.9993

As can be seen from the above analytical results, due to sliding of rubber bearing, the piers are in elastic range under design and severe earthquake. The force response for piers become smaller and the rubber bearing displacements become larger which maybe induce the pounding between the adjacent components.

Seismic response for analytical model II—with consideration of pounding

From the above results of analysis model I, rubber bearing sliding results in the larger bearing displacement which maybe induce the pounding between the adjacent components under severe earthquake. So the analysis of model II is carried out.

If the pier is under the inelastic range, the ratio of the maximum curvature to yield curvature bottom at pier bottom is used to reflect on the deformation response behavior. The calculating results are shown in Table III, Table IV:

TABLE III. PEAK SEISMIC RESPONSE FOR MODEL II UNDER SEVERE EARTHQUAKE

Seismic wave input direction	NO. pier	Force of pounding (KN)	Moment of pier bottom (KN-m)	Shear of pier bottom (KN)	Curvature of bottom of pier (1/m)	Ratio of curvature
In transverse	14#	3.146E3	1.330E4	1.052E3	6.203E-04	0.7794
	16#	3.491E3	1.426E4	1.061E3	6.630E-04	0.8269
	22#	1.400E3	1.235E4	1.147E3	5.874E-04	0.7321
In longitude	1#	7.880E3	6.396E3	2.087E3	5.881E-03	1.8965
	2#	7.935E3	6.524E3	1.560E3	4.456E-03	1.4314
	34#	5.070E3	4.980E3	1.486E3	3.073E-03	1.0233
	35#	8.161E3	6.880E3	2.185E3	5.637E-03	1.7334

To compare the pounding effects of bridge structure, the piers response of model I corresponding to the Table III is given in Table IV.

TABLE IV. SEISMIC RESPONSE OF MODEL I UNDER SEVERE EARTHQUAKE

Seismic wave input direction	No. pier	Force of pounding (KN)	Moment of pier bottom (KN-m)	Curvature of bottom of pier (1/m)	Ratio of curvature
In transverse	14#	6.706E3	5.473E2	2.459E-04	0.3165
	16#	7.951E3	6.230E2	2.926E-04	0.3728
	22#	6.804E3	6.119E2	2.187E-04	0.2780
In longitude	1#	1.486E3	5.641E2	4.534E-04	0.1622
	2#	1.909E3	5.754E2	6.935E-04	0.2473
	34#	1.651E3	4.954E2	6.248E-04	0.2269
	35#	1.307E3	4.846E2	4.070E-04	0.1479

TABLE V. MAXIMUM POUNDING FORCE FOR MODEL II UNDER SEVERE EARTHQUAKE

Seismic wave input direction	Pounding force (kN)	NO. pier
In transverse	7.650E3	0#
	3.339E3	7#
	3.828E3	11#
	1.927E4	36#
In longitude	7.880E3	1#
	7.935E3	2#
	5.070E3	34#
	8.161E3	35#

From the analytical results for model II, pounding of adjacent components results in redistribution of response force for piers and the peak response of piers have large increment. Especially while acceleration input along longitudinal axis, the short piers yield seriously. The effects of shear, moment, curvature for piers bottom caused by pounding is depicted in Figure 5 and Figure 6.

CONCLUSION

In design and construction of urban interchange bridges, the rubber bearings are usually placed on the top of pier directly and the shear force transmitting from superstructures depends on friction between the interfaces. Bearing's sliding might induce not only excessive displacement but also pounding between adjacent components. In this paper, the analysis of this dynamic behavior in urban interchange bridges is carried out through a multi-span simple supported girder bridges. It can be known from the analytical results :

(1) From the seismic response for analytical model without considering pounding effects, due to sliding of rubber bearing, the piers are in elastic range under design and severe earthquake. The force response for piers become smaller and the rubber bearing displacements become larger which maybe induce the pounding between the adjacent components.

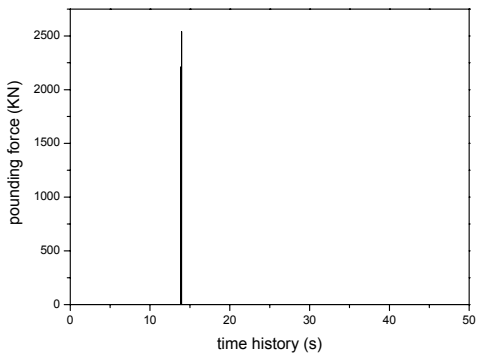

a. Response history for pounding force at the top of pier

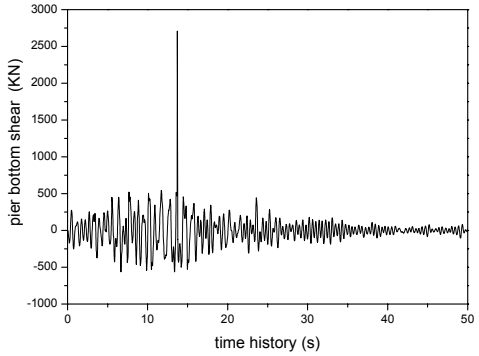

b. Response history for shear at the bottom of pier

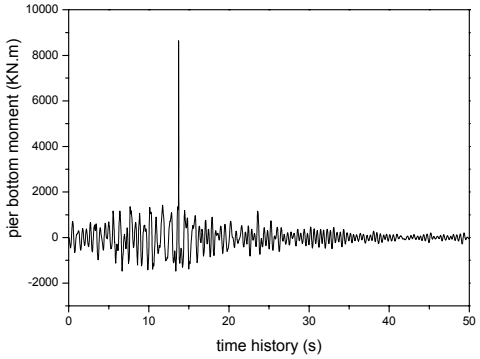

c. Response history for moment at the bottom of pier

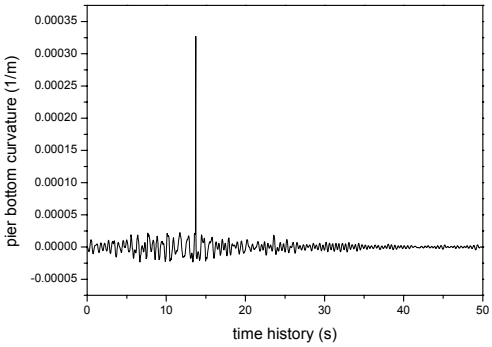

d. response history for curvature at the bottom of pier

Figure 5 Analytical response history for No. 2 pier under severe earthquake with acceleration input along transverse axis

(2) From the seismic response for analytical model with considering pounding effects, pounding of adjacent components results in redistribution of response force for piers and the peak response of pier have large increment . Especially while acceleration input along longitudinal axis, the short piers yield seriously.

REFERENCES

Fan Li-chu. 1997. “Seismic design of highway bridge ”,Hong Kong :Huajie International Publishing Co.Limited，

Fan Li-chu,Hu Shi-de, Ye Ai-jun. 2001, “Seismic design of Long-span bridge” ,.People’s Communication Publishing House (in Chinese)

R S Jangid. 1996. “Seismic response of sliding structures to bidirectional earthquake” excitation.Earthquake Engineering and Structural Dynamics.,25,1301-1305

Parveen K. Malhotra , Moh J.Huang and Anthony F.Shakal .1995. “Seismic Interaction at Separation Joints of An Instrumented Concrete Beidge”, Earthquake Engrg. Struct. Dyn.,24,1055-1067

Robert Jankowski, Krzysztof wilde and Yozo Fujino.1998. “Pounding of Superstructure Segments in Isolated Elevated Bridge During Earthquakes”, Earthquake Engrg. Struct. Dyn., 27, 487-502,

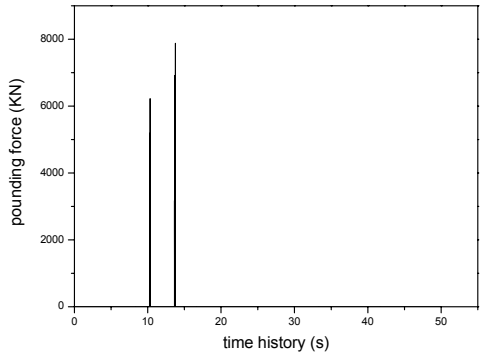

a. Response history for pounding force at the top of pier

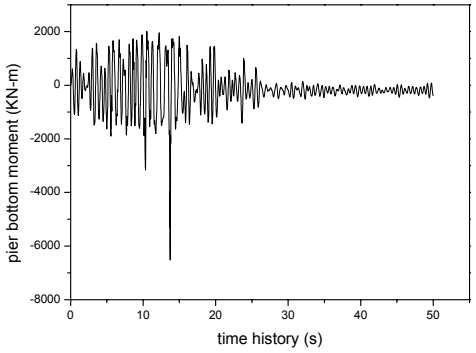

b. Response history for moment at the bottom of pier

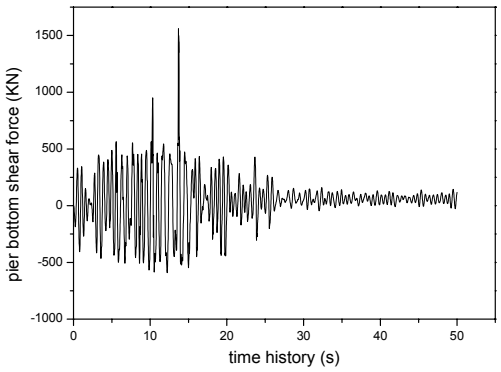

c. Response history for shear at the bottom of pier

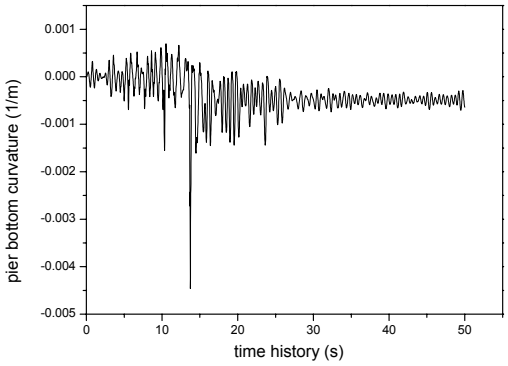

d. Response history for curvature at the bottom of pier

Figure 6 Analytical response history of No.1 pier under severe earthquake with acceleration input along longitudinal axis

Seismic Design and Analysis for Urban Viaducts With a Double Deck

Jian-zhong Li[1], Shi-de Hu[1] and Li-chu Fan[1]

ABSTRACT

The urban viaducts with a double deck in Shanghai are now under construction. According to the China seismic design code for of urban bridges (Draft 2001), the seismic design and analysis for urban viaducts has been finished by State Key Laboratory for Disaster Reduction of Civil Engineering in Tongji University. The three-level seismic design approach corresponding the performance levels is adopted. The analysis results for different column cross section sizes and different reinforcement ratios were investigated.

[1]State Key Laboratory for Disaster Reduction in Civil Engineering, Tongji University, Shanghai 200092, PRC

INTRODUCTION

Seismic design and analysis method for bridges have been improving and advancing based on research findings and lessons learned from past earthquakes. After recent earthquakes, especially the 1989 Loma Prieta, 1994 Notrhridge and 1995 Hyogoken-Nanbu earthquakes, seismic design for highway bridges has been undergoing a critical reappraisal, with the emphasis change from "strength" to "performance". In several countries, seismic design of highway bridges is in the process of fundamental change [1]. In China, a new seismic design code for urban bridges (draft 2001) [2] has been complied by State Key Laboratory for Disaster Reduction of Civil Engineering in Tongji University. The three-level seismic design approach corresponding the performance levels is adopted in this new code.

Based on the new code, the seismic design of the urban viaduct with a double deck in Shanghai has been carried out. The viaduct with a double deck in Shanghai is shown in Figure 1. The pier is Y type with an upper deck for six lanes of urban highway and a lower deck with two lanes of urban light railway system. The superstructure for the upper deck is simple concrete hollow plate girders and for the lower deck is simple box girders, supported on the elastomeric bearings with a span of 30m. The upper and lower columns of the pier are rectangular columns with initial cross section 1.5m ×2.0m and 2.0m ×2.0m, respectively. The pier has a specified concrete compressive strength of 40 Mpa with initial longitudinal steel reinforcement ratio 1.6%. The volumetric ratio of lateral steel reinforcement provided inside the plastic hinge range of the columns is about 0.5%.

SEISMIC ANALYSIS METHODS AND PROCEDURES

Design Criteria

Based on the China seismic design code for urban bridges, the three-level seismic design approach corresponding the performance levels as shown in Figure 2 was adopted for the seismic design of the urban viaduct with a double deck. Three levels of earthquake loads, minor, design and severe earthquakes are defined as ground motion with 63%, 10% and 2% probability of exceedance in 50 years, respectively. Corresponding the three levels of earthquake loads, The earthquake performance levels of I, II, and III are defined as following:

- Performance I: Minor earthquakes should be resisted in the elastic range of structural components without damage.
- Performance II: The structural components may be limited damage, but full access to normal traffic is available almost immediately following a design earthquake.
- Performance III: Severe earthquakes should not cause collapse of all or parts of a viaduct bridge; damage that does occur should be readily detectable and accessible for inspection and repair.

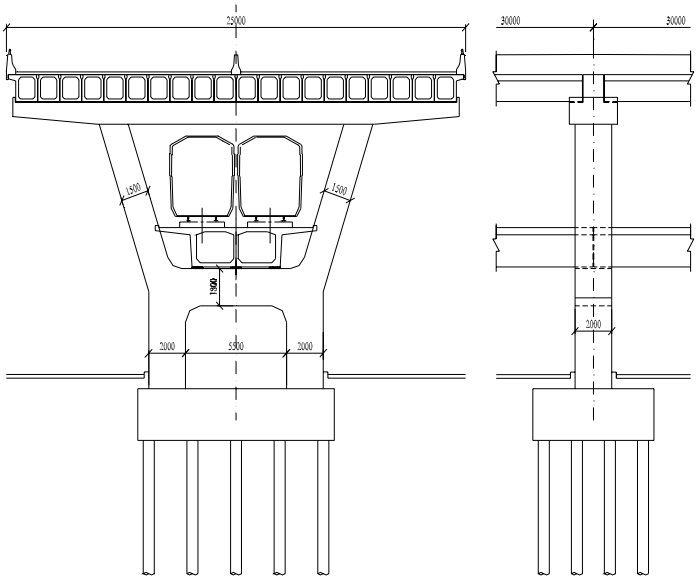

Figure 1. The urban viaduct with a double deck in Shanghai (unit: cm)

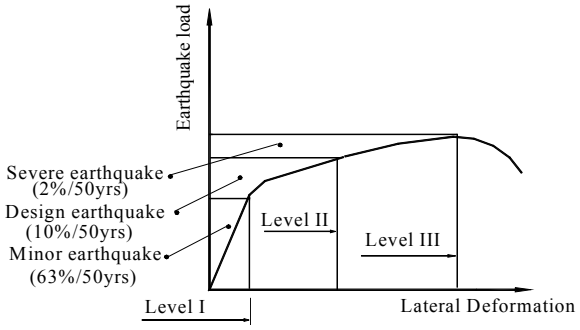

Figure 2. Relationship between earthquake load levels and performance levels

Design Methods and Procedures

For a double-deck viaduct, the upper and lower columns are chosen as the ductile member .The potential plastic hinges should be formed in upper and lower columns of bridges (Figure 3). Plastic hinges may occur at the top and bottom of each upper and lower column when the seismic forces act in the transverse direction, but only at the bottom of the lower columns when seismic forces act in the longitudinal direction.

The three-level seismic design approach for the viaduct bridge with a double deck has evolved as outlined below:

- The multi-modal spectral analysis was used to estimate longitudinal and transverse seismic effects for structures under minor earthquakes. The total stress in concrete and reinforcements for bridge columns under a minor earthquake, weight of structure and 50% loads of train should be limited permissible values to insure the structure components in elastic ranges.

- Nonlinear time history analysis was used determined longitudinal and transverse seismic effects for structures under design and severe earthquakes, respectively. The elastomeric bearings should be designed to resist the maximum shear deformation corresponding to the design earthquake actions. The plastic rotation capacity of the plastic hinge for the upper and
  lower columns of a pier should be design to resist the maximum plastic rotation corresponding to the severe earthquake actions.
- The demands for foundations, cap beams, joints and shear forces for columns were determined in accordance with capacity design principles. These components should be designed to remain essentially elastic when the columns reach its over strength capacity.

The flow charts outlining the steps in the three-level seismic design approach was presented in Figure 4.

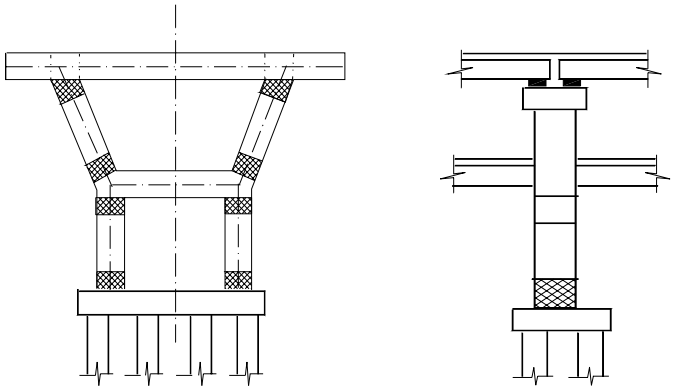

Figure 3. Potential plastic hinge locations for double-deck viaduct

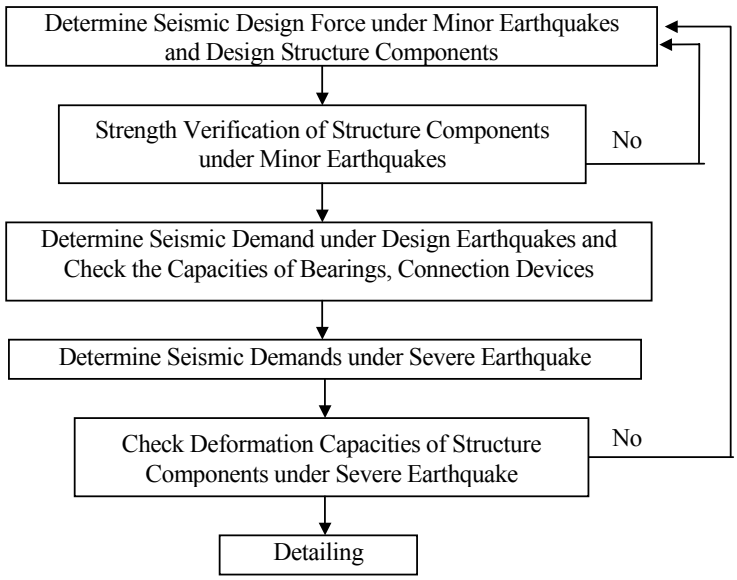

Figure 4. Flow charts outlining the steps in the seismic design

ANALYTICAL MODEL

The analytical model for the viaduct bridge with a double deck is shown in Figure 5. The upper and lower decks were modeled by three-dimensional linear elastic beam-column elements placed at the geometric centroid of the cross section. The inelastic three-dimensional beam-column elements were used to model each upper and lower column of the piers. The general interaction yield surface for a concrete section under the action of axial force combined with biaxial bending suggested by Bresler [3] was adopted. Each elastomeric bearing in viaduct bridges was modeled by a linear spring. The effects of rail and rail fastener were considered in seismic response analysis for lower decks of the viaduct bridge as following:

- The rails were idealized as 3D elastic beam elements;
- The transverse and vertical stiffness of the rail fastener were simulated by linear spring elements;
- The longitudinal interactions between the rails and a lower deck were simulated by nonlinear spring elements with bilinear model.
-

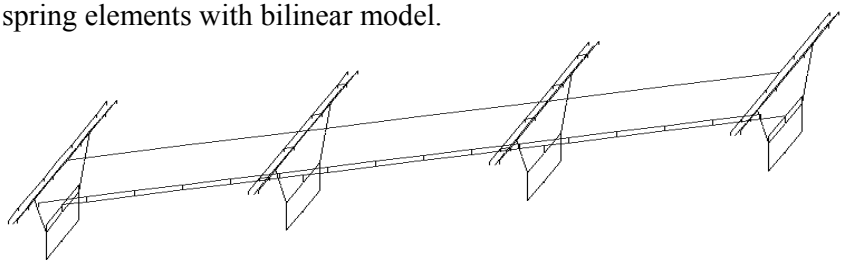

Figure 5. Analytical model for the viaduct bridge with a double deck

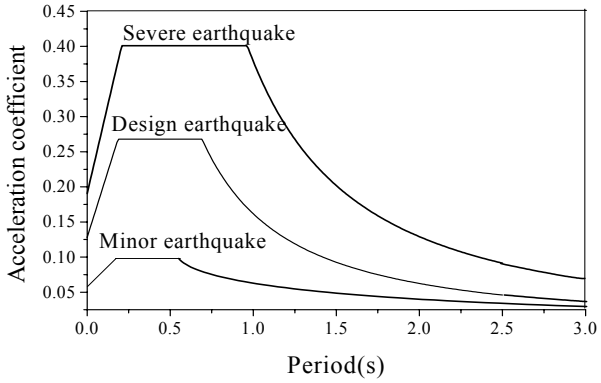

Figure 6. The site-specific acceleration coefficient

EARTHQUAKE LOADING

The site-specific acceleration coefficient and typical site-specific time histories of input acceleration for a minor, design and severe earthquakes were provided. Figure 6 shows the acceleration coefficient for a minor, design and severe earthquakes, respectively.

RESULTS

The computer program IPSABS developed by State Key Laboratory for Disaster Reduction of Civil Engineering in Tongji University was used to perform linear spectral analysis and the nonlinear dynamic time history analysis.

In order to investigate the seismic performance of the double-deck viaduct for different column cross section sizes and reinforcement ratios, the double-deck viaduct with three types of the column cross section size and longitudinal steel reinforcement ratios as shown in TABLE I are analyzed and compared.

TABLE I. THE COLUMN CROSS SECTION SIZES AND STEEL REINFORCEMENT RATIOS FOR DOUBLE-DECK VIADUCT

		Cross section size (cm)	Longitudinal reinforcement ratio (%)	Volumetric ratio of lateral reinforcement (0.5%)
Type 1	Upper column	200×150	1.6	0.5
	Lower column	200×200	1.6	0.5
Type 2	Upper column	180×150	1.2	0.5
	Lower column	180×150	1.2	0.5
Type 3	Upper column	180×130	1.2	0.5
	Lower column	180×130	1.2	0.5

Based on the each column cross section and reinforcement ratio of three types that shown in TABLE I, the shear, flexural strengths and rotation capacities at plastic hinge ranges of the upper and lower columns were determined according to China seismic design code for urban bridges. To assess the response, column bending moments, the maximum relative displacements between the girder and the pier, and plastic rotation in plastic hinge ranges were calculated with the site-specific input acceleration of a minor, design and severe earthquakes, respectively. Parts of import results are discussed as following.

Upper and Lower Column Capacity

Mander's model for confined concrete and unconfined concrete [4] was used to calculate the yield bending moments, yield curvature, ultimate curvature for three types of columns. The rotation capacities of plastic hinge of columns are estimated by [5]:

$$\theta_p = (\phi_u - \phi_y) L_P \tag{1}$$

Where ϕ_y = yield curvature corresponding to the first yield of reinforcements; ϕ_u = curvature capacity at the failure limit state and L_p =equivalent analytical plastic hinge length.

The calculating results for yield bending moments, yield curvature, ultimate curvature and plastic rotation capacities for plastic hinge of columns in the direction of perpendicular the bridge axis are presented in TABLE II.

The demands for cap beams, and shear force demands of columns for three type viaducts determined in accordance with capacity design principles, corresponding to gravity loads are shown in TABLE III.

TABLE II. COLUMN CAPACITIES

		Axial force（kN）	Yield moment（kN-m）	Yield curvature（kN-m）	Ultimate curvature (1/m)	Rotation capacity
Type 1	Upper Column	0.0	9398.0	0.00167	0.082	0.0250
		20000.0	18910.0	0.00226	0.040	0.0110
	Lower Column	0.0	14320.0	0.00120	0.059	0.0153
		20000.0	27540.0	0.00153	0.036	0.0091
Type 2	Upper and lower Column	0.0	5246.00	0.00152	0.069	0.0217
		20000.0	14104.0	0.00210	0.029	0.0089
Type3	Upper and lower Column	0.0	4299.0	0.00178	0.080	0.0245
		20000.0	10085.0	0.00270	0.032	0.0092

TABLE III. THE DEMANDS FOR CAP BEAMS, JOINTS AND SHEAR FORCES FOR COLUMN

	Type 1		Type 2		Type3	
Shear demand for upper column (kN)	3230.0		2893.4		2283.0	
Shear demand for lower column (kN)	7794.0		4785.6		3576.4	
Bending moment demand for upper cap beam (kN-m)	Max	24890.0	Max	15270.2	Max	13699.4
	Min	-11628.0	Min	-3755.84	Min	-2510.0
Bending moment demand for lower cap beam (kN-m)	Max	25830.0	Max	15674.34	Max	14268.0
	Min	-25838.0	Min	-3104.0	Min	-10543.0

Response Analysis Results

The upper and lower columns in viaduct bridge for all three types are worked generally in the elastic range under minor earthquakes and the shear deformations of elastomeric bearings are adequate to resist the design earthquake. The bending moments for columns under minor earthquakes in the direction of perpendicular the bridge axes for three type columns are showing in TABLE IV. The upper and lower columns enter to plastic work range and the maximum plastic rotation at plastic hinge range for the upper and lower columns under severe earthquakes are shown in Figure 7 and TABLE V.

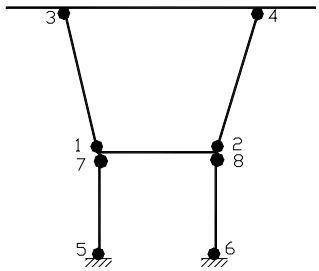

Figure 7. The plastic hinge at upper and lowe column under severe earthque

TABLE IV. THE BENDING MOMENTS FOR COLUMNS UNDER MINOR EARTHQUAKES

	Upper column			Lower column		
	Max. Moment (kN-m)	Max. Axial force (kN)	Min. Axial force (kN)	Max. Moment (kN-m)	Max. Axial force (kN)	Min. Axial force (kN)
Type 1	5515.6	11113.0	9297.7	3477.67	15901.3	10988.6
Type 2	5328.0	8627.0	6460.0	2463.0	13295.0	8364.0
Type 3	5295.0	8123.0	6361.0	2243.0	12372.0	8988.0

TABLE V. THE ROTATION IN PLASTIC RANGE UNDER A SEVERE EARTHQUAKE

	θ_1 and θ_2	θ_3 and θ_4	θ_5 and θ_6	θ_7 and θ_8
Type 1	2.15e-3	1.30e-3	8.01e-4	
Type 2	4.10e-3	1.98e-3	8.01e-4	5.65e-4
Type 3	5.60e-3	2.70e-3	1.25e-3	7.99e-4

DISCUSSION

As mentioned as above, the demands for foundations, cap beams, joints and shear forces for columns are determined when the columns reach its over strength capacity. A proper column cross section size and longitudinal steel reinforcement ratio are very important to design foundation, cap beams and joints. From TABLE III, according to Type 1 design (initial design) of the viaduct bridge, the bending moment and shear force demands for upper and lower cap beams are very high. As the column cross section sizes and longitudinal reinforcement ratios are reduced, the demands for cap beams, and shear forces for columns are reduced largely.

However, the analysis results of three-level seismic design approach show that the Type 2 and Type 3 are adequate to resist minor, design and severe earthquakes, respectively, according to China seismic code for seismic design of urban bridges.

CONCLUSIONS

Based on the new code for seismic design of urban bridges, the three-level seismic design approach corresponding the three-level performances is adopted for the seismic design of the urban viaduct with a double deck. The analysis methods and analysis results were investigated. The analysis results show that a proper column cross section size and longitudinal steel reinforcement ratio are very important to design foundation, cap beams and joints if capacity design principles are adopted to calculate demand for these components.

REFERENCES

Kazuhiko KAWASHIMA, ‘ Seismic Design and Retrofit of Bridge’, Paper No, 2828, 12WCEE, Auckland, New Zealand, 2000.

Stare Key Laboratory for Disaster Reduction of Civil Engineering. ‘China Seismic Code for Urban Bridges (Draft 2001)’, Shanghai, P.R.C, 2001.

Boris Bresler, ‘Design Criteria for Reinforced Column under Axial Load and Biaxial Bending’, ACI Journal. 66(4)(1960) 481-490.

J. B. Mander, M. J. N. Priestley and R. Park.. ‘Theoretical Stress-Stain Model for Confined Concrete’, ASCE Journal of Structure Engineering. 114 (8)(1988) 1804-1826.

M. J. N. Priestley, F. Seible, G. M. Calvi, ‘ Seismic Design And Retrofit Of Bridges’, John Wiley &Sons, New York, 1996.

A Pseudodynamic Test of an Urban Viaduct with a Double-Deck

Tian-bo Peng[1], Shi-de Hu[1], Jian-zhong Li[1] and Li-chu Fan[1]

ABSTRACT

A pseudodynamic test of an urban viaduct with a double-deck was carried out in the structural laboratory of State Key Laboratory for Disaster Reduction in Civil Engineering in Tongji University. The test model and the pseudodynamic method are introduced. The results are shown and investigated.

[1]State Key Laboratory for Disaster Reduction in Civil Engineering, Tongji University, Shanghai 200092, PRC

INTRODUCTION

An urban viaduct with a double-deck is now under construction in Shanghai. Its upper deck is urban arterial highway with six lanes and the lower deck is urban light railway system with two lanes. The pier is Y type, and the superstructure for the upper deck is simple concrete hollow plate girders and for the lower deck is simple box girders, supported on the elastomeric bearings with a span of 30 m.

A pseudodynamic test was performed in the structural laboratory of State Key Laboratory for Disaster Reduction in Civil Engineering in Tongji University to investigate the seismic performance and damage condition of the viaduct. This method is a relatively new structural seismic test method, which combines computers with actuators on line and has some advantages:

1) It's cheaper than shaking table test;

2) Large scale or even full scale model test of large size structures is available;

3) The situation of the specimen can be observed in detail at any moment under test;

4) The effects of damage on the behavior of the structure are physically modeled;

5) Almost all kinds of structures can be tested integrated with the substructuring technique.

Pseudodynamic test method has many advantages compared with other seismic test methods, and has become a popular and credible method abroad.

This method has some disadvantages too:

1) High performance test hardware is required;

2) Strain rate effect cannot be considered in an ordinary pseudodynamic test;

3) Excessive testing time is needed;

4) Test response is often specific to a particular input motion.

SPECIMEN AND TEST SETUP

According to the test capacity of the laboratory, a one fifth scale model shown in figure 1 was adopted. The total height of the specimen is 4.18 m including a foundation 0.44 m thick. The distances from the bottom of lower columns to the center lines of the upper and lower cap beam are 1.76 m and 3.56 m, respectively. The distance between the two lower columns is 1.64 m. Two jacks acted on the top of the upper cap beam and the prestressing wire strand imposed on the lower cap beam are used to simulate the influence of the dead load on the axial force of the four columns. The whole specimen is fixed on the floor with ten screws through the foundation, and cement mortar is also paved between the underside of the foundation and the floor to increase the frictional force. Based on the test data, the foundation's movement is no more than 0.05 mm and is negligible in the test.

According to the simulation law, a one fifth scale specimen was designed. The columns of the specimen are designed on the basis of the height, dimensions and reinforcement content of the prototype. The designs of cap beams and joints are in accordance with the philosophy of capacity design, that is the columns are designed to be ductile members and the two cap beams and the joints

are designed to be capacity protected members, so it's a type of strong-beam weak-column mechanism. The sections of all the components of the specimen designed are shown in figure 2.

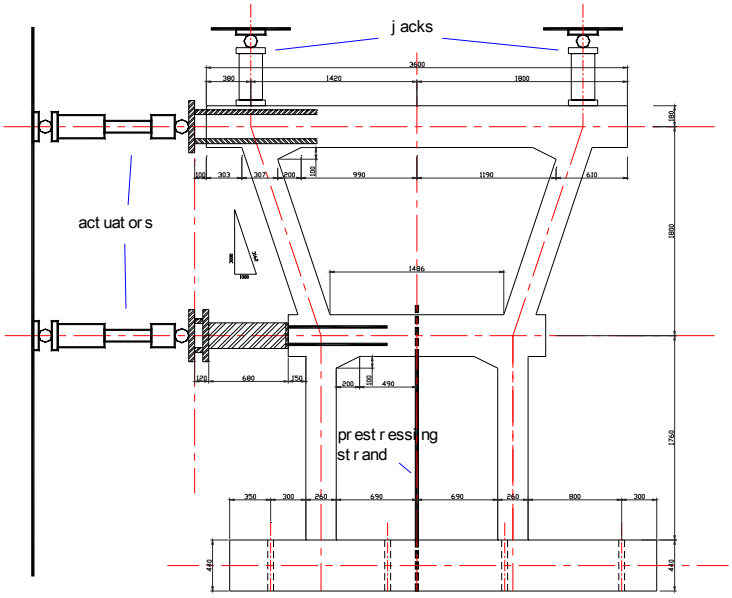

Figure 1. Elevation of the specimen

The design strength of concrete of the prototype is 23.0 Mpa, and the design yield strength of longitudinal reinforcements and hoops are 340 Mpa. In the specimen, the strength of concrete is 44.22 Mpa, and the yield and ultimate strength of longitudinal reinforcements are 355 and 520 Mpa, and which of stirrups are 360 and 455 Mpa, respectively.

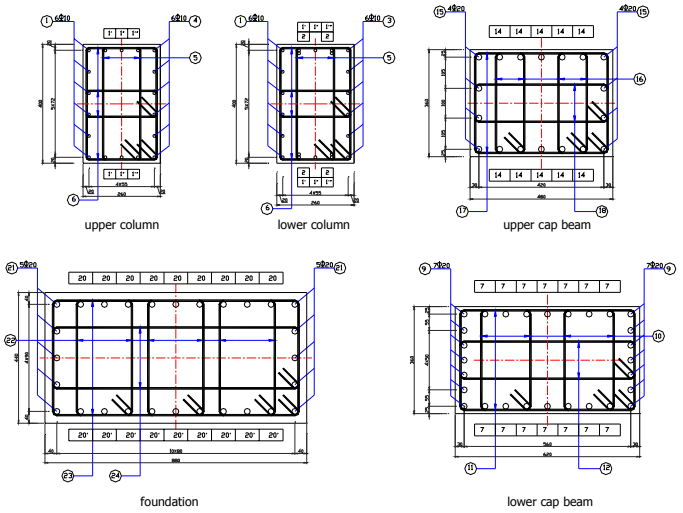

Figure 2. Details of components of the specimen

A site specific time history of input acceleration, called Gong2 wave, is shown in figure 3a). The seismic behavior of the prototype structure is investigated systematically by increasing the maximum of the acceleration history gradually. Because the wave is used to investigate the prototype, the time scale is condensed in the pseudodynamic test. In order to reduce the period of a test, the first two seconds of the condensed earthquake history is removed. The condensed Gong2 wave is shown in figure 3b). El Centro (NS) and Hanshin earthquake record not condensed are also used. The cases of the test are shown in table I.

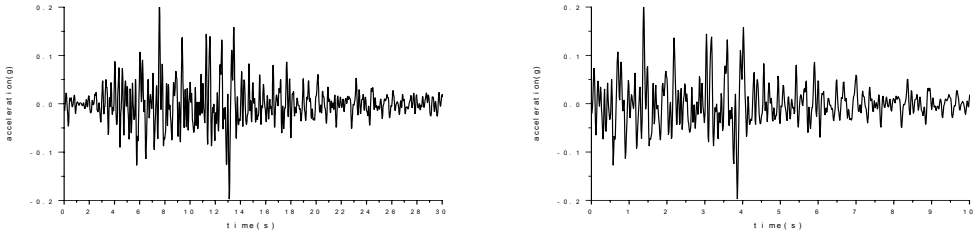

a) Initial wave b) The condensed Gong2 wave

Figure 3. Gong2 wave

TABLE I. CASES OF THE TEST

Case	Wave	Peak of the acceleration history (g)
1	Gong2 wave	0.13
2	Gong2 wave	0.20
3	El Centro wave	0.40
4	Gong2 wave	1.00
5	El Centro wave	0.60
6	Hanshin wave	0.60
7	Gong2 wave	1.20

TEST RESULTS

In the test, data of the displacement and restoring force history of the two cap beams were recorded. Strains of some longitudinal reinforcement bars and stirrups at critical locations were also collected. Some typical results are as follows:

Before the test, the initial tangent stiffness of the specimen was measured, and the shear stiffnesses of the upper and lower structure were 50.0E3 kN/m and 73.5E3 kN/m, respectively. According to the simulation law, the lumped masses on the upper and lower cap beam were 56 ton and 34 ton, respectively. The tolerance limit for every freedom was 0.05 mm, and this was maintained throughout the test.

In case 1, a minor and short crack appeared on the outside of the right lower column, 20 cm above from the bottom. But the crack closed immediately. The displacement histories and hysteretic loops of the interstory shears and drifts of the two parts are shown in figure 4. If there is no specific note, real line and dotted line are used to indicate the data of lower and upper part of the structure

respectively in all the figures of this paper. All the components remained intact, until the maximum displacement of the upper cap beam reached 7.83 mm. With the increase of the displacement, the stiffness of the specimen declined. The equivalent shear stiffnesses of the upper and lower part were 37.2E3 kN/m and 36.9E3 kN/m, from the slope of the line between the positive and negative maximum displacement points of each loop.

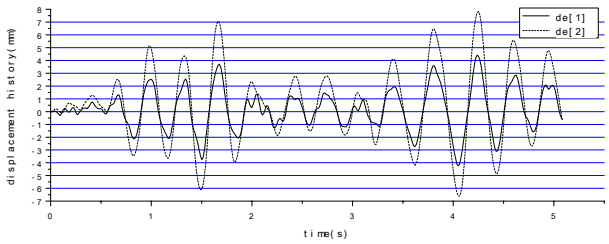

a) Displacement history

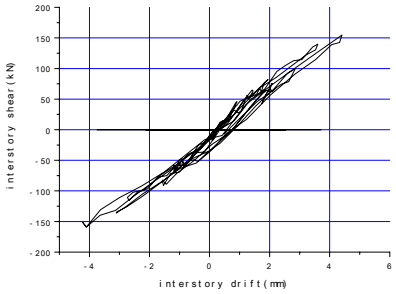

b) Lower hysteretic loop

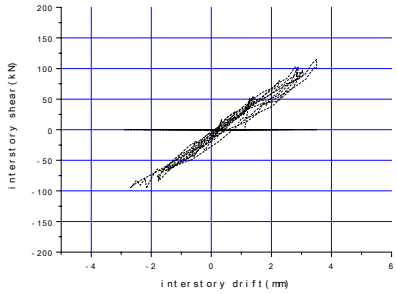

c) Upper hysteretic loop

Figure 4. Data of case 1

In the next case, residual cracks developed first on the outside of lower columns near the bottom, then on the inside near the top of lower columns, and last on the outside of upper columns near the bottom. The displacement histories and hysteretic loops of the case 2 are shown in figure 5, the equivalent shear stiffnesses of the upper and lower part are 18.3E3 kN/m and 19.9E3 kN/m. Because more cracks were observed on the lower columns, the measured stiffness of the lower part reduced more.

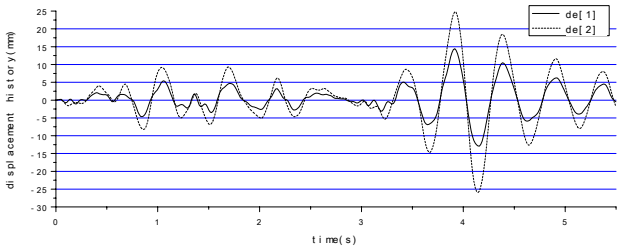

a) Displacement history

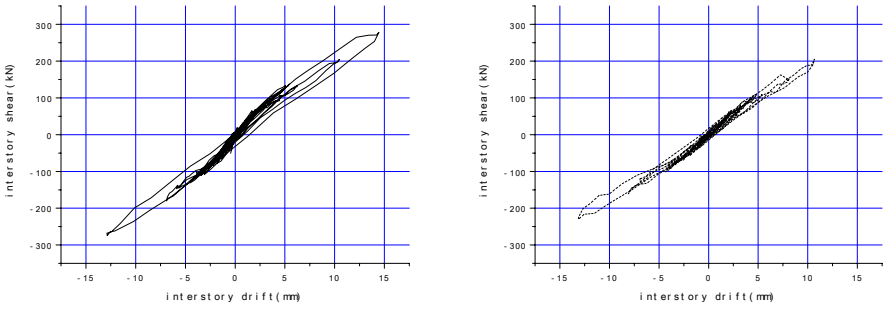

b) Lower hysteretic loop c) Upper hysteretic loop

Figure 5. Data of case 2

Greater nonlinearity was exhibited in the hysteretic loops in case 3, as shown in figure 6. In this case, the observed surface cracks on the outside of the two lower columns near the bottom developed in the form of fish scales. Some of the surface shelled off, but stirrups were not exposed. Cracks distributed relatively uniformly, and 6 cracks with the space of 7 to 8 cm appeared on the outside of the left lower column near the bottom. On the other locations of potential plastic hinge range, which are at the top of lower columns and the bottom of upper columns, cracks appeared relatively densely too.

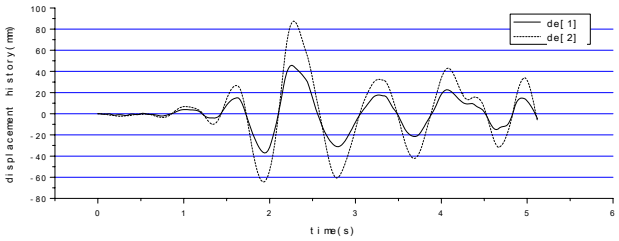

a) Displacement history

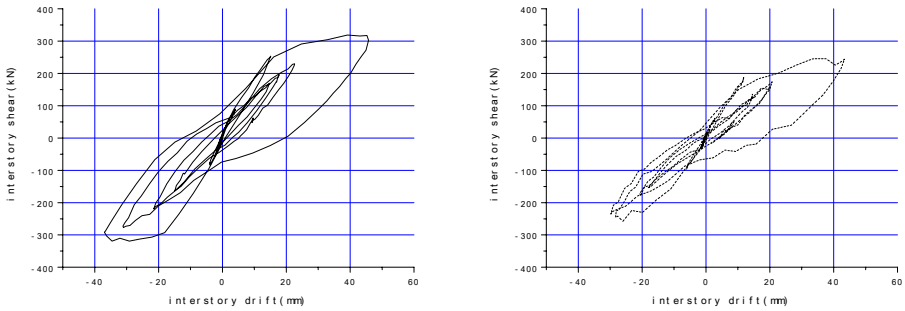

b) Lower hysteretic loop c) Upper hysteretic loop

Figure 6. Data of case 3

Along with the increase of the acceleration peak, the specimen damaged more severely. The concrete surface on the lower columns spalled and several stirrups and longitudinal reinforcements were exposed first. But damage of upper columns developed more quickly, and in case 5, the interstory drift of the upper part exceeded the lower, as shown in figure 8.

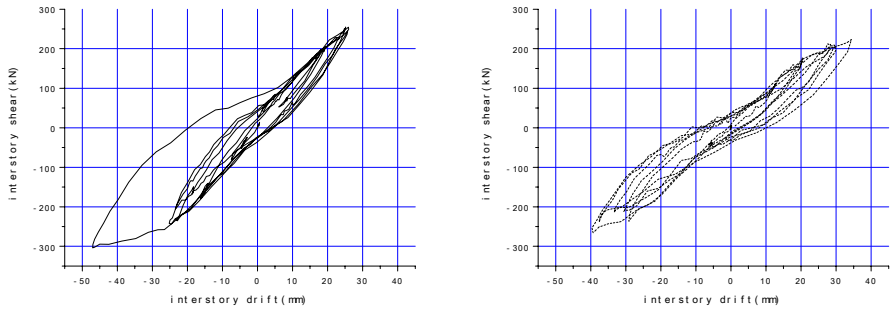

a) Lower hysteretic loop b) Upper hysteretic loop

Figure 7. Data of case 4

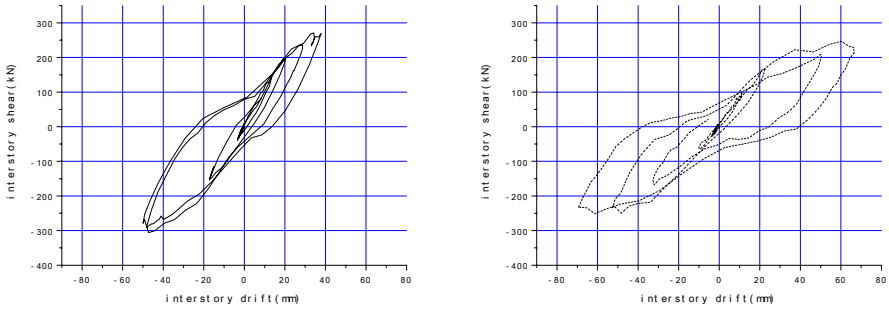

a) Lower hysteretic loop b) Upper hysteretic loop

Figure 8. Data of case 5

After the concrete surface on the outside of the left upper column near the bottom crushed, bars were bared. In case 6, damage was concentrated on the outside of the left upper column, and the maximum interstory drift of the upper reached 136.78 mm. The bared longitudinal reinforcements on the outside of the left upper column became buckled outward lightly in this case, and part of core concrete crushed, which could indicate that the specimen had been destroyed. The displacement histories and hysteretic loops of this case are shown in figure 9.

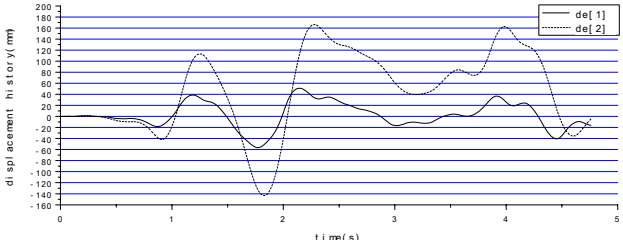

a) Displacement history

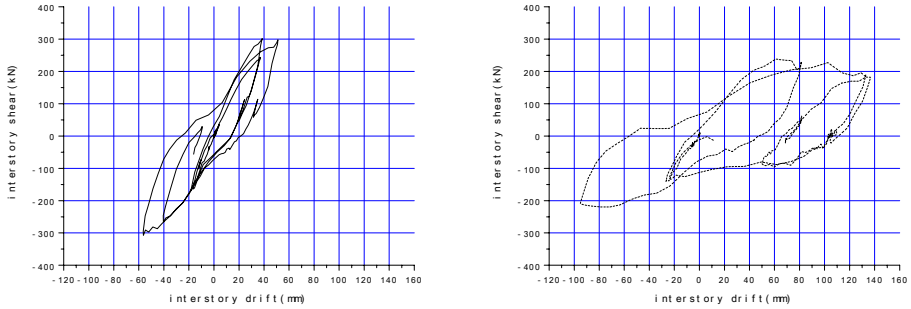

b) Lower hysteretic loop c) Upper hysteretic loop

Figure 9. Data of case 6

At the last case, and soft story effect was found at the upper structure, but the lower part was far from the ultimate state, as shown in figure 10. One of the buckled longitudinal reinforcements of the each upper column fractured, and the structure could not return the initial position. The fractured bar of the upper left column and its location are shown in photograph 1. In all the cases, all the cap beams and joints remained almost intact, and almost no cracks could be found on the surface of all these components.

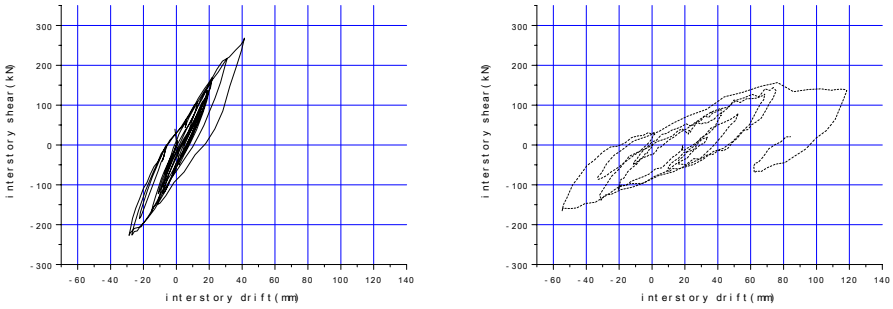

a) Lower hysteretic loop b) Upper hysteretic loop

Figure 10. Data of case 7

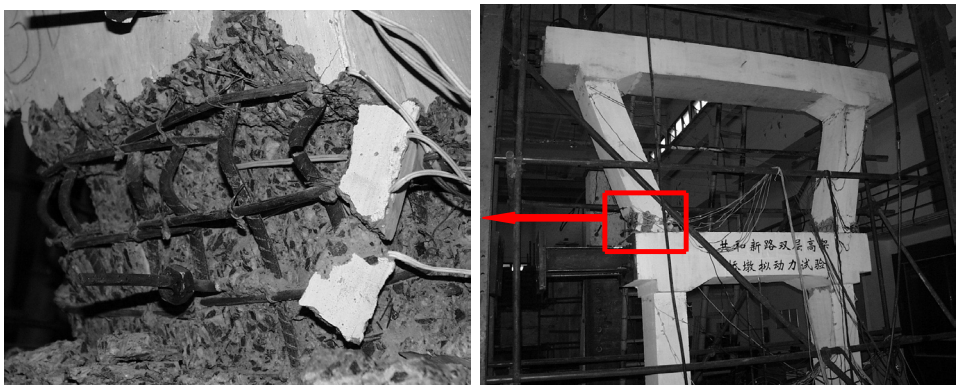

Photograph1. The fractured bar and its location

CONCLUSIONS

The conclusions below can be drawn from the test results of the pier model of the viaduct:

1) The potential plastic hinge locations are at the top and bottom of each column of a pier of a double-deck viaduct, and more plastic deformation and damage are concentrated at the bottoms.
2) Cracks on the lower columns were observed first, but damage of the upper columns was more concentrated, and finally one of the upper columns was destroyed first.
3) The hysteretic loops of the upper and lower structure look like a bow with quite good capacity of energy dissipation, and a certain extent of pinching effect is also shown.

REFERENCES

Zhu, B.L. 1989, Structural Seismic Test, Seismic Publishing House (in Chinese)

Fan, L.C., Li, J.Z., and Wang, J.J.2001, Seismic Design of Viaduct, People's Communication Publishing House (in Chinese)

Fan, L.C., Li, J.Z., and Hu, S.D.2001, Seismic Design Guidebook of Shanghai Gonghexin Road Viaduct (in Chinese)

Seismic Design and Retrofit Strategies of Cable-Supported Bridges: An Overview of Current U.S. Practice

George C. Lee, John Sun and Chuck Seim

ABSTRACT

This paper is a brief review of the current practice of seismic design and retrofit of cable-supported long-span bridges in the United States. It may be regarded as a progress report of the review of typical design practices and retrofit methods of long-span bridges. Full information on this subject is currently being developed by MCEER under a research contract from the U.S. Federal Highway Administration (FHWA).

A major objective of this paper is to provide a basis for discussion by the workshop participants and to call to the attention of PRC and U.S. engineers and researchers about the U.S. FHWA project by requesting their cooperation to supply available information on this subject area (case studies).

George C. Lee, Multidisciplinary Center for Earthquake Engineering Research, University at Buffalo, Red Jacket Quad, Buffalo, NY 14261, USA
John Sun, T. Y. Lin International, 825 Battery St., San Francisco, CA 94111, USA
Chuck Seim, T. Y. Lin International, 825 Battery St., San Francisco, CA 94111, USA

INTRODUCTION

Long-span bridges are a very significant part of the physical infrastructures of our society. In bridge design, long-span bridges are essential structures in the bridge importance category and always need special design attention that is different from regular bridges. In AASHTO specifications, bridges with span length more than 500 feet are considered long-span bridges.

Typical long-span bridges are: cable-stayed bridges, suspension bridges, arch bridges and multi-span continues deck or truss bridges. For the past two decades, more and more long-span bridges were designed and constructed around the world, and some of them are located in high seismic areas. Multi-support excitation, geometrical non-linearity, material non-linearity, and soil-foundation nonlinear interaction have been considered in the analysis, and design.

The investigation of bridge damage in recent large earthquakes have occurred in high seismic prone areas (1994 North-Ridge earthquake and 1995 Kobe earthquake) (Yashinsky 1995, Ritchie 1999) indicate most of the long-span bridges have less seismic vulnerability than short-span regular bridges, and no major damage or collapse had happened to long-span bridges. Because more design attention had been given to long-span bridges, that does not guarantee the long-span bridge function or damage free if a higher intensity earthquake (maximum credible earthquake) occurs near the bridges.

Seismic retrofit strategies of long-span bridges are very different from those used for regular short-medium span highway bridges. Different parts of a long-span bridge may require different strategies (hybrid approach).

In the United States, the AASHTO specifications apply to all highway bridges. Three design methods are included in the provision, which are: coefficient and strength modification factor R (1-3.0/ maximum 5), response spectra design method with one fundamental mode or with multi-mode procedure, and time history method. The design method selection will depend on regularity (bridge with more than 7 spans are considered irregular), importance, and seismic zone.

The hazard risk level is defined by the design spectra spectrum or design ground motion. The design earthquake motions (10% 50 years or 500 return period) and forces specified herein are based upon a low probability of their being exceeded during the normal life expectancy of a bridge. Bridges that are designed and detailed in accordance with the provisions of the specification may suffer damage, but should have low probability of collapse due to seismically-induced ground motions. A return period of 2500 years for a maximum credible earthquake might be used for critical structures such as long-span bridges.

Each state is entitled to implement its own details, design procedure or provisions. In California, CALTRANS has its own guideline for bridge seismic design. And in some states, 2500 return period earthquake (maximum credit earthquake) is used for strength design for essential design. In most states, the AASHTO provision (Division I-A) applies to bridges of conventional slab, beam girder, box girder, and truss superstructure construction with span not exceeding 500 feet. For other types of construction and bridges with span exceeding 500 feet, the owner (state DOT) shall specify and/or approve appropriate provisions for design.

The AASHTO specifications are based the following principles:

1. Small to moderate earthquake should be resisted within the elastic range of the structural components without significant damage.
2. Realistic seismic ground motion intensities and force should be used in the design procedures.
3. Exposure to shaking from large earthquake should not cause collapse of all or part of the bridge. Where possible, damage that does occur should be readily detectable and accessible for inspection and repair.
4. The probability of the coefficient is based on 10% exceeding probability in 50-years or 500-year return period.
5. Acceptable damage is restricted to inelastic hinges in the columns. The foundation should therefore remain in its elastic range.

In California, the majority of the California highway bridges need dynamic analysis design. The seismic performance criteria established by CALTRANS for design and evaluation of bridge is shown in Table I.

TABLE I. SEISMIC PERFORMANCE CRITERIA OF CALTRANS

Ground Motion at Site	Minimum Performance Level	Important Bridge Performance level
Function Evaluation	Immediate Service Level Repairable Damage	Immediate Service Minimum Damage
Safety Evaluation	Limited Service Level Significant Damage	Immediate Service Level Repairable Damage

Seismic performance is assessed at the following two levels of earthquake ground motion:

1. Function evaluation earthquake having 40% probability of occurring during the useful life of the bridge (50, 100, 200).
2. Safety evaluation earthquake which is either the maximum credible earthquake based on the conventional deterministic assessment or an earthquake with an average return period of 1000 to 2000 years.

The seismic requirement for important bridges (long-span bridges are important bridges) are significantly raised to the following level:

1. The structure should remain essentially elastic under the functional evaluation earthquake.
2. The structure should provide service to normal traffic almost immediately following the safety evaluation earthquake. Any damage incurred should be repairable with limited loss of service, i.e., short closure time.

In this paper, seismic design and certain retrofit strategies of cable-supported bridges will be reviewed and discussed.

SOME FUNDAMENTAL ISSUES OF SEISMIC DESIGN

During the past two decades, several cable-supported long-span bridges, approximately 200 meters or longer in span length, have been either seismically retrofitted or constructed in the United States. There are many such bridges constructed throughout the world, particularly in Europe and Asia.

In essence, the design of a long-span cable-supported bridge under seismic loading, like the design of any important bridge, must address a sequence of key issues:

- Determine the site's seismic exposure by developing the seismic hazard evaluation, seismic response spectra, and ground motion time-histories either by deterministic methods of evaluating site-specific historical, seismologic, and geological data, or by probabilistic methods for the region.
- Develop multi-level seismic design events based on the data developed above, in the case of the often adopted two-level (or bi-level) approach, a lower level event that has a 50 percent probability of occurring during the life of the bridge, and a higher level event that has a 5 percent probability of occurring during the life of the bridge. For the usual 75-year life of an ordinary highway bridge in the U. S., this would require developing both 150-year and 1500-year return period seismic design events. Most long-span bridges designed today will survive with good maintenance for 150 years or longer, so developing higher levels of the two-level seismic design event may be warranted.

- Establish a Bridge Performance Policy (BPP) with the owners or operators of the facility. The BPP should consider the economic, social impacts to the local community and the surrounding areas, and the cost to the owner of the bridge under multi-level design seismic events. The BPP is a statement of how the owner wants the bridge to perform in small earthquakes and in large ones with the imposed financial constraints and limited other resources.
- Transfer the bridge performance policies into a site-specific seismic design criteria document to augment the prevailing bridge design specifications.
- Develop several concepts for seismic resisting systems (SRS) based on the gravity resisting system developed for the bridge during the bridge preliminary design phase.
- Design a bridge structural system for these seismic demands and for the seismic design criteria.
- Analyze the structure for global, regional, and local action with linear and nonlinear analysis.
- Refine the design and detailing.
- Verify the design with critical large-scale structural laboratory testing.

More detailed discussion on the seismic design issues listed above are given in the following sections.

Design Seismic Motions

Except for a situation in which a bridge is founded on a single block of rock or for cases that the nearest credible fault line is located at least 50 kilometers away, a rigorous structural time history response evaluation of a long-span cable-supported bridge is fully warranted by the bridge designer. Site-specific multiple-support rock motions and site-specific geotechnical data are essential to performing a realistic linear and nonlinear time history analysis for a long-span cable-supported bridge.

In evaluating the site-specific multiple-support rock motions, the following factors that should be considered are:

- Near-field fault rupture directivity effects: From the recent observations in bridge performance during earthquakes such as the 1989 Loma Prieta Earthquake (USA), the 1994 Northridge Earthquake (USA), the 1995 Kobe Earthquake (Japan), and the 1999 Chi-Chi Earthquake (Taiwan), bridge structures are vulnerable to velocity pulses (called in the U.S. the "Fling Effect" because it results in a large rapid ground displacement). A realistic set of site-specific rock time history motions should be characterized by including a velocity pulse and by its frequency diversity.
- Vertical acceleration effects: A bridge located near an active fault (< 10 kilometers) can experience significant vertical accelerations, which must be accounted for in the design.
- Wave-passage effects to account for traveling seismic waves.
- Compatibility with a coherency function to account for scattering and complex wave propagation phenomena.
- Cross-correlation between the fault-normal and fault-parallel components.

When multiple-support rock motions are used in a free-field analysis to generate inputs for the soil-structural interaction analyses and for inputs to the global bridge response model, site-specific geophysical and geotechnical field and laboratory test data are essential to obtain realistic analyses.

Bridge Performance Policy and Seismic Design Criteria

Bridge Performance Policy is directly related to the level of importance of a bridge to a local community and to the regions it serves. A long-span, cable-supported bridge is usually a landmark Bridge and is often classified as “important” or “critical” infrastructure to the community it serves.

For example, in the case of the San Francisco–Oakland Bay Bridge, the State of California classifies it as a “lifeline” structure. This level of importance requires that the bridge must provide full

service immediately after both a 90-year return period event, called a Functional Evaluation Earthquake, and a 1500-year return period, called a Safety Evaluation Earthquake. The Bridge Performance Policy further states that the bridge may experience minimal or no damage during a Functional Evaluation Earthquake and repairable damage (that can be repaired quickly with minimum interruption of traffic flow) during a Safety Evaluation Earthquake.

Depending on social, political, and economic factors, other landmark bridges may have different requirements stated in the Bridge Performance Policy. Nevertheless, a Bridge Performance Policy is the key item that needs to be fully defined at the beginning so that the seismic design criteria for the bridge can next be established. The performance requirements of key structural elements or sub-structural groups are defined in terms of allowable strains, deformations, and the demand-to-capacity ratios.

Again, taking the case of the San Francisco–Oakland Bay Bridge East Bay Replacement Project as an example, "repairable damage" of the Bridge Performance Policy under Safety Evaluation Earthquakes is ensured by the "Limited Ductility Structure" requirements of the Seismic Design Criteria. The "Limited Ductility" rules set the limits of the maximum concrete compression strain to less than 2/3 of the ultimate concrete strain, and the maximum tensile strain in the reinforcement to less than 2/3 of the defined ultimate steel tensile strain. In addition, the Limited Ductility Structure clauses require that the design provides a clearly defined ductile mechanism for the response to seismic load and with limited nonlinear deformations concentrated to a few specifically chosen elements, such as the tower shear links, the main pier hinging regions, and the top of foundation piles. Maximum residual displacement of any of the elements of the bridge is limited to 300 mm.

Under Functional Evaluation Earthquakes, the "minimal damage" of the Bridge Performance Policy is ensured by the "essentially elastic" requirements of the Seismic Design Criteria. In the Seismic Design Criteria, the term "essentially elastic" is mainly characterized by the elastic response of bridge superstructure and the main tower with strain limits of 0.004 for the concrete in compression and 0.001 for the reinforcing steel in tension.

Seismic Bridge Concept Development

Much like the seismic design of conventional bridges, the seismic design concept for long-span cable-supported bridges should have a clearly identifiable earthquake resisting system (ERS). The bridge's ERS should provide a reliable and uninterrupted load path transmitting seismically induced inertia forces into the ground. The ERS should also provide stable elastic and inelastic displacement capacities to withstand the displacement demands generated by seismic motions. In developing the bridge's optimal ERS system, main span towers and approach span piers should be considered as an integrated seismic system. It may be preferable that devices such as bearings or isolators not be used for considerations of structural simplicity, functional reliability, and continuous maintenance. However, seismic response modification devices can be used effectively when properly employed and when the stand-alone ERS system can not be made adequate to meet the force and displacement demands induced by seismic motions.

Since the main towers of a long-span, cable-supported bridge are the primary gravity-load-carrying members, it is preferable that the seismic lateral loads from the cable-supported system are resisted by the flanking piers and not by the main towers. This concept may require a partial or a fully-integrated design between the approach piers and the main span piers and towers. This consideration is further justified by the fact that post-earthquake repairs of the flanking piers are much easier to repair than the main span towers. However, the towers must be designed for the seismic loading produced at the top of the towers from the seismic forces in the cables.

While towers or pylons are designed traditionally to meet strength demands, their displacement capacities become crucial in ensuring the safety of the bridges under seismic loadings. A recent development using a multi-shaft system for the main tower design presents a new structural system alternative to meet high demands of both axial load carrying capacity and lateral displacement capacity. This concept is discussed in more detail below.

Structural Analysis to Evaluate Demands and Capacities of Bridge Elements

Overall approach of the structural analysis for a cable-supported bridge should include an estimate of force and deformation demands from practical computer models of the bridge- i.e. models that are as simple as possible but that incorporate all significant aspects of ground motion input and structural response.

Global Analysis

In general, for a long-span, cable-supported bridge, the global analysis should be a three-dimensional linear or nonlinear computer program. Both response spectrum and time history analysis methods should be used for design of the long-span, cable-supported bridge.

Time history analysis should be used for models that are largely linear, but that include all significant nonlinearities. These nonlinearities might include:

- Globally nonlinear geometry
- Stay-cable or suspension-cable geometric nonlinearities
- Plastic hinging of piles, piers, and towers
- Rocking of pile caps or piers
- Pounding between structural units
- The action of nonlinear devices such as dampers and restrainers
- The nonlinear behavior of critical areas of the structures such as the bases of towers or the rocking of towers. Simplified representations (e.g. simplified finite element models) of these areas may be included in the global model.

A global model should include appropriate representations of the bridge foundations and soil-structure interaction. From the simple to the complex, the different approaches that might be used to model soil-structure interaction are:

- Linear impedance-matrices and corresponding scattered input motions
- Secant impedance-matrices considering nonlinear soil and/or foundation behavior
- Scattered input motions from time history analysis of the foundation
- If nonlinear soil or foundation behavior or rocking of the foundations is particularly severe, these behaviors may be included in the global model itself

Local Analysis

Local finite element analysis should generally be used to investigate unusual or critical portions of the structure and to determine the behavior of the region studied, in order to incorporate that behavior in the global model in a simplified form.

Parts of the bridge that might be the subject of local analysis are:

- Pile/pile cap connections
- Tower bases, and tower heads
- Joints between the deck and towers

Local models may also be utilized to develop the actual design of unusual portions of the structure, for which design rules are unavailable, or to which code provisions may not apply. We have taken this approach for the seismic retrofit of the Golden Gate Bridge to design the strengthening of the tower bases and the supporting piers, and also for the design of the tower shear links of the new San Francisco–Oakland Bay Bridge, which is discussed below.

Critical Structural Detailing

Proper detailing of structural elements is the link between the structural concept and the completion of a successful project. Proper detailing can never be over-emphasized for design of essential infrastructures, especially for the design of long-span, cable-supported bridges and for seismic designs. Among the many important structural details to ensure the bridge safety against seismic actions, *lateral confinement* in concrete members and *compactness for post-yielding behavior* in steel members are probably the two most decisive factors that can improve bridge performance under earthquake motions.

Lateral confinement. Moderate increase of lateral reinforcement in concrete compression members significantly enhances the post-yield displacement capacity and prevents brittle type shear failures that have been experienced in many concrete bridges in earthquakes during recent decades. This was shown experimentally in the early 1980s at the University of Canterbury, New Zealand, in the late 1980s and in the early 1990s at the University of California, San Diego, and in many other institutions in the U. S.

In addition to the minimum specified transverse reinforcement ratio, currently Caltrans requires that all hoop bars in columns, piers, towers and pylons be spliced with ultimate strength splices or certified butt-welded hoops or be connected by certified mechanical couplers. Traditional "lap-splice" detail that has been used for many years on numerous bridge projects is prohibited. The cost of the lateral confinement reinforcement often is less than 1% of the overall project cost, yet this small cost will have the single most positive effect on good performance of a bridge structure under seismic loading.

Steel plate compactness for post-yielding behavior. Buckling of steel plates is probably the dominant failure mode in steel design under seismic loading. The key design index to control or limit this type of failure is the plate width-to-depth ratios or "b/t" ratios. There appears to be some confusion in current design codes for this critical design index. An example of this confusion would be the definition categories of steel section compactness. Currently, there are four section compactness categories defined in various codes:

Slender section. In this category, local plate buckling will occur before the yielding of the full section occurs.

Compact Section Type A (AASHTO, AISC). In this category, no local plate buckling will occur before the yielding of the full section occurs.

Compact Section Type B (AASHTO, AISC). In this category, yielding can be ensured for nearly the full section and plastic capacity can be developed before the occurrence of local plate buckling. This category can reach a strain level of 2 to 3 times the steel yield strain before any local plate buckling occurs.

Compact section for large strain (ATC–32, AISC Addendum). In this category, the section can endure deformations corresponding to a strain level of 5 times steel yield strain or more before local plate buckling occurs.

In seismic design for steel members of the long-span, cable-supported bridge, the b/t ratios corresponding to the "compact section for large strain" should be used for member sections that are expected to endure significant non-linear or ductile deformations for displacement ductility demand equal to or larger than 2. Extensive damage to steel frames in buildings during the Northridge Earthquake shows how non-ductile steel members can crack if not properly detailed.

The discussion of these decisive factors is to highlight the importance of structural detailing in bridge design, especially for long-span bridges, which are held to high standards in terms of seismic performance and long-term structural durability.

Large Scale Design Verification Laboratory Tests

Often in long-span, cable-supported bridge design, the common state of practice in bridge engineering is pushed, stretched, even broken to ensure the demands arising from social, aesthetic, economic, and public considerations as well as demands from natural and man-induced forces. This

pushing of the edge of the state of practice cannot merely be characterized by uncommonly large size bridge elements, but also by the selected structural system and the materials chosen.

In the case of the new East Bay replacement span of the San Francisco–Oakland Bay Bridge, a panel of engineers and architects that represented the public interest selected a record-setting long-span self-anchored suspension bridge. The bridge engineers, presented with the formidable challenge of designing this unusual structure, developed a new and innovative structural system for the seismic resisting systems. New concepts for key elements in the bridge structural system, such as a four-shaft steel tower connected by deformable steel shear-links, a looped cable anchorage system, multi-shaft seismic force resisting concrete piers, and ductile steel and concrete detailing are all part of essential elements in making the bridge concept a reality.

To ensure high standards in structural safety and the durability of the 150-year design life for the structure, key elements in the bridge structural system were tested in the structural testing laboratory in a scale that is representative of the bridge elements.

Considering the immense investment typically associated with long-span, cable-supported bridges, a verification laboratory test program should be an inherent part of the overall project program, essential not only to ensure structural safety but also to control and reduce the overall cost of the project investment and to advance the state of practice in bridge engineering.

SEISMIC RETROFIT USING RESPONSE MODIFICATION TECHNOLOGIES

Seismic retrofit for cable-supported bridges typically uses "seismic response modification technologies. The two most important factors that affect the structural response of a bridge are stiffness and mass distribution, which determine the frequency content and structural damping of the bridge. As the stiffness and mass of the bridge are not uniformly distributed, irregular responses occur under random earthquake ground motions. The key issue is to first understand the dynamic responses and develop a retrofit strategy to modify or reduce the bridge responses. To a large extent, much of the existing efforts in structural response modifications have been concentrated on:

- "Regularizing the irregularity": Equalizing the stiffness of supporting elements or adding sub-structural systems to equalize the effective seismic demands and the structural capacity.
- Isolation: Increasing the fundamental periods of vibration of the bridge to a point on the design spectrum at which the power of the input motions is lowered.
- Dampers: Increasing the energy-dissipation capacity of the structure, thereby increasing the effective equivalent structural damping to reduce or to limit the base shear and the displacement demands on the substructure.

Engineers and researchers have been accomplishing these objectives with two main approaches:

- Modifying or optimizing the bridge structural response by designing innovative and engineered sub-structural systems or elements, such as multi-shaft piers, sleeved piles, rocking piers, and ductile shear links. This approach is often favored by bridge designers in new construction projects.
- Modifying or optimizing the bridge structural response by using structural response modification "devices" such as isolators, which increase the structure's fundamental period and dampers, which increase the effective damping. Additionally, there are many new developments such as active or semi-active control systems which use devices and/or smart materials. These "smart structure" approaches have not yet been seriously used in bridge engineering practice in the U.S. today.

Obviously, combinations of these two basic approaches can be in most cases cost-effective. This is the basic objective of the current MCEER research task to develop retrofit strategies for long-span

bridges. The following are some typical structural response modification approaches. Some of them are taken from information supplied to MCEER by U.S. bridge designers on cable-supported bridges that are either retrofitted or in the planning and/or construction state (see Figure 1). Specific examples on isolation bearings and various dampers are not provided because their application to cable-supported bridges in the U.S. is only in the very preliminary stage. Many references on their implementation are available, particularly in Japan and China. They are not reviewed in this paper.

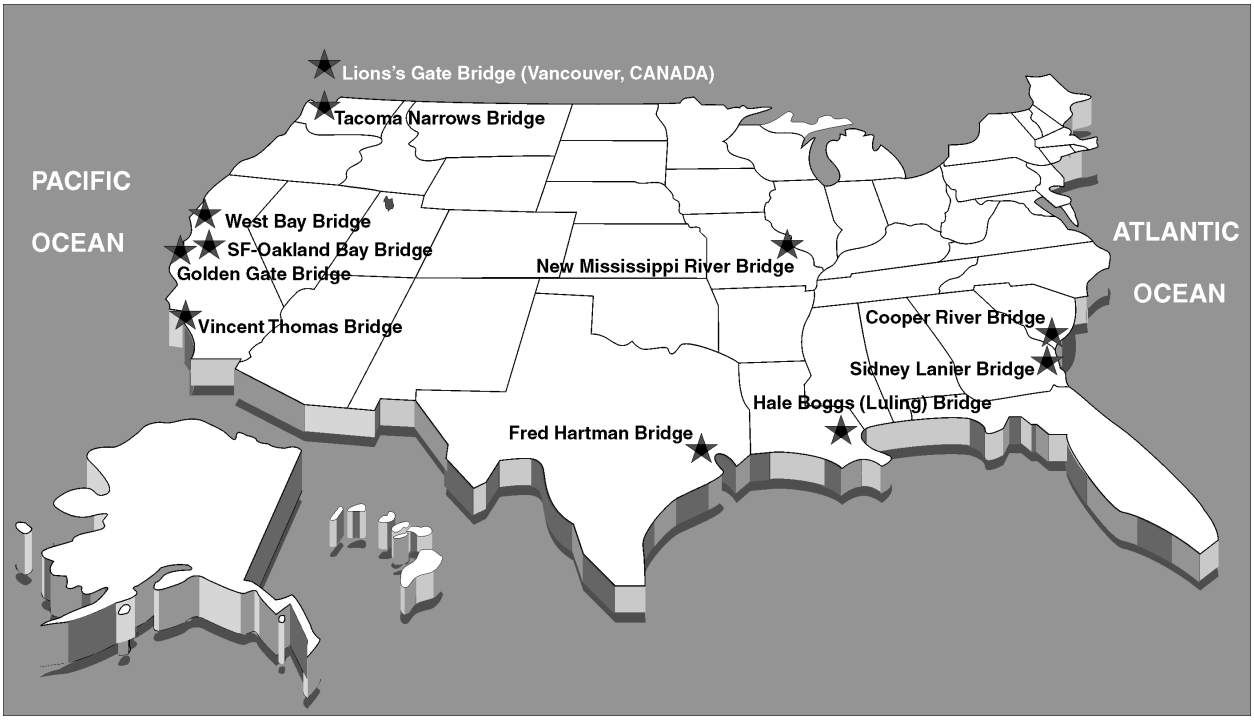

Figure 1. Some earthquake-resisting cable-supported bridges in U.S. (new or retrofitted by response modification technologies)

Multi-Shaft (Column) Concrete Piers

The idea of Multi-Shaft Piers is to split a classic single column pier into a multiple-column pier to increase its flexibility. This leads to significantly increased fundamental periods of the bridge and the displacement capacity of the pier without compromising its shear capacity. This concept was actively explored and used in the final design of the San Francisco–Oakland Bay Bridge Suspension Span. The resulted four-column west-anchorage piers increase the first fundamental period of vibration from 1.5 seconds to 4.0 seconds. This successfully limits the high-density power input of seismic motions within the range of 1.0 to 2.5 seconds. Compared to a classic single-column pier design, the displacement capacity is also enhanced from about 0.3 meters to about 2.0 meters for the 45-meter tall pier.

Multi-Shaft Steel Towers

The Multi-Shaft Concept was also used to improve seismic performance of the single tower supporting the suspension cables of the San Francisco–Oakland Bay Bridge. The single tower was split into four steel shafts connected together with strategically placed ductile shear links.

Sleeved-Pile Foundations

The basic idea of the sleeved pile is to introduce a "soft layer" between the bridge foundation and the ground motion so ground-to-foundation isolation is achieved. This is especially useful in situations in which the geotechnical profile varies under the same bridge foundation. In other situations, this concept

has been used to lower a pier foundation in order to achieve optimal structural response under seismic loads.

Rocking Foundation

It has been recognized that rocking response of a tall bridge pier limits the moment applied to the foundation pier and, consequently, the uplift to one side of the pier. The rocking is also effective in dissipating energy, thus increasing the effective damping in the structure. This concept was studied in the 1960s, and was further studied and applied to a railroad bridge design in New Zealand in the 1970s. Recently, the rocking response mechanism was used for the retrofit design of the steel towers of the Golden Gate Bridge. Special detailing was required to adequately reinforce the lower section of the towers to withstand the rocking pressure. The tops of the two concrete piers were also reinforced by pre-stressing cables to withstand tower base impact loading.

Metallic Dampers

There are numbers of damping devices available today. The underlying energy dissipation mechanism is derived from the inelastic deformation of a metal, usually steel, or an alloy such as lead, to achieve a stable elastic-plastic behavior.

Friction Dampers and Friction Bearings

Friction dampers utilize the mechanism of Coulomb friction between sliding plates of special material to provide energy dissipation. A special class of friction damper, using high-strength bolts, depends on galling action on soft metal inserts. One friction-bearing device combines the concept of a sliding bearing with that of pendulum action, which both dissipates energy and lengthens the fundamental structural period. Even though friction dampers have not been used to any extent in large bridges because they have small energy-absorbing capacities, the friction/pendulum bearing has been used with great economy and structural efficiency.

Viscoelastic Bearing/Dampers

The basic material used in viscoelastic bearing/dampers are layers of copolymer materials interlayered with steel plates to form a stacked bearing that can carry vertical loads, and, when deformed by shear action, they deform and dissipate energy and increase the fundamental period of the structure. They have been used in a number of short-span bridges and in buildings, but rarely in long-span bridges probably because the heavy weight of the bridge requires very large diameter and very thick bearings that are difficult to manufacture.

Viscofluid Dampers

Unlike the viscoelastic dampers that use inelastic deformation as the mechanism for energy dissipation, a viscofluid damper converts the mechanical energy into heat as the piston of a cylindrical damper forces a highly viscous fluid from one chamber to another through an orifice. The viscous fluid also can be placed in a rectangular container and be heat generated by vanes moving through the viscous fluid by mechanical action.

The viscofluid dampers have one other characteristic: they allow movements at slow rates and will provide resistance and energy dissipation when imposed by displacement at higher rates. These characteristics allow them to be used in situations where movements induced by creep, shrinkage, temperature, or traffic should not be restrained under normal service conditions.

Viscofluid dampers will be installed on the 1280-meter main suspension span of the Golden Gate Bridge seismic retrofit between the towers and the stiffening trusses for the main span and for the side spans. These types of dampers also will be installed at the same locations for the seismic retrofit of the twin 704-meter main suspension spans of the San Francisco-Oakland Bay Bridge. However, the new 728-meter main suspension span currently under construction across the Carquinez Straits near the San

Francisco Bay does not utilize viscofluid dampers at the towers because the steel box girder is suspended continuously from end to end and passes through the tower legs.

Tuned Mass Dampers

The principle of a Tuned Mass Damper (TMD) is that the out-of-phase motion of a small spring-mass system can reduce or "damp" out the fundamental period of vibration of a much larger spring-mass system. TMD applications for major bridges in seismic active zones have not been wide spread. This is probably due to the fact that the frequency bandwidth of a typical seismic motion is rather wide. This high-frequency content tends to generate higher modes of vibrations in the structure and the TMD, tuned to the fundamental frequency of the structure, can suppress little of the dynamic response of higher modes in the structure.

TMD was used very effectively for the erection of the towers of the Akaski Kaikyo Bridge and are still in service inside the towers since the bridge was completed. A torsion TMD was installed in 1987 on the Bronx-Whitestone Bridge to effectively suppress the first asymmetric torsion mode by wind excitation.

Tuned Liquid Damper

The basic principle in applying a Tuned Liquid Damper (TLD) to mitigate the structural response is similar to that of a Tuned Mass Damper (TMD). Unlike TMDs, the response of a TLD is highly nonlinear, partially because of liquid sloshing or the presence of orifices. In practice, a TLD does have several advantages over a TMD such as low installation and maintenance cost and long-term reliability of the damping mechanism.

The above are only typical examples. There are many other approaches used in the U.S. that are given in the References without further explanation in this preliminary review.

SUMMARY

This paper is a preliminary review of the recent seismic design and retrofit practice in the U.S. It is presented with two specific purposes: (1) to provide a platform for discussion by the workshop participants to identify future research needs and subject areas suitable for joint research projects to be carried out by PRC and U.S. researchers, and (2) to inform the PRC and U.S. earthquake engineering community of the MCEER project on the development of seismic response modification technologies for long-span bridges and to request their cooperation to provide case studies to MCEER so that a more comprehensive technical volume can result from this study.

The authors apologize for the incompleteness in the review of published information of U.S. efforts on this subject matter.

ACKNOWLEDGEMENTS

The authors acknowledge the financial support of the U.S. Federal Highway Administration (Contract #DTFH61-98-C-00094). Additional support has also been provided by NSF (Contract #EEC-9701471) and State University of New York (Contract #C-000591). They also wish to express their appreciation to those organizations which provide the design and retrofit information on the bridges indicated in Figure 1 (Buckland and Taylor, Ltd.; Caltrans; Modjeski and Masters; Parsons Brinckerhoff; Texas Department of Transportation; T.Y. Lin International; and Washington State Department of Transportation).

REFERENCES

AASHTO. 1998. *LRFD Bridge Design Specifications*, 2nd Edition, Washington, DC: American Association of State Highway and Transportation Officials.

AASHTO. 2001. *Guide Specifications for Seismic Isolation Design*, Washington, DC: American Association of State Highway and Transportation Officials.

Abbas, H., S.P. Singh, and J. Uzarski. 1988. "Seismic Evaluation and Retrofit of Sacramento River Bridge at Rio Vista," *6th US National Conference on Earthquake Engineering*, Seattle, Washington.

Aiken, I.D. and J. M. Kelley. 1990. "Earthquake Simulator Testing and Analytical Studies of the Two Energy-Absorbing Systems for Multistory Structures," Report No. UCB/EERC-90/03, University of California, Berkeley.

Giacomini, M.C. and J.E. Woelfel. 1997, "Retrofitting the Golden Gate Bridge," *J. Civil Engineering*, 67(10).

Ingham, T.J., S. Rodriguez, M.N. Nader, F. Taucer and C. Seim. 1995. "Seismic Retrofit of the Golden Gate Bridge," *Proc. National Seismic Conference on Bridges and Highways*, San Diego, CA, December 10-13.

Jung, H.J., B.F. Spencer, Jr. and I.W. Lee. 2002. "Seismic Protection of a Benchmark Cable-Stayed Bridge Using Magnetorheological Dampers," *Seventh U.S. National Conference on Earthquake Engineering (7NCEE) – Urban Earthquake Risk*, Boston, MA, July 21-25.

Matson, D. 1998. "Experience with Seismic Retrofit of Long-span Bridges," *Structural Engineering World Wide*, Elsevier Science Ltd.

Moon, S.J., L.A. Bergman and P.G. Voulgarios. 2002. "Sliding Mode Control of a Cable-Stayed Bridge Subjected to Seismic Excitation," *Seventh U.S. National Conference on Earthquake Engineering (7NCEE) – Urban Earthquake Risk*, Boston, MA, July 21-25.

Murphy, T.P. and J.M. Kulicki. 2002. "Seismic Issues Affecting the Proposed New Mississippi River Bridge at St. Louis, Missouri," *3rd International Workshop on Performance-Based Seismic Design and Retrofit of Transportation Facilities*, Tokyo Institute of Technology, Tokyo, Japan, July 9-11.

Nader, M. and T.J. Ungham. 1995, "Seismic Retrofit of the Towers of the Golden Gate Bridge," *Proc. National Seismic Conference on Bridges and Highways*, San Diego, CA.

Park, K.S., S.W. Cho, I.W. Lee and H.J. Jung. 2002. "Hybrid Control Strategies for Seismic Protection of a Benchmark Cable-stayed Bridge," *Seventh U.S. National Conference on Earthquake Engineering (7NCEE) – Urban Earthquake Risk*, Boston, MA, July 21-25.

Priestley, M.J.N., F. Seible and G.M. Calvi. 1996. *Seismic Design and Retrofit of Bridges*, John Wiley & Sons, Inc.

Reno, M.L. and M. Pohll. 1997. "Seismic Retrofit of the San Francisco-Oakland Bay Bridge, West Crossing," *Proc. National Seismic Conference on Bridges and Highways*, Sacramento, CA, July.

Somerville, P. 2002. "Characterizing Near Fault Ground Motions for Design and Evaluation of Bridges, *Proc. Third National Seismic Conference and Workshops for Highways and Bridges*, April, pp. 137-148.

Stroh, S. and T. Lovett. 1990, "The Houston Ship Channel Cable-Stayed Bridge," *Proc. 6th US-Japan Bridge Engineering Workshop*, Lake Tahoe, NV, May.

Tang, M.C. 1995. "Seismic Design and Isolation of Long-Span Cable-Stayed and Suspension Bridges." *Proc. Annual Seminar on Construction for Earthquake Hazard Mitigation – Seismic Isolation Retrofit of Structures*, Buffalo, NY, pp. 167-176.

Tang, M.C. 1998. "Cable-stayed Bridges," *Structural Engineering World Wide*, Elsevier Science Ltd.

Trachtenberg, E. 1990, "Brooklyn Bridge Rehabilitation Design and Construction," *Proc. 6th US-Japan Bridge Engineering Workshop*, Lake Tahoe, NV, May.

T.Y. Lin International/Moffat & Nichol Joint Venture. 2000. *Description of Design and Analysis Approach to the Self Anchored Suspension Span of the New San Francisco-Oakland Bay Bridge*, prepared for California Department of Transportation, September.

Seismic Response Analysis of Wuhu Yangtze River Bridge

Xi Zhu[1]

ABSTRACT

The Wuhu Bridge is a cable-stayed bridge with steel truss girder over the main navigable pass of Yangtze River. The seismic ground motion transformed problems are studied at Wuhu bridge site in this paper. The analysis methods of soil-pile-pylon interactions are investigated. The number of modes to provide sufficiently accurate results in this complex bridge structure is discussed. The response spectrum method and the time history analysis method using the identical seismic exciting inputs are compared. The time history analysis of multi-support exciting and response spectrum method for incoherent support motions are implemented. A new improved multi-support response spectrum (IMSRS) method is proposed and comparing the results with that of MSRS method, it is reliable, feasible and timesaving.

[1] College of Civil Engineering and Architecture, Northern Jiaotong University, Beijing, 100044, China

INTRODUCTION

The long-span (180m+312m+180m) cable-stayed bridge (Fig. 1) is built at Wuhu city to cross the main navigable pass of Yangtze River. In fact, it is a continuous truss bridge with the extra doses. It is a highway and railway two-usage bridge. The height of pylon over the bridge deck is only 33.2m.The ratio of pylon height over the length of main span is only 0.106.It is less than the normal value of cable-stayed bridge. The engineering geologic condition of the bridge is more complicated and the conditions of every pier (of Pylon) basis are variant remarkably. The covering soil of the long pylon is 27m depth which is from –43m to –16m in altitude. The bridge foundations are all using large diameter bored piles through the covering soils to reach the rock bed. It is obvious that the soil-pile-pylon interaction of each pylon is different. In order to calculate the seismic responses and dynamic behaviors of each pylon considering the interaction of soil-pile-pylon respectively, the simpler model called Single Pylon Model (SPM) is used. In order to attest the rationality of SPM, more elaborate model called Whole Bridge Model (WBM) is used also.

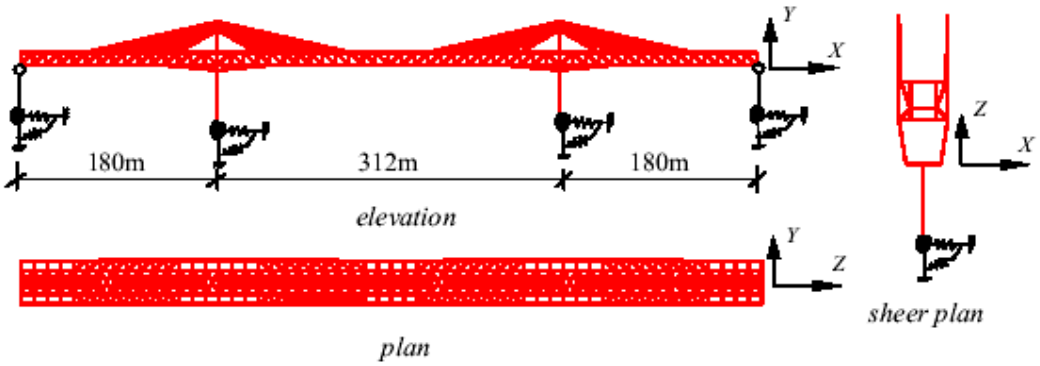

Figure 1 Model of whole bridge

SEISMIC GROUND MOTION AND SOIL-STRUCTURE INTERACTION

The analysis of soil-pile-pylon interaction in SPM mainly consists of two steps. The first step is the free field analysis of earthquake response and the second step is the soil-pile-pylon interaction analysis in which the pile-foundation elasticity-confined to the field is considered. The boundary conditions of far field are provided by the results of the free field analysis.

Seismic response analysis of the free field

The assumptions about the soils are： the surface of the site is horizontal; the soil in one layer is homogeneous; the soil is boundless. The one-dimension soil column model is adapted to simulate the free field. The kinetics equation of the free field is

$$M^G\ddot{U}^G + C^G\dot{U}^G + K^GU^G = -MI^G\ddot{u}_g \qquad (1)$$

in which, U^G displacement vector of 3-dimensional seismic response; $\ddot{u}_g$ acceleration of the base rock; M^G mass matrix with the diagonal elements $m^G{}_i = \frac{1}{2}(\rho_i h_i + \rho_{i+1} h_{i+1})$;K^G stiffness matrix with vertical and horizontal elements respectively $K^G{}_{wi} = \frac{2G_i}{h_i}(\frac{1-\gamma_i}{1-2\gamma_i})$ and $K^G{}_{ui} = \frac{G_i}{h_i}$;$C^G$ Rayleigh damping matrix. In preceding formula: $\rho_i, h_i, G_i, \gamma_i$ are mass per meter, height, shear modulus, Poisson ratio of the ith layer respectively.

The non-linearity of soil is dealt with equivalent linearity method in which the equivalent stiffness and equivalent damping ratio were approached by iteration. The special program is compiled for this purpose.

Design Seismic and input motions

According to Chinese code for Aseismic Design of Railway Engineering at referring to other codes at home and abroad. The seismic input ground motions at the bed rock are provided by the Seismic Bureau of Anhui Province, where the bridge is located. The earthquake ground motion inputs with the exceeding probability in 100 years is 10% was taken for the Functional Evaluation Earthquake. The earthquake ground motion inputs with the exceeding probability in 100 years is 2% was taken for the Safety Evaluation Earthquake.

As the results of seismic risk analysis at the bridge site, there are 12 input motions provided, which include 6 in horizontal and 6 in vertical respectively. One of six input motions in each direction is shown in Figure 2. Its maximum acceleration is 0.952 $m/_{S.S}$ in horizontal direction and 0.436m/ss in vertical direction respectively.

Single Pier(Pylon)Model

A fictitious pile simulates the group piles. The equivalent spring's stiffness at the bottom of cap slab caused by pile's support is computed according $K_{\Phi u} = \sum_{i=1}^{Q} x^2{}_i k_{pi}$,where, Q the total number of piles, k_{pi} the axial stiffness of the ith pile according to Sato assumption, x_i the coordinate of the ith pile. The SPM is shown in Figure3.The characters of the pylon cross sections are shown in TABLE I. The stiffness matrix is assembled by beam elements. In order to reduce the total freedom of the system for accounting soil-pile-pylon is located reasonably with lumped mass in SPM. In order to ensure the comparability, the calculating data in SPM is conformed with those in WBM.

The masses and stiffness influences of the stiffened steel truss and the stayed cables were simply transformed to the piers and pylons. It was built the Single Pier (Pylon) Model.

The allocated mass of main truss and other auxiliary in SPM are shown in TABLE I.

TABLE I. THE ALLOCATED MASS OF MAIN TRUSS AND OTHER AUXILIARY IN SPM(T)

	Long pylon			Short pylon		
	Long.	Ver.	Tran.	Long.	Ver.	Tran.
Joint of pylon and truss	1771	6833	3574	5597	7565	10179
Top of pylon	3330.7	168.3	382.6	4916.0	168.3	548.57

Seismic time history responses for three orthogonal directions located at the pile cap considering soil-pile-pylon interaction were calculated, to get the seismic response spectra at the cap slab in three orthogonal directions respectively. That will be the earthquake inputs when the seismic response of whole bridge is investigated. It will be also provided the spring's stiffness coefficients of the fore cap slabs to account the effects of soil-pile-pylon. It was iterated accurately to approach the constrain condition of the pile foundation, when it was calculated the natural vibration characters and the seismic response with the whole bridge model.

Equation of Soil-Pile-Pylon interaction

The equations of motion considering the soil-pile-pylon interaction are

$$(m_i^{\,p} + m_i^{\,s})\ddot{u}_i + \sum_{j=1}^{n} c_{ij}^{\,p}\dot{u}_j + c_i^{\,s}\dot{u}_i + k_i^{\,s}u_i = -m_i^{\,p}\ddot{u}_g + m_i^{\,s}\ddot{u}_i^{\,G} + c_i^{\,s}\dot{u}_i^{\,G} + k_i^{\,s}u_i^{\,G} \qquad (2)$$

where, u_i the relative displacement of the pile and pylon; u_i^G the relative displacement of the soil.

Equivalent Parameter of Soil-Pile interaction

The equivalent horizontal stiffness between soil and fictitious pile are calculated by Mindlin formula and Elasticity Winkler Assumption. The equivalent vertical stiffness between soil and fictitious pile are calculated according Sato assumption. The equivalent masses of the soil-pile interaction were calculated by the energy equivalent theory.

Seismic Response Spectra

The response spectrum analysis method is used as one method to calculate the seismic response in WBM. Using those 12 seismic input motions of bed rock, 18 acceleration time histories-six respectively in each of longitude, vertical and transverse directions-at top of cap slabs of the pile foundation are analyzed by SPM to get the response spectra at the same

location. Six response spectra are obtained in each direction by Duhamel Integral. The envelope curve of the six response spectra is used as the input motion spectra.

Analysis Results

The Stiffness Coefficient of the Foundation Cap Slab

The foundation spring stiffness of translation, torsion and the coupling each other term that are calculated by SPM are shown in TABLE II.These spring's coefficients are the constraint conditions at the cap slab to alternate the pile foundation in the WBM.

TABLE II. THE CONSTRAINT COEFFICIENTS AT CAP SLAB

		Long pylon	Short pylon
Length of piles	M	30	20
Number of piles		19	17
Diameter of piles	M	3.0	3.0
VE translation	KN/m	1.683E8	4.085E8
TR translation	KN/m	0.116E9	0.439E9
TR coupling	KN/rad	-1.730E9	-7.053E9
TR rotation	KN*m/rad	34.72E9	151.47E9
AL translation	KN/m	0.115E9	0.439E9
AL coupling	KN/rad	1.718E9	7.503E9
AL rotation	KN*m/rad	34.86E9	151.47E9

Envelope Curve of the Response spectra

The envelope curves of the response spectrum at the top of cap slabs which are shown in Figure 4 and TABLE III were calculated by SPM. Those spectra were the input spectra in the WBM.

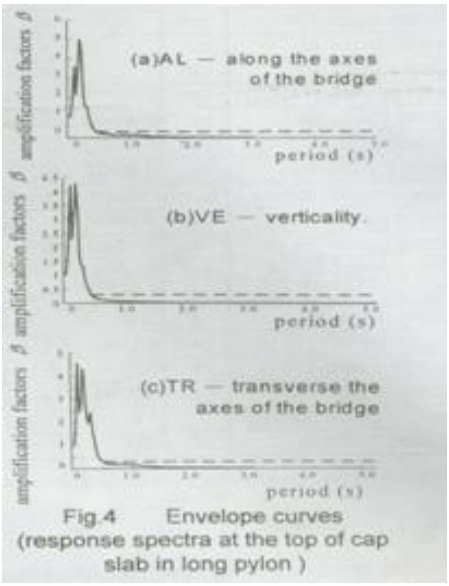

Fig.4 Envelope curves (response spectra at the top of cap slab in long pylon)

TABLE III. THE ENVCELOPE CURVES OF RESPONSE SPECTRUM AT THE TOP OF CAP SLABS

		Displacement (mm)	α_{max} $m/(s*s)$	β_{max}	$\beta_{max} \times \alpha_{max}$ $m/(s*s)$	α_{max} at period s	β_{min} start Period s	$\beta_{min} \times \alpha_{max}$ $m/(s*s)$
Long pylon	AL	3.717	1.4476	5.01996	7.26689	0.20	0.46	0.4343
	VE	2.785	1.0735	4.29193	4.60738	0.20	0.45	0.3221
	TR	3.240	1.2041	4.55865	5.4888	0.12	0.52	0.3612
Short pylon	AL	1.073	0.4034	4.22372	1.7038	0.28	0.56	0.1210
	VE	0.389	0.2784	4.02578	1.1208	0.08	0.44	0.0835
	TR	1.180	0.4103	5.02317	2.0610	0.28	0.60	0.1231

Note: AL-along the axis of the bridge; TR-transverse the axis of the bridge; VE-verticality

Whole Bridge Model

The input locations of seismic ground motions in the Whole Bridge Model are put on the pile cap slabs of four pylons (or piers). The input seismic response spectra are taken from the SPM which is considered the soil-pile-pylon interaction and is enveloped six spectra with same probability condition. The geometric nonlinear effects for cable-stayed are included in the WBM.

Free Vibration Characteristics

The dynamic behaviors of the bridge are calculated by the two proposed models respectively. The natural periods are shown in the TABLE IV and the SPM results are identical with those of WBM.

TABLE IV. THE PERIODS OF BRIDGE IN WBM AND SPM(S)

	WBM	Character of WBM	Long pylon	Short pylon	Character of SPM
1	2.6843	Truss, TR, symmetrical bending			
2	2.4420	Two pylons, AL, floating	2.4369	2.55240	Two pylon, AL
3	2.2460	Truss and pylon, VE, symmetrical bending			
4	1.7088	Long pylon and relevant beam, TR	1.73718		Long pylon, TR
5	1.5718	short pylon and relevant beam, TR		1.68529	Short pylon, TR
6	1.3606	short pylon and relevant beam, TR, torsion			
7	1.3446	long pylon and relevant beam, TR, torsion			
8	1.2982	Short pylon, TR		1.32631	Short pylon's limb TR
9	1.1666	Long pylon, TR	1.23953		long pylon's limb TR
10	1.1624	Russ and pylon, VE, anti-symmetrical bending			
11	1.1484	Truss torsion			

The tangent stiffness matrix of the bridge in its dead load deformed configuration, abstained through an iterative nonlinear static analysis, is utilized in solving the eigenvalue problem. For comparison, four programs were used to calculate the free vibration characteristics. They are the special code 1 by ourselves to account geometric nonlinear effect under dead load, the special code 2 by ourselves and SAP90 and SAP93.The last three codes can't include the nonlinear effects. By examining the computed modes of vibration, the following comments can be made:

(1) Most modes can be categorized as longitudinal, vertical, translateral and purely cable modes.

(2) Strong coupling in the three orthogonal directions occurs in a number of modes. The dominate lateral motion of the bridge truss is strongly coupled with torsion deck and tower vibrations, more over the primarily torsion vibrations are associated with lateral truss motion, and cable vibrations are also present within these modes.

(3) The bridge towers' longitudinal dominant motion is associated with vertical truss vibrations.

(4) The nonlinear effects are not obvious. Because this bridge has a strong stiffen truss, so the natural period of first three modes dominated by the stiffen truss are prolonged less than 3% on considering that the geometric nonlinearity is compared with another. But the natural period from the fourth to ninth which are dominated by the tower are prolonged about 7% to 17% respectively, and the effects of geometric nonlinearity have increased.

SEISMIC RESPONSE OF CABLE-STAYED BRIDGE

Modal contribution ratio

The mode superposition method is widely recognized as a powerful method for calculating the dynamic response of linear structural system with classical damping. The method is attractive because the response of a multi-degree-of-freedom system is expressed as the superposition of modal response, and each modal response is determined from the dynamic analysis of a single-degree-of-freedom system, and these dynamic analysis needs to implement only a few of modes which are significant to the response of total system. Then lots of the calculating efforts will be safe. The number of modes to be included partly depends on modal contribution factor. That will refer to these three ideas, namely, modal participation coefficient vector, modal mass and modal contribution ratio.

The modal participation coefficient vectors are defined as

$$F_x = \Phi^T M E_x, F_y = \Phi^T M E_y, F_z = \Phi^T M E_z \tag{3}$$

in which, M the mass matrix of system, Φ modal vector, and E_x, E_y, E_z as

$$E_x = [1,0,0,1,0,0...]^T, E_y = [0,1,0,0,1,0...]^T, E_z = [0,0,1,0,0,1...]^T$$

The modal masses are the important parameters implying that it is a measure of the degree to which the ith mode participant in the dynamic response.

The modal masses of each mode and each direction are defined as

$$M_{xi} = {F_{xi}}^2, M_{yi} = {F_{yi}}^2, M_{zi} = {F_{zi}}^2 (i = 1,2,..., N) \tag{4}$$

The modal contribution ratio is defined as a ratio, each modal mass is normalized by total mass.

The modal contribution ratio of the ith mode in x direction as: $\gamma_{xi} = \dfrac{M_{xi}}{\sum_{j=1}^{N_x} m_{xj}}, i = 1,2,..., N$

Combining the response contributions of the three orthogonal direction, the total modal contribution ratio of the ith mode:

$$\gamma_i = \frac{M_{xi} + M_{yi} + M_{zi}}{\sum_{j=1}^{N_x} m_{xj} + \sum_{j=1}^{N_y} m_{yj} + \sum_{j=1}^{N_z} m_{zj}}, i = 1,2,..., N \tag{5}$$

In practice, on using mode superposition the modal analysis method can be truncated, and depends on a measure of contribution of the mode to a response quantity. If we take the first n modes to calculate the dynamic response, the total contribution ratio for the first n modes are, respectively

$$R_x = \sum_{i=1}^{n} \gamma_{xi}, R_y = \sum_{i=1}^{n} \gamma_{yi}, R_z = \sum_{i=1}^{n} \gamma_{zi}, R = \sum_{i=1}^{n} \gamma_i \tag{6}$$

The value of R approaching 1, means the contribution of first n modes are enough.

The relationship of the number of accumulated free vibration modes and the value of accumulated total contribution ratio for the Wuhu Yangtze River main navigable bridge is shown in Fig. 5. The total accumulated contribution ratio is reached 0.62 when 30 modes are used, and the R is reached 0.88 when 100 modes are used. R is reached more than 0.90 when 130 modes are used. For this complex long-span bridge, it may be adequate to require R=0.9 or to cut off at first 100 modes.

Response spectrum analysis under identical excitations

Though we use same seismic bed rock inputs with same exceeding probability of 0.1 in 100 years, but the obtained response spectrum respectively at 4 cap slabs of pile foundation are different. The response spectrum of three orthogonal directions at the cap slabs of $10^{\#}$ pylon was selected to conservatively act as the identical seismic inputs for whole bridge. The response spectrum analysis is a procedure for dynamic analysis of a structure subjected to earthquake excitation, but it reduces a series of static analysis. The peak value r_0 of the total response r(t) is estimated by combining the peak modal response r_{io}(I=1,2,…n) according to the complete quadratic combination(CQC) rule. The major results calculated by response spectrum analysis with CQC rule are shown in the TABLE Ⅴ, in order to attest the modes cut off number at 100 is appreciable.

TABLE V. THE RESULTS OF BRIDGE'S IMPORTANT LOCATION WITH VARIOUS MODES' NUMBER

Items	$\frac{q_{30}}{q_{130}}$	$\frac{q_{100}}{q_{130}}$	q_{130}
10#trMtrans.(t-m)	0.878	1.000	52266
10#trQtrans.(t)	0.358	1.000	1947.9
10#trMlog.(t-m)	0.986	1.000	77406
10#trQlog.(t)	0.827	1.000	1267.4
10#trN (t)	0.650	0.967	429.48
11#trMtrans.(t-m)	0.756	1.000	57393
11#trQtrans.(t)	0.300	1.000	2229.6
11#trMlog.(t-m)	0.907	1.000	95432
11#trQlog.(t)	0.453	1.000	2888.5
11#trN (t)	0.530	0.995	529.02
10#tp Δ trans.(cm)	0.979	1.000	4.939
10#tp Δ log.(cm)	0997	1.000	7.848
11#tp Δ trans.(cm)	0.994	1.000	5.285
11#tp Δ log.(cm)	0.974	1.000	8.360
BM Δ trans.(cm)	0.936	1.000	11.65
BM Δ log.(cm)	0.999	1.000	7.879
BM Δ ver.(cm)	0.809	1.000	3.228

(note：tr-tower root; tp-tower top; trans-tranverse; log-longitudial; ver-vertical; M-moment; Q-shear force; Δ-displacement; BM-middle of bridge; q_{30} means the contribution of the first 30 modals, and so forth q_{100}, q_{130}; the note of TABLE Ⅵ and TABLE Ⅶ is same to TABLE Ⅴ.)

Time history analysis of multi-supported linear structures

Using 12 acceleration response spectra of degrees of freedom at 4 top cap slabs of pile foundation, to produce the correspondent artificial seismic records, estimating the time history for every modal coordinate in the first m modal subspace, it has calculated the response values of the modal coordinate time history Z(t) as following expression

$$Z(t) = \sum_{k=1}^{m} a_k u_k(t) + \sum_{k=1}^{m} \sum_{i=1}^{n} b_{ki} s_{ki}(t) \tag{7}$$

in which, $a_k = q^T \gamma_k, k = 1,2,...,m$, $b_{ki} = q^T \Phi_i \beta_{ki}, k = 1,2,...,m, i = 1,2,...,n$

The first part of this response equation represents the components of pseudo static response, and the second part represents the components of dynamic response. It is concerned about the effects of 'local site' through the various exciting inputs.

TABLE VI. THE MAXIMUM VALUE UNDER IDENTICAL EXCITATION COMPARED WITH THE VALUE OF RESPONSE SPECTRUM ANALYSIS

Items	**THistory** Q_h	**RSpectrum** Q_s	Q_h / Q_s
10#trMtrans.(t-m)	46383	45903	1.010
10#trQtrans.(t)	669.49	696.62	0.961
10#trMlog.(t-m)	72043	76323	0.944
10#trQlog.(t)	1076.9	1047.9	1.028
10#trN (t)	205.82	279.12	0.737
11#trMtrans.(t-m)	40946	43401	0.943
11#trQtrans.(t)	646.47	699.27	0.924
11#trMlog.(t-m)	70849	86513	0.819
11#trQlog.(t)	1063.90	1309.40	0.812
11#trN (t)	284.95	280.36	1.016
10#tp Δ trans.(cm)	4.363	4.837	0.902
10#tp Δ log.(cm)	6.424	7.826	0.821
11#tp Δ trans.(cm)	4.408	5.253	0.839
11#tp Δ log.(cm)	6.179	8.143	0.759
BM Δ trans.(cm)	12.816	10.9	1.176
BM Δ log.(cm)	6.202	7.875	0.788
BM Δ ver.(cm)	3.588	2.610	1.375

TABLE VII. THE MAXIMUM RESPONSE VALUE COMPARED WITH IDENTICAL INPUTS AND MULTI-EXCITED INPUTS

Items	Q_1	Q_2	Q_2/Q_1
10#trMtrans.(t-m)	46383	37004	0.798
10#trQtrans.(t)	669.49	755.13	1.128
10#trMlog.(t-m)	72043	62005	0.861
10#trQlog.(t)	1076.9	1574.1	1.437
10#trN (t)	205.82	226.01	1.098
11#trMtrans.(t-m)	40946	25197.82	0.615
11#trQtrans.(t)	646.47	579.38	0.896
11#trMlog.(t-m)	70849	58976	0.832
11#trQlog.(t)	1063.90	1474.41	1.386
11#trN (t)	284.95	174.60	0.613
10#tp Δ trans.(cm)	4.363	4.742	1.087
10#tp Δ log.(cm)	6.424	3.822	0.595
11#tp Δ trans.(cm)	4.408	1.925	0.437
11#tp Δ log.(cm)	6.179	4.433	0.717
BM Δ trans.(cm)	12.816	8.998	0.702
BM Δ log.(cm)	6.202	3.982	0.642
BM Δ ver.(cm)	3.588	3.719	1.037

RESPONSE SPECTRUM METHOD TO SPATIALLY VARYING GROUND MOTION

Multi-support response spectrum (MSRS) method

Recent awareness of the spatial variation of earthquake ground motion, and observations during recent earthquake, notably the Loma Prieta earthquake of October 17, 1989, have clearly demonstrated that seismic ground motions can vary significantly over distance which are of the same order of magnitude as the dimensions of some extended structures, such as long-span bridges. Three phenomena are responsible for these variations：(1) the difference in the arrival time of seismic waves at different stations, denoted as the “wave passage ”effect; (2) the loss of coherence of the motion due to reflections and refraction of the waves in the heterogeneous medium of the ground, as well as due to the difference in the manner of superposition of waves arriving from an extended source at various stations, denoted as “incoherence” effect; (3) the difference in the local soil conditions at each support and the manner in which they influence the amplitude and frequency content of the bedrock motion, denoted as the “local” effect. Nakamura et al. (1993) used the approximate multi-support response spectrum method (MSRS) developed by Der Kiureghian and Neuenhofer (1992), which accounts for spatially varying earthquake ground motion to analyze a complex three-dimensional (3D) model of the Golden Gate Bridge. The method is based on fundamental principles of random vibration theory and

properly accounts for the effects of correlation between the support motions as well as between the modes of the structure. The method works best when the significant segment of the excitation is quasi-stationary ant it is several times longer than the fundamental period of the structure. The combination rule for the mean of the absolute maximum response is given as follows:

$$E[\max|z(t)] = \left[\begin{array}{c} \sum_{k=1}^{m}\sum_{l=1}^{m} a_k a_l \rho_{uk} u_l u_{k,\max} u_{l,\max} + 2\sum_{k=1}^{m}\sum_{l=1}^{m}\sum_{j=1}^{n} a_k b_{1j} \rho_{uk} s_{1j} u_{k,\max} D_l(\omega_j, \zeta_j) + \\ \sum\sum\sum\sum b_{ki} b_{1j} \rho_{ski} s_{1j} D_k(\omega_i, \zeta_i) D_l(\omega_j, \zeta_j) \end{array} \right]^{1/2} \quad (8)$$

in which, the double sum represents the square of the pseudo-static response, the quadruple sum represents the square of the dynamic response, and the triple sum represents a coupling term between the pseudo-static and dynamic response that arises from the covariance between the two components.

Improved multi-support response spectrum (IMSRS) method

An improved multi-support response spectrum (IMSRS) method[7] is deduced by (X.Zhu and H.Liu, 2001) for the structural systems subjected to spatially varying seismic excitations. In the formula, only pseudo-static terms and dynamic terms are included, neglecting the cross contributions of the pseudo-static response and dynamic response and based on the spectral parameters defined by E.H.Zavoni, the analytical solution of those spectral parameters are worked out with the assumptions of the ideal white-noise model and the approximate square frequency transfer function model. The analytical solutions are adopted to analyze the seismic response of this long-span bridge, and the influences of the spatial vibration on the Wuhu bridge are discussed. The improved Multi-supported Response Spectrum (IMSRS) formula can show as following:

$$E[\max|z(t)] = \left[\begin{array}{c} \sum_{k=1}^{m}\sum_{l=1}^{m} a_k a_l \Theta_{kl} u_{k,\max} u_{l,\max} + \sum_{k=1}^{m}\sum_{l=1}^{m}\sum_{i=1}^{n} (\alpha_{kli}\Gamma_{0,k1i} + \beta_{k1i}\Gamma_{2,k1i}) D_k(\omega_j, \xi_j) D_l(\omega_j, \xi_j) - \\ \sum_{k=1}^{m}\sum_{l=1}^{m}\sum_{i=1}^{n} (\lambda_{kli}\Lambda_{l,k1i} + \chi_{k1i}\Lambda_{3,k1i}) D_k(\omega_i, \xi_i) D_l(\omega_j, \xi_j) \end{array} \right]^{1/2}$$

The results of the Wuhu bridge show that the IMSRS method with the analytical solutions of spectra parameters is more convenient and time saving than that of numerical computing, and it is reliable and feasible.

(1) The total seismic response of Wuhu Bridge by MSRS method and IMSRS method are in good agreement with each other. There are approximate analytical solutions in the IMSRS method, so it is simple, obvious and convenient (TABLE VIII).

TABLE VIII. TOTAL RESPONSE OF WUHU BRIDGE BY TWO METHODS

Items	$V_s = V_{app} = 200 m/s$				$V_s = V_{app} = 2000 m/s$			
	d_{l2}^{T} (cm)	d_{r2}^{T} (cm)	M_{l2}^{B} $(kn.m)$	M_{r2}^{B} $(kn.m)$	d_{l2}^{T} (cm)	d_{r2}^{T} (cm)	M_{l2}^{B} $(kn.m)$	M_{r2}^{B} $(kn.m)$
IMSRS	6.58	5.88	658807	490518	7.10	6.51	676021	538790
MSRS	6.34	5.71	700884	466811	6.59	6.06	717461	510590
Error(%)	3.65	2.89	-6.39	483	7.18	6.91	-6.13	5.23

(2) There are relative important influences on the moment response of Wuhu Bridge when the values of V_s and V_{app} are within 100m/s to 600m/s. If the values of V_s and V_{app} are very large, the influences of the 'wave passage' effect and the 'incoherence' effect can be neglected (Figure 6) .The first part of this response equation represents the components of pseudo static response, and the second part represents the components of dynamic response. It is concerned about the effects of 'local site' through the various exciting inputs.

(3) The effect of the 'local site' can enlarge or reduce the seismic response of Wuhu Bridge (TABLE IX). It is reliable to response the influence of the variety of local site for long-span bridge by the multi-supported excited response spectrum method. Fig. 6 shows the curves of the moment response at the bottom of the towers of Wuhu cable-stayed bridge with the varying V_s or V_{app}. Case 1: All the support motions are correlative, i.e. $\gamma_{kl}(i\omega)=1$; Case 2: Only wave passage effects are considered, i.e. $\alpha=0$; Case 3: Only incoherence effects are considered; Case 4: Both wave passage and incoherence effects are considered. The loval site effects are included in all the four cases.

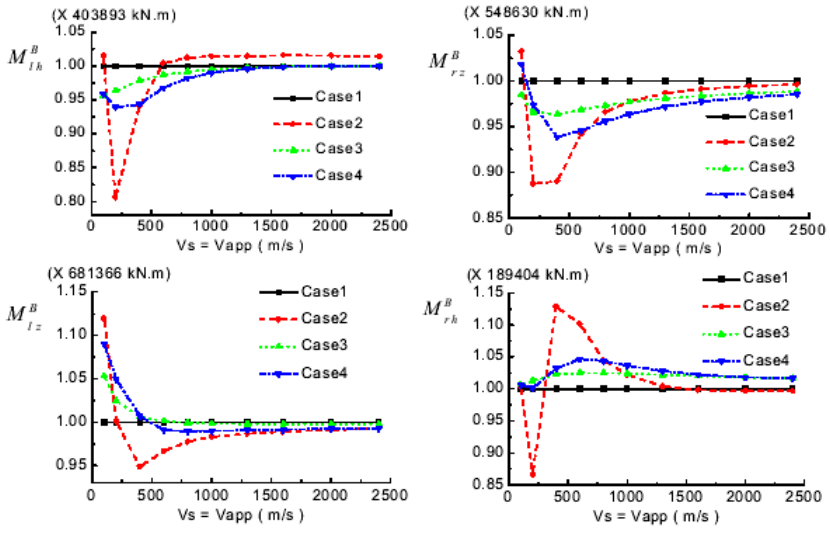

Figure 6. The curves of the moment response with the varying V_s or V_{app}

TABLE Ⅸ. LOCAL SITE EFFECTS OF DISPLACEMENT RESPONSE OF WUHU BRIDGE

Items	d_{lh}^{T} (cm)	d_{rh}^{T} (cm)	d_{h}^{M} (cm)	d_{lz}^{T} (cm)	d_{rz}^{T} (cm)	d_{z}^{M} (cm)	d_{v}^{M} (cm)
Multi-excites	8.91	3.26	9.18	7.29	6.68	6.70	6.47
Min-excites	3.10	3.09	4.27	3.30	3.35	3.32	2.14
Max-excites	9.10	9.07	12.53	11.84	12.04	11.90	8.18
Min/Multi	0.35	0.95	0.47	0.45	0.50	0.50	0.33
Max/Multi	1.02	2.78	1.36	1.65	1.80	1.78	1.26

CONCLUSION

Based on results of this study, the following conclusion were reached:

1. It is necessary that the effects of soil-pile-pier (pylon) interaction should be considered in seismic response analysis for long-span complex bridge with pile foundation. The thickness of the soft soil deposit is variable. Through the difference of deposit the variety response of ground motions is reached. The components of higher frequency will be attenuation and lower frequency will be amplification in the soft deposit layers. The response spectra of each cap slab of pile foundation are different.
2. The soil-pile-pylon interaction is possible and expedient to make these considerations into reality in SPM. The elastic constraints at the top of cap slabs are calculated by SPM for replacing pile foundation in WBM. It is convenient to calculate the response spectrum at the top of cap slabs by SPM. The envelope curves of those spectra are used as input spectra in WBM to evaluate the seismic response.
3. Comparing the results from the accumulated contribution ratio side and the seismic response side, the modes cut off at first 100 modes is better in mode superposition method for seismic response of Wuhu Bridge, to require the accumulated contribution ratio reached 0.9 is appreciate.
4. There are important influences on the long-span bridge subjected to multi-support excitations. An improved multi-support response spectrum (IMSRS) method is proposed for the structure systems subjected to spatially varying seismic excitations. The results are compared with that of the MSRS method. It is shown that the results produced by the two methods are well in agreement with each other, but the proposed method is reliable, feasible and timesaving.

ACKNOWLEDGMENT

This study was supported by the Railing Ministry of P. R. China, GRANT No.96G35©.This support is greatfully acknowledged. The authors wish to thank the Ph.D students Jianping Sun, Kehai Wang, Hongbing Liu and the colleges of the Major Bridge Engineering Bureau for their support in complete process of this project.

REFERENCES

Wiegel, r. l.(et al), 1970. *Earthquake Engineering (chapter 14)*. Prentice-Hall.

R. A. Imbsen, W. D. Liu, "Seismic performance evaluation of long-span bridges", Proceedings of seminar on new developments in earthquake ground motion estimation and implication for engineering design practice, ATC 35-1, March 1994.

Y. Nabamura, A. Derkiureghian, D. Liu, May 1993, "Multiple-support response spectrum analysis of the Golden Gate Bridge", Report No. UCB/EERC-93105.

A. K. Chopra, 1996. "Modal analysis of linear dynamic systems：Physical interpretation", *Journal of Structural Engineering, ASCE*, 122(5).

Transportation Ministry of P. R. China, 1990, *Aseismic Design Code of Highway Engineering,(in Chinese).*

Railway Ministry of P. R. China, 1988, *Aseismic Design Code of Railway Engineering,(in Chinese).*

X.Zhu, & H. Liu: "Seismic Analysis of Cable-stayed Bridge for Multi-supported Excitations", IABSE Conference (84), Seoul, Korean 2001.

H.Liu, X.Zhu, 2000. "Response srectrum analysis of long-span bridge for multi-supported seismic excitations", Proceeding of International Conference on Engineering and Technological Science, 2000, Sience Press, Beijing.

A Study on Shear Strengthening of Reinforced Concrete Beams Using ±45° Glass Fiber Reinforced Polymer

Jie Li[1],Yuan-de Xue[2] and Wen-xiao Li[3]

ABSTRACT

This paper focuses on the effects of fiber orientation and thickness on cracking and ultimate load, stiffness and deflection of the reinforced concrete beams which are strengthened using GFRP in ±45° direction with respect to the beam axis. Two series of the specimens consist of three simply supported beams and three simply supported beams with overhang. The research has presented that effective strain of the FRP is concerned with the FRP thickness and the failure mode varies with the quantities of the FRP. The validity of an anchorage method, using steel plate bonded with epoxy and fixed with bolt, has been verified. A reduced equation of shear strengthening has been put forward. From the analysis of the experimental results the following conclusions can be obtained: The ultimate load and ductility are greatly enhanced if the reinforced concrete beams are strengthened using GFRP in ±45° direction, the stiffness will increase and accordingly the deflection will decrease. It is obvious that the GFRP can effectively confine the diagonal cracking width. Due to the improvement of shear resistance of the reinforced concrete beam, the failure mode will be changed and the shear failure will translate into flexural mode. The more the GFRP quantities are, the less is the effective strain of GFRP. It is worth noting that good anchorage method must be considered in order to prevent FRP fabric from the peel failure, and the reduction of the ultimate capacity may be observed if the thickness of FRP increases.

[1] College of Civil Engineering, Tongji University, 200092,Shanghai, PRC

[2] State Key Laboratory of Concrete Materials Research, Educational Department Key Laboratory of Solid Mechanics, Tongji University, Shanghai 200092,PRC

[3]Department of Engineering Mechanics and Technology, Tongji University, Shanghai 200092,PRC

INTRODUCTION

In practical projects it is often addressed that reinforced concrete members are strengthened for enhancement of shearing resistance. Existing structures could exhibit insufficient shear-resist capacity due to the change of usage, the mistakes of the design or construction and the earthquake and so on. Besides the flexural failure mode may be changed into diagonal failure if the flexural strength increases because of bonding the FRP to the beam tensile region. Especially in seismic zone the strong shear resistance is expected to prevent from brittle failure. Therefore the research of shear retrofit is significant. Many researchers have extensively investigated the mechanism and effects of reinforced concrete beam shear strengthening with FRP composite. [1][2]。A serials of parameters, for example, load condition, support pattern, the ratio of span to depth, the ratio of shear span to depth, concrete strength, flexural reinforcement ratio, shear reinforcement ratio, nominal FRP reinforcement ratio, bond pattern, FRP thickness and orientation, modulus of elasticity, the anchor length, shear strength and thickness of adhesion agent, ultimate elongation and so forth, have effects on efficiency of shear strengthening. Amir M. et. al [3] have proposed a method of shear calculation for RC beam strengthened with FRP in different orientations when the beam have no cracking and have only vertical cracking. The results have a good agreement with those of finite element method and agree with the experimental results. Michael J. Chajes et. al[4] carried out shearing experiment of RC beam strengthened with graphite FRP in ±45° orientation. The shear capacity increased to 151.2%。However it is generally considered that the effects on cracking and ultimate capacity of RC beam strengthened with FRP in ±45° direction cannot be known clearly now. This paper presents a study on the above-mentioned issues and tends to provide experimental database to obtain a reduced equation of shear strength.

THE EXPERIMENTAL PROGRAM

The design of specimens

Two series of specimens are used in the experiment. Three simply supported beams and three simply supported beams with overhang are designated SBF SBF1 SBF2 and EBF EBF1 EBF2 respectively. The size and reinforcement are shown in Figure 1 and Figure 2. It should be noted that the T section simulates the action of floor and the cantilever region is considered the effects of positive and negative moment on the shear strengthening. FRP Composite can provided tension in ±45° direction because there may be three diagonal cracking on the beam with overhang. A steel plate of 6 mm thickness is placed at the upper side of the beam, which is bonded with adhesion agent and anchored by the bolts simultaneously. The thickness of the glass fiber fabric is 0.24 mm. The orientation of the fiber is braided in ±45°

direction. The adhesion agent TYFO produced in America is adopted in the test. All specimens are listed in table I and the concrete mix is shown in table II.

The sketch of test

The load is applied according to four-point flexural test. The location of the P1 and P2, shown in Figure 2, is adjusted so as to produce the same shear force at the two side of the support B. At the same time the shear capacity is designed equally at left and right sections of the support B. One or two hydraulic jacks reacting on a structural frame applied the loads. A steel I-beam distributed the load from the jack to two point load on the specimen.

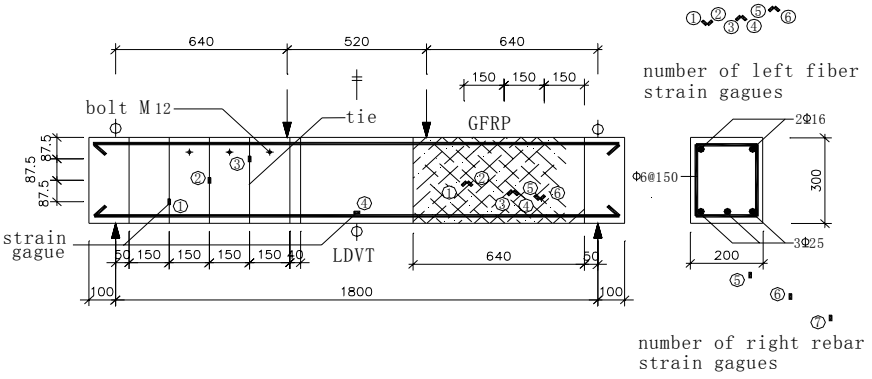

Figure 1. Specimens SBF SBF1 SBF2

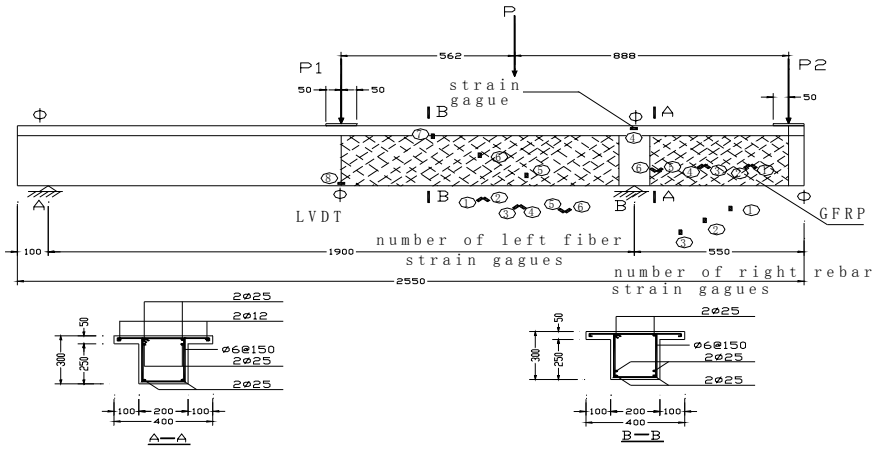

Figure 2. Specimens EBF EBF1 EBF2

The increment of load was 10 kN before cracking and 20 kN after cracking. If the width of cracking or peel of the FRP is obvious, the load was applied monotonically until failure. Test data were collected by a computer acquisition system.

TABLE I LIST OF THE SPECIMENS

specimens	Retrofit condition	The shear span to depth ratio	FRP reinforcement ratio	Transverse steel ratio	fcu (MPa)
SBF	Control	2.32	-	0.2%	40.98
SBF1	One layer		0.24%		40.98
SBF2	Two layers		0.48%		40.98
EBF	Control	1.82 cantilever 1.73 mid-span	-		46.85
EBF1	One layer		0.24%		46.85
EBF2	Two layers		0.48%		46.85

TABLE II CONCRETE MIX

Serial	Water	Cement	Sand	Aggregate	Fly-ash	Water reducer
No. 1	0.45	1	1.55	3.11	/	/
No. 2	0.500	1	1.526	2.380	0.167	0.012

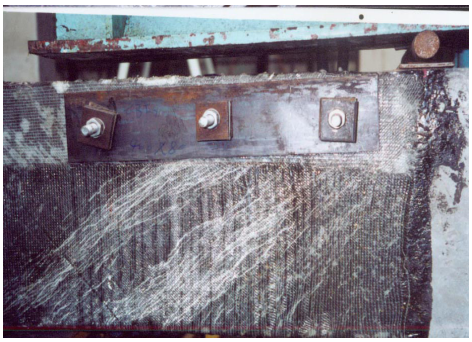

Figure 3 Diagonal white lines

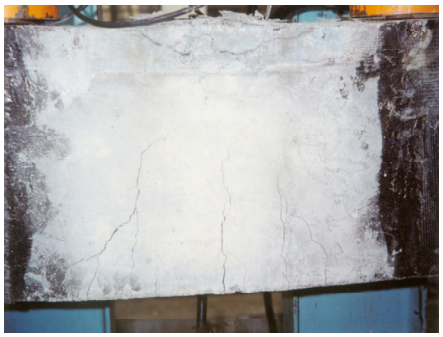

Figure 4 Flexural failure of SBF1

THE OBSERVED BEHAVIOR

Specimen SBF: When the load was applied to 140 kN the first flexural crack appeared at the soffit near the mid-span. The diagonal crack was observed firstly at the load of 150 KN, substantially several flexural cracks occurred. The diagonal cracks gradually increased in

intensity and depth. Critical diagonal crack formed and extended to the point of the load. Finally the crush of the concrete occurred in the shear-compression zone at the ultimate load 313 kN. The width of the major diagonal crack is approximately 2~3 mm., and the deflection is not apparent.

Specimen SBF1: Firstly flexural crack occurred at the mid-span when the load reached 160 kN. Several white lines under the FRP fabric, shown in figure 3, were found near the support at the load of 200 kN, which indicated that concrete had cracked. As the load increased the white lines developed and formed a white strip to location of the bolts. At the load of 429 kN the sound emitted from FRP could be heard and it may be considered that fiber would be peeled from the surface of concrete. Increasing the load to 573 kN the concrete in compression zone crushed, shown in figure 4, and the deflection at the mid-span was greatly obvious. Shear failure changed into bending failure. After the test, the FRP fabric was removed and fine shallow cracks were found on the surface of concrete, as shown in figure 5. Just only small parts of the white lines represented the cracks. There were no major diagonal cracks. And the width of crack is about 0.25 mm.

Specimen SBF2: Flexural and diagonal crack occurring are similar to the specimen SBF2.The deflection in the mid-span is apparent and concrete in compression crushed somewhat at the load 520 kN. Afterwards, the steel plate anchored in shear-compression zone seemed to peel from the concrete. When the load increased to 557 kN cracking was heard and concrete pieces were pull out seriously. The depth of failure was reached under the tie position. The bolts were also dragged out, shown in Figure 6.

Specimen EBF: Two diagonal cracks were shown in the middle of beam depth at the simple span when the load is 200 kN. At the load of 260 kN diagonal crack occurred at the cantilever region. The No. 6 rebar yielded when the load is 310 kN, and the diagonal crack width reached 5 mm. It is indicated that test beam failed in shear mode.

Specimen EBF1: As the load increased to 160 kN the diagonal crack appeared in the simple span where the concrete was not strengthened. White lines could be seen and cracking from the FRP be heard at the load 240 kN and 380 kN respectively. At the ultimate load of 580 kN the fabric adjacent to beam flange was peeled off. But it is regretful that data file which was acquired by computer failed when it is transformed into excel file. Fortunately the ultimate load and maximum fiber strain of No. 4 and No. 6 were recorded.

Specimen EBF2: Much phenomenon was similar to specimen EBF2. At the ultimate load of 529 kN FRP fabric was peeled from concrete near the flange.

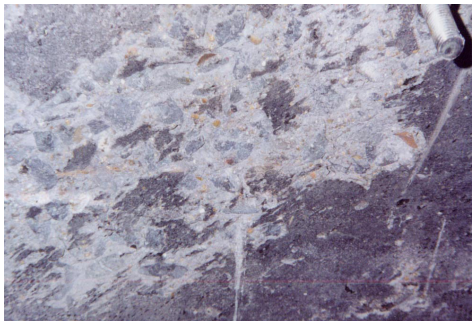

Figure 5 fine diagonal cracks

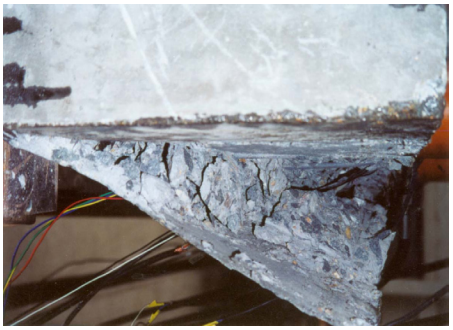

Figure 6 Concrete pieces of SBF2

EXPERIMENTAL RESULTS

Cracking and ultimate load

Accurate cracking load cannot be obtained due to cover of FRP fabric. The cracking load has not being enhanced significantly in terms of the deflection- load curve shown in Figure 7 and Figure 8.

However, the ultimate load increased greatly because the diagonal cracks were confined by FRP in $\pm 45^\circ$ direction. It is worth noting that the specimen SBF1 test indicated the failure mode was changed from shear to flexural pattern. The specimen SBF2 initially showed the tendency of flexural failure but finally failed in peel mode. It is thought that the enhancement of FRP thickness increases the stiffness of FRP, reduces the length of effective bond and adds the peel stress at the end of FRP fabric. If the peel failure is avoided the higher ultimate load would be expected with increasing the quantities of the FRP reinforcement.

Behavior of ductility

Seen from Figure 7 and Figure 8, the ductility of the beam, which was strengthened with FRP in shear, improves significantly. The ratio of SBF2 maximum deflection to that of SBF is 2.5. SBF1 ultimate deflection cannot be obtained due to loose installation of LVDTs, but it is estimated that the ultimate deflection is greater than that of SBF2 on the basis of test observation and the mode of flexural failure.

Analysis of the rebar stress

From figure 9, 10 and 11 it is seen that the rebar stress between the different specimens is almost the same before cracking. After cracking, the rebar strain of beam strengthened is smaller

than that of the beam not strengthened at the same load, especially the beam that was strengthened with two layers FRP fabrics. Hence GFRP can also reduce the rebar stress and share the external force in spite of low modulus of elasticity. Besides if peel failure can be avoided and anchor measurements are adopted suitably the shear strength can be improved greatly.

Fiber strain

Average fiber strains in principle stress direction at the ultimate load are shown as follow: SBF1 is 5865 $\mu\varepsilon$， SBF2 is 4232 $\mu\varepsilon$ and EBF2 is 3553 $\mu\varepsilon$. The strains measured are discrete because of random distribution and non-smoothness of fiber surface. The relationship between the effective strain and the thickness of the FRP will be further researched by experiments.

Measurement of anchor

The method using steel plate and bolt has the function for preventing FRP fabric from debonding. Experiment shows that anchorage function is more effective in rectangular section than T section. It is mentioned that although the steel plate provides another surface of bond to FRP fabric, there are some weak zones that is resulted from concentration of stress in concrete.

THEORETICAL ANALYSES

The summation method is approximately adopted in theoretical analysis for calculating the shear strength of beam. The shear capacity consists of three parts (concrete, rebar and FRP) and the equation is shown as follows:

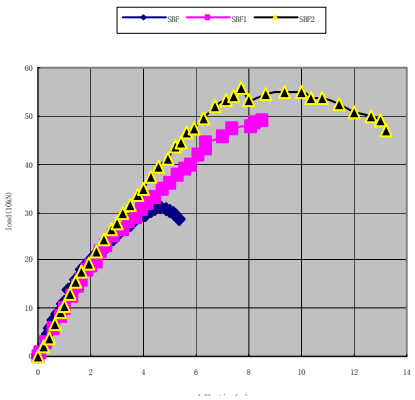

Figure 7 Deflection-load curve

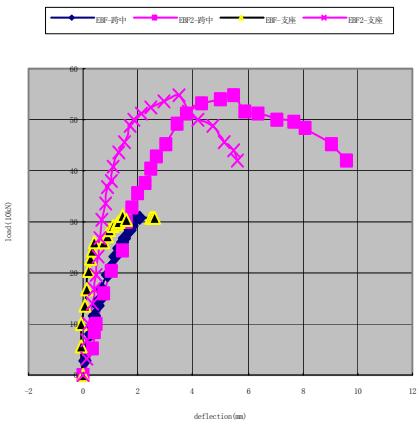

Figure 8 Deflection-load curve

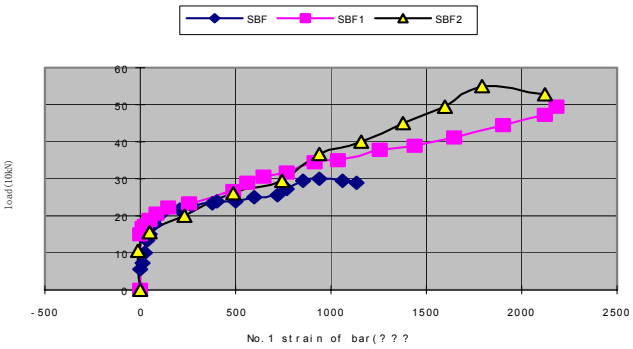

Figure 9 Strain-load curve

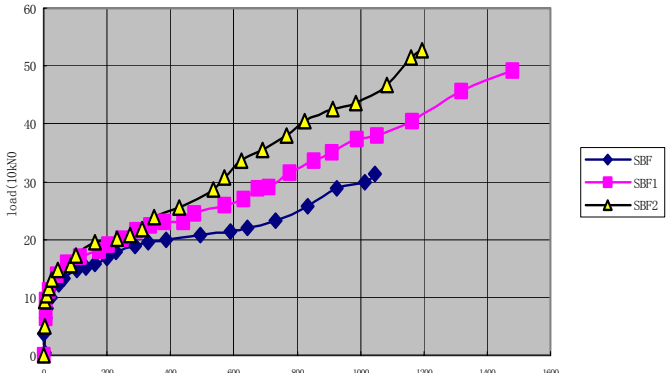

Figure 10 strain-load curve

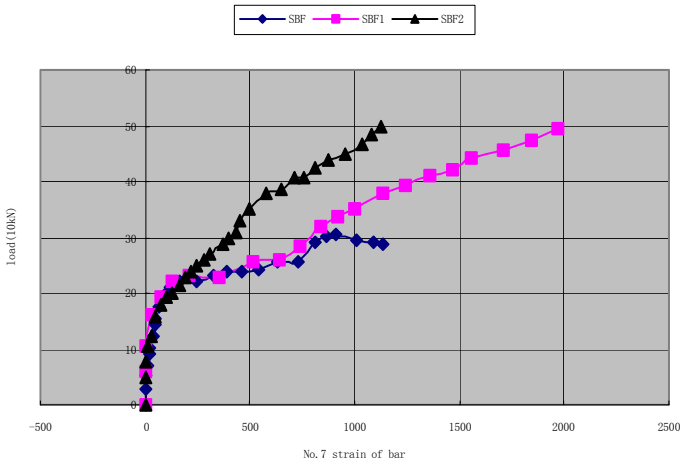

Figure 11 strain-load curve

$$V_u = V_c + V_s + V_f \tag{1}$$

where V_c, V_s and V_f are shear strength of concrete ,rebar and GFRP respectively. V_c, V_s are obtained according to current RC code, V_f can be calculated by the following equation:

$$V_f = \frac{A_f E_f \varepsilon_{fv} (\sin\alpha + \cos\alpha) h_f}{s_f} \tag{2}$$

where $A_f, E_f, \varepsilon_{fv}, h_f, S_f$ are area, the modulus of elasticity of elasticity, effective strain, depth and span of FRP respectively. The effective strains used in calculation obtain from test. The results are listed in table 3. It is worth mentioning that a great deal of aggregation may be exist because the diagonal cracks is constrained by fiber in $\pm 45°$ direction. Considering that the final failure mode is not governed by shear mode, of course, the theoretical results may be approximate. Therefore it is necessary that a suitable equation of shear peel strength should be established, in the view of point of possibility, especially when large amounts of FRP material are used.

TABLE III

Specimen	Experiment KN	Theory KN	Experiment/ Theory	Increment	Failure mode
SBF	313	281	1.11	-	Shear
SBF1	573	456	1.26	1.83	flexural
SBF2	557	528	1.05	1.78	peel
EBF	310	329	0.94	-	Shear
EBF1	580	lost	lost	1.87	peel
EBF2	529	608	0.87	1.71	peel

CONCLUSIONS

（1）If the RC beam is strengthened with GFRP in $\pm 45°$ direction for purpose of shear resistance, the shear strength and stiffness will be increased significantly.

（2）The ultimate deformation and the ductility of the RC beam can be enhanced if using GFRP in $\pm 45°$ direction to retrofit.

（3）The diagonal cracks are constrained effectively by fiber in $\pm 45°$ direction, and the depth and width of cracks can be reduced.

（4）After cracking glass fiber can share the stress of rebar obviously, the more the quantities are, the better the effect is.

（5）The effective strain of GFRP will decrease with increasing GFRP quantities.

ACKNOWLEDGEMENT

Financial support for this study was provided by 863 project No. 2001AA33610

REFERENCES

QuanWang Li , ShuHong Zhao, LiePing Yie, The Experimental Study of Reinforced Concrete Beam Strengthened with CFRP. Proceeding of the first China FRP-concrete structure symposium 2000:242-246

YueXuan Zhang, YuanDe Xue Shear Behavior Research of Concrete-Filled FRP Tubes. Proceeding of the first China FRP-concrete structure symposium 2000:138-145

Amir M.Malek, Hamid Saadatmanesh. Analytical Study of Reinforced Concrete Beams strengthened With Web-Bonded Fiber Reinforced Plastic Plates or Fabrics. ACI Structural Journal. May-June 1998:343-352

Michael J. Chajes, Ted F. Januszka, Dennis R.Mertz .Shear Strengthening of Reinforced Concrete Beams Using Externally Applied Composite Fabrics. ACI Structural Journal. May-June 1995.

Research on Flexural Properties of Hybrid GFRP/CFRP Tube Confined Concrete Beams

Hua Yuan[1],Yuan-de Xue[2] and Wen-xiao Li[3]

ABSTRACT

This paper reports a study on flexural properties of hybrid beams which consist of concrete-filled $\pm 45^{o}$ glass filament-wound FRP square tube with carbon FRP laminates bonded to its tensile side. In order to optimize the utility of characteristic mechanical properties of each element materials, the material and structure designs of that beams are base on such a rule that carbon composite is mainly arranged for bearing tension, confined concrete for compression and $\pm 45^{o}$ plies glass-fiber composite for shear. The constitutive relations of FRP and confined concrete under compression are obtained experimentally and Vecchio and Collins' tensile model of confined concrete is used. The flexural behaviors of beams, which have different hybrid structures, were studied through four-point bending tests. The result shows the synergetic effect of the combination of composite and concrete.

INTRODUCTION

Recently, the usage of fiber-reinforced composites combined with traditional materials in primary structural applications has emerged as one of the most promising developments in the construction industry due to corrosion problems. Diverse concrete-filled FRP tubes (CFFT) are studied for beams. A number of studies about his paper presents a study on a hybrid beam consisted of concrete filled $\pm 45^{o}$ glass filament-wound FRP tube with a carbon FRP laminate bonded to its tension side.

The most common characteristics of combined beams are follows: 1). The designable system allows optimization based on material properties of each component and the state of load carrying. 2) The CFFT replaces conventional reinforcing steel. The enhanced behavior of CFFT

[1] State Key Laboratory of Concrete Materials Research, Tongji University, 200092, Shanghai, PRC

[2] State Key Laboratory of Concrete Materials Research, Educational Department Key Laboratory of Solid Mechanics, Tongji University, shanghai 200092, PRC

[3]Department of Engineering Mechanics and Technology, Tongji University, Shanghai 200092, PRC

beams could allow the use of smaller sections than those which would be required for conventionally reinforced concrete beams . It also increases durability while providing enhanced confinement to the concrete core. 3) FRP shape acts as permanent form for concrete. It greatly enhances ease of handling and erection speeds. Furthermore, FRP jacket reinforced concrete would be more durable than conventional reinforced concrete beam and therefore would require less maintenance and have longer service life. Overall cost is lower.

In 2000, Mirmiran and Shahawy[1] tested round concrete filled 356-mm-diameter and 6.6-mm-wall thickness GFRP winding tube by a series of four point bending tests. Karbhari et al pursued the experimental characterization of the concrete filled carbon shell for girder on short and medium span bridge. The carbon shell geometry used in all the test units of the experimental program is that of a cylindrical tube with an inside diameter of 343 mm and a wall thickness of 10 mm. The carbon/epoxy laminated shell has a lay-up architecture with approximately 80% longitudinal ($\pm 10^o$ helical) and 20% transverse (90^o) fiber reinforcement with an average fiber volume ratio of 55%. In this paper, a novel concrete filled square hybrid GFRP/CFRP tube is studied. The constitutive relations are set up. Applicability of the constitutive relations to hybrid beam is examined.

Experimental analyses on concrete filled hybrid GFRP/CFRP tube beams

Hybrid GFRP/CFRP tube confined concrete beam, shown in Fig. 1, consists of concrete filled $\pm 45^o$ glass fiber winding FRP tube with a thin carbon fiber laminate bonded to its tension side. The thick of GFRP is 2.7 mm and the nominal thick of CFRP 0.11 mm.

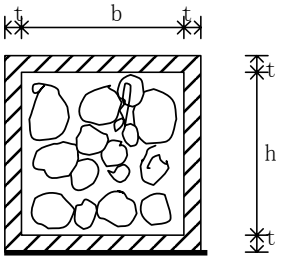

Figure 1 The cross-sectional shape of hybrid GFRP/CFRP tube confined concrete beam

where h=b=50mm; Concrete E_c=28GPa; Carbon fiber E=210 GPa;

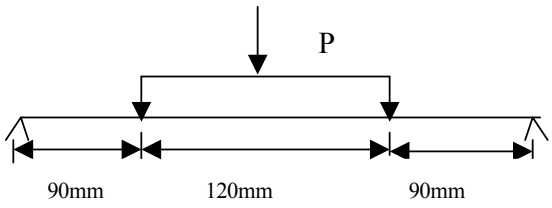

Figure 2. The schematic of beam test setup

The specimens were subjected a four-point flexure tests, the schematic of beam test setup shown in Figure 2. The result of test are shown in Figure 3 and Figure 4.

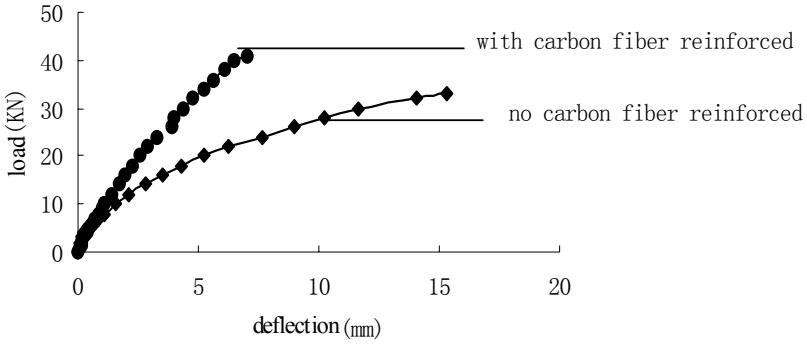

Figure 3. load – deflection diagram

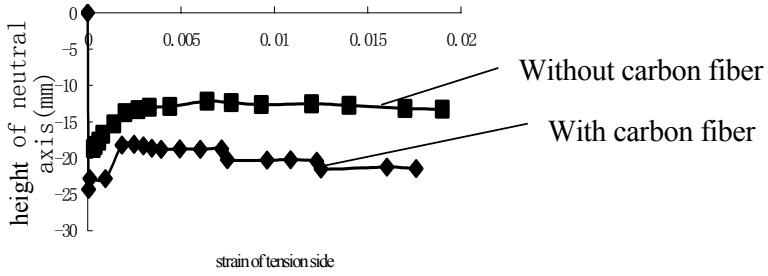

Figure 4 Strain of tension side –height of neutral axis diagram

As shown in Figure 3 and Figure 4, it was noted that when the thick of the GFRP tubes is same, the limit load of the member with carbon fiber reinforced is as 1.2 times as that with no carbon fiber reinforced. The failure bending moment increased from 1.485KN• m to 1.827 KN• m. At the same time, the neutral axis transfers to the tension side due to contribution of carbon fiber. Figure 5 and Figure 6 show the failure of the members.

Figure 5. Picture of concrete filled GFRP tube after failure

Figure 6 Picture of concrete filled hybrid GFRP/CFRP tube after failure

THE CALCULATION MODELS

Tensile model of GFRP

Three slices, dimensions shown in TABLEI, intercepted from a hollow GFRP tube are tested. The specimens after failure are in figure 7

TABLE I DIMENSION OF SPECIMENS

Number	1	2	3
Width (mm)	1.144	1.1964	1.1672
Thickness (mm)	0.1136	0.1184	0.098

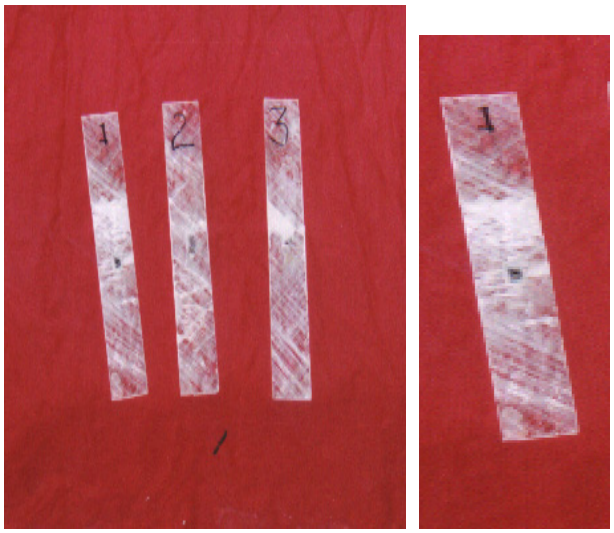

Figure 7 specimens after failure

In order to simplify calculation, the results of test are fitted to get the curve (Figure 8) and Eqn.1.

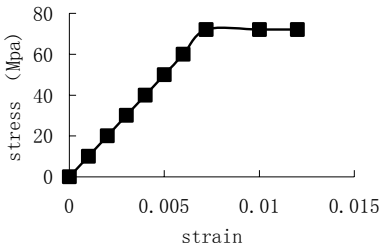

Figure 8 curve of FRP tensile stress-strain

$$\sigma_{FRP} = \begin{cases} 10000\ \varepsilon_{FRP}\ (\text{MPa}) & \varepsilon_{FRP} \le 0.0072 \\ 72\ (\text{MPa}) & \varepsilon_{FRP} > 0.0072 \end{cases} \quad (1)$$

Compressive model of GFRP

Two tubes about 80mm high (dimension shown in TABLE II) intercepted from hollow GFRP are tested. The specimens after failure are shown in Figure 9.

Figure 9 specimens after failure

TABLE II DIMENSION OF SPECIMENS

Number	1	2
Width (mm)	5.325	5.340
Thickness (mm)	0.134	0.136
Height (mm)	80.1	80.5

The results of test are fitted to obtain Figure 10 and Eqn. 2.

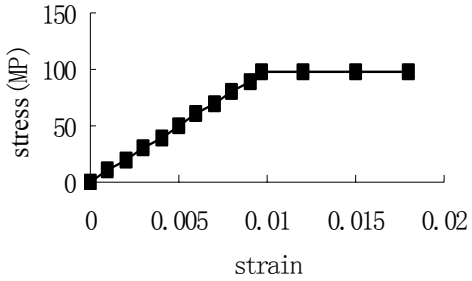

Figure 10 Curve of FRP compressive stress-strain

$$\sigma_{FRP} = \begin{cases} 10000\ \varepsilon_{FRP}\ (\text{MPa}) & \varepsilon_{FRP} \le 0.0097 \\ 97\ (\text{MPa}) & \varepsilon_{FRP} > 0.0097 \end{cases} \quad (2)$$

Tensile model of CFRP

CFRP was bonded to the tension side of a beam in order to bear tensile stress, so carbon fiber was laid parallel to the axis of the beam. Because the thickness of CFRP is much smaller than that of GFRP and dimension of the beam, the strain of the CFRP is thought equal to tension side of GFRP. In calculation stress equals to modulus of elasticity multiplied by strain, namely $\sigma = 2.1 \times 10^5\ \varepsilon_{FRP}$ MPa, while the elastic modulus of carbon.is2.1×10^5 MPa

Compressive model of confined concrete

According to design guidelines in our country, the constitutive relation of concrete in compressive section is shown as Figure.

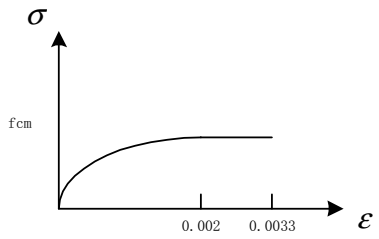

Figure 11 $\sigma - \varepsilon$ diagram of compressive concrete

If $0 < \varepsilon < 0.002$,

$$\sigma = f_{cm}\left[1 - (1 - \varepsilon / \varepsilon_0)^2\right] \quad (3)$$

If $0.002 < \varepsilon < 0.0033$,

$$\sigma = f_{cm} \quad (4)$$

where f_{cm} :flexural strength of concrete； ε_0： yield strain

According to Amir Mirmiran[12] et. al's research , strength of concrete will improve when it is confined. Magnifying coefficient is given by test.

Two blocks of same height were cut from a beam. One block was shucked off FRP. (The dimensions are shown in TABLE III). Two blocks were tested under compression. The results are shown in Figure 12.and the specimens after failure are shown in figure 3

TABLE III DIMENSION OF SPECIMENS

Plain concrete block		FRP confined concrete block		
Height (mm)	Side (mm)	Height (mm)	Side (mm)	Thick of FRP tube (mm)
76.0	52.5	76.0	57.82	2.66

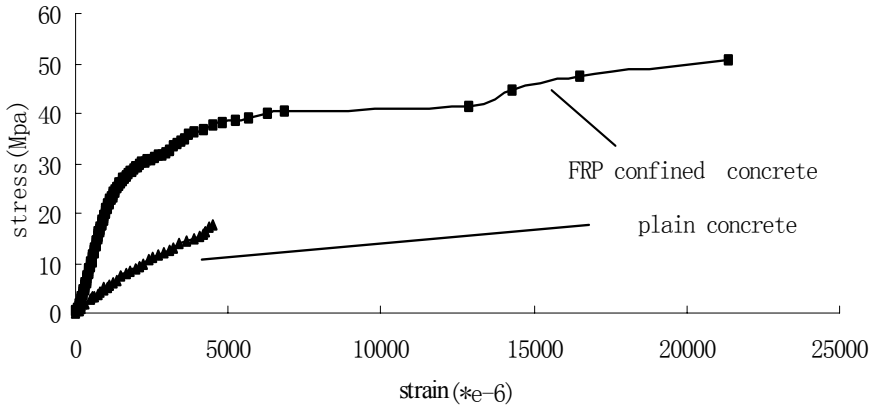

Fig. 12 Curve of stress-strain of plain concrete and FRP confined concrete in compression

According to the test, compressive strength of FRP confined concrete is much higher than that of plain concrete. The ratio of two failure stresses is 2.5.

Figure 13 Specimens after failure

According to Amir Mirmiran[13]and Xue Yuande et al[6]´s researches, and the manuscript of Technology Code of Fiber Reinforced Composite Strengthening Concrete Structure, a calculation equation was put forward:

$$N_u = \alpha_1 \left[\left(f_c + 8 r_1 \frac{E_f \varepsilon_{cf} n t_f}{h} \right) A_c + A_s' f_y' \right] \tag{5}$$

where: N_u —carrying load of strengthened member;

α_1 —Strength coefficient, according to regulations (GBJ10),taken 0.9;

f_c —Compressive strength of concrete core;

r_1 —Strength of concrete effecting coefficient $r_1 = 0.8 + \frac{60 - c}{150}$;

c —Strength grade of concrete;

E_f —Elastic modulus of fabric, taken elastic modulus of FRP tube;

ε_{cf} —Permitting strain of fabric under compression. According to the test, take longitudinal strain 0.004488 as permitting strain. Permitting strain of fabric under compression is 0.004488× 0.48=0.0021 due to Poisson's ratio of $\pm 45^{\circ}$ winding FRP tube is 0.48

n —Layers of fabric;

t_f —Thickness of single layer of fabric;

h —Side of member section;

A_c —Area of concrete section;

A_c' —Area of steel section. It is 0 in this paper;

f_y' —Compressive strength of steel. It is 0 in this paper;

When t_f=1.65mm, reinforcement ratio is 1.36 on calculation. The value is smaller than that obtained from test. 1.36 is adopted in this paper on account of safety. Compressive model of confined concrete is shown in Fig. 14.

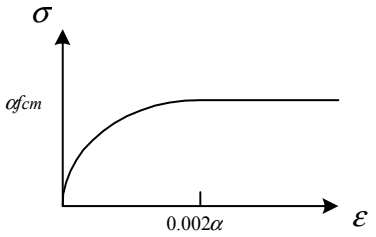

Figure 14 curve of concrete $\sigma - \varepsilon$ under compression

When $0 < \varepsilon < 0.002\alpha$, $\sigma = \alpha f_{cm}\left[1 - (1 - \varepsilon/\varepsilon_0)^2\right]$ (6)

When $\varepsilon > 0.002\alpha$, $\sigma = \alpha f_{cm}$ (7)

Where: α : compressive reinforcing coefficient of confined concrete

f_{cm} : flexural compressive strength of concrete

Tensile model of confined concrete

According to guidelines, concrete in tension section does not work after crack, so carrying load capacity of concrete in tension section usually is neglected.

But according to Amir Mirmiran、Vecchio and Collins [14], FRP Confined concrete in tension section works all the time. The result is also proved in our test.

The model Vecchio and Collins[14]obtained is used in this paper. It is shown in Figure14.

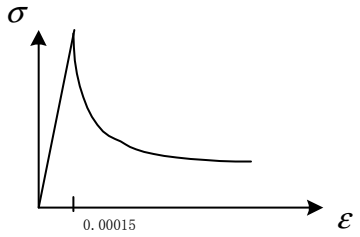

Figure 15 Tensile $\sigma - \varepsilon$ of confined concrete diagram

When $0 < \varepsilon < 0.00015$ 时 , $\sigma = E_c \times \varepsilon$ (8)

When $\varepsilon > 0.00015$ 时, $\sigma = \frac{\beta f_{cr}}{1 + \sqrt{200\ \varepsilon}}$ (9)

Where：E_c elastic modulus of concrete；

f_{cr} : Crack stress of concrete；

β : Reinforcing coefficient of concrete under tension（β=1 in order for safety）

CALCULATING CARRYING LOAD OF HYBRID GFRP/CFRP TUBE CONFINED CONCRETE BEAM

Specimen is same as above

Assumption of calculation

1. Plane sections remain plane and normal to the neutral axis after bending.
2. Perfect bond exists between concrete and the FRP tube.
3. The constitutive relations above are suitable to the calculation.

Calculating program frame

Figure 16 shows the Calculating program frame.

Result analysis

Moments in different strains are shown in table IV by test and calculation respectively. From the table IV, it is found that the results tested are close to but not equal to that calculated. The main reasons are:(1)there are perhaps some errors using nominal thick of the carbon fiber instead of real thick of CFRP in calculation .(2) Carbon fiber is controlled in elastic range in practical use. When elastic model is used, there is bigger error in state of larger strain than smaller strain.

TABLE IV COMPARISON THE RESULT WITH THAT OF CALCULATION

Item		Result of test	Result of calculation
moment/KN.m	ε =0.0075	0.810	0.790
	ε =0.014	1.305	1.049
	ε =0.0176	1.485	1.16

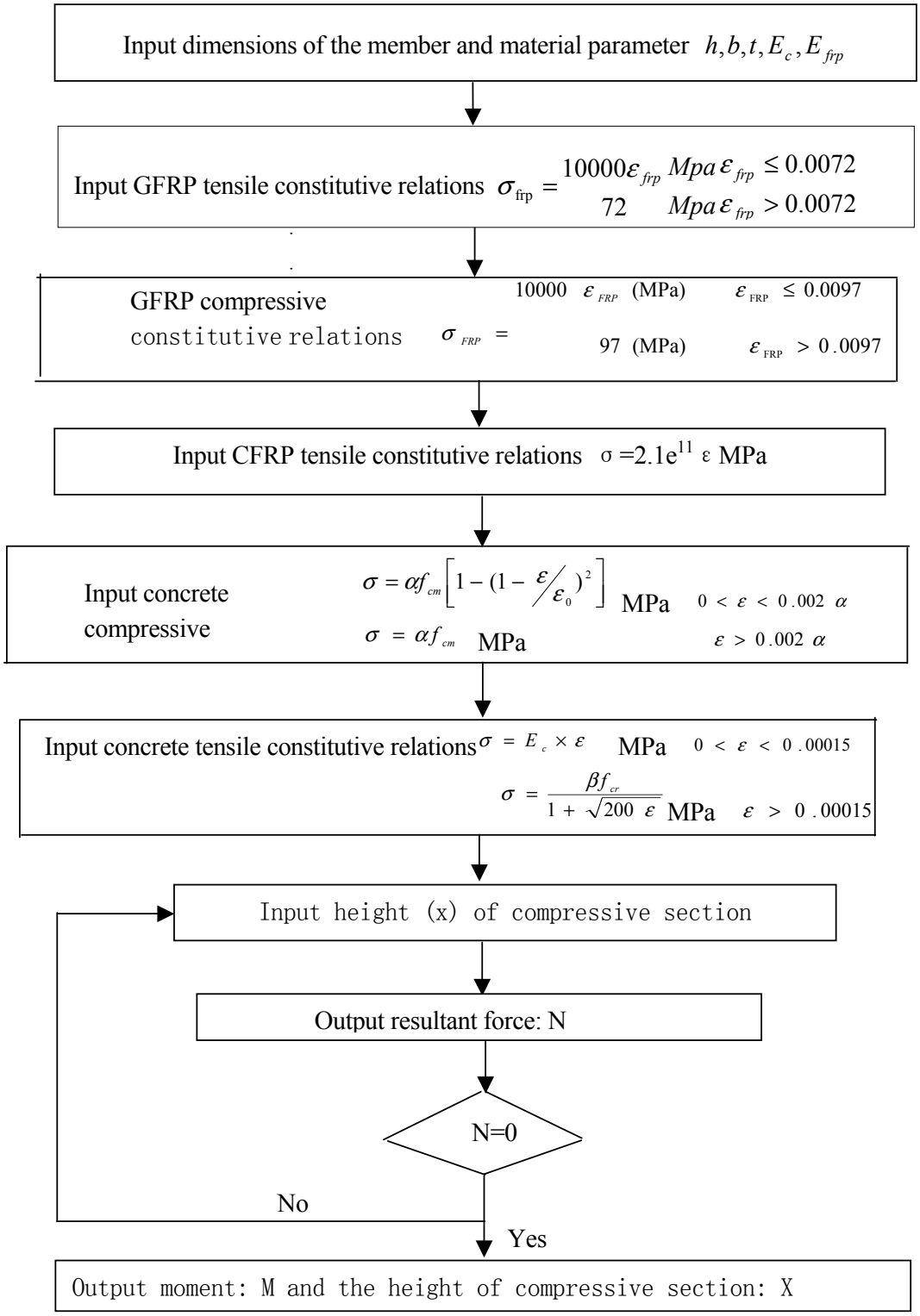

Figure 16 FRP confined concrete beam calculating program frame

CONCLUSION

1. Hybrid beams were designed, manufactured and tested. This innovative design produces highly optimized behavior with a pronounced synergetic effect. In hybrid beam, carbon composite works in tension, concrete filling works mainly in compression and $\pm 45^{o}$ glass fiber composite works in shear
2. The numerical model used for this analysis was implemented. This model predicts with reasonable accuracy the moments. This model is still in progress.

ACKNOWLEDGEMENT

Financial support for this study was provided by 863 projects No.2001AA33610

REFERENCES

Amir Mirmiran, et al. Large Beam-column Tests on Concrete-Filled Composite Tubes [A]. ACI Structural Journal, 2000,97(2):268-276

Karbhari V M, Seible F, et al. Structural characterization of fiber-reinforced composite short-and medium-span bridge system [J]. Applied Composite Materials, 2000, (7): 151-182

Zhao J study on FRP confined concrete [D]. Shanghai: Department of Engineering Mechanics and Technology, Tongji University, 1997.

Zhao J and Xue Y D. Primary Research on FRP Tube Confined Concrete [A]. Proceedings of the 12th Glass fiber Reinforced Plastics/Composite[C] , Qindao: Glassfiber reinforced plastics/composite agent,1997:232-237.

Xue Y D, Zhao, J. Primary Research on FRP Confined Concrete[A]. Proceedings of International Conference of the Mechanical Test on Material and Structure[C], Hongkong, 1998: 274-278

Zhang Y X. Study on property of FRP confined concrete [D]. Shanghai: Department of Engineering Mechanics and Technology, Tongji University 2000.

Zhang Y X, Xue Y D. The basic property of FRP tube confined concrete [A] ，Glassfiber reinforced plastics/composite, 1999,6:21-23

Xue Y D, Zhang Y X. Study on shear property of FRP tube confined concrete [A], Proceedings of the 1st Chinese Academic Conference of FRP/Concrete Structure [C], Beijing. 2000,6:138-145

Yuan H, Xue Y D. Study on basic property of FRP tube confined concrete [J]. Concrete and cement products,2000(6):34-36.

Fan L.C, Zhuo W. D, Xue Y. D., Research on Seismic Property of FRP Jacket RC pier [A], Proceedings of the 1st Chinese Academic Conference of FRP / Concrete Structure [C], Beijing. 2000,6:113-117.

Xue Y D, Yuan H ,et al. Fiber reinforced polymer confined concrete combined component [J].journal of building materials,2002,1:1-8.

Amir Mirmiran，Mohsen Shahawy and Michael Samaan . Strength and Ductility of Hybrid FRP-Concrete Beam-Columns [J] ，Journal of Structural Engineering, 1999; 10

Amir Mirmiran, Mohsen Shahawy. Effect of Column Parameters on FRP-Confined Concrete [J]. Journal of Composites for Construction, 1998, 175-185.

Vecchi F J and Collins M P. The modified compression-field theory for reinforced concrete elements subjected to shear [J]. ACI Structural Journal, 1998, (3-4): 219-185

PRC-US Workshop Agenda

October 8, AM: Four invited papers (30 minutes for each)

9:00-9:10: Opening speech
9:10-10:10: Two papers
1. Brief introduction of the study trends of SLDRCE, *by Li-chu Fan*
2. Performance-based seismic design of highway systems, *by Ian G. Buckle*

10:10-10:30: *Coffee break*
10:30-11:30: Two papers
3. Mitigate earthquake hazard & risk for highway bridges through planning, design and retrofitting (extended abstract), *by W. Phillip Yen*
4. Seismic safety evaluation of large scale interchange system in Shanghai, introduced by *Li-chu Fan,* and presented by *Li-ying Nie*

October 8, PM: Seven papers (20 minutes for each)

2:30-3:50: Four papers
5. A new approach to analysis of soil-pile-structure interactions for long-span bridges, *by Jamshid Ghaboussi*
6. Preliminary study of hydrodynamic effects on seismic response of bridges, *by Jun-jie wang*
7. Observed pile and pipeline performance in the full-scale lateral spread experiment, *by Scott A. Ashford*
8. Seismic response of railway bridges considering track restriction, *by Gui-ping Yan*

3:50-4:10: *Coffee break*
4:10-5:10: Three papers
9. Seismic design and retrofit guidelines for bridges in New Jersey, a low-to-moderate seismic hazard area, *by H.A. Capers*
10. Generation of response spectrum compatible non-stationary ground motions based on phase difference spectra, *by Qing-shan Yang*
11. The seismic retrofit of the Golden Gate Bridge, *by Charles Seim, P.E.*

5:10-6:00: *Visit to SLDRCE* (wind tunnel, bridge laboratory and shaking table)

October 8, Evening, **20:00:** ***Reception*** (Radission hotel)

October 9, AM: Seven papers(20 minutes for each)

9:00-10:20: Four papers
12. Response of seismic isolated bridges using M-DOF model and 2D excitation, *by G.C. Lee*
13. Aseismic conceptual design of bridge tower of long-span cable-stayed bridges, *by Ai-jun Ye*
14. Analytical investigation of the response of LuPu bridge with added viscous dampers, *by Shi-de Hu*
15. Seismic performance and retrofit of a 24-span freeway bridge, *by M. Saiidi*

10:20-10:40: *Coffee break*
10:40-11:40: Three papers

16. A study on shear strengthening of reinforced concrete beams using ±45º glass fiber reinforced polymer, *by Yuan-de Xue*
17. Seismic design and analysis for urban viaducts with a double deck, *by Jian-zhong Li*
18. A pseudodynamic test of an urban viaduct with a double-deck, *by Tian-bo Peng*

October 9, PM: Two invited papers (30 minutes for each) plus summary and recommendations for future research

2:30-3:30: Two invited papers

19. Seismic design and retrofit strategies of cable-supported bridge: An overview of current practice, introduced *by G.C. Lee,* presented *by J. Sun*
20. Seismic response analysis of Wuhu Yangtze River Bridge, *by Xi zhu*

3:30-3:50: *Coffee break*

3:50-5:20: Summary and recommendations for future research (8th floor of new bridge building)

October 9, Evening, 19:00: ***Banquet*** (Radisson hotel)

October 10: Technical tour to Lupu bridge and sightseeing in Shanghai

Participants

U.S. Participants

Scott A. Ashford
Department of Structural Engineering
University of California, San Diego
La Jolla, CA 92093-0085
sashford@ucsd.edu

Ian G. Buckle
Department of Civil Engineering
MS 258
University of Nevada, Reno
Reno, NV 89557
igbuckle@unr.edu

Harry Allen Capers
Structural Engineering (State Bridge Engineer)
New Jersey Department of Transportation
PO Box 615
Trenton, New Jersey 08625-0615
harry.capers@dot.state.nj.us

Jamshid Ghaboussi
Department of Civil and Environmental Engineering
University of Illinois at Urbana-Champaign
Urbana, IL 61801

George C. Lee
MCEER
University of Buffalo
Red Jacket Quad
Buffalo, NY 14261 **gclee@acsu.buffalo.edu**

M.Saiidi
Civil Engineering Department
University of Nevada, Reno
Reno, NV 89557
saiidi@unr.edu

Charles Seim, P.E.
T.Y.Lin International
825 Battery St.
San Francisco, CA., 94111
cseim@tylin.com

John Sun
T.Y.Lin International
825 Battery St.
San Francisco, CA., 94111
isun@tylin.com

Jane Stoyle
MCEER
University of Buffalo
Red Jacket Quad
Buffalo, NY 14261
jestoyle@mceermail.buffalo.edu

W. Phillip Yen
Office of Infrastructure, R&D Federal Highway Administration
6300 Georgetown,Pike
McLean, VA 20121
wen-huei.Yen@fhwa.dot.gov

PRC Participants

Suwen Chen
College of Civil Enginering
Tongji University
Shanghai,China
Current address:
MCEER
University of Buffalo
Red Jacket Quad
Buffalo, NY 14261
sc75@buffalo.edu

Lichu Fan
Department of Bridge Engineering
Tongji University
Siping Road, 1239#,
200092, Shanghai, China
Lcfan@mail.tongji.edu.cn

Shidi Hu
Department of Bridge Engineering
Tongji University
Siping Road, 1239#,
200092, Shanghai, China
Hushidec@online.sh.cn

Jianzhong Li
Department of Bridge Engineering
Tongji University
Siping Road, 1239#,
200092, Shanghai, China
lijianzh@mail.tongji.edu.cn

Liying Nie
Department of Bridge Engineering
Tongji University
Siping Road, 1239#,
200092, Shanghai, China
nly1972@163.com,nly1972@etang.com

Tianbo Peng
Department of Bridge Engineering
Tongji University
Siping Road, 1239#,
200092, Shanghai, China
ptbsy@163.com

Junjie Wang
Department of Bridge Engineering
Tongji University
Siping Road, 1239#,
200092, Shanghai, China
jjwang@mail.tongji.edu.cn

Zhiqiang Wang
Department of Bridge Engineering
Tongji University
Siping Road, 1239#,
200092, Shanghai, China
wangzhiq@mail.tongji.edu.cn

Yan Xu
Department of Bridge Engineering
Tongji University
Siping Road, 1239#,
200092, Shanghai, China
Helen_xyz@163.com

Guiping Yan
College of Engineering and Architecture
Northern Jiaotong University
Bejing,100044,PRC
gpyanql101@hotmail.com

Qingshan Yang
College of Engineering and Architecture
Northern Jiaotong University
Bejing,100044,PRC
qshyang6620@sina.com

Aijun Ye
Department of Bridge Engineering
Tongji University
Siping Road, 1239#,
200092, Shanghai, China
yeaijun@mail.tongji.edu.cn

Xi Zhu
College of Engineering and Architecture
Northern Jiaotong University
Bejing,100044,PRC
hjw2003@sina.com

Multidisciplinary Center for Earthquake Engineering Research
List of Technical Reports

The Multidisciplinary Center for Earthquake Engineering Research (MCEER) publishes technical reports on a variety of subjects related to earthquake engineering written by authors funded through MCEER. These reports are available from both MCEER Publications and the National Technical Information Service (NTIS). Requests for reports should be directed to MCEER Publications, Multidisciplinary Center for Earthquake Engineering Research, State University of New York at Buffalo, Red Jacket Quadrangle, Buffalo, New York 14261. Reports can also be requested through NTIS, 5285 Port Royal Road, Springfield, Virginia 22161. NTIS accession numbers are shown in parenthesis, if available.

NCEER-87-0001 "First-Year Program in Research, Education and Technology Transfer," 3/5/87, (PB88-134275, A04, MF-A01).

NCEER-87-0002 "Experimental Evaluation of Instantaneous Optimal Algorithms for Structural Control," by R.C. Lin, T.T. Soong and A.M. Reinhorn, 4/20/87, (PB88-134341, A04, MF-A01).

NCEER-87-0003 "Experimentation Using the Earthquake Simulation Facilities at University at Buffalo," by A.M. Reinhorn and R.L. Ketter, to be published.

NCEER-87-0004 "The System Characteristics and Performance of a Shaking Table," by J.S. Hwang, K.C. Chang and G.C. Lee, 6/1/87, (PB88-134259, A03, MF-A01). This report is available only through NTIS (see address given above).

NCEER-87-0005 "A Finite Element Formulation for Nonlinear Viscoplastic Material Using a Q Model," by O. Gyebi and G. Dasgupta, 11/2/87, (PB88-213764, A08, MF-A01).

NCEER-87-0006 "Symbolic Manipulation Program (SMP) - Algebraic Codes for Two and Three Dimensional Finite Element Formulations," by X. Lee and G. Dasgupta, 11/9/87, (PB88-218522, A05, MF-A01).

NCEER-87-0007 "Instantaneous Optimal Control Laws for Tall Buildings Under Seismic Excitations," by J.N. Yang, A. Akbarpour and P. Ghaemmaghami, 6/10/87, (PB88-134333, A06, MF-A01). This report is only available through NTIS (see address given above).

NCEER-87-0008 "IDARC: Inelastic Damage Analysis of Reinforced Concrete Frame - Shear-Wall Structures," by Y.J. Park, A.M. Reinhorn and S.K. Kunnath, 7/20/87, (PB88-134325, A09, MF-A01). This report is only available through NTIS (see address given above).

NCEER-87-0009 "Liquefaction Potential for New York State: A Preliminary Report on Sites in Manhattan and Buffalo," by M. Budhu, V. Vijayakumar, R.F. Giese and L. Baumgras, 8/31/87, (PB88-163704, A03, MF-A01). This report is available only through NTIS (see address given above).

NCEER-87-0010 "Vertical and Torsional Vibration of Foundations in Inhomogeneous Media," by A.S. Veletsos and K.W. Dotson, 6/1/87, (PB88-134291, A03, MF-A01). This report is only available through NTIS (see address given above).

NCEER-87-0011 "Seismic Probabilistic Risk Assessment and Seismic Margins Studies for Nuclear Power Plants," by Howard H.M. Hwang, 6/15/87, (PB88-134267, A03, MF-A01). This report is only available through NTIS (see address given above).

NCEER-87-0012 "Parametric Studies of Frequency Response of Secondary Systems Under Ground-Acceleration Excitations," by Y. Yong and Y.K. Lin, 6/10/87, (PB88-134309, A03, MF-A01). This report is only available through NTIS (see address given above).

NCEER-87-0013 "Frequency Response of Secondary Systems Under Seismic Excitation," by J.A. HoLung, J. Cai and Y.K. Lin, 7/31/87, (PB88-134317, A05, MF-A01). This report is only available through NTIS (see address given above).

NCEER-87-0014 "Modelling Earthquake Ground Motions in Seismically Active Regions Using Parametric Time Series Methods," by G.W. Ellis and A.S. Cakmak, 8/25/87, (PB88-134283, A08, MF-A01). This report is only available through NTIS (see address given above).

NCEER-87-0015 "Detection and Assessment of Seismic Structural Damage," by E. DiPasquale and A.S. Cakmak, 8/25/87, (PB88-163712, A05, MF-A01). This report is only available through NTIS (see address given above).

NCEER-87-0016 "Pipeline Experiment at Parkfield, California," by J. Isenberg and E. Richardson, 9/15/87, (PB88-163720, A03, MF-A01). This report is available only through NTIS (see address given above).

NCEER-87-0017 "Digital Simulation of Seismic Ground Motion," by M. Shinozuka, G. Deodatis and T. Harada, 8/31/87, (PB88-155197, A04, MF-A01). This report is available only through NTIS (see address given above).

NCEER-87-0018 "Practical Considerations for Structural Control: System Uncertainty, System Time Delay and Truncation of Small Control Forces," J.N. Yang and A. Akbarpour, 8/10/87, (PB88-163738, A08, MF-A01). This report is only available through NTIS (see address given above).

NCEER-87-0019 "Modal Analysis of Nonclassically Damped Structural Systems Using Canonical Transformation," by J.N. Yang, S. Sarkani and F.X. Long, 9/27/87, (PB88-187851, A04, MF-A01).

NCEER-87-0020 "A Nonstationary Solution in Random Vibration Theory," by J.R. Red-Horse and P.D. Spanos, 11/3/87, (PB88-163746, A03, MF-A01).

NCEER-87-0021 "Horizontal Impedances for Radially Inhomogeneous Viscoelastic Soil Layers," by A.S. Veletsos and K.W. Dotson, 10/15/87, (PB88-150859, A04, MF-A01).

NCEER-87-0022 "Seismic Damage Assessment of Reinforced Concrete Members," by Y.S. Chung, C. Meyer and M. Shinozuka, 10/9/87, (PB88-150867, A05, MF-A01). This report is available only through NTIS (see address given above).

NCEER-87-0023 "Active Structural Control in Civil Engineering," by T.T. Soong, 11/11/87, (PB88-187778, A03, MF-A01).

NCEER-87-0024 "Vertical and Torsional Impedances for Radially Inhomogeneous Viscoelastic Soil Layers," by K.W. Dotson and A.S. Veletsos, 12/87, (PB88-187786, A03, MF-A01).

NCEER-87-0025 "Proceedings from the Symposium on Seismic Hazards, Ground Motions, Soil-Liquefaction and Engineering Practice in Eastern North America," October 20-22, 1987, edited by K.H. Jacob, 12/87, (PB88-188115, A23, MF-A01). This report is available only through NTIS (see address given above).

NCEER-87-0026 "Report on the Whittier-Narrows, California, Earthquake of October 1, 1987," by J. Pantelic and A. Reinhorn, 11/87, (PB88-187752, A03, MF-A01). This report is available only through NTIS (see address given above).

NCEER-87-0027 "Design of a Modular Program for Transient Nonlinear Analysis of Large 3-D Building Structures," by S. Srivastav and J.F. Abel, 12/30/87, (PB88-187950, A05, MF-A01). This report is only available through NTIS (see address given above).

NCEER-87-0028 "Second-Year Program in Research, Education and Technology Transfer," 3/8/88, (PB88-219480, A04, MF-A01).

NCEER-88-0001 "Workshop on Seismic Computer Analysis and Design of Buildings With Interactive Graphics," by W. McGuire, J.F. Abel and C.H. Conley, 1/18/88, (PB88-187760, A03, MF-A01). This report is only available through NTIS (see address given above).

NCEER-88-0002 "Optimal Control of Nonlinear Flexible Structures," by J.N. Yang, F.X. Long and D. Wong, 1/22/88, (PB88-213772, A06, MF-A01).

NCEER-88-0003 "Substructuring Techniques in the Time Domain for Primary-Secondary Structural Systems," by G.D. Manolis and G. Juhn, 2/10/88, (PB88-213780, A04, MF-A01).

NCEER-88-0004 "Iterative Seismic Analysis of Primary-Secondary Systems," by A. Singhal, L.D. Lutes and P.D. Spanos, 2/23/88, (PB88-213798, A04, MF-A01).

NCEER-88-0005 "Stochastic Finite Element Expansion for Random Media," by P.D. Spanos and R. Ghanem, 3/14/88, (PB88-213806, A03, MF-A01).

NCEER-88-0006 "Combining Structural Optimization and Structural Control," by F.Y. Cheng and C.P. Pantelides, 1/10/88, (PB88-213814, A05, MF-A01).

NCEER-88-0007 "Seismic Performance Assessment of Code-Designed Structures," by H.H-M. Hwang, J-W. Jaw and H-J. Shau, 3/20/88, (PB88-219423, A04, MF-A01). This report is only available through NTIS (see address given above).

NCEER-88-0008 "Reliability Analysis of Code-Designed Structures Under Natural Hazards," by H.H-M. Hwang, H. Ushiba and M. Shinozuka, 2/29/88, (PB88-229471, A07, MF-A01). This report is only available through NTIS (see address given above).

NCEER-88-0009 "Seismic Fragility Analysis of Shear Wall Structures," by J-W Jaw and H.H-M. Hwang, 4/30/88, (PB89-102867, A04, MF-A01).

NCEER-88-0010 "Base Isolation of a Multi-Story Building Under a Harmonic Ground Motion - A Comparison of Performances of Various Systems," by F-G Fan, G. Ahmadi and I.G. Tadjbakhsh, 5/18/88, (PB89-122238, A06, MF-A01). This report is only available through NTIS (see address given above).

NCEER-88-0011 "Seismic Floor Response Spectra for a Combined System by Green's Functions," by F.M. Lavelle, L.A. Bergman and P.D. Spanos, 5/1/88, (PB89-102875, A03, MF-A01).

NCEER-88-0012 "A New Solution Technique for Randomly Excited Hysteretic Structures," by G.Q. Cai and Y.K. Lin, 5/16/88, (PB89-102883, A03, MF-A01).

NCEER-88-0013 "A Study of Radiation Damping and Soil-Structure Interaction Effects in the Centrifuge," by K. Weissman, supervised by J.H. Prevost, 5/24/88, (PB89-144703, A06, MF-A01).

NCEER-88-0014 "Parameter Identification and Implementation of a Kinematic Plasticity Model for Frictional Soils," by J.H. Prevost and D.V. Griffiths, to be published.

NCEER-88-0015 "Two- and Three- Dimensional Dynamic Finite Element Analyses of the Long Valley Dam," by D.V. Griffiths and J.H. Prevost, 6/17/88, (PB89-144711, A04, MF-A01).

NCEER-88-0016 "Damage Assessment of Reinforced Concrete Structures in Eastern United States," by A.M. Reinhorn, M.J. Seidel, S.K. Kunnath and Y.J. Park, 6/15/88, (PB89-122220, A04, MF-A01). This report is only available through NTIS (see address given above).

NCEER-88-0017 "Dynamic Compliance of Vertically Loaded Strip Foundations in Multilayered Viscoelastic Soils," by S. Ahmad and A.S.M. Israil, 6/17/88, (PB89-102891, A04, MF-A01).

NCEER-88-0018 "An Experimental Study of Seismic Structural Response With Added Viscoelastic Dampers," by R.C. Lin, Z. Liang, T.T. Soong and R.H. Zhang, 6/30/88, (PB89-122212, A05, MF-A01). This report is available only through NTIS (see address given above).

NCEER-88-0019 "Experimental Investigation of Primary - Secondary System Interaction," by G.D. Manolis, G. Juhn and A.M. Reinhorn, 5/27/88, (PB89-122204, A04, MF-A01).

NCEER-88-0020 "A Response Spectrum Approach For Analysis of Nonclassically Damped Structures," by J.N. Yang, S. Sarkani and F.X. Long, 4/22/88, (PB89-102909, A04, MF-A01).

NCEER-88-0021 "Seismic Interaction of Structures and Soils: Stochastic Approach," by A.S. Veletsos and A.M. Prasad, 7/21/88, (PB89-122196, A04, MF-A01). This report is only available through NTIS (see address given above).

NCEER-88-0022 "Identification of the Serviceability Limit State and Detection of Seismic Structural Damage," by E. DiPasquale and A.S. Cakmak, 6/15/88, (PB89-122188, A05, MF-A01). This report is available only through NTIS (see address given above).

NCEER-88-0023 "Multi-Hazard Risk Analysis: Case of a Simple Offshore Structure," by B.K. Bhartia and E.H. Vanmarcke, 7/21/88, (PB89-145213, A05, MF-A01).

NCEER-88-0024 "Automated Seismic Design of Reinforced Concrete Buildings," by Y.S. Chung, C. Meyer and M. Shinozuka, 7/5/88, (PB89-122170, A06, MF-A01). This report is available only through NTIS (see address given above).

NCEER-88-0025 "Experimental Study of Active Control of MDOF Structures Under Seismic Excitations," by L.L. Chung, R.C. Lin, T.T. Soong and A.M. Reinhorn, 7/10/88, (PB89-122600, A04, MF-A01).

NCEER-88-0026 "Earthquake Simulation Tests of a Low-Rise Metal Structure," by J.S. Hwang, K.C. Chang, G.C. Lee and R.L. Ketter, 8/1/88, (PB89-102917, A04, MF-A01).

NCEER-88-0027 "Systems Study of Urban Response and Reconstruction Due to Catastrophic Earthquakes," by F. Kozin and H.K. Zhou, 9/22/88, (PB90-162348, A04, MF-A01).

NCEER-88-0028 "Seismic Fragility Analysis of Plane Frame Structures," by H.H-M. Hwang and Y.K. Low, 7/31/88, (PB89-131445, A06, MF-A01).

NCEER-88-0029 "Response Analysis of Stochastic Structures," by A. Kardara, C. Bucher and M. Shinozuka, 9/22/88, (PB89-174429, A04, MF-A01).

NCEER-88-0030 "Nonnormal Accelerations Due to Yielding in a Primary Structure," by D.C.K. Chen and L.D. Lutes, 9/19/88, (PB89-131437, A04, MF-A01).

NCEER-88-0031 "Design Approaches for Soil-Structure Interaction," by A.S. Veletsos, A.M. Prasad and Y. Tang, 12/30/88, (PB89-174437, A03, MF-A01). This report is available only through NTIS (see address given above).

NCEER-88-0032 "A Re-evaluation of Design Spectra for Seismic Damage Control," by C.J. Turkstra and A.G. Tallin, 11/7/88, (PB89-145221, A05, MF-A01).

NCEER-88-0033 "The Behavior and Design of Noncontact Lap Splices Subjected to Repeated Inelastic Tensile Loading," by V.E. Sagan, P. Gergely and R.N. White, 12/8/88, (PB89-163737, A08, MF-A01).

NCEER-88-0034 "Seismic Response of Pile Foundations," by S.M. Mamoon, P.K. Banerjee and S. Ahmad, 11/1/88, (PB89-145239, A04, MF-A01).

NCEER-88-0035 "Modeling of R/C Building Structures With Flexible Floor Diaphragms (IDARC2)," by A.M. Reinhorn, S.K. Kunnath and N. Panahshahi, 9/7/88, (PB89-207153, A07, MF-A01).

NCEER-88-0036 "Solution of the Dam-Reservoir Interaction Problem Using a Combination of FEM, BEM with Particular Integrals, Modal Analysis, and Substructuring," by C-S. Tsai, G.C. Lee and R.L. Ketter, 12/31/88, (PB89-207146, A04, MF-A01).

NCEER-88-0037 "Optimal Placement of Actuators for Structural Control," by F.Y. Cheng and C.P. Pantelides, 8/15/88, (PB89-162846, A05, MF-A01).

NCEER-88-0038 "Teflon Bearings in Aseismic Base Isolation: Experimental Studies and Mathematical Modeling," by A. Mokha, M.C. Constantinou and A.M. Reinhorn, 12/5/88, (PB89-218457, A10, MF-A01). This report is available only through NTIS (see address given above).

NCEER-88-0039 "Seismic Behavior of Flat Slab High-Rise Buildings in the New York City Area," by P. Weidlinger and M. Ettouney, 10/15/88, (PB90-145681, A04, MF-A01).

NCEER-88-0040 "Evaluation of the Earthquake Resistance of Existing Buildings in New York City," by P. Weidlinger and M. Ettouney, 10/15/88, to be published.

NCEER-88-0041 "Small-Scale Modeling Techniques for Reinforced Concrete Structures Subjected to Seismic Loads," by W. Kim, A. El-Attar and R.N. White, 11/22/88, (PB89-189625, A05, MF-A01).

NCEER-88-0042 "Modeling Strong Ground Motion from Multiple Event Earthquakes," by G.W. Ellis and A.S. Cakmak, 10/15/88, (PB89-174445, A03, MF-A01).

NCEER-88-0043 "Nonstationary Models of Seismic Ground Acceleration," by M. Grigoriu, S.E. Ruiz and E. Rosenblueth, 7/15/88, (PB89-189617, A04, MF-A01).

NCEER-88-0044 "SARCF User's Guide: Seismic Analysis of Reinforced Concrete Frames," by Y.S. Chung, C. Meyer and M. Shinozuka, 11/9/88, (PB89-174452, A08, MF-A01).

NCEER-88-0045 "First Expert Panel Meeting on Disaster Research and Planning," edited by J. Pantelic and J. Stoyle, 9/15/88, (PB89-174460, A05, MF-A01).

NCEER-88-0046 "Preliminary Studies of the Effect of Degrading Infill Walls on the Nonlinear Seismic Response of Steel Frames," by C.Z. Chrysostomou, P. Gergely and J.F. Abel, 12/19/88, (PB89-208383, A05, MF-A01).

NCEER-88-0047 "Reinforced Concrete Frame Component Testing Facility - Design, Construction, Instrumentation and Operation," by S.P. Pessiki, C. Conley, T. Bond, P. Gergely and R.N. White, 12/16/88, (PB89-174478, A04, MF-A01).

NCEER-89-0001 "Effects of Protective Cushion and Soil Compliancy on the Response of Equipment Within a Seismically Excited Building," by J.A. HoLung, 2/16/89, (PB89-207179, A04, MF-A01).

NCEER-89-0002 "Statistical Evaluation of Response Modification Factors for Reinforced Concrete Structures," by H.H-M. Hwang and J-W. Jaw, 2/17/89, (PB89-207187, A05, MF-A01).

NCEER-89-0003 "Hysteretic Columns Under Random Excitation," by G-Q. Cai and Y.K. Lin, 1/9/89, (PB89-196513, A03, MF-A01).

NCEER-89-0004 "Experimental Study of `Elephant Foot Bulge' Instability of Thin-Walled Metal Tanks," by Z-H. Jia and R.L. Ketter, 2/22/89, (PB89-207195, A03, MF-A01).

NCEER-89-0005 "Experiment on Performance of Buried Pipelines Across San Andreas Fault," by J. Isenberg, E. Richardson and T.D. O'Rourke, 3/10/89, (PB89-218440, A04, MF-A01). This report is available only through NTIS (see address given above).

NCEER-89-0006 "A Knowledge-Based Approach to Structural Design of Earthquake-Resistant Buildings," by M. Subramani, P. Gergely, C.H. Conley, J.F. Abel and A.H. Zaghw, 1/15/89, (PB89-218465, A06, MF-A01).

NCEER-89-0007 "Liquefaction Hazards and Their Effects on Buried Pipelines," by T.D. O'Rourke and P.A. Lane, 2/1/89, (PB89-218481, A09, MF-A01).

NCEER-89-0008 "Fundamentals of System Identification in Structural Dynamics," by H. Imai, C-B. Yun, O. Maruyama and M. Shinozuka, 1/26/89, (PB89-207211, A04, MF-A01).

NCEER-89-0009 "Effects of the 1985 Michoacan Earthquake on Water Systems and Other Buried Lifelines in Mexico," by A.G. Ayala and M.J. O'Rourke, 3/8/89, (PB89-207229, A06, MF-A01).

NCEER-89-R010 "NCEER Bibliography of Earthquake Education Materials," by K.E.K. Ross, Second Revision, 9/1/89, (PB90-125352, A05, MF-A01). This report is replaced by NCEER-92-0018.

NCEER-89-0011 "Inelastic Three-Dimensional Response Analysis of Reinforced Concrete Building Structures (IDARC-3D), Part I - Modeling," by S.K. Kunnath and A.M. Reinhorn, 4/17/89, (PB90-114612, A07, MF-A01). This report is available only through NTIS (see address given above).

NCEER-89-0012 "Recommended Modifications to ATC-14," by C.D. Poland and J.O. Malley, 4/12/89, (PB90-108648, A15, MF-A01).

NCEER-89-0013 "Repair and Strengthening of Beam-to-Column Connections Subjected to Earthquake Loading," by M. Corazao and A.J. Durrani, 2/28/89, (PB90-109885, A06, MF-A01).

NCEER-89-0014 "Program EXKAL2 for Identification of Structural Dynamic Systems," by O. Maruyama, C-B. Yun, M. Hoshiya and M. Shinozuka, 5/19/89, (PB90-109877, A09, MF-A01).

NCEER-89-0015 "Response of Frames With Bolted Semi-Rigid Connections, Part I - Experimental Study and Analytical Predictions," by P.J. DiCorso, A.M. Reinhorn, J.R. Dickerson, J.B. Radziminski and W.L. Harper, 6/1/89, to be published.

NCEER-89-0016 "ARMA Monte Carlo Simulation in Probabilistic Structural Analysis," by P.D. Spanos and M.P. Mignolet, 7/10/89, (PB90-109893, A03, MF-A01).

NCEER-89-P017 "Preliminary Proceedings from the Conference on Disaster Preparedness - The Place of Earthquake Education in Our Schools," Edited by K.E.K. Ross, 6/23/89, (PB90-108606, A03, MF-A01).

NCEER-89-0017 "Proceedings from the Conference on Disaster Preparedness - The Place of Earthquake Education in Our Schools," Edited by K.E.K. Ross, 12/31/89, (PB90-207895, A012, MF-A02). This report is available only through NTIS (see address given above).

NCEER-89-0018 "Multidimensional Models of Hysteretic Material Behavior for Vibration Analysis of Shape Memory Energy Absorbing Devices, by E.J. Graesser and F.A. Cozzarelli, 6/7/89, (PB90-164146, A04, MF-A01).

NCEER-89-0019 "Nonlinear Dynamic Analysis of Three-Dimensional Base Isolated Structures (3D-BASIS)," by S. Nagarajaiah, A.M. Reinhorn and M.C. Constantinou, 8/3/89, (PB90-161936, A06, MF-A01). This report has been replaced by NCEER-93-0011.

NCEER-89-0020 "Structural Control Considering Time-Rate of Control Forces and Control Rate Constraints," by F.Y. Cheng and C.P. Pantelides, 8/3/89, (PB90-120445, A04, MF-A01).

NCEER-89-0021 "Subsurface Conditions of Memphis and Shelby County," by K.W. Ng, T-S. Chang and H-H.M. Hwang, 7/26/89, (PB90-120437, A03, MF-A01).

NCEER-89-0022 "Seismic Wave Propagation Effects on Straight Jointed Buried Pipelines," by K. Elhmadi and M.J. O'Rourke, 8/24/89, (PB90-162322, A10, MF-A02).

NCEER-89-0023 "Workshop on Serviceability Analysis of Water Delivery Systems," edited by M. Grigoriu, 3/6/89, (PB90-127424, A03, MF-A01).

NCEER-89-0024 "Shaking Table Study of a 1/5 Scale Steel Frame Composed of Tapered Members," by K.C. Chang, J.S. Hwang and G.C. Lee, 9/18/89, (PB90-160169, A04, MF-A01).

NCEER-89-0025 "DYNA1D: A Computer Program for Nonlinear Seismic Site Response Analysis - Technical Documentation," by Jean H. Prevost, 9/14/89, (PB90-161944, A07, MF-A01). This report is available only through NTIS (see address given above).

NCEER-89-0026 "1:4 Scale Model Studies of Active Tendon Systems and Active Mass Dampers for Aseismic Protection," by A.M. Reinhorn, T.T. Soong, R.C. Lin, Y.P. Yang, Y. Fukao, H. Abe and M. Nakai, 9/15/89, (PB90-173246, A10, MF-A02). This report is available only through NTIS (see address given above).

NCEER-89-0027 "Scattering of Waves by Inclusions in a Nonhomogeneous Elastic Half Space Solved by Boundary Element Methods," by P.K. Hadley, A. Askar and A.S. Cakmak, 6/15/89, (PB90-145699, A07, MF-A01).

NCEER-89-0028 "Statistical Evaluation of Deflection Amplification Factors for Reinforced Concrete Structures," by H.H.M. Hwang, J-W. Jaw and A.L. Ch'ng, 8/31/89, (PB90-164633, A05, MF-A01).

NCEER-89-0029 "Bedrock Accelerations in Memphis Area Due to Large New Madrid Earthquakes," by H.H.M. Hwang, C.H.S. Chen and G. Yu, 11/7/89, (PB90-162330, A04, MF-A01).

NCEER-89-0030 "Seismic Behavior and Response Sensitivity of Secondary Structural Systems," by Y.Q. Chen and T.T. Soong, 10/23/89, (PB90-164658, A08, MF-A01).

NCEER-89-0031 "Random Vibration and Reliability Analysis of Primary-Secondary Structural Systems," by Y. Ibrahim, M. Grigoriu and T.T. Soong, 11/10/89, (PB90-161951, A04, MF-A01).

NCEER-89-0032 "Proceedings from the Second U.S. - Japan Workshop on Liquefaction, Large Ground Deformation and Their Effects on Lifelines, September 26-29, 1989," Edited by T.D. O'Rourke and M. Hamada, 12/1/89, (PB90-209388, A22, MF-A03).

NCEER-89-0033 "Deterministic Model for Seismic Damage Evaluation of Reinforced Concrete Structures," by J.M. Bracci, A.M. Reinhorn, J.B. Mander and S.K. Kunnath, 9/27/89, (PB91-108803, A06, MF-A01).

NCEER-89-0034 "On the Relation Between Local and Global Damage Indices," by E. DiPasquale and A.S. Cakmak, 8/15/89, (PB90-173865, A05, MF-A01).

NCEER-89-0035 "Cyclic Undrained Behavior of Nonplastic and Low Plasticity Silts," by A.J. Walker and H.E. Stewart, 7/26/89, (PB90-183518, A10, MF-A01).

NCEER-89-0036 "Liquefaction Potential of Surficial Deposits in the City of Buffalo, New York," by M. Budhu, R. Giese and L. Baumgrass, 1/17/89, (PB90-208455, A04, MF-A01).

NCEER-89-0037 "A Deterministic Assessment of Effects of Ground Motion Incoherence," by A.S. Veletsos and Y. Tang, 7/15/89, (PB90-164294, A03, MF-A01).

NCEER-89-0038 "Workshop on Ground Motion Parameters for Seismic Hazard Mapping," July 17-18, 1989, edited by R.V. Whitman, 12/1/89, (PB90-173923, A04, MF-A01).

NCEER-89-0039 "Seismic Effects on Elevated Transit Lines of the New York City Transit Authority," by C.J. Costantino, C.A. Miller and E. Heymsfield, 12/26/89, (PB90-207887, A06, MF-A01).

NCEER-89-0040 "Centrifugal Modeling of Dynamic Soil-Structure Interaction," by K. Weissman, Supervised by J.H. Prevost, 5/10/89, (PB90-207879, A07, MF-A01).

NCEER-89-0041 "Linearized Identification of Buildings With Cores for Seismic Vulnerability Assessment," by I-K. Ho and A.E. Aktan, 11/1/89, (PB90-251943, A07, MF-A01).

NCEER-90-0001 "Geotechnical and Lifeline Aspects of the October 17, 1989 Loma Prieta Earthquake in San Francisco," by T.D. O'Rourke, H.E. Stewart, F.T. Blackburn and T.S. Dickerman, 1/90, (PB90-208596, A05, MF-A01).

NCEER-90-0002 "Nonnormal Secondary Response Due to Yielding in a Primary Structure," by D.C.K. Chen and L.D. Lutes, 2/28/90, (PB90-251976, A07, MF-A01).

NCEER-90-0003 "Earthquake Education Materials for Grades K-12," by K.E.K. Ross, 4/16/90, (PB91-251984, A05, MF-A05). This report has been replaced by NCEER-92-0018.

NCEER-90-0004 "Catalog of Strong Motion Stations in Eastern North America," by R.W. Busby, 4/3/90, (PB90-251984, A05, MF-A01).

NCEER-90-0005 "NCEER Strong-Motion Data Base: A User Manual for the GeoBase Release (Version 1.0 for the Sun3)," by P. Friberg and K. Jacob, 3/31/90 (PB90-258062, A04, MF-A01).

NCEER-90-0006 "Seismic Hazard Along a Crude Oil Pipeline in the Event of an 1811-1812 Type New Madrid Earthquake," by H.H.M. Hwang and C-H.S. Chen, 4/16/90, (PB90-258054, A04, MF-A01).

NCEER-90-0007 "Site-Specific Response Spectra for Memphis Sheahan Pumping Station," by H.H.M. Hwang and C.S. Lee, 5/15/90, (PB91-108811, A05, MF-A01).

NCEER-90-0008 "Pilot Study on Seismic Vulnerability of Crude Oil Transmission Systems," by T. Ariman, R. Dobry, M. Grigoriu, F. Kozin, M. O'Rourke, T. O'Rourke and M. Shinozuka, 5/25/90, (PB91-108837, A06, MF-A01).

NCEER-90-0009 "A Program to Generate Site Dependent Time Histories: EQGEN," by G.W. Ellis, M. Srinivasan and A.S. Cakmak, 1/30/90, (PB91-108829, A04, MF-A01).

NCEER-90-0010 "Active Isolation for Seismic Protection of Operating Rooms," by M.E. Talbott, Supervised by M. Shinozuka, 6/8/9, (PB91-110205, A05, MF-A01).

NCEER-90-0011 "Program LINEARID for Identification of Linear Structural Dynamic Systems," by C-B. Yun and M. Shinozuka, 6/25/90, (PB91-110312, A08, MF-A01).

NCEER-90-0012 "Two-Dimensional Two-Phase Elasto-Plastic Seismic Response of Earth Dams," by A.N. Yiagos, Supervised by J.H. Prevost, 6/20/90, (PB91-110197, A13, MF-A02).

NCEER-90-0013 "Secondary Systems in Base-Isolated Structures: Experimental Investigation, Stochastic Response and Stochastic Sensitivity," by G.D. Manolis, G. Juhn, M.C. Constantinou and A.M. Reinhorn, 7/1/90, (PB91-110320, A08, MF-A01).

NCEER-90-0014 "Seismic Behavior of Lightly-Reinforced Concrete Column and Beam-Column Joint Details," by S.P. Pessiki, C.H. Conley, P. Gergely and R.N. White, 8/22/90, (PB91-108795, A11, MF-A02).

NCEER-90-0015 "Two Hybrid Control Systems for Building Structures Under Strong Earthquakes," by J.N. Yang and A. Danielians, 6/29/90, (PB91-125393, A04, MF-A01).

NCEER-90-0016 "Instantaneous Optimal Control with Acceleration and Velocity Feedback," by J.N. Yang and Z. Li, 6/29/90, (PB91-125401, A03, MF-A01).

NCEER-90-0017 "Reconnaissance Report on the Northern Iran Earthquake of June 21, 1990," by M. Mehrain, 10/4/90, (PB91-125377, A03, MF-A01).

NCEER-90-0018 "Evaluation of Liquefaction Potential in Memphis and Shelby County," by T.S. Chang, P.S. Tang, C.S. Lee and H. Hwang, 8/10/90, (PB91-125427, A09, MF-A01).

NCEER-90-0019 "Experimental and Analytical Study of a Combined Sliding Disc Bearing and Helical Steel Spring Isolation System," by M.C. Constantinou, A.S. Mokha and A.M. Reinhorn, 10/4/90, (PB91-125385, A06, MF-A01). This report is available only through NTIS (see address given above).

NCEER-90-0020 "Experimental Study and Analytical Prediction of Earthquake Response of a Sliding Isolation System with a Spherical Surface," by A.S. Mokha, M.C. Constantinou and A.M. Reinhorn, 10/11/90, (PB91-125419, A05, MF-A01).

NCEER-90-0021 "Dynamic Interaction Factors for Floating Pile Groups," by G. Gazetas, K. Fan, A. Kaynia and E. Kausel, 9/10/90, (PB91-170381, A05, MF-A01).

NCEER-90-0022 "Evaluation of Seismic Damage Indices for Reinforced Concrete Structures," by S. Rodriguez-Gomez and A.S. Cakmak, 9/30/90, PB91-171322, A06, MF-A01).

NCEER-90-0023 "Study of Site Response at a Selected Memphis Site," by H. Desai, S. Ahmad, E.S. Gazetas and M.R. Oh, 10/11/90, (PB91-196857, A03, MF-A01).

NCEER-90-0024 "A User's Guide to Strongmo: Version 1.0 of NCEER's Strong-Motion Data Access Tool for PCs and Terminals," by P.A. Friberg and C.A.T. Susch, 11/15/90, (PB91-171272, A03, MF-A01).

NCEER-90-0025 "A Three-Dimensional Analytical Study of Spatial Variability of Seismic Ground Motions," by L-L. Hong and A.H.-S. Ang, 10/30/90, (PB91-170399, A09, MF-A01).

NCEER-90-0026 "MUMOID User's Guide - A Program for the Identification of Modal Parameters," by S. Rodriguez-Gomez and E. DiPasquale, 9/30/90, (PB91-171298, A04, MF-A01).

NCEER-90-0027 "SARCF-II User's Guide - Seismic Analysis of Reinforced Concrete Frames," by S. Rodriguez-Gomez, Y.S. Chung and C. Meyer, 9/30/90, (PB91-171280, A05, MF-A01).

NCEER-90-0028 "Viscous Dampers: Testing, Modeling and Application in Vibration and Seismic Isolation," by N. Makris and M.C. Constantinou, 12/20/90 (PB91-190561, A06, MF-A01).

NCEER-90-0029 "Soil Effects on Earthquake Ground Motions in the Memphis Area," by H. Hwang, C.S. Lee, K.W. Ng and T.S. Chang, 8/2/90, (PB91-190751, A05, MF-A01).

NCEER-91-0001 "Proceedings from the Third Japan-U.S. Workshop on Earthquake Resistant Design of Lifeline Facilities and Countermeasures for Soil Liquefaction, December 17-19, 1990," edited by T.D. O'Rourke and M. Hamada, 2/1/91, (PB91-179259, A99, MF-A04).

NCEER-91-0002 "Physical Space Solutions of Non-Proportionally Damped Systems," by M. Tong, Z. Liang and G.C. Lee, 1/15/91, (PB91-179242, A04, MF-A01).

NCEER-91-0003 "Seismic Response of Single Piles and Pile Groups," by K. Fan and G. Gazetas, 1/10/91, (PB92-174994, A04, MF-A01).

NCEER-91-0004 "Damping of Structures: Part 1 - Theory of Complex Damping," by Z. Liang and G. Lee, 10/10/91, (PB92-197235, A12, MF-A03).

NCEER-91-0005 "3D-BASIS - Nonlinear Dynamic Analysis of Three Dimensional Base Isolated Structures: Part II," by S. Nagarajaiah, A.M. Reinhorn and M.C. Constantinou, 2/28/91, (PB91-190553, A07, MF-A01). This report has been replaced by NCEER-93-0011.

NCEER-91-0006 "A Multidimensional Hysteretic Model for Plasticity Deforming Metals in Energy Absorbing Devices," by E.J. Graesser and F.A. Cozzarelli, 4/9/91, (PB92-108364, A04, MF-A01).

NCEER-91-0007 "A Framework for Customizable Knowledge-Based Expert Systems with an Application to a KBES for Evaluating the Seismic Resistance of Existing Buildings," by E.G. Ibarra-Anaya and S.J. Fenves, 4/9/91, (PB91-210930, A08, MF-A01).

NCEER-91-0008 "Nonlinear Analysis of Steel Frames with Semi-Rigid Connections Using the Capacity Spectrum Method," by G.G. Deierlein, S-H. Hsieh, Y-J. Shen and J.F. Abel, 7/2/91, (PB92-113828, A05, MF-A01).

NCEER-91-0009 "Earthquake Education Materials for Grades K-12," by K.E.K. Ross, 4/30/91, (PB91-212142, A06, MF-A01). This report has been replaced by NCEER-92-0018.

NCEER-91-0010 "Phase Wave Velocities and Displacement Phase Differences in a Harmonically Oscillating Pile," by N. Makris and G. Gazetas, 7/8/91, (PB92-108356, A04, MF-A01).

NCEER-91-0011 "Dynamic Characteristics of a Full-Size Five-Story Steel Structure and a 2/5 Scale Model," by K.C. Chang, G.C. Yao, G.C. Lee, D.S. Hao and Y.C. Yeh," 7/2/91, (PB93-116648, A06, MF-A02).

NCEER-91-0012 "Seismic Response of a 2/5 Scale Steel Structure with Added Viscoelastic Dampers," by K.C. Chang, T.T. Soong, S-T. Oh and M.L. Lai, 5/17/91, (PB92-110816, A05, MF-A01).

NCEER-91-0013 "Earthquake Response of Retaining Walls; Full-Scale Testing and Computational Modeling," by S. Alampalli and A-W.M. Elgamal, 6/20/91, to be published.

NCEER-91-0014 "3D-BASIS-M: Nonlinear Dynamic Analysis of Multiple Building Base Isolated Structures," by P.C. Tsopelas, S. Nagarajaiah, M.C. Constantinou and A.M. Reinhorn, 5/28/91, (PB92-113885, A09, MF-A02).

NCEER-91-0015 "Evaluation of SEAOC Design Requirements for Sliding Isolated Structures," by D. Theodossiou and M.C. Constantinou, 6/10/91, (PB92-114602, A11, MF-A03).

NCEER-91-0016 "Closed-Loop Modal Testing of a 27-Story Reinforced Concrete Flat Plate-Core Building," by H.R. Somaprasad, T. Toksoy, H. Yoshiyuki and A.E. Aktan, 7/15/91, (PB92-129980, A07, MF-A02).

NCEER-91-0017 "Shake Table Test of a 1/6 Scale Two-Story Lightly Reinforced Concrete Building," by A.G. El-Attar, R.N. White and P. Gergely, 2/28/91, (PB92-222447, A06, MF-A02).

NCEER-91-0018 "Shake Table Test of a 1/8 Scale Three-Story Lightly Reinforced Concrete Building," by A.G. El-Attar, R.N. White and P. Gergely, 2/28/91, (PB93-116630, A08, MF-A02).

NCEER-91-0019 "Transfer Functions for Rigid Rectangular Foundations," by A.S. Veletsos, A.M. Prasad and W.H. Wu, 7/31/91, to be published.

NCEER-91-0020 "Hybrid Control of Seismic-Excited Nonlinear and Inelastic Structural Systems," by J.N. Yang, Z. Li and A. Danielians, 8/1/91, (PB92-143171, A06, MF-A02).

NCEER-91-0021 "The NCEER-91 Earthquake Catalog: Improved Intensity-Based Magnitudes and Recurrence Relations for U.S. Earthquakes East of New Madrid," by L. Seeber and J.G. Armbruster, 8/28/91, (PB92-176742, A06, MF-A02).

NCEER-91-0022 "Proceedings from the Implementation of Earthquake Planning and Education in Schools: The Need for Change - The Roles of the Changemakers," by K.E.K. Ross and F. Winslow, 7/23/91, (PB92-129998, A12, MF-A03).

NCEER-91-0023 "A Study of Reliability-Based Criteria for Seismic Design of Reinforced Concrete Frame Buildings," by H.H.M. Hwang and H-M. Hsu, 8/10/91, (PB92-140235, A09, MF-A02).

NCEER-91-0024 "Experimental Verification of a Number of Structural System Identification Algorithms," by R.G. Ghanem, H. Gavin and M. Shinozuka, 9/18/91, (PB92-176577, A18, MF-A04).

NCEER-91-0025 "Probabilistic Evaluation of Liquefaction Potential," by H.H.M. Hwang and C.S. Lee," 11/25/91, (PB92-143429, A05, MF-A01).

NCEER-91-0026 "Instantaneous Optimal Control for Linear, Nonlinear and Hysteretic Structures - Stable Controllers," by J.N. Yang and Z. Li, 11/15/91, (PB92-163807, A04, MF-A01).

NCEER-91-0027 "Experimental and Theoretical Study of a Sliding Isolation System for Bridges," by M.C. Constantinou, A. Kartoum, A.M. Reinhorn and P. Bradford, 11/15/91, (PB92-176973, A10, MF-A03).

NCEER-92-0001 "Case Studies of Liquefaction and Lifeline Performance During Past Earthquakes, Volume 1: Japanese Case Studies," Edited by M. Hamada and T. O'Rourke, 2/17/92, (PB92-197243, A18, MF-A04).

NCEER-92-0002 "Case Studies of Liquefaction and Lifeline Performance During Past Earthquakes, Volume 2: United States Case Studies," Edited by T. O'Rourke and M. Hamada, 2/17/92, (PB92-197250, A20, MF-A04).

NCEER-92-0003 "Issues in Earthquake Education," Edited by K. Ross, 2/3/92, (PB92-222389, A07, MF-A02).

NCEER-92-0004 "Proceedings from the First U.S. - Japan Workshop on Earthquake Protective Systems for Bridges," Edited by I.G. Buckle, 2/4/92, (PB94-142239, A99, MF-A06).

NCEER-92-0005 "Seismic Ground Motion from a Haskell-Type Source in a Multiple-Layered Half-Space," A.P. Theoharis, G. Deodatis and M. Shinozuka, 1/2/92, to be published.

NCEER-92-0006 "Proceedings from the Site Effects Workshop," Edited by R. Whitman, 2/29/92, (PB92-197201, A04, MF-A01).

NCEER-92-0007 "Engineering Evaluation of Permanent Ground Deformations Due to Seismically-Induced Liquefaction," by M.H. Baziar, R. Dobry and A-W.M. Elgamal, 3/24/92, (PB92-222421, A13, MF-A03).

NCEER-92-0008 "A Procedure for the Seismic Evaluation of Buildings in the Central and Eastern United States," by C.D. Poland and J.O. Malley, 4/2/92, (PB92-222439, A20, MF-A04).

NCEER-92-0009 "Experimental and Analytical Study of a Hybrid Isolation System Using Friction Controllable Sliding Bearings," by M.Q. Feng, S. Fujii and M. Shinozuka, 5/15/92, (PB93-150282, A06, MF-A02).

NCEER-92-0010 "Seismic Resistance of Slab-Column Connections in Existing Non-Ductile Flat-Plate Buildings," by A.J. Durrani and Y. Du, 5/18/92, (PB93-116812, A06, MF-A02).

NCEER-92-0011 "The Hysteretic and Dynamic Behavior of Brick Masonry Walls Upgraded by Ferrocement Coatings Under Cyclic Loading and Strong Simulated Ground Motion," by H. Lee and S.P. Prawel, 5/11/92, to be published.

NCEER-92-0012 "Study of Wire Rope Systems for Seismic Protection of Equipment in Buildings," by G.F. Demetriades, M.C. Constantinou and A.M. Reinhorn, 5/20/92, (PB93-116655, A08, MF-A02).

NCEER-92-0013 "Shape Memory Structural Dampers: Material Properties, Design and Seismic Testing," by P.R. Witting and F.A. Cozzarelli, 5/26/92, (PB93-116663, A05, MF-A01).

NCEER-92-0014 "Longitudinal Permanent Ground Deformation Effects on Buried Continuous Pipelines," by M.J. O'Rourke, and C. Nordberg, 6/15/92, (PB93-116671, A08, MF-A02).

NCEER-92-0015 "A Simulation Method for Stationary Gaussian Random Functions Based on the Sampling Theorem," by M. Grigoriu and S. Balopoulou, 6/11/92, (PB93-127496, A05, MF-A01).

NCEER-92-0016 "Gravity-Load-Designed Reinforced Concrete Buildings: Seismic Evaluation of Existing Construction and Detailing Strategies for Improved Seismic Resistance," by G.W. Hoffmann, S.K. Kunnath, A.M. Reinhorn and J.B. Mander, 7/15/92, (PB94-142007, A08, MF-A02).

NCEER-92-0017 "Observations on Water System and Pipeline Performance in the Limón Area of Costa Rica Due to the April 22, 1991 Earthquake," by M. O'Rourke and D. Ballantyne, 6/30/92, (PB93-126811, A06, MF-A02).

NCEER-92-0018 "Fourth Edition of Earthquake Education Materials for Grades K-12," Edited by K.E.K. Ross, 8/10/92, (PB93-114023, A07, MF-A02).

NCEER-92-0019 "Proceedings from the Fourth Japan-U.S. Workshop on Earthquake Resistant Design of Lifeline Facilities and Countermeasures for Soil Liquefaction," Edited by M. Hamada and T.D. O'Rourke, 8/12/92, (PB93-163939, A99, MF-E11).

NCEER-92-0020 "Active Bracing System: A Full Scale Implementation of Active Control," by A.M. Reinhorn, T.T. Soong, R.C. Lin, M.A. Riley, Y.P. Wang, S. Aizawa and M. Higashino, 8/14/92, (PB93-127512, A06, MF-A02).

NCEER-92-0021 "Empirical Analysis of Horizontal Ground Displacement Generated by Liquefaction-Induced Lateral Spreads," by S.F. Bartlett and T.L. Youd, 8/17/92, (PB93-188241, A06, MF-A02).

NCEER-92-0022 "IDARC Version 3.0: Inelastic Damage Analysis of Reinforced Concrete Structures," by S.K. Kunnath, A.M. Reinhorn and R.F. Lobo, 8/31/92, (PB93-227502, A07, MF-A02).

NCEER-92-0023 "A Semi-Empirical Analysis of Strong-Motion Peaks in Terms of Seismic Source, Propagation Path and Local Site Conditions, by M. Kamiyama, M.J. O'Rourke and R. Flores-Berrones, 9/9/92, (PB93-150266, A08, MF-A02).

NCEER-92-0024 "Seismic Behavior of Reinforced Concrete Frame Structures with Nonductile Details, Part I: Summary of Experimental Findings of Full Scale Beam-Column Joint Tests," by A. Beres, R.N. White and P. Gergely, 9/30/92, (PB93-227783, A05, MF-A01).

NCEER-92-0025 "Experimental Results of Repaired and Retrofitted Beam-Column Joint Tests in Lightly Reinforced Concrete Frame Buildings," by A. Beres, S. El-Borgi, R.N. White and P. Gergely, 10/29/92, (PB93-227791, A05, MF-A01).

NCEER-92-0026 "A Generalization of Optimal Control Theory: Linear and Nonlinear Structures," by J.N. Yang, Z. Li and S. Vongchavalitkul, 11/2/92, (PB93-188621, A05, MF-A01).

NCEER-92-0027 "Seismic Resistance of Reinforced Concrete Frame Structures Designed Only for Gravity Loads: Part I - Design and Properties of a One-Third Scale Model Structure," by J.M. Bracci, A.M. Reinhorn and J.B. Mander, 12/1/92, (PB94-104502, A08, MF-A02).

NCEER-92-0028 "Seismic Resistance of Reinforced Concrete Frame Structures Designed Only for Gravity Loads: Part II - Experimental Performance of Subassemblages," by L.E. Aycardi, J.B. Mander and A.M. Reinhorn, 12/1/92, (PB94-104510, A08, MF-A02).

NCEER-92-0029 "Seismic Resistance of Reinforced Concrete Frame Structures Designed Only for Gravity Loads: Part III - Experimental Performance and Analytical Study of a Structural Model," by J.M. Bracci, A.M. Reinhorn and J.B. Mander, 12/1/92, (PB93-227528, A09, MF-A01).

NCEER-92-0030 "Evaluation of Seismic Retrofit of Reinforced Concrete Frame Structures: Part I - Experimental Performance of Retrofitted Subassemblages," by D. Choudhuri, J.B. Mander and A.M. Reinhorn, 12/8/92, (PB93-198307, A07, MF-A02).

NCEER-92-0031 "Evaluation of Seismic Retrofit of Reinforced Concrete Frame Structures: Part II - Experimental Performance and Analytical Study of a Retrofitted Structural Model," by J.M. Bracci, A.M. Reinhorn and J.B. Mander, 12/8/92, (PB93-198315, A09, MF-A03).

NCEER-92-0032 "Experimental and Analytical Investigation of Seismic Response of Structures with Supplemental Fluid Viscous Dampers," by M.C. Constantinou and M.D. Symans, 12/21/92, (PB93-191435, A10, MF-A03). This report is available only through NTIS (see address given above).

NCEER-92-0033 "Reconnaissance Report on the Cairo, Egypt Earthquake of October 12, 1992," by M. Khater, 12/23/92, (PB93-188621, A03, MF-A01).

NCEER-92-0034 "Low-Level Dynamic Characteristics of Four Tall Flat-Plate Buildings in New York City," by H. Gavin, S. Yuan, J. Grossman, E. Pekelis and K. Jacob, 12/28/92, (PB93-188217, A07, MF-A02).

NCEER-93-0001 "An Experimental Study on the Seismic Performance of Brick-Infilled Steel Frames With and Without Retrofit," by J.B. Mander, B. Nair, K. Wojtkowski and J. Ma, 1/29/93, (PB93-227510, A07, MF-A02).

NCEER-93-0002 "Social Accounting for Disaster Preparedness and Recovery Planning," by S. Cole, E. Pantoja and V. Razak, 2/22/93, (PB94-142114, A12, MF-A03).

NCEER-93-0003 "Assessment of 1991 NEHRP Provisions for Nonstructural Components and Recommended Revisions," by T.T. Soong, G. Chen, Z. Wu, R-H. Zhang and M. Grigoriu, 3/1/93, (PB93-188639, A06, MF-A02).

NCEER-93-0004 "Evaluation of Static and Response Spectrum Analysis Procedures of SEAOC/UBC for Seismic Isolated Structures," by C.W. Winters and M.C. Constantinou, 3/23/93, (PB93-198299, A10, MF-A03).

NCEER-93-0005 "Earthquakes in the Northeast - Are We Ignoring the Hazard? A Workshop on Earthquake Science and Safety for Educators," edited by K.E.K. Ross, 4/2/93, (PB94-103066, A09, MF-A02).

NCEER-93-0006 "Inelastic Response of Reinforced Concrete Structures with Viscoelastic Braces," by R.F. Lobo, J.M. Bracci, K.L. Shen, A.M. Reinhorn and T.T. Soong, 4/5/93, (PB93-227486, A05, MF-A02).

NCEER-93-0007 "Seismic Testing of Installation Methods for Computers and Data Processing Equipment," by K. Kosar, T.T. Soong, K.L. Shen, J.A. HoLung and Y.K. Lin, 4/12/93, (PB93-198299, A07, MF-A02).

NCEER-93-0008 "Retrofit of Reinforced Concrete Frames Using Added Dampers," by A. Reinhorn, M. Constantinou and C. Li, to be published.

NCEER-93-0009 "Seismic Behavior and Design Guidelines for Steel Frame Structures with Added Viscoelastic Dampers," by K.C. Chang, M.L. Lai, T.T. Soong, D.S. Hao and Y.C. Yeh, 5/1/93, (PB94-141959, A07, MF-A02).

NCEER-93-0010 "Seismic Performance of Shear-Critical Reinforced Concrete Bridge Piers," by J.B. Mander, S.M. Waheed, M.T.A. Chaudhary and S.S. Chen, 5/12/93, (PB93-227494, A08, MF-A02).

NCEER-93-0011 "3D-BASIS-TABS: Computer Program for Nonlinear Dynamic Analysis of Three Dimensional Base Isolated Structures," by S. Nagarajaiah, C. Li, A.M. Reinhorn and M.C. Constantinou, 8/2/93, (PB94-141819, A09, MF-A02).

NCEER-93-0012 "Effects of Hydrocarbon Spills from an Oil Pipeline Break on Ground Water," by O.J. Helweg and H.H.M. Hwang, 8/3/93, (PB94-141942, A06, MF-A02).

NCEER-93-0013 "Simplified Procedures for Seismic Design of Nonstructural Components and Assessment of Current Code Provisions," by M.P. Singh, L.E. Suarez, E.E. Matheu and G.O. Maldonado, 8/4/93, (PB94-141827, A09, MF-A02).

NCEER-93-0014 "An Energy Approach to Seismic Analysis and Design of Secondary Systems," by G. Chen and T.T. Soong, 8/6/93, (PB94-142767, A11, MF-A03).

NCEER-93-0015 "Proceedings from School Sites: Becoming Prepared for Earthquakes - Commemorating the Third Anniversary of the Loma Prieta Earthquake," Edited by F.E. Winslow and K.E.K. Ross, 8/16/93, (PB94-154275, A16, MF-A02).

NCEER-93-0016 "Reconnaissance Report of Damage to Historic Monuments in Cairo, Egypt Following the October 12, 1992 Dahshur Earthquake," by D. Sykora, D. Look, G. Croci, E. Karaesmen and E. Karaesmen, 8/19/93, (PB94-142221, A08, MF-A02).

NCEER-93-0017 "The Island of Guam Earthquake of August 8, 1993," by S.W. Swan and S.K. Harris, 9/30/93, (PB94-141843, A04, MF-A01).

NCEER-93-0018 "Engineering Aspects of the October 12, 1992 Egyptian Earthquake," by A.W. Elgamal, M. Amer, K. Adalier and A. Abul-Fadl, 10/7/93, (PB94-141983, A05, MF-A01).

NCEER-93-0019 "Development of an Earthquake Motion Simulator and its Application in Dynamic Centrifuge Testing," by I. Krstelj, Supervised by J.H. Prevost, 10/23/93, (PB94-181773, A-10, MF-A03).

NCEER-93-0020 "NCEER-Taisei Corporation Research Program on Sliding Seismic Isolation Systems for Bridges: Experimental and Analytical Study of a Friction Pendulum System (FPS)," by M.C. Constantinou, P. Tsopelas, Y-S. Kim and S. Okamoto, 11/1/93, (PB94-142775, A08, MF-A02).

NCEER-93-0021 "Finite Element Modeling of Elastomeric Seismic Isolation Bearings," by L.J. Billings, Supervised by R. Shepherd, 11/8/93, to be published.

NCEER-93-0022 "Seismic Vulnerability of Equipment in Critical Facilities: Life-Safety and Operational Consequences," by K. Porter, G.S. Johnson, M.M. Zadeh, C. Scawthorn and S. Eder, 11/24/93, (PB94-181765, A16, MF-A03).

NCEER-93-0023 "Hokkaido Nansei-oki, Japan Earthquake of July 12, 1993, by P.I. Yanev and C.R. Scawthorn, 12/23/93, (PB94-181500, A07, MF-A01).

NCEER-94-0001 "An Evaluation of Seismic Serviceability of Water Supply Networks with Application to the San Francisco Auxiliary Water Supply System," by I. Markov, Supervised by M. Grigoriu and T. O'Rourke, 1/21/94, (PB94-204013, A07, MF-A02).

NCEER-94-0002 "NCEER-Taisei Corporation Research Program on Sliding Seismic Isolation Systems for Bridges: Experimental and Analytical Study of Systems Consisting of Sliding Bearings, Rubber Restoring Force Devices and Fluid Dampers," Volumes I and II, by P. Tsopelas, S. Okamoto, M.C. Constantinou, D. Ozaki and S. Fujii, 2/4/94, (PB94-181740, A09, MF-A02 and PB94-181757, A12, MF-A03).

NCEER-94-0003 "A Markov Model for Local and Global Damage Indices in Seismic Analysis," by S. Rahman and M. Grigoriu, 2/18/94, (PB94-206000, A12, MF-A03).

NCEER-94-0004 "Proceedings from the NCEER Workshop on Seismic Response of Masonry Infills," edited by D.P. Abrams, 3/1/94, (PB94-180783, A07, MF-A02).

NCEER-94-0005 "The Northridge, California Earthquake of January 17, 1994: General Reconnaissance Report," edited by J.D. Goltz, 3/11/94, (PB193943, A10, MF-A03).

NCEER-94-0006 "Seismic Energy Based Fatigue Damage Analysis of Bridge Columns: Part I - Evaluation of Seismic Capacity," by G.A. Chang and J.B. Mander, 3/14/94, (PB94-219185, A11, MF-A03).

NCEER-94-0007 "Seismic Isolation of Multi-Story Frame Structures Using Spherical Sliding Isolation Systems," by T.M. Al-Hussaini, V.A. Zayas and M.C. Constantinou, 3/17/94, (PB193745, A09, MF-A02).

NCEER-94-0008 "The Northridge, California Earthquake of January 17, 1994: Performance of Highway Bridges," edited by I.G. Buckle, 3/24/94, (PB94-193851, A06, MF-A02).

NCEER-94-0009 "Proceedings of the Third U.S.-Japan Workshop on Earthquake Protective Systems for Bridges," edited by I.G. Buckle and I. Friedland, 3/31/94, (PB94-195815, A99, MF-A06).

NCEER-94-0010 "3D-BASIS-ME: Computer Program for Nonlinear Dynamic Analysis of Seismically Isolated Single and Multiple Structures and Liquid Storage Tanks," by P.C. Tsopelas, M.C. Constantinou and A.M. Reinhorn, 4/12/94, (PB94-204922, A09, MF-A02).

NCEER-94-0011 "The Northridge, California Earthquake of January 17, 1994: Performance of Gas Transmission Pipelines," by T.D. O'Rourke and M.C. Palmer, 5/16/94, (PB94-204989, A05, MF-A01).

NCEER-94-0012 "Feasibility Study of Replacement Procedures and Earthquake Performance Related to Gas Transmission Pipelines," by T.D. O'Rourke and M.C. Palmer, 5/25/94, (PB94-206638, A09, MF-A02).

NCEER-94-0013 "Seismic Energy Based Fatigue Damage Analysis of Bridge Columns: Part II - Evaluation of Seismic Demand," by G.A. Chang and J.B. Mander, 6/1/94, (PB95-18106, A08, MF-A02).

NCEER-94-0014 "NCEER-Taisei Corporation Research Program on Sliding Seismic Isolation Systems for Bridges: Experimental and Analytical Study of a System Consisting of Sliding Bearings and Fluid Restoring Force/Damping Devices," by P. Tsopelas and M.C. Constantinou, 6/13/94, (PB94-219144, A10, MF-A03).

NCEER-94-0015 "Generation of Hazard-Consistent Fragility Curves for Seismic Loss Estimation Studies," by H. Hwang and J-R. Huo, 6/14/94, (PB95-181996, A09, MF-A02).

NCEER-94-0016 "Seismic Study of Building Frames with Added Energy-Absorbing Devices," by W.S. Pong, C.S. Tsai and G.C. Lee, 6/20/94, (PB94-219136, A10, A03).

NCEER-94-0017 "Sliding Mode Control for Seismic-Excited Linear and Nonlinear Civil Engineering Structures," by J. Yang, J. Wu, A. Agrawal and Z. Li, 6/21/94, (PB95-138483, A06, MF-A02).

NCEER-94-0018 "3D-BASIS-TABS Version 2.0: Computer Program for Nonlinear Dynamic Analysis of Three Dimensional Base Isolated Structures," by A.M. Reinhorn, S. Nagarajaiah, M.C. Constantinou, P. Tsopelas and R. Li, 6/22/94, (PB95-182176, A08, MF-A02).

NCEER-94-0019 "Proceedings of the International Workshop on Civil Infrastructure Systems: Application of Intelligent Systems and Advanced Materials on Bridge Systems," Edited by G.C. Lee and K.C. Chang, 7/18/94, (PB95-252474, A20, MF-A04).

NCEER-94-0020 "Study of Seismic Isolation Systems for Computer Floors," by V. Lambrou and M.C. Constantinou, 7/19/94, (PB95-138533, A10, MF-A03).

NCEER-94-0021 "Proceedings of the U.S.-Italian Workshop on Guidelines for Seismic Evaluation and Rehabilitation of Unreinforced Masonry Buildings," Edited by D.P. Abrams and G.M. Calvi, 7/20/94, (PB95-138749, A13, MF-A03).

NCEER-94-0022 "NCEER-Taisei Corporation Research Program on Sliding Seismic Isolation Systems for Bridges: Experimental and Analytical Study of a System Consisting of Lubricated PTFE Sliding Bearings and Mild Steel Dampers," by P. Tsopelas and M.C. Constantinou, 7/22/94, (PB95-182184, A08, MF-A02).

NCEER-94-0023 “Development of Reliability-Based Design Criteria for Buildings Under Seismic Load,” by Y.K. Wen, H. Hwang and M. Shinozuka, 8/1/94, (PB95-211934, A08, MF-A02).

NCEER-94-0024 “Experimental Verification of Acceleration Feedback Control Strategies for an Active Tendon System,” by S.J. Dyke, B.F. Spencer, Jr., P. Quast, M.K. Sain, D.C. Kaspari, Jr. and T.T. Soong, 8/29/94, (PB95-212320, A05, MF-A01).

NCEER-94-0025 “Seismic Retrofitting Manual for Highway Bridges,” Edited by I.G. Buckle and I.F. Friedland, published by the Federal Highway Administration (PB95-212676, A15, MF-A03).

NCEER-94-0026 “Proceedings from the Fifth U.S.-Japan Workshop on Earthquake Resistant Design of Lifeline Facilities and Countermeasures Against Soil Liquefaction,” Edited by T.D. O’Rourke and M. Hamada, 11/7/94, (PB95-220802, A99, MF-E08).

NCEER-95-0001 "Experimental and Analytical Investigation of Seismic Retrofit of Structures with Supplemental Damping: Part 1 - Fluid Viscous Damping Devices," by A.M. Reinhorn, C. Li and M.C. Constantinou, 1/3/95, (PB95-266599, A09, MF-A02).

NCEER-95-0002 "Experimental and Analytical Study of Low-Cycle Fatigue Behavior of Semi-Rigid Top-And-Seat Angle Connections," by G. Pekcan, J.B. Mander and S.S. Chen, 1/5/95, (PB95-220042, A07, MF-A02).

NCEER-95-0003 "NCEER-ATC Joint Study on Fragility of Buildings," by T. Anagnos, C. Rojahn and A.S. Kiremidjian, 1/20/95, (PB95-220026, A06, MF-A02).

NCEER-95-0004 "Nonlinear Control Algorithms for Peak Response Reduction," by Z. Wu, T.T. Soong, V. Gattulli and R.C. Lin, 2/16/95, (PB95-220349, A05, MF-A01).

NCEER-95-0005 "Pipeline Replacement Feasibility Study: A Methodology for Minimizing Seismic and Corrosion Risks to Underground Natural Gas Pipelines," by R.T. Eguchi, H.A. Seligson and D.G. Honegger, 3/2/95, (PB95-252326, A06, MF-A02).

NCEER-95-0006 "Evaluation of Seismic Performance of an 11-Story Frame Building During the 1994 Northridge Earthquake," by F. Naeim, R. DiSulio, K. Benuska, A. Reinhorn and C. Li, to be published.

NCEER-95-0007 "Prioritization of Bridges for Seismic Retrofitting," by N. Basöz and A.S. Kiremidjian, 4/24/95, (PB95-252300, A08, MF-A02).

NCEER-95-0008 "Method for Developing Motion Damage Relationships for Reinforced Concrete Frames," by A. Singhal and A.S. Kiremidjian, 5/11/95, (PB95-266607, A06, MF-A02).

NCEER-95-0009 "Experimental and Analytical Investigation of Seismic Retrofit of Structures with Supplemental Damping: Part II - Friction Devices," by C. Li and A.M. Reinhorn, 7/6/95, (PB96-128087, A11, MF-A03).

NCEER-95-0010 "Experimental Performance and Analytical Study of a Non-Ductile Reinforced Concrete Frame Structure Retrofitted with Elastomeric Spring Dampers," by G. Pekcan, J.B. Mander and S.S. Chen, 7/14/95, (PB96-137161, A08, MF-A02).

NCEER-95-0011 "Development and Experimental Study of Semi-Active Fluid Damping Devices for Seismic Protection of Structures," by M.D. Symans and M.C. Constantinou, 8/3/95, (PB96-136940, A23, MF-A04).

NCEER-95-0012 "Real-Time Structural Parameter Modification (RSPM): Development of Innervated Structures," by Z. Liang, M. Tong and G.C. Lee, 4/11/95, (PB96-137153, A06, MF-A01).

NCEER-95-0013 "Experimental and Analytical Investigation of Seismic Retrofit of Structures with Supplemental Damping: Part III - Viscous Damping Walls," by A.M. Reinhorn and C. Li, 10/1/95, (PB96-176409, A11, MF-A03).

NCEER-95-0014 "Seismic Fragility Analysis of Equipment and Structures in a Memphis Electric Substation," by J-R. Huo and H.H.M. Hwang, (PB96-128087, A09, MF-A02), 8/10/95.

NCEER-95-0015 "The Hanshin-Awaji Earthquake of January 17, 1995: Performance of Lifelines," Edited by M. Shinozuka, 11/3/95, (PB96-176383, A15, MF-A03).

NCEER-95-0016 "Highway Culvert Performance During Earthquakes," by T.L. Youd and C.J. Beckman, available as NCEER-96-0015.

NCEER-95-0017 "The Hanshin-Awaji Earthquake of January 17, 1995: Performance of Highway Bridges," Edited by I.G. Buckle, 12/1/95, to be published.

NCEER-95-0018 "Modeling of Masonry Infill Panels for Structural Analysis," by A.M. Reinhorn, A. Madan, R.E. Valles, Y. Reichmann and J.B. Mander, 12/8/95, (PB97-110886, MF-A01, A06).

NCEER-95-0019 "Optimal Polynomial Control for Linear and Nonlinear Structures," by A.K. Agrawal and J.N. Yang, 12/11/95, (PB96-168737, A07, MF-A02).

NCEER-95-0020 "Retrofit of Non-Ductile Reinforced Concrete Frames Using Friction Dampers," by R.S. Rao, P. Gergely and R.N. White, 12/22/95, (PB97-133508, A10, MF-A02).

NCEER-95-0021 "Parametric Results for Seismic Response of Pile-Supported Bridge Bents," by G. Mylonakis, A. Nikolaou and G. Gazetas, 12/22/95, (PB97-100242, A12, MF-A03).

NCEER-95-0022 "Kinematic Bending Moments in Seismically Stressed Piles," by A. Nikolaou, G. Mylonakis and G. Gazetas, 12/23/95, (PB97-113914, MF-A03, A13).

NCEER-96-0001 "Dynamic Response of Unreinforced Masonry Buildings with Flexible Diaphragms," by A.C. Costley and D.P. Abrams," 10/10/96, (PB97-133573, MF-A03, A15).

NCEER-96-0002 "State of the Art Review: Foundations and Retaining Structures," by I. Po Lam, to be published.

NCEER-96-0003 "Ductility of Rectangular Reinforced Concrete Bridge Columns with Moderate Confinement," by N. Wehbe, M. Saiidi, D. Sanders and B. Douglas, 11/7/96, (PB97-133557, A06, MF-A02).

NCEER-96-0004 "Proceedings of the Long-Span Bridge Seismic Research Workshop," edited by I.G. Buckle and I.M. Friedland, to be published.

NCEER-96-0005 "Establish Representative Pier Types for Comprehensive Study: Eastern United States," by J. Kulicki and Z. Prucz, 5/28/96, (PB98-119217, A07, MF-A02).

NCEER-96-0006 "Establish Representative Pier Types for Comprehensive Study: Western United States," by R. Imbsen, R.A. Schamber and T.A. Osterkamp, 5/28/96, (PB98-118607, A07, MF-A02).

NCEER-96-0007 "Nonlinear Control Techniques for Dynamical Systems with Uncertain Parameters," by R.G. Ghanem and M.I. Bujakov, 5/27/96, (PB97-100259, A17, MF-A03).

NCEER-96-0008 "Seismic Evaluation of a 30-Year Old Non-Ductile Highway Bridge Pier and Its Retrofit," by J.B. Mander, B. Mahmoodzadegan, S. Bhadra and S.S. Chen, 5/31/96, (PB97-110902, MF-A03, A10).

NCEER-96-0009 "Seismic Performance of a Model Reinforced Concrete Bridge Pier Before and After Retrofit," by J.B. Mander, J.H. Kim and C.A. Ligozio, 5/31/96, (PB97-110910, MF-A02, A10).

NCEER-96-0010 "IDARC2D Version 4.0: A Computer Program for the Inelastic Damage Analysis of Buildings," by R.E. Valles, A.M. Reinhorn, S.K. Kunnath, C. Li and A. Madan, 6/3/96, (PB97-100234, A17, MF-A03).

NCEER-96-0011 "Estimation of the Economic Impact of Multiple Lifeline Disruption: Memphis Light, Gas and Water Division Case Study," by S.E. Chang, H.A. Seligson and R.T. Eguchi, 8/16/96, (PB97-133490, A11, MF-A03).

NCEER-96-0012 "Proceedings from the Sixth Japan-U.S. Workshop on Earthquake Resistant Design of Lifeline Facilities and Countermeasures Against Soil Liquefaction, Edited by M. Hamada and T. O'Rourke, 9/11/96, (PB97-133581, A99, MF-A06).

NCEER-96-0013 "Chemical Hazards, Mitigation and Preparedness in Areas of High Seismic Risk: A Methodology for Estimating the Risk of Post-Earthquake Hazardous Materials Release," by H.A. Seligson, R.T. Eguchi, K.J. Tierney and K. Richmond, 11/7/96, (PB97-133565, MF-A02, A08).

NCEER-96-0014 "Response of Steel Bridge Bearings to Reversed Cyclic Loading," by J.B. Mander, D-K. Kim, S.S. Chen and G.J. Premus, 11/13/96, (PB97-140735, A12, MF-A03).

NCEER-96-0015 "Highway Culvert Performance During Past Earthquakes," by T.L. Youd and C.J. Beckman, 11/25/96, (PB97-133532, A06, MF-A01).

NCEER-97-0001 "Evaluation, Prevention and Mitigation of Pounding Effects in Building Structures," by R.E. Valles and A.M. Reinhorn, 2/20/97, (PB97-159552, A14, MF-A03).

NCEER-97-0002 "Seismic Design Criteria for Bridges and Other Highway Structures," by C. Rojahn, R. Mayes, D.G. Anderson, J. Clark, J.H. Hom, R.V. Nutt and M.J. O'Rourke, 4/30/97, (PB97-194658, A06, MF-A03).

NCEER-97-0003 “Proceedings of the U.S.-Italian Workshop on Seismic Evaluation and Retrofit,” Edited by D.P. Abrams and G.M. Calvi, 3/19/97, (PB97-194666, A13, MF-A03).

NCEER-97-0004 "Investigation of Seismic Response of Buildings with Linear and Nonlinear Fluid Viscous Dampers," by A.A. Seleemah and M.C. Constantinou, 5/21/97, (PB98-109002, A15, MF-A03).

NCEER-97-0005 "Proceedings of the Workshop on Earthquake Engineering Frontiers in Transportation Facilities," edited by G.C. Lee and I.M. Friedland, 8/29/97, (PB98-128911, A25, MR-A04).

NCEER-97-0006 "Cumulative Seismic Damage of Reinforced Concrete Bridge Piers," by S.K. Kunnath, A. El-Bahy, A. Taylor and W. Stone, 9/2/97, (PB98-108814, A11, MF-A03).

NCEER-97-0007 "Structural Details to Accommodate Seismic Movements of Highway Bridges and Retaining Walls," by R.A. Imbsen, R.A. Schamber, E. Thorkildsen, A. Kartoum, B.T. Martin, T.N. Rosser and J.M. Kulicki, 9/3/97, (PB98-108996, A09, MF-A02).

NCEER-97-0008 "A Method for Earthquake Motion-Damage Relationships with Application to Reinforced Concrete Frames," by A. Singhal and A.S. Kiremidjian, 9/10/97, (PB98-108988, A13, MF-A03).

NCEER-97-0009 "Seismic Analysis and Design of Bridge Abutments Considering Sliding and Rotation," by K. Fishman and R. Richards, Jr., 9/15/97, (PB98-108897, A06, MF-A02).

NCEER-97-0010 "Proceedings of the FHWA/NCEER Workshop on the National Representation of Seismic Ground Motion for New and Existing Highway Facilities," edited by I.M. Friedland, M.S. Power and R.L. Mayes, 9/22/97, (PB98-128903, A21, MF-A04).

NCEER-97-0011 "Seismic Analysis for Design or Retrofit of Gravity Bridge Abutments," by K.L. Fishman, R. Richards, Jr. and R.C. Divito, 10/2/97, (PB98-128937, A08, MF-A02).

NCEER-97-0012 "Evaluation of Simplified Methods of Analysis for Yielding Structures," by P. Tsopelas, M.C. Constantinou, C.A. Kircher and A.S. Whittaker, 10/31/97, (PB98-128929, A10, MF-A03).

NCEER-97-0013 "Seismic Design of Bridge Columns Based on Control and Repairability of Damage," by C-T. Cheng and J.B. Mander, 12/8/97, (PB98-144249, A11, MF-A03).

NCEER-97-0014 "Seismic Resistance of Bridge Piers Based on Damage Avoidance Design," by J.B. Mander and C-T. Cheng, 12/10/97, (PB98-144223, A09, MF-A02).

NCEER-97-0015 “Seismic Response of Nominally Symmetric Systems with Strength Uncertainty,” by S. Balopoulou and M. Grigoriu, 12/23/97, (PB98-153422, A11, MF-A03).

NCEER-97-0016 “Evaluation of Seismic Retrofit Methods for Reinforced Concrete Bridge Columns,” by T.J. Wipf, F.W. Klaiber and F.M. Russo, 12/28/97, (PB98-144215, A12, MF-A03).

NCEER-97-0017 “Seismic Fragility of Existing Conventional Reinforced Concrete Highway Bridges,” by C.L. Mullen and A.S. Cakmak, 12/30/97, (PB98-153406, A08, MF-A02).

NCEER-97-0018 “Loss Asssessment of Memphis Buildings,” edited by D.P. Abrams and M. Shinozuka, 12/31/97, (PB98-144231, A13, MF-A03).

NCEER-97-0019 “Seismic Evaluation of Frames with Infill Walls Using Quasi-static Experiments,” by K.M. Mosalam, R.N. White and P. Gergely, 12/31/97, (PB98-153455, A07, MF-A02).

NCEER-97-0020 “Seismic Evaluation of Frames with Infill Walls Using Pseudo-dynamic Experiments,” by K.M. Mosalam, R.N. White and P. Gergely, 12/31/97, (PB98-153430, A07, MF-A02).

NCEER-97-0021 “Computational Strategies for Frames with Infill Walls: Discrete and Smeared Crack Analyses and Seismic Fragility,” by K.M. Mosalam, R.N. White and P. Gergely, 12/31/97, (PB98-153414, A10, MF-A02).

NCEER-97-0022 "Proceedings of the NCEER Workshop on Evaluation of Liquefaction Resistance of Soils," edited by T.L. Youd and I.M. Idriss, 12/31/97, (PB98-155617, A15, MF-A03).

MCEER-98-0001 "Extraction of Nonlinear Hysteretic Properties of Seismically Isolated Bridges from Quick-Release Field Tests," by Q. Chen, B.M. Douglas, E.M. Maragakis and I.G. Buckle, 5/26/98, (PB99-118838, A06, MF-A01).

MCEER-98-0002 "Methodologies for Evaluating the Importance of Highway Bridges," by A. Thomas, S. Eshenaur and J. Kulicki, 5/29/98, (PB99-118846, A10, MF-A02).

MCEER-98-0003 "Capacity Design of Bridge Piers and the Analysis of Overstrength," by J.B. Mander, A. Dutta and P. Goel, 6/1/98, (PB99-118853, A09, MF-A02).

MCEER-98-0004 "Evaluation of Bridge Damage Data from the Loma Prieta and Northridge, California Earthquakes," by N. Basoz and A. Kiremidjian, 6/2/98, (PB99-118861, A15, MF-A03).

MCEER-98-0005 "Screening Guide for Rapid Assessment of Liquefaction Hazard at Highway Bridge Sites," by T. L. Youd, 6/16/98, (PB99-118879, A06, not available on microfiche).

MCEER-98-0006 "Structural Steel and Steel/Concrete Interface Details for Bridges," by P. Ritchie, N. Kauhl and J. Kulicki, 7/13/98, (PB99-118945, A06, MF-A01).

MCEER-98-0007 "Capacity Design and Fatigue Analysis of Confined Concrete Columns," by A. Dutta and J.B. Mander, 7/14/98, (PB99-118960, A14, MF-A03).

MCEER-98-0008 "Proceedings of the Workshop on Performance Criteria for Telecommunication Services Under Earthquake Conditions," edited by A.J. Schiff, 7/15/98, (PB99-118952, A08, MF-A02).

MCEER-98-0009 "Fatigue Analysis of Unconfined Concrete Columns," by J.B. Mander, A. Dutta and J.H. Kim, 9/12/98, (PB99-123655, A10, MF-A02).

MCEER-98-0010 "Centrifuge Modeling of Cyclic Lateral Response of Pile-Cap Systems and Seat-Type Abutments in Dry Sands," by A.D. Gadre and R. Dobry, 10/2/98, (PB99-123606, A13, MF-A03).

MCEER-98-0011 "IDARC-BRIDGE: A Computational Platform for Seismic Damage Assessment of Bridge Structures," by A.M. Reinhorn, V. Simeonov, G. Mylonakis and Y. Reichman, 10/2/98, (PB99-162919, A15, MF-A03).

MCEER-98-0012 "Experimental Investigation of the Dynamic Response of Two Bridges Before and After Retrofitting with Elastomeric Bearings," by D.A. Wendichansky, S.S. Chen and J.B. Mander, 10/2/98, (PB99-162927, A15, MF-A03).

MCEER-98-0013 "Design Procedures for Hinge Restrainers and Hinge Sear Width for Multiple-Frame Bridges," by R. Des Roches and G.L. Fenves, 11/3/98, (PB99-140477, A13, MF-A03).

MCEER-98-0014 "Response Modification Factors for Seismically Isolated Bridges," by M.C. Constantinou and J.K. Quarshie, 11/3/98, (PB99-140485, A14, MF-A03).

MCEER-98-0015 "Proceedings of the U.S.-Italy Workshop on Seismic Protective Systems for Bridges," edited by I.M. Friedland and M.C. Constantinou, 11/3/98, (PB2000-101711, A22, MF-A04).

MCEER-98-0016 "Appropriate Seismic Reliability for Critical Equipment Systems: Recommendations Based on Regional Analysis of Financial and Life Loss," by K. Porter, C. Scawthorn, C. Taylor and N. Blais, 11/10/98, (PB99-157265, A08, MF-A02).

MCEER-98-0017 "Proceedings of the U.S. Japan Joint Seminar on Civil Infrastructure Systems Research," edited by M. Shinozuka and A. Rose, 11/12/98, (PB99-156713, A16, MF-A03).

MCEER-98-0018 "Modeling of Pile Footings and Drilled Shafts for Seismic Design," by I. PoLam, M. Kapuskar and D. Chaudhuri, 12/21/98, (PB99-157257, A09, MF-A02).

MCEER-99-0001 "Seismic Evaluation of a Masonry Infilled Reinforced Concrete Frame by Pseudodynamic Testing," by S.G. Buonopane and R.N. White, 2/16/99, (PB99-162851, A09, MF-A02).

MCEER-99-0002 "Response History Analysis of Structures with Seismic Isolation and Energy Dissipation Systems: Verification Examples for Program SAP2000," by J. Scheller and M.C. Constantinou, 2/22/99, (PB99-162869, A08, MF-A02).

MCEER-99-0003 "Experimental Study on the Seismic Design and Retrofit of Bridge Columns Including Axial Load Effects," by A. Dutta, T. Kokorina and J.B. Mander, 2/22/99, (PB99-162877, A09, MF-A02).

MCEER-99-0004 "Experimental Study of Bridge Elastomeric and Other Isolation and Energy Dissipation Systems with Emphasis on Uplift Prevention and High Velocity Near-source Seismic Excitation," by A. Kasalanati and M. C. Constantinou, 2/26/99, (PB99-162885, A12, MF-A03).

MCEER-99-0005 "Truss Modeling of Reinforced Concrete Shear-flexure Behavior," by J.H. Kim and J.B. Mander, 3/8/99, (PB99-163693, A12, MF-A03).

MCEER-99-0006 "Experimental Investigation and Computational Modeling of Seismic Response of a 1:4 Scale Model Steel Structure with a Load Balancing Supplemental Damping System," by G. Pekcan, J.B. Mander and S.S. Chen, 4/2/99, (PB99-162893, A11, MF-A03).

MCEER-99-0007 "Effect of Vertical Ground Motions on the Structural Response of Highway Bridges," by M.R. Button, C.J. Cronin and R.L. Mayes, 4/10/99, (PB2000-101411, A10, MF-A03).

MCEER-99-0008 "Seismic Reliability Assessment of Critical Facilities: A Handbook, Supporting Documentation, and Model Code Provisions," by G.S. Johnson, R.E. Sheppard, M.D. Quilici, S.J. Eder and C.R. Scawthorn, 4/12/99, (PB2000-101701, A18, MF-A04).

MCEER-99-0009 "Impact Assessment of Selected MCEER Highway Project Research on the Seismic Design of Highway Structures," by C. Rojahn, R. Mayes, D.G. Anderson, J.H. Clark, D'Appolonia Engineering, S. Gloyd and R.V. Nutt, 4/14/99, (PB99-162901, A10, MF-A02).

MCEER-99-0010 "Site Factors and Site Categories in Seismic Codes," by R. Dobry, R. Ramos and M.S. Power, 7/19/99, (PB2000-101705, A08, MF-A02).

MCEER-99-0011 "Restrainer Design Procedures for Multi-Span Simply-Supported Bridges," by M.J. Randall, M. Saiidi, E. Maragakis and T. Isakovic, 7/20/99, (PB2000-101702, A10, MF-A02).

MCEER-99-0012 "Property Modification Factors for Seismic Isolation Bearings," by M.C. Constantinou, P. Tsopelas, A. Kasalanati and E. Wolff, 7/20/99, (PB2000-103387, A11, MF-A03).

MCEER-99-0013 "Critical Seismic Issues for Existing Steel Bridges," by P. Ritchie, N. Kauhl and J. Kulicki, 7/20/99, (PB2000-101697, A09, MF-A02).

MCEER-99-0014 "Nonstructural Damage Database," by A. Kao, T.T. Soong and A. Vender, 7/24/99, (PB2000-101407, A06, MF-A01).

MCEER-99-0015 "Guide to Remedial Measures for Liquefaction Mitigation at Existing Highway Bridge Sites," by H.G. Cooke and J. K. Mitchell, 7/26/99, (PB2000-101703, A11, MF-A03).

MCEER-99-0016 "Proceedings of the MCEER Workshop on Ground Motion Methodologies for the Eastern United States," edited by N. Abrahamson and A. Becker, 8/11/99, (PB2000-103385, A07, MF-A02).

MCEER-99-0017 "Quindío, Colombia Earthquake of January 25, 1999: Reconnaissance Report," by A.P. Asfura and P.J. Flores, 10/4/99, (PB2000-106893, A06, MF-A01).

MCEER-99-0018 "Hysteretic Models for Cyclic Behavior of Deteriorating Inelastic Structures," by M.V. Sivaselvan and A.M. Reinhorn, 11/5/99, (PB2000-103386, A08, MF-A02).

MCEER-99-0019 "Proceedings of the 7th U.S.- Japan Workshop on Earthquake Resistant Design of Lifeline Facilities and Countermeasures Against Soil Liquefaction," edited by T.D. O'Rourke, J.P. Bardet and M. Hamada, 11/19/99, (PB2000-103354, A99, MF-A06).

MCEER-99-0020 "Development of Measurement Capability for Micro-Vibration Evaluations with Application to Chip Fabrication Facilities," by G.C. Lee, Z. Liang, J.W. Song, J.D. Shen and W.C. Liu, 12/1/99, (PB2000-105993, A08, MF-A02).

MCEER-99-0021 "Design and Retrofit Methodology for Building Structures with Supplemental Energy Dissipating Systems," by G. Pekcan, J.B. Mander and S.S. Chen, 12/31/99, (PB2000-105994, A11, MF-A03).

MCEER-00-0001 "The Marmara, Turkey Earthquake of August 17, 1999: Reconnaissance Report," edited by C. Scawthorn; with major contributions by M. Bruneau, R. Eguchi, T. Holzer, G. Johnson, J. Mander, J. Mitchell, W. Mitchell, A. Papageorgiou, C. Scaethorn, and G. Webb, 3/23/00, (PB2000-106200, A11, MF-A03).

MCEER-00-0002 "Proceedings of the MCEER Workshop for Seismic Hazard Mitigation of Health Care Facilities," edited by G.C. Lee, M. Ettouney, M. Grigoriu, J. Hauer and J. Nigg, 3/29/00, (PB2000-106892, A08, MF-A02).

MCEER-00-0003 "The Chi-Chi, Taiwan Earthquake of September 21, 1999: Reconnaissance Report," edited by G.C. Lee and C.H. Loh, with major contributions by G.C. Lee, M. Bruneau, I.G. Buckle, S.E. Chang, P.J. Flores, T.D. O'Rourke, M. Shinozuka, T.T. Soong, C-H. Loh, K-C. Chang, Z-J. Chen, J-S. Hwang, M-L. Lin, G-Y. Liu, K-C. Tsai, G.C. Yao and C-L. Yen, 4/30/00.

MCEER-00-0004 "Seismic Retrofit of End-Sway Frames of Steel Deck-Truss Bridges with a Supplemental Tendon System: Experimental and Analytical Investigation," by G. Pekcan, J.B. Mander and S.S. Chen, 7/1/00.

MCEER-00-0005 "Sliding Fragility of Unrestrained Equipment in Critical Facilities," by W.H. Chong and T.T. Soong, 7/5/00.

MCEER-00-0006 "Seismic Response of Reinforced Concrete Bridge Pier Walls in the Weak Direction," by N. Abo-Shadi, M. Saiidi and D. Sanders, 7/17/00.

MCEER-00-0007 "Low-Cycle Fatigue Behavior of Longitudinal Reinforcement in Reinforced Concrete Bridge Columns," by J. Brown and S.K. Kunnath, 7/23/00.

MCEER-00-0008 "Soil Structure Interaction of Bridges for Seismic Analysis," I. PoLam and H. Law, 9/25/00.

MCEER-00-0009 "Proceedings of the First MCEER Workshop on Mitigation of Earthquake Disaster by Advanced Technologies (MEDAT-1), edited by M. Shinozuka, D.J. Inman and T.D. O'Rourke, 11/10/00.

MCEER-00-0010 "Development and Evaluation of Simplified Procedures for Analysis and Design of Buildings with Passive Energy Dissipation Systems," by O.M. Ramirez, M.C. Constantinou, C.A. Kircher, A.S. Whittaker, M.W. Johnson, J.D. Gomez and C. Chrysostomou, 11/16/01.

MCEER-00-0011 "Dynamic Soil-Foundation-Structure Interaction Analyses of Large Caissons," by C-Y. Chang, C-M. Mok, Z-L. Wang, R. Settgast, F. Waggoner, M.A. Ketchum, H.M. Gonnermann and C-C. Chin, 12/30/00.

MCEER-00-0012 "Experimental Evaluation of Seismic Performance of Bridge Restrainers," by A.G. Vlassis, E.M. Maragakis and M. Saiid Saiidi, 12/30/00.

MCEER-00-0013 "Effect of Spatial Variation of Ground Motion on Highway Structures," by M. Shinozuka, V. Saxena and G. Deodatis, 12/31/00.

MCEER-00-0014 "A Risk-Based Methodology for Assessing the Seismic Performance of Highway Systems," by S.D. Werner, C.E. Taylor, J.E. Moore, II, J.S. Walton and S. Cho, 12/31/00.

MCEER-01-0001 “Experimental Investigation of P-Delta Effects to Collapse During Earthquakes,” by D. Vian and M. Bruneau, 6/25/01.

MCEER-01-0002 “Proceedings of the Second MCEER Workshop on Mitigation of Earthquake Disaster by Advanced Technologies (MEDAT-2),” edited by M. Bruneau and D.J. Inman, 7/23/01.

MCEER-01-0003 "Sensitivity Analysis of Dynamic Systems Subjected to Seismic Loads," by C. Roth and M. Grigoriu, 9/18/01.

MCEER-01-0004 "Overcoming Obstacles to Implementing Earthquake Hazard Mitigation Policies: Stage 1 Report," by D.J. Alesch and W.J. Petak, 12/17/01.

MCEER-01-0005 "Updating Real-Time Earthquake Loss Estimates: Methods, Problems and Insights," by C.E. Taylor, S.E. Chang and R.T. Eguchi, 12/17/01.

MCEER-01-0006 "Experimental Investigation and Retrofit of Steel Pile Foundations and Pile Bents Under Cyclic Lateral Loadings," by A. Shama, J. Mander, B. Blabac and S. Chen, 12/31/01.

MCEER-02-0001 "Assessment of Performance of Bolu Viaduct in the 1999 Duzce Earthquake in Turkey" by P.C. Roussis, M.C. Constantinou, M. Erdik, E. Durukal and M. Dicleli, 5/8/02.

MCEER-02-0002 "Seismic Behavior of Rail Counterweight Systems of Elevators in Buildings," by M.P. Singh, Rildova and L.E. Suarez, 5/27/02.

MCEER-02-0003 "Development of Analysis and Design Procedures for Spread Footings," by G. Mylonakis, G. Gazetas, S. Nikolaou and A. Chauncey, 10/02/02.

MCEER-02-0004 "Bare-Earth Algorithms for Use with SAR and LIDAR Digital Elevation Models," by C.K. Huyck, R.T. Eguchi and B. Houshmand, 10/16/02.

MCEER-02-0005 "Review of Energy Dissipation of Compression Members in Concentrically Braced Frames," by K.Lee and M. Bruneau, 10/18/02.

MCEER-03-0001 "Experimental Investigation of Light-Gauge Steel Plate Shear Walls for the Seismic Retrofit of Buildings" by J. Berman and M. Bruneau, 5/2/03.

MCEER-03-0002 "Statistical Analysis of Fragility Curves," by M. Shinozuka, M.Q. Feng, H. Kim, T. Uzawa and T. Ueda, 6/16/03.

MCEER-03-0003 "Proceedings of the Eighth U.S.-Japan Workshop on Earthquake Resistant Design f Lifeline Facilities and Countermeasures Against Liquefaction," edited by M. Hamada, J.P. Bardet and T.D. O'Rourke, 6/30/03.

MCEER-03-0004 "Proceedings of the PRC-US Workshop on Seismic Analysis and Design of Special Bridges," edited by L.C. Fan and G.C. Lee, 7/15/03.

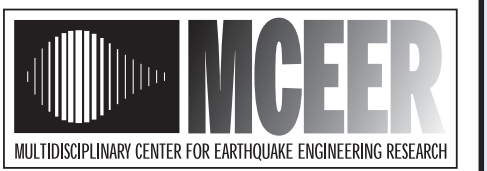

MULTIDISCIPLINARY CENTER FOR EARTHQUAKE ENGINEERING RESEARCH

A National Center of Excellence in Advanced Technology Applications

University at Buffalo, State University of New York
Red Jacket Quadrangle ▪ Buffalo, New York 14261
Phone: (716) 645-3391 ▪ Fax: (716) 645-3399
E-mail: *mceer@mceermail.buffalo.edu* ▪ WWW Site *http://mceer.buffalo.edu*

University at Buffalo *The State University of New York*